Microwave Studies of Gas-Phase Molecules and Complexes: Automation, Structure, and Electronic Analysis

A DISSERTATION
SUBMITTED TO THE FACULTY OF THE
UNIVERSITY OF MINNESOTA
BY

Nathan K. Love

IN PARTIAL FULLFILLMENT OF THE REQUIREMENTS
FOR THE DEGREE OF
DOCTOR OF PHILOSOPHY

Dr. Kenneth R. Leopold Advisor

September 2022

Acknowledgements

Firstly, I would like to thank my advisor, Ken Leopold, for the important role that he played in my graduate studies. When I was a first year student looking to join a group, Ken's group uniquely stood out as kind and welcoming. After nearly five years of researching in the Leopold Lab, I have learned that the group's qualities are the direct result of its patient, engaging, and warm-hearted leader, Ken. His mentorship and support were integral to the quality and quantity of research that I produced during my graduate studies. Additionally, there are very few classically trained pianists I know that would be willing to graciously listen to "screamo" music!

Next, I would like to thank my group mates, Anna Huff and C.J. Smith. Both were instrumental (pun intended) in training me in on the microwave spectrometer and teaching me best practices for working with vacuum equipment and gases. Anna and C.J. were both warm, welcoming, and patient with me as a first year graduate student who knew next to nothing about microwave spectroscopy at the time. I would like to extend a continued thanks to Anna who critically and importantly engaged in the testing of my automation programs and the discussion of their improvement.

Next, I want to thank the "Boundary Waters Crew" as we have come to be known. A huge thanks to Dan for first inviting me to join his Dungeons and Dragons campaign through which I met this group of friends – Dan, Casey, Nicole, Nick, Becca, and Celeste. Thank you all for creating a loving community and allowing me to lead you all to my favorite place in the world – the Boundary Waters Canoe Area. I hope that we will continue to have future expeditions into nature together.

The next group I would like to thank are the members of my metalcore band. Graduate school is often stressful and the world events that occurred during these five years were not easy to handle or process. Together we were able to create something beautiful (and loud) while providing a crucial mode of stress relief for me. There are things worth screaming about!

Finally, I would like to thank my extensive and loving support system consisting of all my family and friends (including those aforementioned). To my mom, my dad, Anna, Nick, Bag – I could not have completed these graduate studies without your endless support and love. To my loving and supportive girlfriend Jasmine who was particularly compassionate during the latter portion of my graduate studies during which my future was uncertain. To my close friends – Aashish, Jesse, Swayne, H.P., and many others – for reminding me that there is more to life than graduate school and letting me continually and absolutely punish them in Mario Kart. Lastly, to Pastor Steph and the many community members of Mill City Church for affirming that science and faith are not mutually exclusive in the slightest.

Table of Contents

List of Tables

List of Figures

Introduction

Gas phase molecular clusters comprised of two or more molecules represent a unique bridge between the molecular and bulk phases of matter. The intermolecular interactions that exist at the core of weakly bound clusters and complexes are ultimately responsible for the aggregation and properties of bulk matter. Through the study of these intermolecular forces, one is able to describe how fundamental interactions at the molecular level ultimately mold the physical properties of bulk matter in the liquid and solid phases. Furthermore, the analysis of intermolecular interactions within pre-reactive complexes can provide valuable insight into chemical properties and reactivity as it scales to the bulk phase.

Techniques such as photoelectron, multiphoton, optical, and infrared spectroscopy as well as mass spectrometry have been used to study a wide variety of molecular cluster properties including dynamics, reactivity, electronics, and molecular/complex structure.[1-11] The research presented in this thesis employs Fourier transform microwave spectroscopy to observe and characterize small molecules and complexes. This method provides acutely specific information about structure through the analysis of rotational transitions whose frequencies are primarily related to the inertial moments of a freely rotating molecule or complex. With ample isotopic data, highly accurate bond lengths, angles, and dihedral angles can be determined through a Kraitchman analysis.[12] In some cases, the presence of large amplitude motion or a nucleus with a quadrupole moment can provide additional insight into internal dynamics or electronic properties, albeit at the cost of an increase in spectral complexity.

The observed microwave spectra in this work are always supported by high level calculations. Small deviations between theoretical and experimental structure often result in significant deviation in the frequencies of observed rotational transitions so it is important to choose a reliable level of theory. In recent years, the Leopold Lab most frequently has used Density Functional Theory (DFT) calculations to predict structure which have proven to be a dependable and accurate method for small molecules and complexes. However, some of the work described here also utilizes second order Møller-

Plesset perturbation methods (MP2) which was found to be particularly accurate for predicting both the nuclear quadrupole coupling constants and complex structure for some of the systems studied. More expensive coupled cluster calculations are also described in this work to provide more accurate minimum and transition state energies for reaction pathways.

The Leopold Lab houses a tandem cavity and chirped-pulse spectrometer which allows for switching between methods without the need to break vacuum. The instrument was originally built in 1995[13] to house a Balle-Flygare cavity spectrometer, of the type originally designed in 1981.[14] The chirped-pulse method, which was developed by Brooks Pate in 2008,[15] was added to the existing instrument along an axis orthogonal to the cavity axis in 2013.[16] The newer chirped-pulse system is a broadband method capable of measuring spectra 3 GHz at a time ranging between 6 and 18 GHz, whereas the narrowband cavity method is limited to spectral windows of only 1 MHz between 2.5 and 19.3 GHz. However, the cavity method importantly provides higher resolution and improved sensitivity, thus being capable of resolving closely spaced transitions and observing weak transitions such as those due to ^{18}O isotopologues in natural abundance. Despite the power of the broadband method, the data collection and transfer of the chirped-pulse method of the Leopold Lab spectrometer originally required manual manipulation due to memory limitations of the oscilloscope. In addition to the chemical work in this thesis, the automation of the chirped-pulse method is described.

Orthogonal to both the cavity and the chirped-pulse methods is the molecular source in which samples are either pulsed through a nozzle or injected via a hypodermic needle directed along the flow axis of the expansion through the nozzle orifice. The two methods of sample introduction can be used simultaneously which allows for on-the-fly mixing of reactive samples prior to supersonic expansion into the vacuum system.

For my dissertation, I have first used microwave spectroscopy coupled with computational chemistry to study molecules on the brink of chemical change. Second, I have developed several programs that have automated the collection, averaging, and analysis of rotational spectra.

In 2015, a novel product of the reaction between a carboxylic acid and sulfur trioxide was observed to form in a supersonic expansion in the Leopold Lab.[17] These products were named carboxylic sulfuric anhydrides (CSAs) because their hydrolysis would result in the formation of sulfuric acid and a carboxylic acid. After initial discovery with formic acid,[17] a series of CSAs formed from various carboxylic acids (RCOOH, CH_3,[18] CF_3,[19] CH_2=CH,[20] and HCC[21]) were subsequently studied showing that the reaction was generalizable and had overall low barriers to reaction. Additionally, the reactivity of acetic sulfuric anhydride (ASA) with water at the molecular level was studied through the observation of the ASA-H_2O complex.[22]

The study of CSAs has prompted the investigation of a series of compounds with similar structure and promising prereactive behavior, carboxylic anhydrides, which are the foci of Chapters 1, 2, and 3. The molecules studied include trifluoroacetic,[23] pivalic,[24] and acetic anhydrides as well as the mixed pivalic trifluoroacetic, benzoic trifluoroacetic, acetic trifluoroacetic, acetic pivalic, and acetic difluoroacetic anhydrides. Subjects of study throughout these chapters include conformational analysis, structural determination, and internal rotation. Of particular note in Chapter 3, the case of acetic anhydride's double methyl rotor spectrum is fit and analyzed despite significant spectral complexity.

Chapter 2 additionally describes the development, functionality, and success of the Data Analysis Package for Productive and Enthusiastic Rotational Spectroscopists (DAPPERS).[24] Over the past decade, observed rotational spectra have become increasingly dense and difficult to assign manually prompting the genesis of automated assignment programs. While DAPPERS is not the first of these programs, it does offer a uniquely fast and accurate assignment algorithm. The spectral density and variety of carboxylic anhydrides proved to be perfect test cases for DAPPERS' automated spectral

assignment algorithm. DAPPERS was also used to assign spectra donated graciously by other rotational spectroscopy labs internationally to aid in development and showcase the robust capabilities of the spectral assignment software.

Chapter 4 explores the microsolvation of the trifluoroacetic, pivalic, and pivalic trifluoroacetic anhydrides through the analysis of their monohydrates. In general, microsolvation studies analyze the stepwise addition of water molecules to a chemical substrate which can in turn provide useful information about reactivity as it scales to the bulk phase. As previously mentioned, ASA was observed to complex with one molecule of water in which ASA behaved as a hydrogen bond donor.[22] The carboxylic anhydrides in this study do not feature the acidic hydrogens of CSAs and therefore must interact with water by behaving either as a hydrogen bond acceptor or an electrophile. This study describes the impact of R group electronic character on the microsolvation of carboxylic anhydrides by a single water molecule.

In Chapter 5, focus is returned to CSAs centering on pivalic sulfuric anhydride. As previously mentioned, the barriers to CSA formation through the reaction of a carboxylic acid and sulfur trioxide are generally low with the exception of trifluoroacetic sulfuric anhydride (TFASA).[19] During the reaction, the highly electron withdrawing and relatively massive CF_3 group must rotate 60 degrees in addition to reaching the pericyclic transition state common to all CSAs. A comparison to ASA,[18] which features a similar rotation of the electron donating and lightweight CH_3 group, does not distinguish whether the higher barrier of TFASA is due to the CF_3 group's mass or to its electron withdrawing character. Pivalic acid was chosen because it is both electron donating like the CH_3 group of ASA and has a comparable mass to the CF_3 rotor of TFASA. In this chapter, the impact of R group of RCOOH on the energetics of this generalized reaction is additionally analyzed with computational methods.

Departing from anhydrides, Chapter 6 details the observation of trimethylammonium triflate as the result of separate injection of trimethylamine (TMA) and the superacid trifluoromethanesulfonic acid (triflic acid).[25] In a similar vein to the microsolvation studies

of Chapter 4, proton transfer is a ubiquitous process that readily occurs in the bulk phase but is actually rare in small molecular complexes. Previous work from our lab on the nitric acid–TMA complex utilized the quadrupolar ^{14}N nuclei of the nitric acid and TMA nitrogen atoms to probe the degree of proton transfer with the result that only partial proton transfer occurs.[26] Recent work in our lab examined the microsolvation of triflic acid which demonstrated that three water molecules were necessary for proton transfer to occur in the gas phase for even this superacid.[27] This work showcases full proton transfer between triflic acid and one molecule of TMA to form a gas phase ion pair as evidenced by the experimentally determined nuclear quadrupole coupling constants of the nitrogen atom and further supported by computational analysis.

Finally, Chapter 7 describes the "Chirp-o-matic" and "Data Averager" which were developed to automate the measurement and processing of chirped-pulse spectra. The implementation of these programs greatly simplified the data collection and averaging processes and have become tools used daily in the Leopold lab.

Chapter 1: A Microwave and Computational Study of Trifluoroacetic Anhydride

Adapted with permission from Nathan Love, C.J. Smith, Anna K. Huff and K. R. Leopold. *J. Mol. Spectrosc.* **2019**, *365*, pp. 111210-1-4.

Overview

The microwave spectrum of trifluoroacetic anhydride ($CF_3COOCOCF_3$) has been recorded by chirped-pulse and cavity Fourier transform microwave spectroscopy. A dense *b*-type spectrum containing several P, Q, and R branch progressions has been assigned and fit to the Watson A-reduced asymmetric rotor Hamiltonian. No evidence of tunneling or internal rotation of the CF_3 groups was observed. DFT calculations of the rotational constants are in good agreement with experimental results.

Introduction

Recently, our laboratory has become interested in the chemistry and spectroscopy of acid anhydrides. To date, this has involved microwave and computational studies characterizing the mixed anhydrides derived from sulfuric acid and a series of carboxylic acids, $RCOOSO_2OH$ (R = H[1], CH_3[2], CF_3[3], CH_2=CH[4], and HCC[5]). Interest in these molecules stems from their potential role in the nucleation of atmospheric aerosol and the possibility that their hydrolysis may influence aerosol composition. With this latter feature in mind, we recently investigated the water complex of acetic sulfuric anhydride, viz., $CH_3COOSO_2OH–H_2O$.[6]

Carboxylic sulfuric anhydrides are relatively unknown in the chemical literature, but carboxylic acid anhydrides, i.e., those derived from the condensation of two carboxylic acids, are much more familiar. Several have been the subject of detailed microwave work.[7-15] In light of our interest in hydrolysis, we have recently recorded the spectrum of the water complex of trifluoroacetic anhydride ($CF_3COOCOCF_3$, TFAA). As a first step toward assigning the rather complex spectrum observed, we have also recorded and assigned that of the TFAA monomer. That spectrum, and a series of supporting DFT calculations, are the subject of this note.

Experimental and Theoretical Methods and Results

Spectra were initially observed using a chirped-pulse Fourier transform microwave spectrometer, whose construction has been described elsewhere.[16] A mixture of 0.5% TFAA in argon was expanded through a 1.25 in. x 0.0085 in. 3D-printed rectangular slit nozzle[16] at a stagnation pressure of 1.3 atm and chirped-pulse spectra were taken in 3 GHz segments between 6 and 18 GHz. Transition frequencies were typically measured with an accuracy of ~10 kHz. A relatively dense *b*-type spectrum was observed, featuring well over 250 transitions from the R and Q branches alone. The $J'_{1,J'} \leftarrow J''_{0,J''}$ and $J'_{0,J'} \leftarrow J''_{1,J''}$ progressions were quickly assigned with J'' ranging from 6 to 21 and 8 to 20 respectively, yielding a fit highly predictive of the remaining TFAA transitions. Approximately half of the transitions measured belonged to various Q branch progressions, one of which is shown in Figure 1.1.

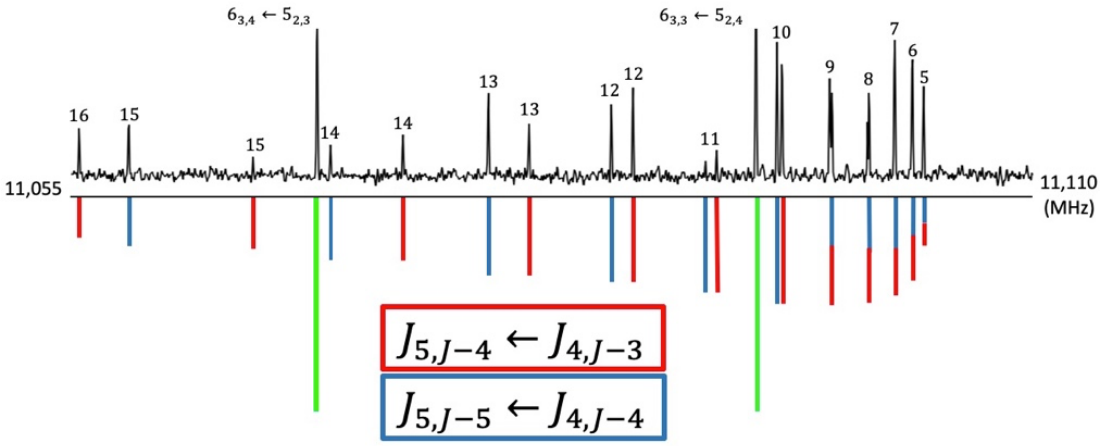

Figure 1.1 Excerpt of the TFAA Rotational Spectrum

A portion of the chirped-pulse microwave spectrum of trifluoroacetic anhydride showing the K_a''= 4 Q branch series from J = 5 to 16. This spectrum represents the average of 100,000 free induction decay signals, each with a data collection time of 20 μs. The top trace is the experimental spectrum and the bottom trace depicts the predictions from the fitted spectrum using an estimated temperature of 2 K. Transitions shown in red are $J_{5,J-4} \leftarrow J_{4,J-3}$. Transitions shown in blue are $J_{5,J-5} \leftarrow J_{4,J-4}$. The transitions shown in green are intervening R branch lines.

The top trace is the experimental spectrum and the bottom trace is the calculated spectrum using the fitted constants and an estimated temperature of 2 K. Note that while the nozzle temperature is not known, the calculated relative intensities are reasonably commensurate with experimental observation.

Several pairs of transitions involving high K_a values were unresolved in the chirped-pulse spectrum and were subsequently recorded using the cavity spectrometer, which provided a typical accuracy of ~4 kHz. An example is shown in Figure 1.2. In addition to resolving closely spaced pairs of transitions in the R and Q branches, the cavity spectrometer was used to measure several progressions of P branch transitions between 4.5 and 7.1 GHz. A final fit of 297 transitions (261 distinct frequencies) was obtained using the SPFIT program of Pickett[17] and the resulting spectroscopic constants are given in Table 1.1. Observed frequencies, assignments, and residuals from the least squares fit are provided as Appendix A. Overall, the majority of the residuals were smaller than the estimated uncertainties, indicating the suitability of the Hamiltonian used to treat the spectrum. The vast majority

of observed lines in the chirped-pulse spectrum were assigned, with only 30 lines in the spectrum remaining unassigned, and no attempt was made to pursue the acquisition of spectra arising from any of the ^{13}C isotopologues.

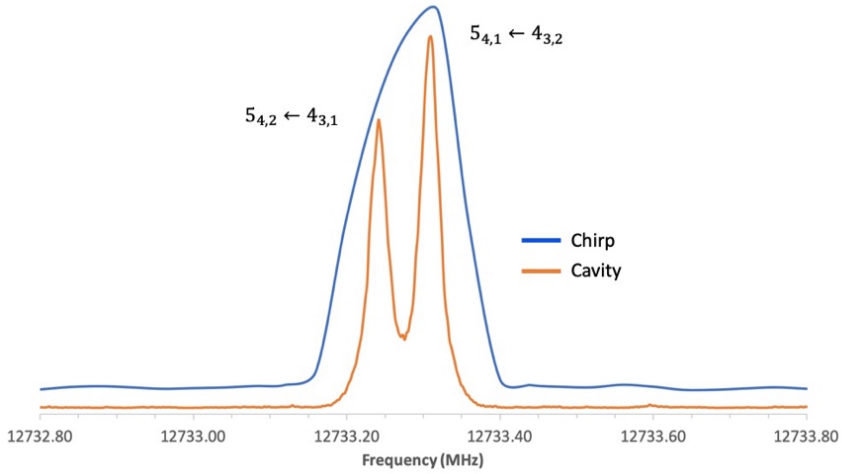

Figure 1.2 A Comparison of TFAA Chirp and Cavity Spectra

The $5_{42} \leftarrow 4_{31}$ and $5_{41} \leftarrow 4_{32}$ transitions of trifluoroacetic anhydride, overlapped in the chirped-pulse spectrum and resolved on the cavity spectrometer. The predicted splitting is 66 kHz, and the observed splitting is 68 kHz. The cavity and chirped-pulse spectra represent the average of 2,800 and 100,000 free induction decay signals respectively.

Table 1.1 Spectroscopic Constants of Trifluoroacetic Anhydride

	Experimental	Calculated[a]
A (MHz)	1643.510188(42)	1651
B (MHz)	426.630935(39)	431
C (MHz)	392.365649(43)	395
Δ_J (kHz)	0.013121(77)	
Δ_{JK} (kHz)	0.09423(16)	
Δ_K (kHz)	0.1402(13)	
δ_J (Hz)	–2.644(45)	
$P_{aa}{}^c$	1082.556237(89)	1073
$P_{bb}{}^c$	205.474643(89)	206
$P_{cc}{}^c$	102.025168(89)	99.6
N	297 (261)[b]	
RMS (kHz)	5.2	

(a) Obtained from M06-2X/6-311++G(3df) calculations.
(b) Number of transitions in fit. The number in parenthesis denotes the number of distinct frequencies.
(c) Calculated from the fitted rotational constants.

In addition to the experimental work, calculations to determine the minimum energy structure of TFAA were performed at the M06-2X/6-311++G(3df) level of theory using the Gaussian09 suite of programs.[18] The optimized geometry is shown in Figure 1.3 and Cartesian coordinates are provided in Appendix A. The calculated rotational constants are included in Table 1.1. The two carbonyl groups are not coplanar at the minimum energy configuration, but instead form an O-C-C-O dihedral angle of 34 deg. When the two carbonyl groups are constrained to the same plane, with all other structural parameters allowed to relax, the resulting energy is 0.3 kcal/mol higher than that at the minimum energy structure. The barrier for the internal rotation of a single CF_3 group, V_3, was calculated by rotating the CF_3 60 deg from its minimum energy orientation and optimizing the resulting transition state geometry. The resulting value was determined to be 1.3 kcal/mol. Similar calculations involving simultaneous rotation of both CF_3 rotors gave a barrier of 2.6 kcal/mol (exactly twice the single-rotor value), as expected since the two rotors are equivalent and quite spatially separated. The calculated dipole moment is 1.2 D and lies entirely along the *b*-inertial axis, consistent with the observation of a purely *b*-type spectrum.

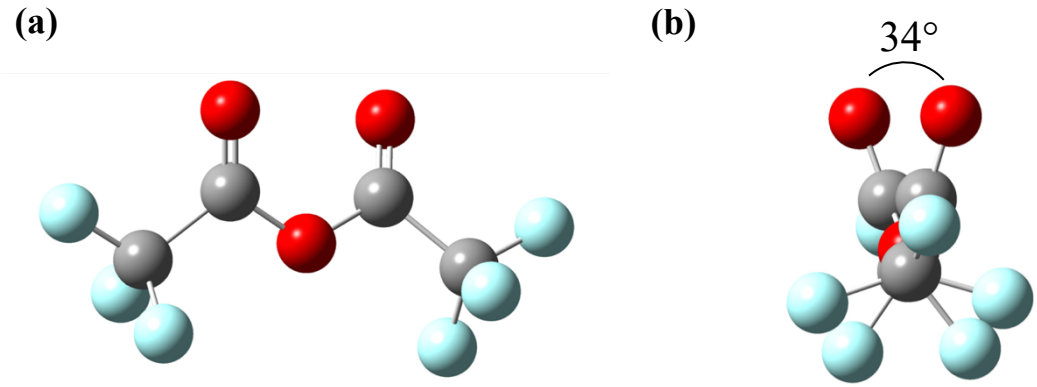

Figure 1.3 Computational Structure of TFAA
The structure of trifluoroacetic anhydride, calculated using the M06-2X/6-311++G(3df) level/basis set. (a) Side view. (b) End-on view emphasizing the dihedral angle between the two carbonyl groups.

Discussion

As seen in Table 1.1, the rotational constants and planar moments calculated at the M06-2X/6-311++G(3df) level of theory are in reasonable agreement with experiment. Because the two carbonyl groups are not coplanar, there is a double minimum potential with a 0.3 kcal/mol barrier through which the system can pass via a twisting motion. While such a potential, in principle, gives rise to a pair of tunneling states, no evidence of a second state was observed in this work. Transitions across the tunneling doublet would not be allowed because they do not invert μ_b and thus, the only manifestation of a second state would be the observation of a second *b*-type spectrum. The absence of such a spectrum suggests that either tunneling through the barrier does not occur (the effective barrier is high), that the excited tunneling state is too high in energy to be populated in the supersonic jet (the effective barrier is low), or that its vibrationally averaged rotational constants of the ground and excited tunneling states are so similar that the two states cannot be distinguished at the experimental resolution. While it is not possible to rigorously establish which of these scenarios is correct, the necessity of moving numerous heavy atoms through a finite barrier suggests that the tunneling frequency is very low and that tunneling is not a prominent feature of this system.

Chemical intuition would suggest that the existence of a barrier in the planar configuration arises from repulsion between the carbonyl oxygens. The 34 deg dihedral angle between the two carbonyl groups is similar to the analogous angle in acetic anhydride, which has a value of 47 deg calculated from the atomic coordinates given in the Supporting Information of a recent gas phase electron diffraction study.[19] Interestingly, a microwave study of formic acetic anhydride has established that the carbonyl groups are coplanar, but are *anti* to one another in the gas phase.[10] It seems reasonable that such a configuration is not particularly favorable in trifluoroacetic anhydride, as significant repulsions between the fluorines and the carbonyl oxygens would be expected to occur.

Also absent from the observed spectrum are any signatures of internal rotation of the CF_3 group. This is not surprising in light of the reduced barrier for CF_3 internal rotation. Using the barrier of V_3 determined above and the calculated moment of inertia of the CF_3 about

its pseudo-C_3 axis, the reduced barrier, $s = 4V_3/9F$, has a value over 800 (where F is the inverse reduced moment of inertia of the rotor).[20] Thus, the system is well in the high barrier limit. This is quite reasonable, as no evidence of internal rotation was observed in trifluoroacetic sulfuric anhydride (CF_3COOSO_2OH)[3] or in the ground vibrational state of trifluoroacetic acid itself.[21]

Conclusion

The microwave spectrum of trifluoroacetic anhydride has been observed and is in good agreement with predictions from density functional theory. A dense *b*-type spectrum is readily fit to a Watson A-reduced Hamiltonian with no evidence of CF_3 internal rotation or the presence of a second tunneling state. This study provides a useful baseline for future investigations of molecular complexes containing the anhydride.

Acknowledgement

This work was supported by the National Science Foundation (Grant No. CHE 1563324) and the Minnesota Supercomputing Institute.

Chapter 2: A New Program for the Assignment and Fitting of Dense Rotational Spectra based on Spectral Progressions: Application to the Microwave Spectrum of Pivalic Anhydride

Adapted with permission from Nathan Love, Anna K. Huff and K. R. Leopold. *J. Mol. Spectrosc.* **2020**, *370*, pp. 111294.

Overview

A new computerized package for the rapid processing and analysis of dense rotational spectra is described. The package is based on the automated identification of user-specified spectral progressions and interacts with the operator through a simple graphical user interface. In addition to containing an algorithm for obtaining spectral assignments, the package includes a peak-finder with adjustable baseline drift compensation, seamless interfacing with Pickett's SPFIT and SPCAT programs, and a number of visualization features. The utility of the program is illustrated through its application to the analysis of new spectra of pivalic anhydride, $(CH_3)_3CCOOCOC(CH_3)_3$. Spectra of the parent, as well as all isotopologues with single heavy-atom substitution, are reported, as are calculations for the parent species at the M06-2X/6-311++G(3df,3pd) level of theory. The central oxygen atom is poorly located due to its proximity to the center of mass of the molecule, but a Kraitchman analysis of the fitted rotational constants otherwise provides a detailed structural characterization of the heavy-atom frame. The two carbonyl groups are not coplanar, but rather form a dihedral angle of 53.9(39) deg.

Introduction

In recent years, technological advances in the acquisition of molecular rotational spectra have led to a dramatic increase in the size and complexity of species that can be studied.[1,2] The concomitant complexity of the resulting spectra is often compounded by factors such as multi-component samples, the presence of more than one molecular conformation, the occurrence of naturally abundant isotopologues, and the population of excited vibrational states. Thus, spectra may contain tens of thousands of transitions, and it has become increasingly unfeasible to generate spectral assignments by hand. Automated algorithms that aid in the assigning and fitting of such spectra have been developed over a period of many years[3-11] with powerful programs such as Autofit,[12] PGOPHER,[13] JB95,[14] the AABS package,[15] and SPFIT/SPCAT[16] emerging as some of the most important and widely used tools today. Many additional programs exist, however, and can be found on the Programs for ROtational SPEctroscopy website (http://www.ifpan.edu.pl/~kisiel/prospe.htm).

Dense spectra of large molecules typically feature large ranges of *J* quantum numbers. Accordingly, spectra can be logically organized into progressions of distinct transition types, as discussed in detail by Cooke and Ohring.[17] Complex spectra, which result from the overlay of multiple progressions, can then be readily understood in terms of these simple sequences. This paper describes a new program, "DAPPERS" (Data Analysis Package for Productive and Enthusiastic Rotational Spectroscopists), which features a dynamic fit searching algorithm that intelligently assigns spectral progressions embedded in even the most dense spectra with extremely rapid runtimes (a few seconds). The algorithm accurately identifies members of a series and then fits them together as a single progression or ultimately combines them in a single fit with other identified progressions or individual transitions. All fits are done using a built-in wrapper interface for Pickett's SPFIT program. DAPPERS also features a number of spectral processing tools, such as a graphical peak finder with adjustable baseline compensation, that can greatly aid in the assignment and fitting of rotational spectra.

In addition to describing the basic features of DAPPERS, this paper illustrates its applicability to new spectra of a moderately large molecule, pivalic anhydride, shown below.

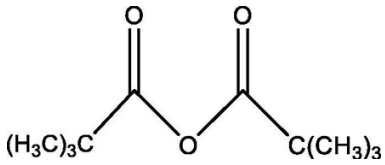

Our laboratory has recently become interested in acid anhydrides, initially in the form of carboxylic sulfuric anhydrides ($RCOOSO_2OH$),[18] with the eventual goal of studying their water complexes as hydrolysis precursor complexes. One such complex, $CH_3COOSO_2OH–H_2O$,[19] has already been studied. Recently, however, this interest has been extended to more familiar analogues derived from the condensation of two carboxylic acids i.e., species of the form RCOOCOR′. Trifluoroacetic anhydride (TFAA), the first of these carboxylic analogues investigated in our laboratory, featured a relatively dense *b*-type spectrum with the presence of several spectral progressions.[20] Pivalic anhydride was chosen as the example for DAPPERS because it was predicted to also have a dense spectrum with multiple superimposed sequences. Although it does not exhibit complicating features such as internal rotation, hyperfine structure, Coriolis coupling, or multiple conformers, the spectrum consists of multiple progressions that are so intertwined as to render them difficult to identify by visual inspection. We take this as the operational definition of a "dense" spectrum for which an autofitting routine has value. Moreover, beyond its role as a test case for DAPPERS, pivalic anhydride extends the study of acid anhydrides by replacing the small, electron withdrawing fluorines of TFAA with bulky, electron releasing methyl groups, thus allowing an exploration of steric and electronic effects on structure (and ultimately complexation).

Methods and Results

The 6–18 GHz chirped-pulse spectrum of pivalic anhydride was measured in 3 GHz segments with the tandem chirped-pulse and cavity spectrometer which has been described elsewhere.[21,22] Pivalic anhydride, obtained from Sigma Aldrich, was introduced into the system by flowing argon over a ~1 ml sample in a reservoir located a short distance from

the pulsed nozzle. The reservoir was heated to 60 °C and the resulting pivalic anhydride-argon mixture was injected through a 0.020 in I.D. (inner diameter) needle along the axis of a cone nozzle as described previously.[23] The pressure behind the hypodermic needle was 0.4 atm and the stagnation pressure (behind the nozzle) was 1.3 atm. A 30 MHz segment of the observed spectrum is shown in Figure 2.1.

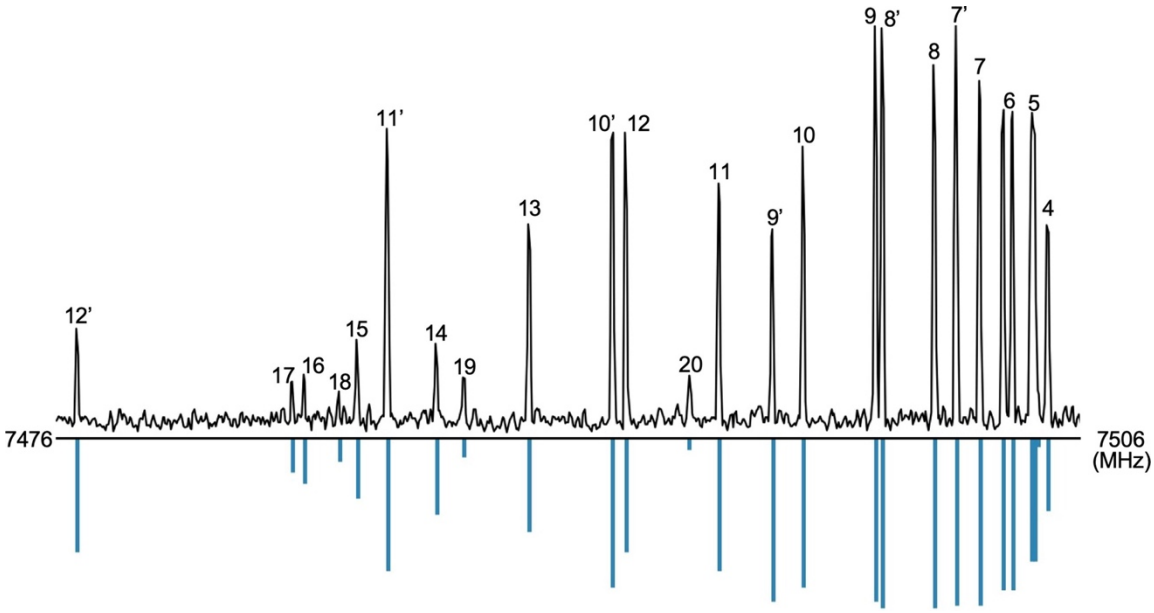

Figure 2.1 Excerpt of the PiA Rotational Spectrum

A 30 MHz wide segment of the chirped-pulse spectrum of pivalic anhydride. This spectrum represents the Fourier transform of the average of 60,000 free induction decay signals and includes two Q branch progressions with $K_p = 4 \leftarrow 3$. The two progressions converge in frequency as J decreases. The J value for each transition is labeled at the top of the corresponding peak and primes are used to differentiate transitions from the two progressions. Transitions with $J = 4$, 5, and 6 are not differentiated due to their small splitting. The stick spectrum on the bottom shows the frequencies predicted with the fitted spectroscopic constants.

Frequencies from the chirped-pulse spectrum were measured with a typical uncertainty of ~12 kHz. As described in more detail below, DAPPERS was then used to assign and fit 255 *b*-type Q and R branch transitions with a root mean square residual of 3.5 kHz in under four minutes. Several sets of unresolved transitions in the chirped-pulse spectrum were purposefully not included at this stage and were subsequently re-measured and resolved on the cavity spectrometer before being added to the final fit. For these measurements, the typical accuracy was 1–2 kHz. Six transitions with frequencies greater than 18 GHz were also observed and measured as sidebands on the chirped-pulse system. The final set of 273

assigned transitions (226 distinct frequencies) was fit to a Watson A-reduced Hamiltonian in the I^r representation using Pickett's SPFIT program,[16] again as implemented through its interface with DAPPERS. The rms residual was 4.0 kHz and the resulting spectroscopic constants are given in Table 2.1.

Table 2.1 Spectroscopic Constants of Pivalic Anhydride

	Parent	**^{13}C6/^{13}C19**	**^{13}C15/^{13}C28**	**^{13}C1/^{13}C4**
***A* [MHz]**	1517.933464(96)	1517.59351(38)	1505.57981(31)	1516.44983(29)
***B* [MHz]**	456.765702(84)	454.42014(13)	453.31905(36)	456.19730(11)
***C* [MHz]**	434.61336(10)	432.46261(12)	432.39949(21)	434.05910(11)
Δ_J **[kHz]**	0.01240(17)	0.01328(74)	0.0125(19)	0.01190(77)
Δ_{JK} **[kHz]**	0.23806(84)	0.2330(88)	0.2415(51)	0.2413(71)
Δ_K **[kHz]**	-0.1149(29)	-0.104(13)	-0.140(15)	-0.139(11)
δ_J **[kHz]**	-0.000202(92)	-	-	-
δ_K **[kHz]**	0.057(22)	-	-	-
***N*[a]**	273 (226)	30 (25)	23 (22)	22 (21)
σ **[kHz]**	4.0	3.2	1.9	1.8

	^{13}C7/^{13}C20	**^{13}C11/^{13}C24**	**^{18}O2/^{18}O5**	**^{18}O3**
***A* [MHz]**	1516.11388(48)	1503.80983(41)	1490.29342(66)	1517.32316(89)
***B* [MHz]**	451.34081(20)	454.36876(39)	455.170(40)	457.20(12)
***C* [MHz]**	429.68338(33)	431.46526(33)	431.938(43)	434.15(12)
Δ_J **[kHz]**	0.0132(17)	0.0093(35)	-	-
Δ_{JK} **[kHz]**	0.229(13)	0.2296(64)	0.286(30)	-
Δ_K **[kHz]**	-0.114(18)	-0.157(14)	-0.153(41)	-
δ_J **[kHz]**	-	-	-	-
δ_K **[kHz]**	-	-	-	-
***N*[a]**	20 (19)	19 (18)	16 (10)	6 (5)
σ **[kHz]**	1.6	2.1	1.7	3.1

(a) Number in parentheses denotes the number of distinct frequencies in a fit

A listing of fitted transitions, assignments, and residuals appears in Appendix A and a sample spectrum showing the $5_{4,2} \leftarrow 4_{3,1}$ and $5_{4,1} \leftarrow 4_{3,2}$ transitions, as resolved on the cavity spectrometer, is shown in Figure 2.2.

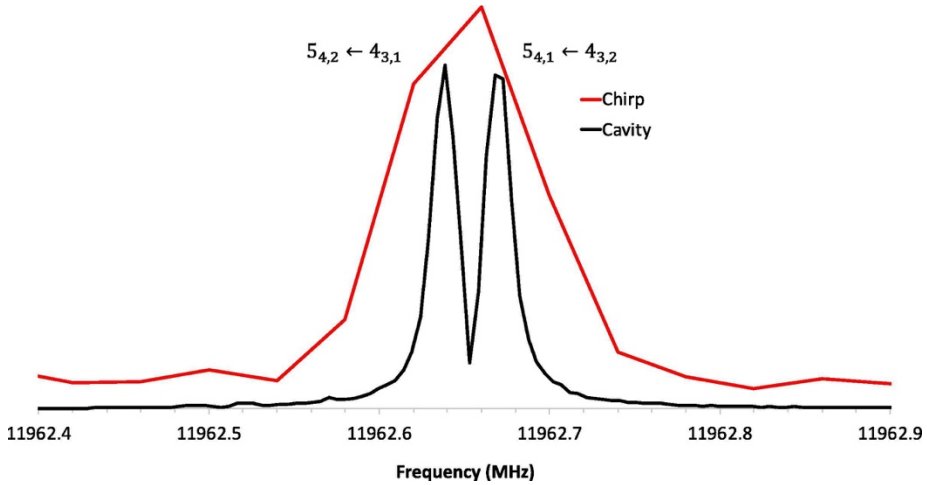

Figure 2.2 A Comparison of PiA Chirp and Cavity Spectra

Bottom trace shows the $5_{4,2} \leftarrow 4_{3,1}$ and $5_{4,1} \leftarrow 4_{3,2}$ transitions of the parent form of pivalic anhydride, as observed on the cavity spectrometer. This spectrum represents the average of 24,000 free induction decays. The calculated splitting is 24 kHz and the observed splitting is 22 kHz. The top trace shows the same pair of transitions as observed on the chirped-pulse system.

Due to the C_2 symmetry of the molecule, there are five singly-substituted ^{13}C isotopologues, and two singly-substituted ^{18}O isotopologues. Rotational constants were predicted for each species using the results of the parent fit, and spectra were readily located in natural abundance on the cavity spectrometer. (A few ^{13}C peaks resulting from pairs of unresolved transitions were observed on the chirped-pulse system as well.) Due to the equivalence of pairs of atoms on both sides of the bridging oxygen, spectra from all isotopologues, except those from that bridging oxygen, were observed at approximately twice the expected intensity based on relative isotope abundances. The scope of the data sets for the isotopically substituted species was, in each case, insufficient to determine all of the quartic centrifugal distortion constants and thus, when necessary, these values were constrained to those determined for the parent species. Transition frequencies, assignments, and residuals for all isotopologues studied are also given in the Appendix B, and the fitted spectroscopic constants are included in Table 2.1.

The minimum energy structure of pivalic anhydride was obtained at the M06-2X/6-311++G(3df,3pd) level of theory using the Gaussian16 suite[24] of programs. The optimized geometry is shown in Figure 2.3 and calculated structural parameters are summarized in Table 2.2.

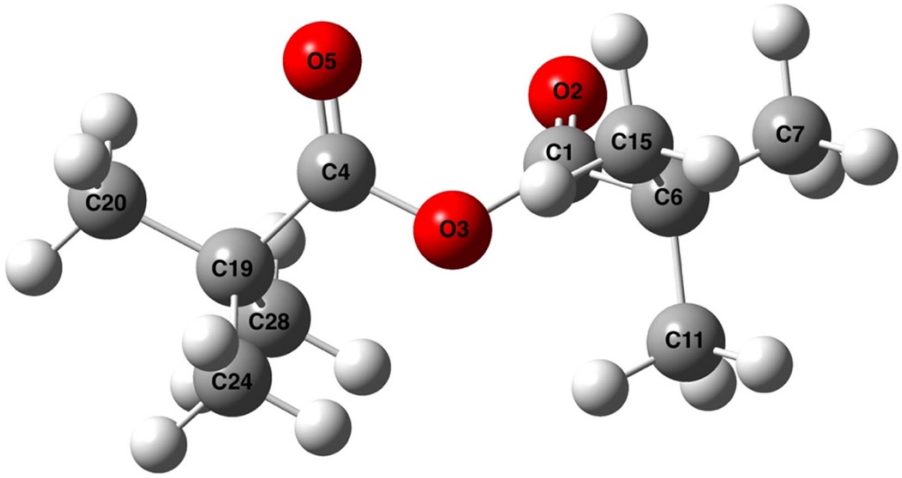

Figure 2.3 Computational Structure of PiA

The structure of pivalic anhydride calculated at the M06-2X/6-311++G(3df,3pd) level/basis. Note that the *b*-axis is the C_2 symmetry axis.

Table 2.2 Structural Parameters for PiA[a]

Bond Lengths [Å]	M06-2X/ 6-311++G(3df,3dp)	Experimental
C1-C4	2.38469	2.3507(26)
C1-O2 and C4-O5	1.18739	1.20(15)
C1-C6 and C4-C19	1.51561	1.509(11)
C6-C7 and C19-C20	1.52467	1.513(13)
C6-C11 and C19-C24	1.53291	1.530(16)
C6-C15 and C19-C28	1.53521	1.587(42)
Bond Angles [°]		
O2-C1-C6 and O5-C4-C19	126.84045	124.0(42)
C1-C6-C7 and C4-C19-C20	108.69499	111.5(14)
C1-C6-C11 and C4-C19-C24	109.73163	110.8(15)
C1-C6-C15 and C4-C19-C28	107.33107	106.3(32)
C7-C6-C11 and C20-C19-C24	110.58700	111.6(16)
C7-C6-C15 and C20-C19-C28	110.48638	108.9(33)
C11-C6-C15 and C24-C19-C28	109.94094	107.4(33)
Dihedral Angles [°]		
O2-C1-C4-O5	59.47312	53(38)
O2-C1-C6-C7 and O5-C4-C19-C20	5.17758	2.28(24)
O2-C1-C6-C11 and O5-C4-C19-C24	126.22455	127(10)
O2-C1-C6-C15 and O5-C4-C19-C28	114.33716	116(11)

(a) Atom numberings refer to Figure 2.3.

(b) The C1···C4 distance does not correspond to the length of a bond but is quoted here because the C1-O3-C4 angle and the C1-O3 and O3-C4 bond lengths are not determined.

The structure is similar to that predicted for trifluoroacetic anhydride,[20] with a C_2 axis of symmetry and non-coplanar arrangement of the carbonyl groups. However, the 59 deg O2-C1-C4-O5 dihedral angle calculated at this level of theory is 25 deg larger than that in the trifluoroacetic analog at the same level of theory. In principle, the resulting double well potential associated with a scissoring motion of the two C=O groups gives rise to a pair of tunneling states. However, the calculated barrier, obtained by re-optimizing the geometry with the dihedral angle constrained to zero, has a rather large value of 1.7 kcal/mol. Indeed, no second state was observed and, as mentioned previously, the observed spectrum was adequately fit to a semi-rigid rotor Hamiltonian. The predicted rotational constants for the parent isotopologue, *A*, *B*, and *C*, are 1537, 459, and 438 MHz respectively, and agree with their experimentally determined values to within 1.3%, 0.5%, and 0.8%, respectively. The predicted dipole moment is 3.6 D and lies entirely along the *b*-inertial axis, consistent with the observation of only *b*-type rotational transitions. Cartesian coordinates for the predicted structure are provided in Appendix B.

Structure Analysis

With isotopic substitution on each of the heavy atoms of the molecule, Kraitchman's equations[25] can be used to determine the structure of the heavy atom frame. The analysis was implemented using Kisiel's KRA program[26] and the resulting atomic coordinates are given in Table 2.3. The signs of the coordinates are not determined experimentally but have been inferred based on the theoretical structure. Quoted uncertainties include the Costain correction, as described in the KRA documentation. Note that O3 is excluded from this tabulation as, in the theoretical structure, it lies within 0.25 Å of the center of mass of the molecule, rendering the Kraitchman analysis unreliable. Indeed, the bond distance between either carbonyl carbon and the bridging oxygen was calculated to be 1.78 Å with Kraitchman's equations, quite different from the more realistic value of 1.38 Å predicted by theory. A comparison of the experimentally determined structural parameters and those predicted by M06-2X/6-311++G(3df,3pd) theory is included in Table 2.2. As indicated in the table, bond lengths and bond angles are duplicated on two sides of the molecule due to symmetry.

Table 2.3 Experimental Coordinates for PiA

	X [Å]	Y [Å]	Z [Å]
C1	1.1273(13)	0.4652(32)	-0.3325(45)
O2	1.108(17)	1.530(12)	-0.884(23)
C4	-1.1273(13)	0.4652(32)	0.3325(45)
O5	-1.108(17)	1.530(12)	0.884(23)
C6	-2.39181(63)	-0.2720(55)	0.036(42)
C7	3.62498(42)	0.4741(32)	-0.4269(35)
C11	2.36345(65)	-1.70342(90)	-0.5042(31)
C15	2.41031(63)	-0.3627(42)	1.62022(94)
C19	-2.39181(63)	-0.2720(55)	-0.036(42)
C20	-3.62498(42)	0.4741(32)	0.4269(35)
C24	-2.36345(65)	-1.70342(90)	0.5042(31)
C28	-2.41031(63)	-0.3627(42)	-1.62022(94)

(a) Atom numbering refers to Figure 2.3
(b) The Kraitchman analysis gives only the absolute values of the coordinates. Signs have been inferred based on the computed structure (Figure 2.3).

The DAPPERS Package

As noted above, chirped-pulse spectral data were processed using the DAPPERS package. The package is coded in LabVIEW, but has been complied into an executable file, therefore eliminating the need to have LabVIEW installed by the user. A single installer for the DAPPERS package, as well as extensive documentation, test files, and installation instructions, can be downloaded at www.chem.umn.edu/groups/kleopold. The program features an intuitive and dynamic graphical user interface that requires no prior programming experience and automatically formats and executes Pickett SPFIT and SPCAT files. This section outlines some of the basic features of the package.

Graphical Peak Finder: Peak finding programs are widely used to identify and catalogue transitions in a raw spectral file that have intensities greater than a user selected threshold. While many programs utilize a global threshold for this purpose, spectra with drifting baselines are better served by more refined methods. One solution is to apply a baseline correction to the spectrum, but this involves the modification of raw experimental data. DAPPERS handles the problem by allowing the calculation of *local* thresholds within a

user-defined window. For example, for a 50 MHz window, a separate baseline value is calculated for every 50 MHz segment of the spectrum. The windows can be as small as 1 MHz or as large as the entire spectrum. The local thresholds determined within each windowed segment are then stitched together to form a piece-wise threshold function that can be uniformly raised or lowered to a user selected intensity level. A traditional, global threshold (without calculation of a baseline value) is also available.

The Algorithm: The core feature of the package is the algorithm that intelligently identifies experimental spectral progressions with user-specified quantum number identities. Examples of these "quantum filtered" series would be the *a*-type R branch progression $2_{0,2} \leftarrow 1_{0,1}$, $3_{0,3} \leftarrow 2_{0,2}$, etc., or the *b*-type Q branch progression $10_{4,6} \leftarrow 10_{3,7}$, $11_{4,7} \leftarrow 11_{3,8}$, etc. The identification is based on the relationships between different transitions from a corresponding progression in a predicted spectrum. (Using the industry standard of Pickett's SPCAT program, this would be a .cat file.) The searching algorithm selects experimental frequencies that may belong to a given spectral progression, starting with the lowest (user specified) *J*, and then applies successively refined criteria to identify additional members of the series. The criteria are summarized in Table 2.4.

Table 2.4 The Three Tests Used to Identify Spectral Progressions

Test	When is it applied?	Equation[a]
Starter Test	When searching for the first transition in a fit.	$\nu_1^{guess} = \nu_1^{pred}$
Ratio Test	When searching for the second transition in a fit.	$\nu_2^{guess} = \nu_1^{Obs}\left[\frac{\nu_2^{Pred}}{\nu_1^{Pred}}\right]$
Derivative Ratio Test	When searching for the N^{th} transition in a fit ($N > 2$)	$\nu_N^{guess} = \left(\nu_{N-1}^{Obs} - \nu_{N-2}^{Obs}\right)\left[\frac{\nu_N^{Pred} - \nu_{N-1}^{Pred}}{\nu_{N-1}^{Pred} - \nu_{N-2}^{Pred}}\right] + \nu_{N-1}^{Obs}$

(a) ν^{Pred} is determined from estimated constants, e.g., from a .cat file produced by SPCAT.

The first test (the starter test) provides initial assignments, and utilizes a "starter window", which represents the maximum anticipated discrepancy between the observed and predicted frequencies for the lowest *J* member of the series. Depending on a number of factors including molecular size, prediction accuracy, and experimental frequency range,

reasonable starter window values can range from 10 to 10,000 MHz. Fortunately, larger starter windows do not drastically affect the efficiency of the algorithm (within reason). This means that, although well-predicted rotational constants are helpful, one does not necessarily need highly accurate information about the molecule in order to assign its spectrum.

Once candidates for the lowest J member of the series are identified, a "ratio test" is applied. This test identifies experimental transitions that may be candidates for the next member of the series, based on their predicted ratio as determined in the .cat file (within a generally smaller window). Finally, the "derivative ratio test" utilizes ratios of the predicted and observed differences between previous members of the series (rather than the frequencies themselves) to select candidates for the next member of the series.

Experimental peaks are only assigned if their frequencies lie within the appropriate user-specified windows. With dense spectra and liberal window sizes, more than one set of transitions may initially be identified as belonging to a particular quantum filtered progression. However, once fit individually, these may be combined with other quantum filtered progressions and fit simultaneously using Pickett's SPFIT program to test their compatibility. Once a good fit is obtained, the spectrum can be further scoured to locate, assign, and fit transitions that were not contained in the spectral progressions. DAPPERS seamlessly integrates with Pickett's programs at each stage of the process, allowing properly formatted input files to be created via an easy-to-use graphical user interface.

For pivalic anhydride, three distinct R branch progressions involving $K_p' = 0$ ($8_{0,8} \leftarrow 7_{1,7}$, $9_{0,9} \leftarrow 8_{1,8}$, etc.), $K_p' = 1$ ($6_{1,6} \leftarrow 5_{0,5}$, $7_{1,7} \leftarrow 6_{0,6}$, etc.), and $K_p' = 3$ ($3_{3,1} \leftarrow 2_{2,0}$, $4_{3,2} \leftarrow 3_{2,1}$, etc.) were readily identified. Based on these progressions, the full spectrum was scoured, yielding the identification and fitting of a total of 255 b-type transitions in four minutes. Remaining transitions that appeared as sidebands in the chirped-pulse spectrum were then readily assigned, and a number of predicted lines were observed on the cavity spectrometer before generating the final fit.

Performance: In addition to its application to pivalic anhydride, DAPPERS has been tested on a number of published spectra whose density arises from the presence of conformers,[27] excited vibrational states,[28,29] and isotopologues.[28,29,30] For example, in 21 min, a proficient user was able to correctly assign and fit well over 4000 mm wave transitions to the ground vibrational state of 2-chloropyridine[29] in a spectrum containing over 10,000 lines (arising from 23 vibrationally excited states and the 35/37Cl isotopologues). DAPPERS has also been used to fit several other sets of published, dense rotational spectra in the microwave frequency region including trifluoroacetic anhydride,[20] perillyl alcohol,[27] 3,3,3-trifluoro-1,2-epoxypropane,[30] and 1-hexanal.[12] In these tests, the fitting algorithm has effectively handled dense rotational spectra with different types (*a*-, *b*-, and *c*-), branches (P, Q, and R), frequency regions (microwave and millimeter wave), and molecular sizes and asymmetry parameters. It is easy to learn and has been successfully used by college sophomores with only several weeks of spectroscopic experience. The extensive documentation noted above and included in Appendix I guides the user through operation and "best practices".

Among the spectra we have tested so far, significant variation in approach has not been required. Typically, one obtains initial assignments by looking for several intense R branch progressions with low K_p values from one or more types of spectra (*a*-, *b*-, or *c*-), and then combining these progressions to produce a fit with centrifugal distortion that is predictive of remaining transitions from different types and branches. To date, once a full spectrum has been assigned, we have not encountered any instances of misassignments or erroneous alternate fits.

Specific tests were conducted to assess the effect of the molecular asymmetry parameter on the accuracy of guess frequencies derived from the ratio and derivative ratio tests. This is useful for setting the sizes of the windows utilized in these tests. A graphical representation of the relationship between the accuracy of guess frequencies and the asymmetry parameters for both the ratio and derivative ratio tests can be seen in Figure 2.4.

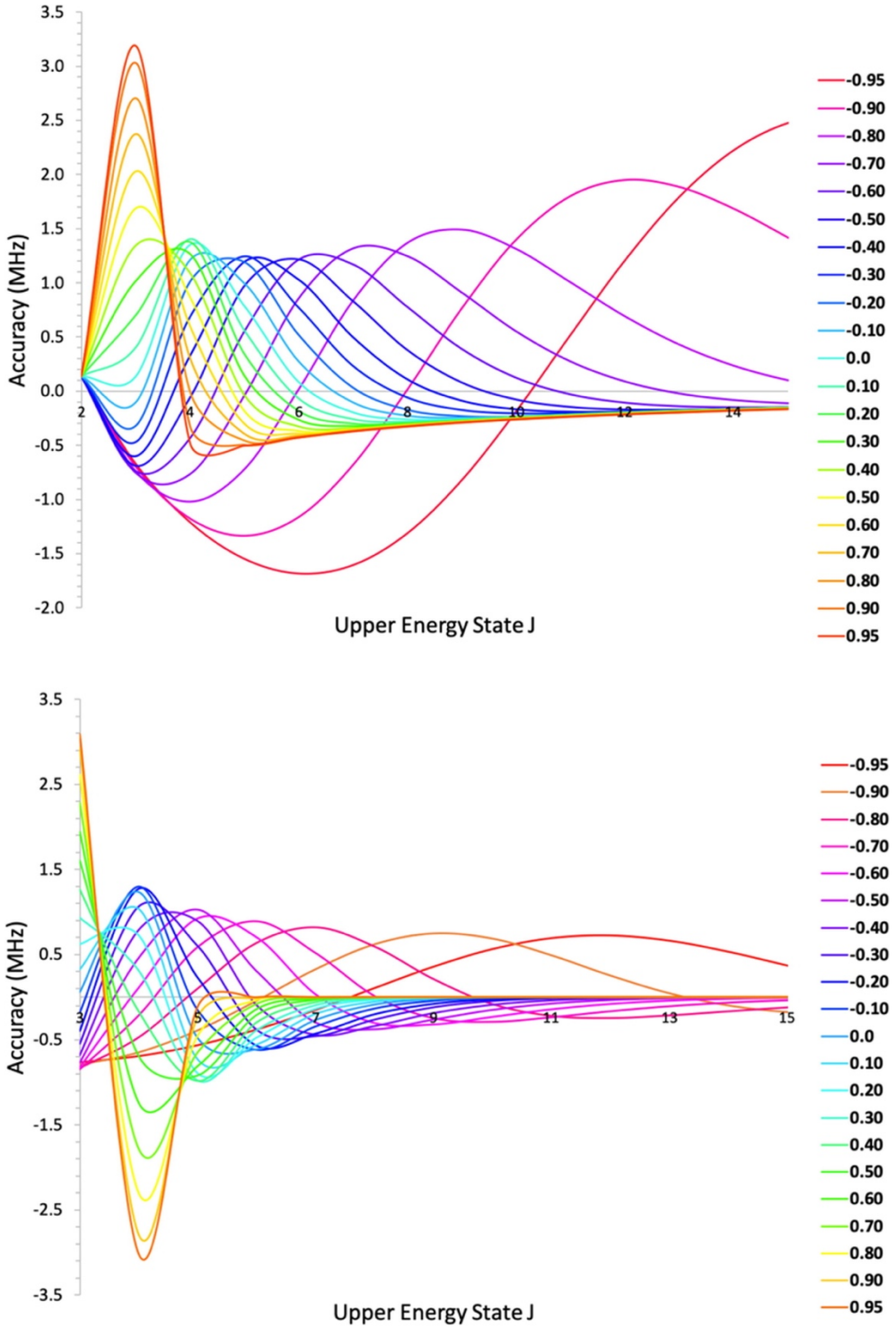

Figure 2.4 DAPPERS Algorithm Accuracy Curves
Plots comparing the accuracies of the ratio test (top) and derivative ratio test (bottom) for varying asymmetry parameters between −0.95 and 0.95. *J* values are along the horizontal axis and the deviations of the algorithm's guess frequencies from their hypothetical experimental values are on the vertical axis. See text for discussion.

The curves in Figure 2.4 that correspond to an asymmetry parameter of −0.95 represent the accuracy of the algorithm guesses that were obtained for the R branch, *b*-type progression $J'_{1,J'} \leftarrow J''_{0,J''}$ of trifluoroacetic anhydride (TFAA).[20] The remaining curves were calculated by fixing all experimental constants for TFAA except for B, which was then varied to produce the range of asymmetry parameters. The predicted frequencies thus generated were compared against a hypothetical experimental spectrum obtained by scaling the new *A*, *B*, and *C* according to the ratio of the observed TFAA constants and those obtained from the DFT calculations. The figure shows that, regardless of asymmetry parameter, the ratio and derivative ratio tests are reliable to within a few MHz. Other progressions were tested and, while the shape of the curves were found to vary, similar accuracies were obtained.

The core algorithm uses parallel computing to significantly speed up performance, and assignment and fitting of spectra are not limited by the runtime of the algorithm itself. Indeed, with reasonably chosen window sizes for the three test algorithms, runtimes generally take no longer than a few seconds, even for very dense spectra. These runtimes, however, can be further minimized, if desired, by using an abridged peak list containing only the most intense experimental peaks and searching for progressions that are likely to be most intense. A significant advantage of this approach can be to reduce the number of trial progressions that need to be evaluated and merged, and may be particularly useful for spectra that contain weak lines from rare isotopologues in natural abundance or high energy conformers with reduced population. A built-in spectral "scrubber" facilitates the creation of spectral files containing subsets of the data, and ensures that they receive different files names so that abridged spectra cannot be accidentally confused with original, raw data.

The current version of DAPPERS was designed to analyze asymmetric top spectra with quartic and sextic centrifugal distortion but is currently not capable of handling internal rotation, Coriolis coupling, or nuclear hyperfine structure (unless it is collapsed to near or within the experimental resolution). Because DAPPERS' algorithm searches for spectral progressions, a minimum of 3 or 4 transitions per progression is required in the

experimental data set and thus, the routine is neither applicable (nor needed) for light molecules with sparse spectra. Finally, since DAPPERS utilizes SPCAT and SPFIT for the prediction and fitting of spectra, it is subject to the same limitations as those programs (notably limited to a maximum *J* value of 369 for SPCAT and 999 for SPFIT).

Discussion

The experimentally determined structural parameters for pivalic anhydride given in Table 2.2 are seen to be in generally quite good agreement with the corresponding values determined at the M06-2X/6-311++G(3df,3pd) level of theory. Of particular interest is the O2-C1-C4-O5 dihedral angle of 53.9(39) deg, which measures the degree to which the two carbonyl groups are not coplanar. This value is in very reasonable agreement with the DFT result of 59 deg. Overall, the extensive isotopic substitution and the good agreement between experimental and theoretical values indicates that the reported structural parameters should be quite reliable.

The structure of pivalic anhydride may be compared with that of the related compound, trifluoroacetic anhydride,[20] in which the $C(CH_3)_3$ is replaced by the more electron withdrawing CF_3 group. For this purpose, we compare only the computational results since a complete experimental structure determination for trifluoroacetic anhydride was not reported. The calculations in that work, however, were performed at the M06-2X/6-311++G(3df) level of theory and should be comparable to those reported here. (Note that trifluoroacetic anhydride contains no hydrogen atoms.) In the calculated structure of pivalic anhydride, the C=O bond lengths are 1.187 Å. This value is slightly longer than the 1.175 Å value obtained for trifluoroacetic anhydride from the coordinates provided in the Supplementary Material of reference 20. The expansion of the carbonyl bond is slight in pivalic anhydride and may result, at least in part, from a stabilization of the $C^{+}{-}O^{-}$ resonance structure of the carbonyl group by the more electron releasing substituent.

A larger difference between the two compounds is seen in the dihedral angle formed by the two carbonyl groups (59 deg computed for pivalic anhydride and only 34 deg for trifluoroacetic anhydride). A plausible explanation for the difference may be increased

repulsion between the two carbonyl oxygens in pivalic anhydride resulting from the replacement of the electron withdrawing fluorine atoms with electron releasing methyl groups. In this regard, it is interesting to note that the 1.7 kcal/mol barrier at the coplanar configuration calculated in this work for pivalic anhydride is about five times larger than the 0.3 kcal/mol barrier obtained for trifluoroacetic anhydride. Some caution is warranted in applying this argument, however, since the equivalent angle has been observed to be 180 deg in formic anhydride[31,32] and formic acetic anhydride,[33] where the carbonyl groups are coplanar, but opposed. As is often the case with conformation, multiple electronic and steric factors may contribute to determining the minimum energy geometry.

The variety of programs that are now available for automated spectral fitting[5-16] provides workers in the field with an array of options for handling increasingly dense rotational spectra. DAPPERS' focus on spectral progressions provides an alternative and easy-to-use approach which should add to the pool of resources that can be harnessed to rapidly process spectra. Further work will be needed to handle spectral features such as hyperfine structure, internal rotation, and Coriolis coupling, but for a variety of semi-rigid asymmetric top molecules, the routine has so far proven quite effective at solving dense spectra of the kind that can now be easily recorded with chirped-pulse methods.

Conclusion

Eight isotopologues of pivalic anhydride have been observed by chirped-pulse and cavity Fourier transform microwave spectroscopy and the resulting spectroscopic constants provide reliable information about the structure of the heavy atom frame. The two carbonyl groups are syn to one another but are not coplanar. M06-2X/6-311++G(3df,3pd) calculations have provided additional structural information, as well as a value for the energetic barrier at the planar configuration (1.7 kcal/mol relative to the equilibrium geometry). The chirped-pulse spectrum provides an early demonstration of the utility of a new spectral processing program (DAPPERS) which provides start-to-finish spectral assignment and fitting based on the identification of spectral progressions. Currently, the program is applicable to semi-rigid asymmetric top molecules with dense rotational

spectra but, in principle, could be adapted to analyze spectra with features such as internal rotation, Coriolis coupling, and nuclear hyperfine structure.

Acknowledgements

This work was supported by the National Science Foundation (Grant No. CHE 1563324) and the Minnesota Supercomputing Institute. We are grateful to Brian Esselman (UW Madison), Helen Leung (Amherst College), Mark Marshall (Amherst College), Fan Xie (University of Alberta), and Yunji Xu (University of Alberta) for providing their experimental spectral files which were critical to the development and testing of DAPPERS.

Chapter 3: Conformational Analysis of Carboxylic Acid Anhydrides: A Microwave and Computational Study

Overview

The microwave spectra of six carboxylic acid anhydrides, RCOOCOR' (R,R') = (CH_3,CH_3), (CH_3,CF_3), (CH_3,$C(CH_3)_3$), (CH_3,CF_2H), ($C(CH_3)_3$,CF_3), and (C_6H_5,CF_3), have been observed. Using M06-2X/6-311++G(d,p) and MP2/6-311++G(d,p) calculations, non-planar *cis* conformers have been predicted for all observed anhydrides, and two types of non-planar *trans* conformers have been predicted for anhydrides with a methyl group. Methyl rotation energy profiles with irregularities were calculated for non-planar *trans* anhydrides which likely arise due to the intermolecular interaction between the methyl rotor and the adjacent carbonyl as well as the interaction between the same methyl and the attached carbonyl. DAPPERS was used to easily assign all or portions of each anhydride's microwave spectrum. For pivalic trifluoracetic anhydride, (R,R') = ($C(CH_3)_3$,CF_3), a Kraitchman analysis enabled the determination of most of the heavy atom structural parameters which were then used to validate the level of theory used. Lastly, the impact of the R group electronic character on the structure of the anhydride functional group has been analyzed using theoretical structures.

Introduction

The simplest possible carboxylic acid anhydride, formic anhydride, was first characterized by electron diffraction in 1972[1] and then by microwave spectroscopy in 1975.[2] In these works, conformational analyses of the anhydride functional group (O=C–O–C=O) were performed with respect to the two O=C–O–C torsional angles. In both instances, the planar rotamer with syn-periplanar and anti-periplanar torsional angles (sp,ap) was observed. Formic acetic anhydride, a mixed carboxylic anhydride derived from both formic and acetic acid, was studied by Raman and IR spectroscopy in 1971,[3] electron diffraction in 1996,[4] and then by microwave spectroscopy in 2013.[5] The conformational analyses from both works showed that the (sp,ap) conformer was again the only observed conformer of mixed formic acetic anhydride. This (sp,ap) conformer can alternatively be described as planar *trans* with respect to the relative orientation of the two carbonyl groups.

While previous attempts to measure the microwave spectrum of the next logical anhydride, acetic anhydride, have proved elusive,[5] acetic anhydride was successfully studied by Raman and IR spectroscopy in 1971[6] and then by electron diffraction in 2000.[7] In the electron diffraction study, acetic anhydride was observed in two new conformations, syn-periplanar/syn-periplanar (sp,sp) and syn-periplanar/anti-clinal (sp,ac), which can alternatively be described as non-planar cis and non-planar *trans* respectively. Note that the use of the term non-planar is in reference to the O=C–O–C=O plane and ignores non-planar R groups. The non-planar *trans* conformer notably features an intramolecular hydrogen bond between the weakly acidic alpha proton and the adjacent carbonyl oxygen forming a six atom ring. The non-planar *cis* conformation of acetic anhydride has a C_2 axis of symmetry but lacks a mirror plane presumably due to the co-repulsion of the adjacent carbonyl oxygen atoms. Two carboxylic anhydrides recently studied by our group, trifluoroacetic anhydride[8] and pivalic anhydride,[9] have also been observed in the non-planar *cis* conformation. Additionally, a fourth anhydride conformation has previously been observed in the microwave studies of maleic[10] and phthalic anhydride[11] which are ring-locked to a planar *cis* orientation of the two carbonyls.

Here we report the microwave spectra of the following carboxylic anhydrides: pivalic trifluoroacetic anhydride, benzoic trifluoroacetic anhydride, acetic trifluoroacetic anhydride, acetic pivalic anhydride, acetic difluoroacetic anhydride, and acetic anhydride. In this work, we will explore the conformational landscape of carboxylic anhydrides with a focus on how the electronic character of different R groups impact structure. Furthermore, we will discuss the internal rotation of different conformers of methyl containing carboxylic acid anhydrides.

Experimental Methods and Results

Acetic anhydride and D6-acetic anhydride were purchased from Sigma-Aldrich. The mixed carboxylic anhydrides were not commercially available and required synthesis. There are several literature methods for the preparation of mixed carboxylic anhydrides,[5,12,13] but the procedure associated with the reaction scheme depicted in Figure 3.1[12] was chosen because it boasts 100% atom economy and no further distillation or purification is necessary assuming the reaction goes to completion and is kept dry.

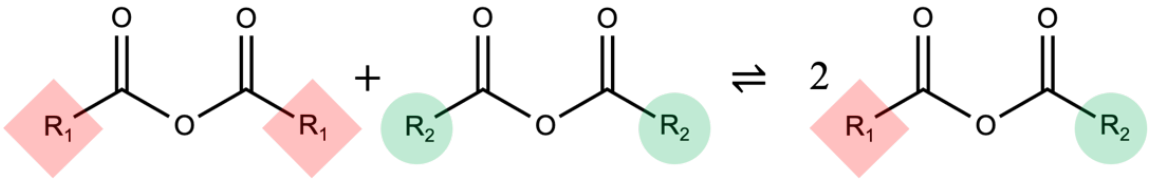

Figure 3.1 Mixed Carboxylic Anhydride Reaction Scheme
The reaction scheme used in the synthesis of the five mixed anhydrides in this study.

The post-reaction mixtures were observed as clear, pale-yellow liquids with the exception of acetic difluoroacetic anhydride which appeared as a deep mahogany colored liquid. The microwave spectra of the anhydrides were separately measured with our tandem chirped-pulse and cavity microwave spectrometer which has been described elsewhere.[14,15] The anhydrides were introduced to the system by flowing argon with a backing pressure of 0.6 atm over a 1.5 mL sample stored in a stainless-steel reservoir. The reservoir was gently heated to 45 °C and 50 °C for benzoic trifluoroacetic anhydride and acetic pivalic anhydride respectively. Heating was not necessary for the other four anhydrides. The resulting mixture of argon and anhydride vapors was then flowed through

a 0.016 in. inner diameter needle along the axis of a stainless-steel cone nozzle through which argon was simultaneously pulsed at a stagnation pressure of 1.0 atm to facilitate the expansion. Chirped-pulse spectra were initially measured followed by spot checks with the cavity method to resolve dense regions of broadband spectra. The ^{13}C and ^{18}O isotopologues of pivalic trifluoroacetic anhydride and one ^{13}C isotopologue of benzoic trifluoroacetic anhydride were observed in natural abundance only with the cavity method.

Spectra of pivalic trifluoroacetic anhydride, benzoic trifluoroacetic anhydride, the A states of the mixed acetic anhydrides, and the AA state of acetic anhydride were easily assigned and fit to semi-rigid rotor Watson A-reduced Hamiltonians in the I^r representation using Pickett's SPFIT[16] through the DAPPERS[9] package. Isotopic substitutions were measured for all carbon and oxygen atoms in the structure of pivalic trifluoroacetic anhydride apart from the bridging oxygen, which was determined to be too close to the center of mass to provide any meaningful information. Only two isotopologues (parent and $^{13}C4$) were observed for benzoic trifluoroacetic anhydride due to lower signal intensity. Fitted parameters for the parent spectra of the pivalic trifluoroacetic and benzoic trifluoroacetic anhydrides are shown in Tables 3.1 and 3.2 respectively, and the fitted parameters for all isotopologues are shown for both species in Tables 3.3 and 3.4 respectively. The structures of pivalic trifluoroacetic and benzoic trifluoracetic anhydride with Gaussian atomic numberings relevant to the following Kraitchman analysis are shown in Figure 3.2. A portion of the PiTFAA chirped-pulse spectrum is shown in Figure 3.3 and an example of a measured cavity spectrum is shown in Figure 3.4.

Table 3.1 Fitted and Computed Spectroscopic Constants of Parent Pivalic Trifluoroacetic Anhydride

	Experimental	M06-2X[a]	MP2[a]
A **[MHz]**	1579.471847(33)	1576	1577
B **[MHz]**	441.570027(19)	445	442
C **[MHz]**	413.612330(17)	413	415
Δ_J **[kHz]**	0.015313(43)		
Δ_{JK} **[kHz]**	0.15106(24)		
Δ_K **[kHz]**	0.01691(93)		
δ_J **[kHz]**	0.000179(17)		
δ_K **[kHz]**	0.1561(62)		
$\lvert\mu_a\rvert$ **[D]**	Strong	3.1	3.0
$\lvert\mu_b\rvert$ **[D]**	Strong	2.7	2.3
$\lvert\mu_c\rvert$ **[D]**	Weak	0.5	0.5
N	509 (405)[a]		
σ **[kHz]**	3.4		

(a) Basis set is 6-311++G(d,p)
(b) Number in parenthesis denotes number of distinct frequencies in the fit

Table 3.2 Fitted and Computed Spectroscopic Constants of Parent Benzoic Trifluoroacetic Anhydride

	Experimental	M06-2X[a]	MP2[a]
A **[MHz]**	1450.101414(68)	1443	1444
B **[MHz]**	299.142841(10)	302	299
C **[MHz]**	266.407241(14)	267	267
Δ_J **[kHz]**	0.007362(18)		
Δ_{JK} **[kHz]**	0.01494(23)		
Δ_K **[kHz]**	0.5192(16)		
δ_J **[kHz]**	0.0019020(93)		
δ_K **[kHz]**	-0.0403(17)		
$\lvert\mu_a\rvert$ **[D]**	Strong	4.3	4.1
$\lvert\mu_b\rvert$ **[D]**	Strong	2.6	2.2
$\lvert\mu_c\rvert$ **[D]**	-	0.1	0.1
N	516 (432)[b]		
σ **[kHz]**	4.1		

(a) Basis set is 6-311++G(d,p)
(b) Number in parenthesis denotes number of distinct frequencies in the fit

Table 3.3 Fitted Spectroscopic Constants for all Pivalic Trifluoroacetic Anhydride Isotopologues[a,b,]

	Parent	**^{13}C1**	**^{18}O2**	**^{13}C4**	**^{18}O5**
***A* [MHz]**	1579.471847(33)	1577.5276(21)	1547.5540(37)	1577.5114(12)	1547.9550(76)
***B* [MHz]**	441.570027(19)	441.21440(11)	440.40123(16)	440.834004(69)	439.59609(37)
***C* [MHz]**	413.612330(17)	413.21605(11)	411.12198(22)	412.898937(66)	410.49618(39)
Δ_J **[kHz]**	0.015313(43)	0.01479(73)	0.0120(14)	0.01572(41)	0.0153(31)
Δ_{JK} **[kHz]**	0.15106(24)	0.1521(26)	0.163(24)	0.1507(26)	0.148(52)
Δ_K **[kHz]**	0.01691(93)	[0.01691]	[0.01691]	[0.01691]	[0.01691]
δ_J **[kHz]**	0.000179(17)	[0.000179]	[0.000179]	[0.000179]	[0.000179]
δ_K **[kHz]**	0.1561(62)	[0.1561]	[0.1561]	[0.1561]	[0.1561]
N	509 (405)[c]	23	12	24 (22)[*]	11
σ **[kHz]**	3.4	0.8	2.4	1.0	1.8

	^{13}C6	**^{13}C7**	**^{13}C11**	**^{13}C15**	**^{13}C19**
***A* [MHz]**	1578.91835(88)	1579.2585(18)	1578.4910(20)	1565.2244(29)	1563.7159(11)
***B* [MHz]**	439.15065(11)	439.682640(85)	435.98533(18)	438.40141(20)	439.10238(10)
***C* [MHz]**	411.45017(10)	411.941731(95)	408.67345(17)	411.55067(14)	410.65979(11)
Δ_J **[kHz]**	0.01536(48)	0.01513(53)	0.01455(81)	0.0147(10)	0.01419(42)
Δ_{JK} **[kHz]**	0.1596(59)	0.1426(32)	0.1485(38)	0.170(17)	0.1491(29)
Δ_K **[kHz]**	[0.01691]	[0.01691]	[0.01691]	[0.01691]	[0.01691]
δ_J **[kHz]**	[0.000179]	[0.000179]	[0.000179]	[0.000179]	[0.000179]
δ_K **[kHz]**	[0.1561]	[0.1561]	[0.1561]	[0.1561]	[0.1561]
N	19	21	23	18	22
σ **[kHz]**	0.6	1.1	1.4	2.1	0.8

(a) Atom numbering is given in Figure 3.2

(b) Numbers in square brackets were constrained to parent values

(c) Number in parenthesis denotes the number of distinct frequencies in a fit

Table 3.4 Fitted Spectroscopic Constants for both Benzoic Trifluoroacetic Anhydride Isotopologues[a,b]

	Parent	^{13}C4
A **[MHz]**	1450.101414(68)	1446.1135(29)
B **[MHz]**	299.142841(10)	299.07098(26)
C **[MHz]**	266.407241(14)	266.22315(11)
Δ_J **[kHz]**	0.007362(18)	0.00790(41)
Δ_{JK} **[kHz]**	0.01494(23)	[0.01494]
Δ_K **[kHz]**	0.5192(16)	[0.5192]
δ_J **[kHz]**	0.0019020(93)	0.00237(33)
δ_K **[kHz]**	-0.0403(17)	[-0.0403]
N	516 (432)[c]	20
σ **[kHz]**	4.1	1.3

(a) Atom numbering is given in Figure 3.2
(b) Numbers in square brackets were constrained to parent values
(c) Number in parenthesis denotes the number of distinct frequencies in a fit

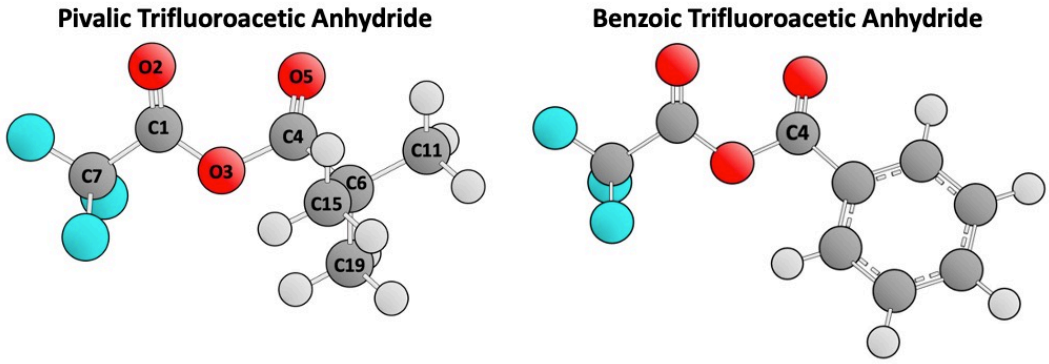

Figure 3.2 Isotopically Labelled Anhydride Structures
The structures of pivalic trifluoroacetic anhydride and benzoic trifluoroacetic anhydride determined with M06-2X/6-311++G(d,p) calculations. Atoms for which ^{13}C and ^{18}O isotopologue spectra were observed have been labelled with the exception of O3 in pivalic trifluoroacetic anhydride which was not observed due to proximity to the principal axis system origin. Only one isotopologue of benzoic trifluoracetic anhydride (^{13}C4) was pursued

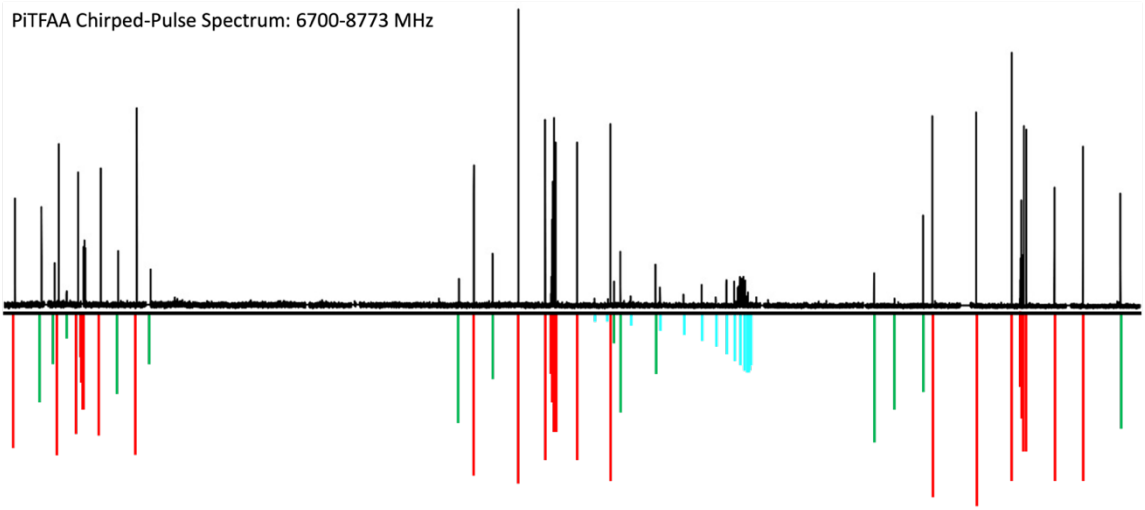

Figure 3.3 Excerpt of the Pivalic Trifluoroacetic Anhydride Chirped-Pulse Spectrum
A portion of the pivalic trifluoroacetic anhydride (PiTFAA) chirped-pulse spectrum between 6700 and 8733 MHz showing three *J* clusters of transitions. The below spectrum is the fitted simulated spectrum. Red transitions are R branch *a*-type, green transitions are R branch *b*-type, and teal transitions are Q branch *b*-type.

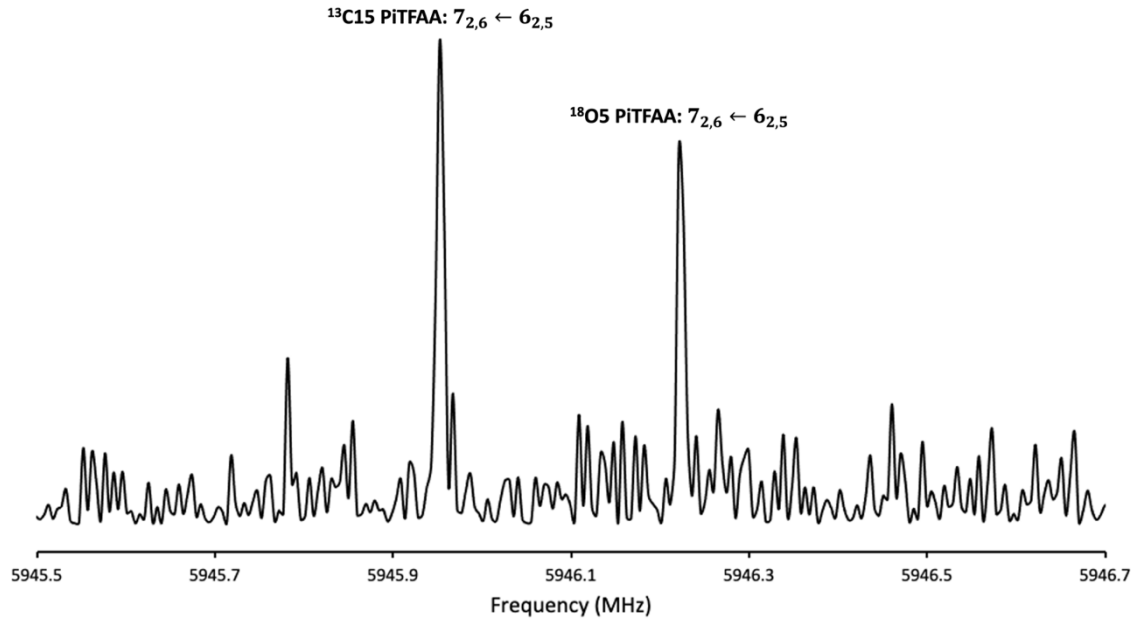

Figure 3.4 Excerpt of the Pivalic Trifluoroacetic Anhydride Cavity Spectrum
A portion of the cavity spectrum of PiTFAA. This particular segment happens to include transitions from both ^{18}O5 and ^{13}C15 PiTFAA isotopologues.

Regarding the three mixed acetic anhydrides, the fitted constants of the A states were combined with theoretical internal rotor parameters (described later) to produce a simulated spectrum that was highly predictive of the remaining E state transitions. The

two states were then fit together with XIAM[17] using rotational and quartic distortion parameters as well as the V_3 barrier heights, the rotor polar angles, and internal rotation distortion parameters. The fitted parameters for acetic trifluoroacetic, acetic pivalic, and acetic difluoroacetic anhydride are shown in Tables 3.5, 3.6, and 3.7 respectively.

For acetic anhydride, the parameters from the DAPPERS AA state fit were combined with predicted internal rotor parameters (discussed later) and were helpful in assigning some of the K_p = 0 and 1 transitions of the other four torsional states. However many transitions were still up to many hundreds of kHz off from their expected frequencies based on the XIAM simulated spectrum. The closed loops shown in Figure 3.5 were used to confidently assign over 200 transitions spread across all five torsional states (AA, EA, AE, EE_j, and E_iE). The assigned transitions were fit together with XIAM using rotational and quartic distortion parameters as well as the V_3 methyl rotor barrier heights, the polar angles ε and δ, and the internal rotation distortion parameters $D_{\pi 2J}$, $D_{\pi 2K}$, and $D_{\pi 2-}$.[18] Additionally, the inclusion of the top-top coupling term V_{cc} improved the predictions of the higher K_p = 2 and 3 transition frequencies and dropped the RMS by nearly 100 kHz, but V_{cc} was highly correlated to both V_3 parameters. It should also be noted that the inclusion of the V_6 parameter and other additional internal rotor parameters available from XIAM_mod was thoroughly attempted with no success.[19] The only remaining transitions in the chirped-pulse spectra were those of acetic acid, a known impurity of acetic anhydride. Fitted spectroscopic constants of the final fit and a K_p = 0 and 1 only fit for the parent acetic anhydride are shown in Table 3.8. The assignment and fitting process of the D6-acetic anhydride microwave spectrum was mostly similar to that of the parent, except the top-top coupling parameter and some internal rotor distortion constants were not needed to achieve an acceptable fit. The hyperfine splitting of the six deuterium atoms was not resolved. The fitted parameters compared to the computational constants for the D6-acetic anhydride are shown in Table 3.9 as well as the parameters of a K_p = 0 and 1 only fit mirroring the parent table. Assigned transitions with labelled torsional states where appropriate can be found in Appendix C for all six observed anhydride spectra.

Table 3.5 Fitted and Computed Spectroscopic Constants of Acetic Trifluoroacetic Anhydride

	Experimental	**M06-2X[b]**			**MP2[b]**	
Conformer	*cis*	*cis*	CH_3 *trans*^{90}	CH_3 *trans*^{120}	*cis*	CH_3 *trans*^{120}
***A* [MHz]**	2648.74070(26)	2669	2677	2692	2626	2673
***B* [MHz]**	817.827036(76)	825	818	800	817	788
***C* [MHz]**	737.724205(73)	741	740	764	740	776
Δ_J [kHz]	.05513(28)					
Δ_{JK} [kHz]	.35033(97)					
Δ_K [kHz]	.0769(47)					
δ_J [kHz]	.00048(13)					
F_o [GHz]	[158.1]	158.1	158.3	157.8	157.6	157.4
V_3 [cm^{-1}]	326.610(95)	311	273	273	324	286
ε [deg]	22.003(62)	21	25	32	25	70
δ [deg]	129.933(57)	127	106	108	128	140
$D_{\pi 2K}$ [MHz]	-0.0408(55)					
$D_{\pi 2-}$ [MHz]	-0.0202(13)					
N	290					
σ [kHz]	4.1					
$\lvert\mu_a\rvert$ [D]	Strong	2.2	1.3	1.6	2.3	1.8
$\lvert\mu_b\rvert$ [D]	Strong	3.1	1.8	1.4	2.7	1.2
$\lvert\mu_c\rvert$ [D]	Weak	0.8	1.5	2.2	0.8	2.3
Rel. E. [kcal/mol]	-	0	0.803	0.857	0	0.946

(a) Numbers in square brackets were constrained to parent values

(b) Basis set is 6-311++G(d,p)

Table 3.6 Fitted and Computed Spectroscopic Constants of Acetic Pivalic Anhydride

	Experimental	**M06-2X[b]**		**MP2[b]**		
Conformer	*cis*	*cis*	CH_3 *trans*^{90}	*cis*	CH_3 *trans*^{90}	CH_3 *trans*^{120}
A **[MHz]**	2398.50252(38)	2415	2428	2398	2420	2429
B **[MHz]**	845.01595(17)	848	843	844	836	818
C **[MHz]**	786.23188(20)	788	761	782	769	796
Δ_J **[kHz]**	0.19103(67)					
Δ_{JK} **[kHz]**	0.3428(58)					
Δ_K **[kHz]**	0.1693(62)					
δ_J **[kHz]**	-0.02605(30)					
δ_K **[kHz]**	0.201(55)					
F_o**[GHz]**	[158.3]	158.3	158.5	157.8	158.1	157.4
V_3 **[cm^{-1}]**	268.569(33)	247	278	240	177	177
ε **[deg]**	152.484(39)	151	157	151	153	146
δ **[deg]**	138.784(30)	136	106	136	104	110
$D_{\pi 2J}$ **[MHz]**	-0.14593(85)					
$D_{\pi 2K}$ **[MHz]**	0.3713(32)					
N	290					
σ **[kHz]**	4.1					
$\lvert\mu_a\rvert$ **[D]**	Weak	0.7	2.1	0.7	1.9	1.4
$\lvert\mu_b\rvert$ **[D]**	Strong	3.7	0.9	3.4	0.8	0.8
$\lvert\mu_c\rvert$ **[D]**	Weak	0.3	1.8	0.2	2.0	2.7
Rel. E. [kcal/mol]	-	0.193	0	0	0.844	0.773

(a) Numbers in square brackets were constrained to parent values

(b) Basis set is 6-311++G(d,p)

Table 3.7 Fitted and Computed Spectroscopic Constants of Acetic Difluoroacetic Anhydride

	Experimental	**M06-2X[b]**				**MP2[b]**		
Conformer	CF_2H *trans*^{90}	*cis*	CF_2H *trans*^{90}	CH_3 *trans*^{90}	CH_3 *trans*^{120}	*cis*	CF_2H *trans*^{90}	CH_3 *trans*^{120}
A **[MHz]**	2910.06378(45)	2879	2930	2983	3035	2855	2872	3032
B **[MHz]**	1182.89553(17)	1020	1199	1010	995	1011	1195	985
C **[MHz]**	989.46343(13)	920	996	918	934	921	998	935
Δ_J **[kHz]**	0.1837(14)							
Δ_{JK} **[kHz]**	0.3229(70)							
Δ_K **[kHz]**	0.392(14)							
δ_J **[kHz]**	0.03318(67)							
δ_K **[kHz]**	-0.246(35)							
F_o **[GHz]**	[158.0]	158.1	158.0	158.3	157.9	157.7	157.6	157.4
V_3 **[cm^{-1}]**	252.646(19)	305	257	248	248	315	246	272
ε **[deg]**	95.28(66)	18	95	18	16	19	78	10
δ **[deg]**	149.802(26)	122	148	109	109	123	147	110
$D_{\pi 2J}$ **[MHz]**	0.06020(58)							
$D_{\pi 2K}$ **[MHz]**	-0.3379(35)							
N	178							
σ **[kHz]**	4.1							
$\lvert\mu_a\rvert$ **[D]**	Strong	0.4	3.2	0.0	0.1	0.6	2.9	0.4
$\lvert\mu_b\rvert$ **[D]**	Weak	2.1	0.9	2.8	2.6	1.9	0.9	2.4
$\lvert\mu_c\rvert$ **[D]**	Weak	0.8	0.5	0.5	0.6	0.9	0.4	0.3
Rel. E. [kcal/mol]	-	1.039	0	1.883	1.887	0	0.360	0.946

(a) Numbers in square brackets were constrained to parent values
(b) Basis set is 6-311++G(d,p)

Table 3.8 Fitted and Computed Spectroscopic Constants of Parent Acetic Anhydride[a]

	Full Fit	K=0 and 1 Fit	M06-2X[b]		MP2[b]		
Conformer	generalized *trans*[c]		*cis*	CH_3 *trans*^{90}	*cis*	CH_3 *trans*^{90}	CH_3 *trans*^{120}
A **[MHz]**	5253.5921(87)	5253.535(66)	5552	5350	5442	5261	5188
B **[MHz]**	1825.7289(38)	1825.83(11)	1811	1895	1801	1864	1800
C **[MHz]**	1642.5558(33)	1642.46(11)	1541	1535	1542	1574	1696
Δ_J **[kHz]**	1.864(41)	2.55(73)					
Δ_{JK} **[kHz]**	12.80(14)	9.4(44)					
Δ_K **[kHz]**	-12.87(66)	-69(55)					
δ_J **[kHz]**	-0.494(16)	-0.475(47)					
δ_K **[kHz]**	65.0(12)	116(55)					
F_o^{R1} **[GHz]**	[158.5]	[158.5]	158.3	158.5	157.8	158.1	157.5
V_3^{R1} **[cm^{-1}]**	242.5(19)	246.7(19)	290	280	295	194	194
ε^{R1} **[deg]**	24.15(11)	24.048(39)	25	19	34	23	27
δ^{R1} **[deg]**	73.890(23)	73.956(39)	87	81	41	81	72
$D_{\pi 2J}^{R1}$ **[MHz]**	0.462(16)	0.493(88)					
$D_{\pi 2K}^{R1}$ **[MHz]**	-1.881(59)	-2.095(64)					
$D_{\pi 2-}^{R1}$ **[MHz]**	-2.365(62)	-2.525(64)					
F_o^{R2} **[GHz]**	[157.9]	[157.9]	158.3	158.3	157.8	157.9	157.9
V_3^{R2} **[cm^{-1}]**	207.8(19)	212.1(19)	290	222	295	186	161
ε^{R2} **[deg]**	40.01(13)	40.164(47)	25	26	34	33	48
δ^{R2} **[deg]**	28.359(37)	28.327(15)	87	34	41	33	28
$D_{\pi 2J}^{R2}$ **[MHz]**	-0.0975(64)	-0.0986(30)					
$D_{\pi 2K}^{R2}$ **[MHz]**	-0.862(33)	-0.912(28)					
$D_{\pi 2-}^{R2}$ **[MHz]**	1.462(49)	1.618(41)					
V_{cc} **[cm^{-1}]**	21.6(19)	26.1(20)					
N	244	152					
σ **[kHz]**	57.6	13.9					
$\lvert\mu_a\rvert$ **[D]**	Strong		0.0	2.0	0.0	1.7	1.2
$\lvert\mu_b\rvert$ **[D]**	Strong		4.0	0.7	3.6	0.7	0.9
$\lvert\mu_c\rvert$ **[D]**	Strong		0.0	1.9	0.0	2.2	2.8
Rel. E. [kcal/mol]	-		0.133	0	0.000	0.770	0.665

(a) Numbers in square brackets were constrained to parent values

(b) Basis set is 6-311++G(d,p)

(c) See text for discussion of what the "generalized *trans*" conformer means

Table 3.9 Fitted and Computed Spectroscopic Constants of D6-Acetic Anhydride[a]

	Full Fit	K=0 and 1 Fit	M06-2X[b]		MP2[b]		
Conformer	generalized *trans*[c]		*cis*	CH_3 *trans*^{90}	*cis*	CH_3 *trans*^{90}	CH_3 *trans*^{120}
***A* [MHz]**	4592.2901(26)	4592.301(12)	4892	4636	4807	4567	4555
***B* [MHz]**	1599.8448(13)	1599.841(69)	1553	1668	1545	1640	1573
***C* [MHz]**	1440.6333(14)	1440.636(67)	1337	1360	1337	1393	1482
Δ_J **[kHz]**	1.8348(97)	1.82(44)					
Δ_{JK} **[kHz]**	11.371(49)	11.2(27)					
Δ_K **[kHz]**	-11.64(19)	-					
δ_J **[kHz]**	-0.3121(59)	-0.317(42)					
δ_K **[kHz]**	66.76(43)	66(33)					
F_o^{R1} **[GHz]**	[79.0]	[79.0]	79.2	79.3	79.0	79.1	78.8
V_3^{R1} **[cm^{-1}]**	184.99(11)	185.1(15)	290	280	295	194	194
ε^{R1} **[deg]**	18.27(82)	16.24(93)	30	18	31	21	20
δ^{R1} **[deg]**	70.583(52)	70.44(11)	40	77	40	78	69
$D_{\pi 2\text{-}}{}^{R1}$ **[MHz]**	-0. 965772(24)	-0.77661(12)					
F_o^{R2} **[GHz]**	[79.0]	[79.0]	79.2	79.2	79.0	79.0	79.0
V_3^{R2} **[cm^{-1}]**	174.453(61)	174.50(83)	290	222	295	186	161
ε^{R2} **[deg]**	48.92(77)	55.68(68)	30	30	31	39	59
δ^{R2} **[deg]**	26.71(15)	26.96(15)	40	31	40	30	27
$D_{\pi 2K}{}^{R2}$ **[MHz]**	-0.91841(52)	-0.89617(14)					
N	175	90					
σ **[kHz]**	14.3	12.2					
$\lvert\mu_a\rvert$ **[D]**	Strong		0.0	1.9	0.0	1.7	1.1
$\lvert\mu_b\rvert$ **[D]**	Strong		4.0	0.9	3.6	0.9	1.3
$\lvert\mu_c\rvert$ **[D]**	Strong		0.0	1.9	0.0	2.1	2.6
Rel. E. [kcal/mol]	-		0.133	0	0.000	0.770	0.665

(a) Numbers in square brackets were constrained to parent values

(b) Basis set is 6-311++G(d,p)

(c) See text for discussion of what the "generalized *trans*" conformer means

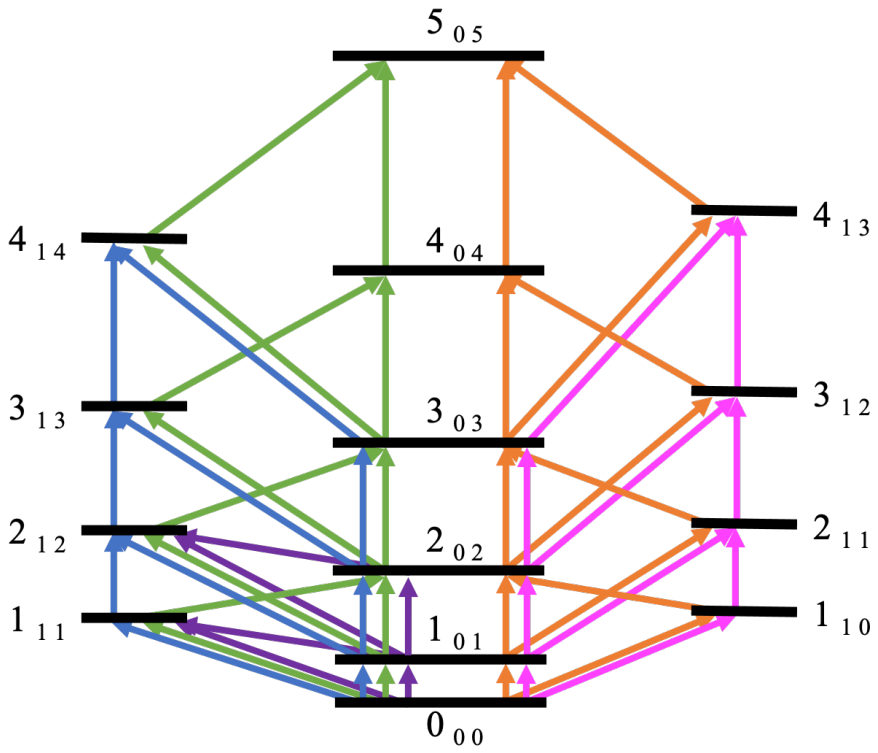

Figure 3.5 Acetic Anhydride Closed Loops
Energy diagram depicting the 16 unique closed loops used to assign one of the five torsional states of the acetic anhydride microwave spectrum. Identical sets of closed loops were found for each of the other four torsional states. The color-coding highlights closed loops with similar transitions differing only by *J*.

Kraitchman Analysis

The full heavy-atom structure was determined for the pivalic trifluoracetic acid species in order to validate the levels of theory used. A Kraitchman analysis[20] was performed using the measured isotopic substitutions enabling the determination of most of the structural parameters describing the heavy atom frame. Kisiel's KRA program was used to perform the analysis using Costain uncertainties as described in the KRA documentation.[21] The resulting atomic coordinates are included in the Table 3.10 and the corresponding structural parameters derived from these coordinates are shown in Table 3.11 with a comparison to computational values from the M06-2X/6-311++G(d,p) and MP2/6-311++G(d,p) structures. The signs of the atomic coordinates were inferred based on the theoretical structures. For the benzoic trifluoracetic acid species, the spectrum of the one ^{13}C isotopologue was well predicted by the computed structure. In light of these results, extensive isotopic substitution was not pursued for the remaining systems studied.

Table 3.10 Experimental Coordinates for Pivalic Trifluoroacetic Anhydride[a]

	X [Å]	Y [Å]	Z [Å]
C1	-0.9225(16)	0.5678(27)	0.2702(56)
O2	-0.9798(15)	1.65200(91)	0.7775(19)
C4	1.3470(11)	0.5475(28)	-0.3154(48)
O5	1.4055(11)	1.62953(93)	-0.8021(19)
C6	2.51335(60)	-0.3390(44)	0.041(36)
C7	-2.21823(68)	-0.2076(73)	-0.021(69)
C11	3.82563(40)	0.3941(38)	-0.2175(70)
C15	2.39401(63)	-0.6094(25)	1.60152(95)
C19	2.44610(62)	-1.67265(90)	-0.6745(22)

(a) Signs are inferred from the theoretical structure.

Table 3.11 Structural Parameters for Pivalic Trifluoroacetic Anhydride[a]

Bond Lengths [Å]	**Experimental**	**M06-2X**	**MP2**
C1-C4[b]	2.3439(27)	2.39960	2.39335
C1-O2	1.1984(36)	1.18218	1.19841
C4-O5	1.1880(34)	1.18217	1.19426
C1-C7	1.538(13)	1.54445	1.54257
C4-C6	1.5217(34)	1.51268	1.50923
C6-C11	1.5355(32)	1.52806	1.52946
C6-C15	1.5341(13)	1.53750	1.53852
C6-C19	1.5417(41)	1.53721	1.53765
Bond Angles [°]			
O2-C1-C7	119.8(40)	123.50341	124.11573
O5-C4-C6	127.14(84)	128.78457	129.29484
C4-C6-C11	108.76(38)	108.18616	108.53619
C4-C6-C15	107.96(55)	108.21947	108.05172
C4-C6-C19	109.59(51)	109.00710	109.28216
C11-C6-C15	110.55(69)	110.65390	110.43957
C11-C6-C19	110.37(44)	110.66047	110.49926
C15-C6-C19	109.55(43)	110.04394	109.97541
Dihedral Angles [°]			
O2-C1-C4-O5	46.6(16)	43.01157	50.30319
O5-C4-C6-C11	0.0993(60)	0.62424	1.76777
O5-C4-C6-C15	120.1(48)	119.30946	118.01251
O5-C4-C6-C19	120.6(46)	121.01929	122.33903

(a) Atom numberings refer to Figure 3.2

(b) The C1-C4 distance does not correspond to the length of a bond but is quoted here because the C1-O3-C4 angle and the C1-O3 and O3-C4 bond lengths are not determined.

Computational Methods and Results

The minimum energy and transition state structures of all six carboxylic anhydrides were predicted with M06-2X/6-311++G(d,p) and MP2/6-311++G(d,p) calculations with the Gaussian16 suite of programs.[22] Four types of anhydride conformers were predicted and are shown in Figure 3.6. The carbonyls are oriented in the same general direction for the non-planar *cis* conformer, while those of the *trans* conformers are oriented in opposite directions as shown in the figure. Non-planar *cis* conformers were predicted for all six carboxylic anhydrides, but *trans* conformers were only predicted for anhydrides with at least one R group containing a weakly acidic alpha hydrogen (R = CH_3 or CF_2H). As shown by the dotted lines in Figure 3.6, the *trans* conformers are partially stabilized by a weak internal hydrogen bond between this weakly acidic alpha hydrogen and the adjacent carbonyl oxygen forming a six membered ring. The CH_3 *trans*^{90} and CH_3 *trans*^{120} conformers represent the two minima that are passed through during the threefold internal rotation of said hydrogen bonded methyl groups. The M06-2X and MP2 scans of the hydrogen bonded methyl rotation energy profiles are shown in Figure 3.7. Note that "90" and "120" in the CH_3 *trans*^{90} and CH_3 *trans*^{120} denotations refer to the approximate dihedral angle between the carbonyl adjacent to the methyl rotor and the weakly acidic alpha proton at which the respective minima occur. Interestingly, the CH_3 *trans*^{120} conformers appeared as inflections in the M06-2X energy profiles rather than minima for acetic and acetic pivalic anhydrides, while the CH_3 *trans*^{90} conformers appeared as inflections in the MP2 energy profiles of acetic difluoroacetic and acetic trifluoroacetic anhydrides. The final structure in Figure 3.6 is the CF_2H *trans*^{90} conformer which was only predicted for acetic difluoroacetic anhydride. In this structure, the hydrogen bonded alpha hydrogen is that of the difluoromethyl group rather than that of the methyl group in the CH_3 *trans*^{90} and CH_3 *trans*^{120} conformers. An analogous CF_2H *trans*^{120} is not possible, again presumably due to steric repulsions between the carbonyl and fluorine atom which would be eclipsed in this theoretical conformation.

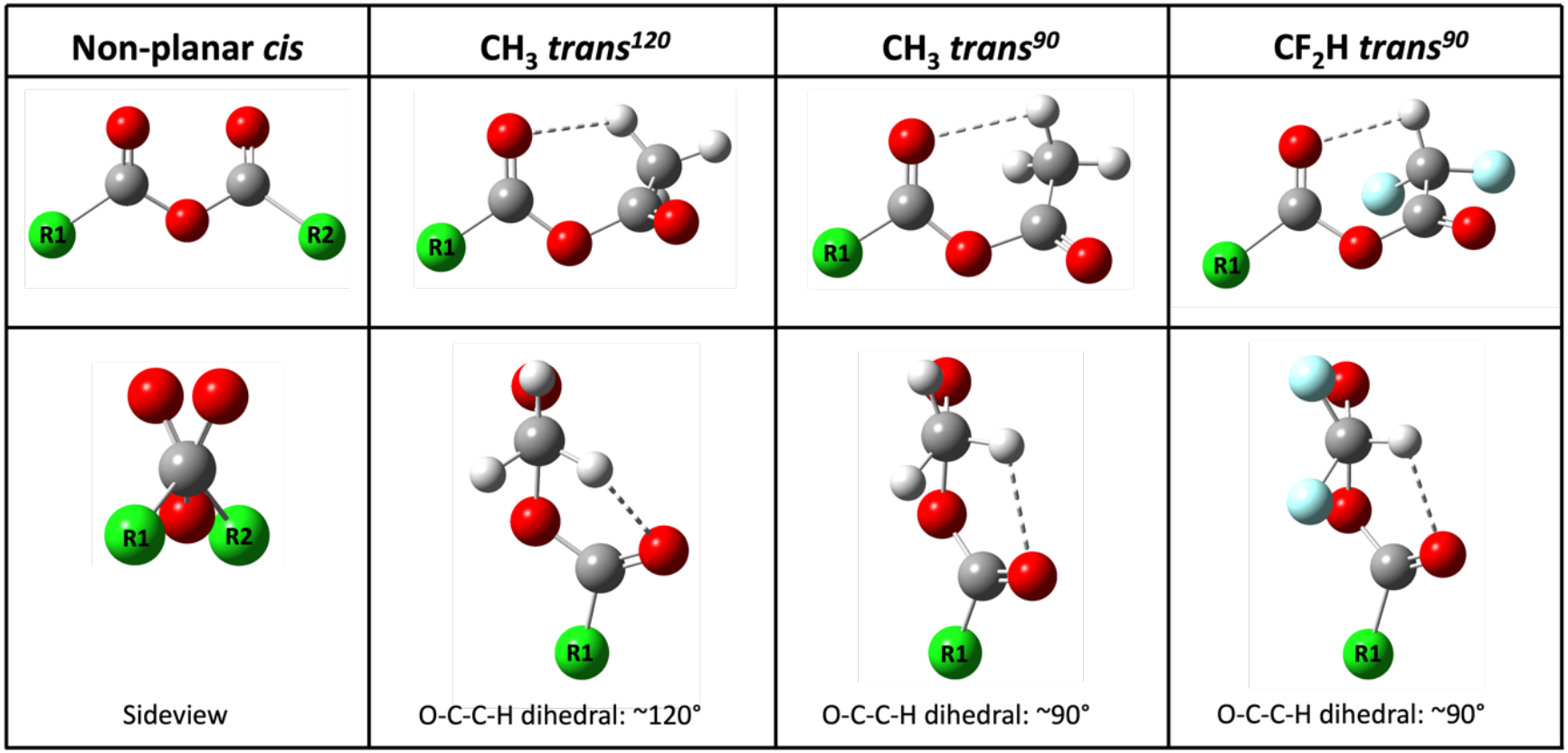

Figure 3.6 Predicted Structures of Carboxylic Anhydrides
The three non-planar carboxylic anhydride conformers predicted in this study. Note that the CF_2H *trans*^{90} conformer is the same conformer as the CH_3 *trans*^{90} conformer, but the difluoromethyl group is hydrogen bonded rather than the methyl group. This conformer is only predicted for acetic difluoroacetic anhydride. The dashed lines highlight the internal hydrogen bond in the *trans* conformers. The lower view of the *trans* conformers is viewed through the C–C bond of the O=C–C–H dihedral angle (H refers to the hydrogen bonded methyl hydrogen).

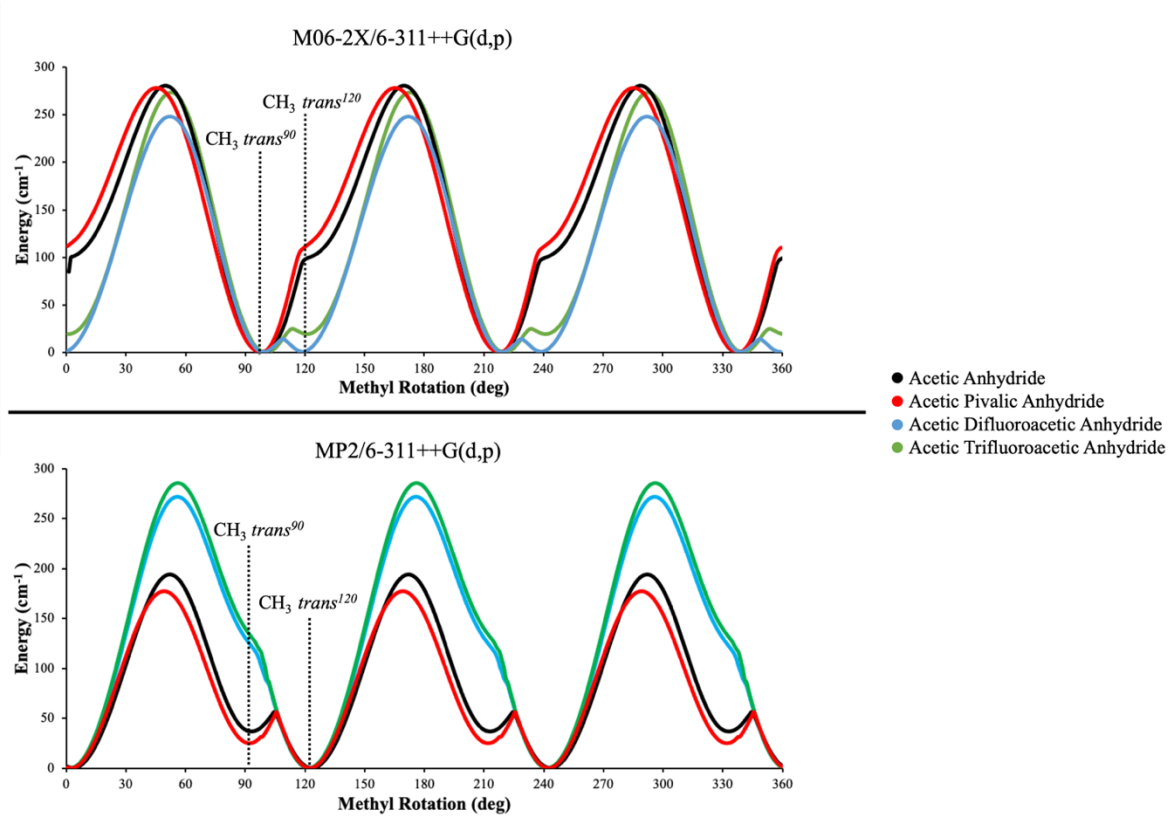

Figure 3.7 Energy Profiles of the *trans* Acetic Anhdydrides

The M06-2X/6-311++(d,p) and MP2/6-311++(d,p) one degree stepwise energy profile scans of the three *trans* oriented mixed acetic anhydride methyl groups and the R1 methyl group of either *trans* conformer of acetic anhydride (see Figure 3.8 for R1 labelling). The fixed scan coordinate is the O=C–C–H dihedral angle between the hydrogen bonded alpha proton and the attached carbonyl (not the adjacent hydrogen bonded carbonyl). The CH_3 $trans^{90}$ and CH_3 $trans^{120}$ conformers are labelled on each plot. Note that the profiles of the non-planar *cis* conformers, the CF_2H $trans^{90}$ conformer of acetic difluoroacetic anhydride, and the R1 methyl in all acetic anhydride conformers were normal V_3 energy profiles. Note also that in both methods the acetic anhydrides with electron donating R groups (acetic and acetic pivalic anhydride) have very similar profile shapes. In contrast, the anhydrides with electron withdrawing R groups (acetic difluoroacetic and acetic trifluoroacetic anhydride) have very similar profile shapes.

The predicted rotational constants, dipole moments, internal rotor constants, and relative energies of the conformers predicted with both M06-2X and MP2 calculations are compared to the fitted spectroscopic constants for each anhydride (Tables 3.1, 3.2, and 3.5-3.8). The predicted V_3 barriers to internal rotation were obtained from transition state calculations for the non-planar *cis* conformers of the acetic and mixed acetic anhydrides as well as for the CF_2H *trans*^{90} conformer of acetic difluoroacetic anhydride. Unfortunately, methyl internal rotation transition state calculations for the CH_3 *trans*^{90} and CH_3 *trans*^{120} conformers were unsuccessful, so V_3 barriers were taken from the scanned energy profiles shown in Figure 3.7. The rotational constants of the methyl rotors (F_o) and the polar angles (ε and δ), which describe the orientation of the rotors' pseudo C_3 axis relative to the inertial axes of the molecule, are also reported. Two sets of internal rotor parameters are reported for the conformers of acetic anhydride. The methyl R groups are distinguished with the labels "R1" and "R2" in Figure 3.8 for each conformer of acetic anhydride. Cartesian coordinates for all energy minimum and transition state structures are included in Appendix C.

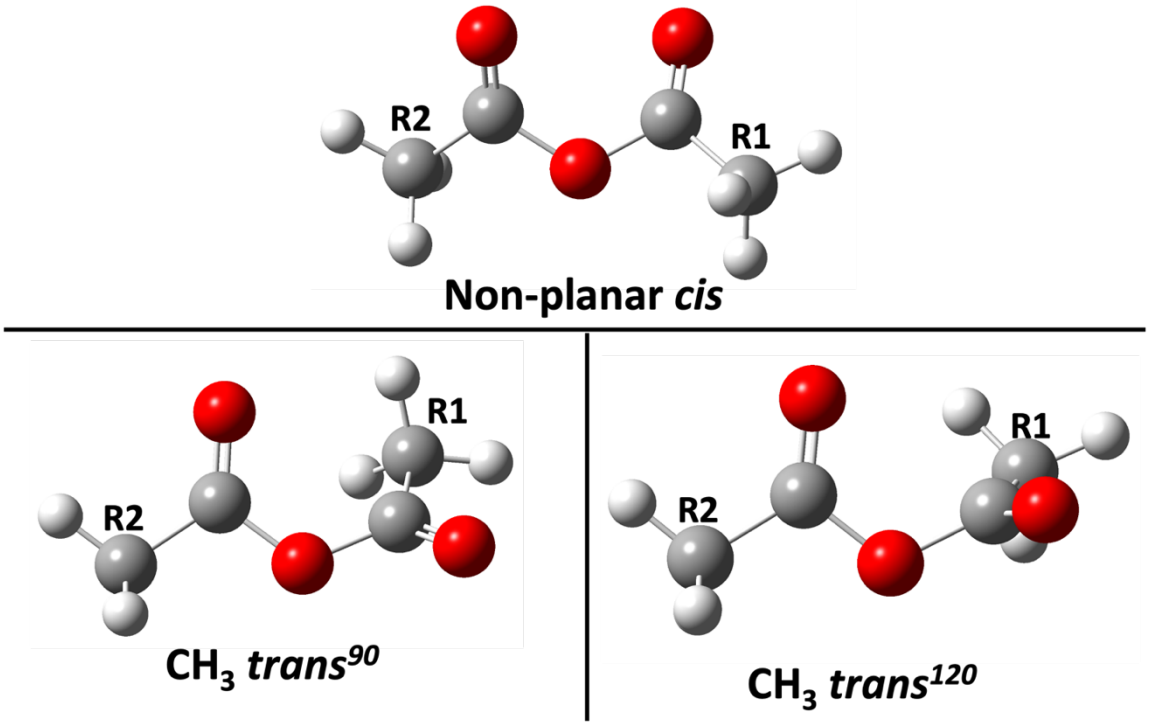

Figure 3.8 Conformers of Acetic Anhydride
The three predicted conformers of acetic anhydride with the methyl groups labelled R1 and R2. Note that R1 and R2 in the non-planar *cis* conformer are equivalent due to the C_2 symmetry axis.

Discussion

Only the non-planar *cis* conformer was predicted for the pivalic trifluoroacetic and benzoic trifluoroacetic anhydrides. Note that the trifluoroacetic[8] and pivalic anhydrides[9] were previously observed in the non-planar *cis* conformation as well, and that all four of these anhydrides lack weakly acidic alpha hydrogens needed for the non-planar *trans* conformer. The rotational constants in Tables 3.1 and 3.2 show very good agreement between experimental, M06-2X, and MP2 rotational constants for both anhydrides. Additionally, the experimental structural parameters in Table 3.11 are in very good agreement with the values calculated by both the M06-2X and MP2 methods, providing further validation of their use for these carboxylic acid anhydrides.

For the four acetic anhydrides, the CH_3 *trans*^{90} and CH_3 *trans*^{120} conformers were predicted in addition to the non-planar *cis* conformer. In the CH_3 *trans*^{120} conformer, one hydrogen of the methyl group is eclipsed relative to the attached carbonyl which is the expected lowest energy orientation for a methyl group attached to a carbonyl given steric interactions.[23-25] The CH_3 *trans*^{90} conformer is possibly stabilized through the weak intramolecular hydrogen bond, though it is unclear whether this hydrogen bond is stronger than that of the CH_3 *trans*^{120} conformer based on the structural parameters shown in Table 3.12. Note that the hydrogen bond distances are slightly shorter for the CH_3 *trans*^{90} conformer, but the hydrogen bond angles are less linear than those of the CH_3 *trans*^{120} conformer. No angles in Table 3.12 are particularly close to ideal linearity likely due to ring strain in the cyclic six atom ring formed by the hydrogen bond.

Table 3.12 Hydrogen Bonding in the *trans*^{90} and *trans*^{120} Conformers

Anhydride			H-Bond Angle (deg)		H-Bond Distance (Å)	
R1	**R2**	**Method[a,b]**	**CH_3 *trans*^{90}**	**CH_3 *trans*^{120}**	**CH_3 *trans*^{90}**	**CH_3 *trans*^{120}**
CH_3	CF_3	M06-2X	98.2	112.2	2.50	2.52
CH_3	CF_2H	M06-2X	98.9	111.7	2.50	2.53
CH_3	CH_3	MP2	95.8	109.0	2.53	2.59
CH_3	$C(CH_3)_3$	MP2	94.3	108.8	2.55	2.59

(a) Some minima were not calculated with each method as described in the text so both methods cannot be compared for all four anhydrides
(b) Basis set is 6-311++G(d,p) for both methods

The MP2 calculations predicted CH_3 *trans*^{120} conformers for all four acetic anhydrides, but only CH_3 *trans*^{90} conformers for the acetic and acetic pivalic anhydrides. In contrast, CH_3 *trans*^{90} conformers were predicted for all four acetic anhydrides using the M06-2X method and CH_3 *trans*^{120} conformers were only predicted for the acetic trifluoroacetic and acetic difluoroacetic anhydrides. While the two computational methods differ in their ability to identify a distinct minimum, both clearly show the development of another interaction as the methyl group is rotated as represented by the "inflections" in Figure 3.7. Whether one or two minima are predicted likely comes down to the numerical details of the method used. Finally, Figure 3.7 shows low barriers between the CH_3 *trans*^{90} and CH_3 *trans*^{120} minima when both conformers are predicted. As will be discussed below, it is unclear what spectral effects should be expected from an irregular methyl rotation that propagates through two distinct minima each with unique rotational constants such as those shown in Figure 3.7.

Three total conformers were predicted for acetic trifluoroacetic anhydride as shown in Table 3.5. The rotational constants and V_3 barrier of the CH_3 *trans*^{120} conformer predicted with the M06-2X method are very similar to those from the analogous MP2 structure, but the polar angles disagree somewhat significantly across methods. The experimental rotational constants are in reasonable agreement with all predicted constants regardless of method and thus do not distinguish which conformer was observed. However, the fitted V_3 barrier and δ polar angle are only in good agreement to those of the predicted non-planar *cis* conformer (for both M06-2X and MP2 methods) indicating that the *cis* conformer was indeed observed. Furthermore, the non-planar *cis* conformer is predicted to be the global minimum by over 0.8 kcal/mol by both the M06-2X and MP2 methods. Lastly, strong *a*- and *b*-type spectra and a weak *c*-type spectrum were observed which is only consistent with the predicted dipole moments of the non-planar *cis* conformer.

For acetic pivalic anhydride, the non-planar *cis* and CH_3 *trans*^{90} conformers were predicted with both methods while the CH_3 *trans*^{120} was only predicted with MP2 calculations. Constants between the two conformers predicted with both methods are in very good agreement with the exception of the V_3 barriers of the CH_3 *trans*^{90} conformers which differ

by over 100 cm^{-1}. This difference is perhaps the result of the difference in energy profile shape between methods (see Figure 3.7). Similar to acetic trifluoroacetic anhydride, the rotational constants in Table 3.6 cannot be used to definitively distinguish which conformer was observed for acetic pivalic anhydride. The internal rotor constants continue the ambiguity with the exception of the polar angle δ whose fitted value is significantly closer to the non-planar *cis* value (both M06-2X and MP2) than those of the *trans* conformers. Importantly, a strong *b*-type spectrum was observed which is only compatible with the predicted dipole moments of the non-planar *cis* conformer. Furthermore, the MP2 energies indicate the non-planar *cis* conformer is the global minimum by approximately 0.8 kcal/mol, while the M06-2X predicts the *cis* conformer to be less than 0.2 kcal/mol higher in energy than the CH_3 $trans^{90}$ conformer which is plausibly within the range of computational error. Therefore, we conclude that the non-planar *cis* conformer was more than likely observed for acetic pivalic anhydride.

For acetic difluoroacetic anhydride, the CF_2H $trans^{90}$ conformer is predicted in addition to the non-planar *cis*, CH_3 $trans^{90}$, and CH_3 $trans^{120}$ conformers. The CF_2H $trans^{90}$ conformer also features an internal hydrogen bond, but in its case it involves the difluoromethyl group's alpha hydrogen rather than that of the methyl group. While there is still internal rotation for this conformer, the energy profile does not feature the irregularities shown in Figure 3.7 because the methyl group is not involved in the hydrogen bond. The predicted rotational and internal rotor constants of the CF_2H $trans^{90}$ conformer are in significantly better agreement with the fitted constants (both M06-2X and MP2), which clearly indicates that the CF_2H $trans^{90}$ conformer was observed. Moreover, the M06-2X energies predict the CF_2H $trans^{90}$ conformer to be the global minimum by over 1.0 kcal/mol. The 1.8 kcal/mol difference in M06-2X energies between the CH_3 $trans^{90}$ and CF_2H $trans^{90}$ conformer of acetic difluoroacetic anhydride is likely the result of the increased hydrogen bonding ability of the difluoromethyl hydrogen which has been previously described to be isosteric and isopolar to a hydroxyl with respect to hydrogen bonding.[26] The MP2 energies predict the non-planar *cis* conformer to be the lowest energy conformer but by only 0.360 kcal/mol which is again possibly due to computational error. Relative intensity of

the *a-, b-*, and *c*-type transitions exclude the *cis* conformer and also favor the CF_2H *trans*^{90} conformer.

In the case of acetic anhydride, non-planar *cis* and CH_3 *trans*^{90} conformers were predicted with both computational methods, but the CH_3 *trans*^{120} conformer was only predicted with MP2 calculations. Note that these are minima on the potential energy surface but that does not guarantee that they represent two distinct vibrationally averaged species. As shown in Table 3.8, the rotational constants for the conformers predicted with both methods are fairly similar, but there are key differences for many of the internal rotor parameters. The non-planar *cis* conformer is easily ruled out because two distinct sets of fitted internal rotor parameters were obtained. Furthermore, strong *a*-, *b*-, and *c*-type spectra were observed which is incompatible with the predicted dipole moments of the C_2 symmetrical non-planar *cis* conformer. This leaves only the CH_3 *trans*^{90} and CH_3 *trans*^{120} conformers both of which are minima in the MP2 energy profile of the R1 methyl group's rotation shown in Figure 3.7. The predicted constants and polar angles of both *trans* conformers are in moderate agreement to the fitted values, though this agreement does not definitively establish which *trans* conformer was observed (the V_3 barriers are discussed in the following paragraph). As previously discussed, both conformers are very close in energy with a small barrier between the two minima, so it is possible that the observed transitions are influenced by the vibrational averaging between these two theoretical conformers as the methyl rotates. Additionally, a comparison of the fitted and predicted constants of the D6-acetic anhydride isotopologue is shown in Table 3.9 and the results parallel those of the parent: poor agreement with the non-planar *cis* conformer and generally good agreement between either *trans* conformer. Therefore, we can conclude only that acetic anhydride was observed generally as a *trans* conformer, though it cannot be established whether a CH_3 *trans*^{90} or CH_3 *trans*^{120} conformer was observed as these may or may not be distinct species. Note that the inclusion of K_p = 2 and 3 does not significantly change any of the fitted parameters for either the parent or D6-acetic anhydrides.

The relatively good agreement between the observed and predicted polar angles were used to correlate the fitted V_3^{R1} and V_3^{R2} values to their respective rotors as labelled in

Figure 3.8. Interestingly, the fitted V_3 values were in fairly poor agreement with the barriers of any predicted conformer with any method. Note that acetic anhydride is the only molecule in this study observed in a CH_3 *trans* conformer for which the irregular V_3 energy profiles were predicted. The poor agreement between the fitted and predicted V_3 barrier for the R1 methyl (labelled in Figure 3.8) is likely correlated to the irregular energy profiles shown in Figure 3.7. It is entirely possible that such an irregular V_3 profile cannot be easily fit using existing programs. While the energy profile of the R2 methyl is predicted to be "regular", there is still poor agreement between fitted and predicted V_3 barriers which may be the result of coupling between the R1 and R2 tops. The significant impact of the top-top coupling constant, V_{cc}, on the fit and the high correlation of V_{cc} to both V_3 barriers may indicate that the two rotors are highly coupled which could impact the normalcy of the R2 energy profile of methyl rotation. The recently assigned microwave spectrum of 4,5-dimethylthiazole[27] (45DMTA) bears some striking similarities to the case of acetic anhydride which notably also includes two coupled methyl rotors with poorly predicted V_3 barriers and an XIAM fit with a V_{cc} term highly correlated to the V_3 parameters. In their study, the magnitude and sign of XIAM's V_{cc} was confirmed with a BELGI-C_s-2Tops[28] fit in which BELGI's analogous coupling parameter was fitted without correlation. Unfortunately, the fully asymmetric two top version of BELGI needed to fit the *trans* conformer of acetic anhydride has yet to be developed, so a similar comparison between BELGI and XIAM fits cannot be made to confirm the value of V_{cc} in the case of acetic anhydride.

Finally, the majority of carboxylic anhydrides studied by microwave spectroscopy have been observed in the non-planar *cis* conformation including four of the anhydrides in this study. While the structural differences between non-planar *trans* conformers have already been discussed, a similar comparison of non-planar *cis* conformers is warranted. Variations in structure within non-planar *cis* anhydrides arise due to the electronic character of the two anhydride R groups. It is expected that more electron withdrawing R groups, such as trifluoromethyl, would decrease the electron density about the adjacent carbonyl oxygen while electron donating groups, such as *t*-butyl, would have the opposite effect. This variance in electron density about carbonyl oxygens in anhydrides likely

impacts the degree of repulsion between carbonyls in *cis* anhydrides, though an energy decomposition analysis would be an interesting study into this interaction. The overall electronic character of the R groups on anhydride structure can be quantified by the through space dihedral angle between the carbonyl groups in which greater carbonyl dihedral angles indicate greater repulsion. The predicted carbonyl dihedral angles for all predicted non-planar *cis* anhydride conformations are shown in Table 3.13. Theoretical dihedral angles are compared here because experimental values have only been determined for pivalic and pivalic trifluoroacetic anhydride. Note again that the Kraitchman analyses of both of these molecules have shown wonderful agreement between experimental and theoretical structures. As can be seen in Table 3.13, the two highly electron withdrawing trifluoromethyl groups of trifluoroacetic anhydride result in the smallest dihedral angle, while the two highly electron donating *t*-butyl groups of pivalic anhydride produce the largest angle. The predicted dihedral angles of the remaining anhydrides lie between these two extrema and are in good agreement with the expected trend in carbonyl dihedral values which is predicted by the different combinations of electron donating and withdrawing R groups.

Table 3.13 Theoretical Carbonyl Dihedral Angles in Non-Planar *cis* Conformers

R_1	Electronic Character	R_2	Electronic Character	C=O Dihedral [deg] M06-2X	C=O Dihedral [deg] MP2
$-CF_3$	e^- withdrawing	$-CF_3$	e^- withdrawing	32.6	40.1
$-CF_3$	e^- withdrawing	$-CH_3$	e^- donating	39.5	44.6
$-CF_3$	e^- withdrawing	$-C_6H_5$	e^- donating	40.4	47.5
$-CF_3$	e^- withdrawing	$-C(CH_3)_3$	e^- donating	43.0	50.3
$-CH_3$	e^- donating	$-CH_3$	e^- donating	52.3[a]	50.7[a]
$-CH_3$	e^- donating	$-C(CH_3)_3$	e^- donating	56.2	54.9
$-C(CH_3)_3$	e^- donating	$-C(CH_3)_3$	e^- donating	57.8	57.0

(a) Acetic anhydride's non-planar *cis* conformation was observed in previous electron diffraction studies.

The jet-cooled microwave experiments reported here are expected to access only the lowest energy forms of the anhydrides studied, and we note that conformers of only slightly higher energy have been identified for some systems. Thus, observations at higher temperatures are, in many cases, likely to be influenced by the presence of two or more conformers. That said, the results of this study, combined with those of several others

already in the literature, provide a glimpse of the conformational complexity accessible to carboxylic acid anhydrides. All systems studied have a local potential energy minimum at nonplanar *cis* geometry. Regarding the lowest energy configurations, however, planar *trans* configurations allow for intramolecular hydrogen bonding and represent the global minimum, as demonstrated by the planar structures of formic[1-3] and formic acetic anhydrides.[4,5] In the absence of at least one formic hydrogen, however, the planarity is sacrificed, presumably due to steric effects of bulkier groups. The alpha methyl hydrogens of acetic anhydride still support a *trans* configuration, albeit a nonplanar one. Bulkier groups such as CF_3 or $C(CH_3)_3$ appear to drive a transition to a global minimum with a nonplanar *cis* geometry, with the nonplanarity plausibly arising due to repulsion of the carbonyl oxygens. An exception noted in this study is the case of acetic difluoroacetic anhydride in which CF_2H hydrogen is a sufficiently strong hydrogen bond donor to stabilize a nonplanar *trans* structure. Only in cases of ring-locked anhydrides such as maleic[10] and phthalic[11] anhydrides, are the *cis* structures planar.

Conclusion

The microwave spectra of six carboxylic anhydrides have been measured and assigned. Non-planar *cis* structures were predicted for all anhydrides, and CH_3 $trans^{90}$ and CH_3 $trans^{120}$ conformers were additionally predicted for acetic, acetic trifluoroacetic, acetic pivalic, and acetic difluoroacetic anhydride (as well as the CF_2H $trans^{90}$ conformer for acetic difluoroacetic anhydride). A generalized *trans* conformer was observed for acetic anhydride, the CF_2H $trans^{90}$ conformer was observed for acetic difluoroacetic anhydride, and the non-planar *cis* conformer was observed for the remaining four anhydrides. A nearly complete experimental determination of the structure of the heavy atom skeleton was performed for pivalic trifluoroacetic anhydride through a Kraitchman analysis. Irregularities in the energy profiles of methyl rotation were calculated for the CH_3 $trans^{90}$ and CH_3 $trans^{120}$ conformers of the acetic anhydrides. Partial agreement between the CH_3 $trans^{90}$ and CH_3 $trans^{120}$ conformers of acetic anhydride indicate that the observed transitions may have been the result of vibrational averaging between these two conformers. Furthermore, variations in structure across non-planar *cis* and *trans* conformers of carboxylic anhydrides were investigated with respect to the electronic

character of different R groups. The differences between non-planar *cis* conformers of different anhydrides are possibly due to varying degrees of repulsion between carbonyl groups based on the electronic impact of their R groups, though this effect could be better analyzed with energy decomposition studies. Finally, a set of guidelines is given for predicting what conformers are possible for any given carboxylic anhydride based on its R groups.

Acknowledgements

This work was supported by the National Science Foundation (Grant No. CHE 1563324) and the Minnesota Supercomputing Institute.

Chapter 4: A Microwave and Computational Study of Carboxylic Acid Anhydride Monohydrates: A Competition between Intermolecular Interactions

Overview

The microwave spectra of the monohydrates of trifluoroacetic, pivalic, and pivalic trifluoroacetic anhydrides, have been recorded. Theoretical structures have been predicted using B3LYP, M06-2X, and MP2 calculations with 6-311++G(nd,np)$_{n=1-3}$ basis sets. While only one conformer was predicted for the trifluoroacetic and pivalic anhydride water complexes, two conformers were predicted for the mixed pivalic trifluoroacetic anhydride monohydrate in which water interacts with either side of the molecule. The various computational methods disagreed as to which conformer was the global minimum for the mixed anhydride monohydrate, but a comparison of experimental and theoretical constants clearly indicates which conformer was observed. Water tunneling states were observed for the for some isotopologues of pivalic and the mixed anhydride's monohydrates, but not for the water complex with trifluoroacetic anhydride. Lastly, the impact of the varying carboxylic anhydride R group electronic effects was analyzed with respect to the intermolecular interactions directing water complexation.

Introduction

The analysis of gas phase molecular clusters consisting of pre-reactive species provides an interesting insight into the intermolecular interactions governing systems that would otherwise readily undergo chemical change in the bulk phase. Through the application of microwave spectroscopy and computational analysis, pre-reactive complexes and their resulting products have been analyzed for proton transfer,[1-6] hydrolysis and hydration,[6-16] and pericyclic[17-21] reactions for example. Information gained from these studies includes but is not limited to reaction energetics, the minimum number of solvent molecules needed to facilitate chemical change, relative orientation of moieties, and the types of intermolecular interactions that bind complexes together. The chemical media of interest in this study are carboxylic acid anhydrides which are well known to readily react with water to produce two equivalents of carboxylic acids through bulk phase hydrolysis according to the following balanced chemical equation:

$$RCOOCOR + H_2O \rightleftharpoons 2\,RCOOH \qquad (2)$$

While the above equation is balanced by one equivalent of water, the hydrolysis of a carboxylic anhydride by one molecule of water is highly unlikely to proceed in the gas phase without the stabilizing effects of bulk phase solvation. However, analyzing the stepwise solvation of carboxylic anhydrides with water could provide further context as to how the first water molecule interacts with the anhydride as well as what is the minimum number of water molecules needed to facilitate gas phase hydrolysis.

In gas phase complexes, water has been observed to behave as either a hydrogen bond acceptor, a hydrogen bond donor, or a nucleophile interacting with an electrophilic center. The versatility of water's ability to interact sets up a competition when complexing with molecules that feature multiple interaction sites. For example, the trifluoroacetic acid monohydrate features an electrophilic carbonyl carbon and a carbonyl oxygen capable of accepting a hydrogen bond, but the water molecule is only observed to interact with trifluoroacetic acid's hydrogen bond donating hydroxyl group.[8] In the monohydrate of acetic sulfuric anhydride, which features all three interaction sites, water was observed to

behave as both a hydrogen bond donor and acceptor but did not interact with the electrophilic carbonyl carbon.[16] In comparison to these two cases, carboxylic anhydrides feature both an electrophilic center and a hydrogen bond acceptor but lack an acidic hydrogen.

In this study, the dominant intermolecular interaction by a single water molecule in the complexation to various carboxylic anhydrides will be assessed using microwave spectroscopy supported with computational analysis. The anhydrides studied include trifluoroacetic anhydride (TFAA), pivalic anhydride (PiA), and pivalic trifluoroacetic anhydride (PiTFAA), the latter of which is an asymmetrical, mixed anhydride that features both the trifluoromethyl and *t*-butyl R groups of TFAA and PiA respectively. These R groups with opposite electronic character have been specifically chosen so that their electronic impact on the hydration of acid anhydrides can be analyzed. The trifluoromethyl groups of TFAA improve the electrophilicity of the carbonyl carbons and decrease the hydrogen bond accepting ability of the carbonyl oxygens, whereas the opposite is true for the electron donating *t*-butyl groups of PiA. The complexation of water to PiTFAA sets the stage for an interesting competition between the two halves of the mixed anhydride featuring R groups with opposing electronic effects. The central focus of this study is to determine what intermolecular interactions are dominant in a complex formed between a single water molecule and a carboxylic anhydride with varying electronic properties.

Experimental Methods and Results

TFAA Monohydrate

TFAA with 99% purity was obtained from Sigma Aldrich. The sample was pulsed into our system as a 0.9% Ar–TFAA gas mixture through a stainless steel conical nozzle whose configuration is described elsewhere.[21] Water was introduced by bubbling argon through a glass bubbler at a stagnation pressure of 0.6 atm and flowing the resulting Ar–H_2O mixture through a stainless steel hypodermic needle with an inner diameter of 0.016 inches in the direction of the supersonic expansion. Chirped-pulse spectra were initially collected from 6-18 GHz consisting of 400,000 averaged free induction decays (FIDs) using our tandem chirped-pulse[22] and cavity[23] microwave spectrometer.[24,25] A beta version of the

DAPPERS program[26] was used to assign three distinct progressions of transitions. The peaks in these progressions were each comprised of two *b*-type and two *c*-type transitions that were near-degenerate and unresolvable with the resolution of our instrument resulting in summed intensities. The fit of the three combined progressions was sufficient in predicting the remaining *a*, *b*, and *c*-type transitions, which were subsequently measured with the more sensitive cavity method. D_2O and DHO species were easily located using shifted rotational constants based on the relationship between the experimental and predicted constants from the parent monohydrate. Note that deuterium hyperfine was too collapsed to resolve for all isotopologues of the three anhydride monohydrates. The fitted spectroscopic parameters for all TFAA monohydrate isotopologues are shown in Table 4.1.

Table 4.1 Spectroscopic Constants of the TFAA Monohydrate[a]

	TFAA-H_2O	*TFAA-DOH*	*TFAA-D_2O*
A (MHz)	1154.259850(88)	1132.72180(38)	1109.34712(12)
B (MHz)	397.74570(14)	397.48644(32)	395.87442(10)
C (MHz)	366.55343(13)	364.05003(26)	362.008800(97)
Δ_J (kHz)	0.01686(55)	0.0161(15)	0.01820(39)
Δ_{JK} (kHz)	0.1196(36)	0.1530(43)	0.16400(93)
Δ_K (kHz)	0.1622(33)	0.1260(60)	0.1320(16)
δ_J (kHz)	-0.00060(19)	[-0.00060]	[-0.00060]
δ_K (kHz)	0.131(53)	[0.131]	[0.131]
N	174 (117)[b]	94 (37)[b]	129 (59)[b]
no. of a-type	22	2	9
no. of b-type	90	47	62
no. of c-type	62	39	58
RMS (kHz)	2.7	5.3	2.1

(a) Distortion constants in square brackets are fixed to those of the parent.
(b) Numbers in parenthesis denotes number of distinct frequencies

PiA Monohydrate

PiA of 99% purity was purchased from Sigma Aldrich. PiA is a solid at room temperature and has a much lower vapor pressure than TFAA, so an alternate method of introduction to the vacuum system was required. Argon was flowed at a pressure of 0.6 atm over 1 mL of PiA stored in a heated reservoir a short distance away from the pulse nozzle. The

reservoir was heated to 60 °C which was the optimized temperature for signal intensity. The resulting Ar–PiA mixture was then passed through a stainless-steel needle with an inner diameter of 0.020 inches. Water was introduced into the system by flowing argon through a glass water bubbler at a stagnation pressure of 1.3 atm and pulsing the resulting Ar–H_2O mixture into the vacuum system through a stainless-steel cone nozzle.

Chirped-pulse spectra were collected in three segments from 9-18 GHz with 200,000 averaged FIDs in each segment. Only four PiA–H_2O complex peaks were measured in the chirped-pulse spectra due to relatively low signal intensity. The principles of the DAPPERS assignment algorithm were applied to these four transitions, and 47 additional *a* and *b*-type transitions were discovered using the cavity method. All observed transitions were split closely into two states with peaks in an approximate 3:1 intensity ratio. The existence of such states is common in water complexes and arises due to the possibility of an interchange between the two water hydrogens via rotation of the water moiety. D_2O and DHO species were easily located using shifted rotational constants based on the relationship between the experimental and predicted constants from the parent monohydrate. Observed spectroscopic constants for all isotopologues and states for the PiA monohydrate are shown in Table 4.2.

Table 4.2 Spectroscopic Constants of the PiA Monohydrate[a]

	PiA-H_2O: State A	*PiA-H_2O: State B*	*PiA-DOH*	*PiA-D_2O*
A (MHz)	974.02978(27)	974.0414(20)	962.1560(18)	944.38142(90)
B (MHz)	436.558625(28)	436.55925(15)	436.48724(11)	435.194433(62)
C (MHz)	370.190169(28)	370.191533(74)	368.590488(73)	364.656374(42)
Δ_J (kHz)	0.015380(89)	0.01590(28)	0.01426(41)	0.01438(21)
Δ_{JK} (kHz)	0.1614(25)	0.163(10)	0.169(19)	0.1893(62)
Δ_K (kHz)	0.1375(58)	0.245(64)	[0.1375]	[0.1375]
δ_K (kHz)	0.0279(40)	-	0.036(17)	0.0431(59)
N	28	19	18	29
no. of a-type	10	6	11	22
no. of b-type	18	13	7	7
RMS (kHz)	0.7	1.0	0.6	0.8

(a) Distortion constants in square brackets are fixed to those of the parent.

PiTFAA Monohydrate

PiTFAA was readily synthesized according to a literature procedure[27] in which 7 ml (50 mmol) of TFAA was added to 10 ml (50 mmol) of PiA and mixed thoroughly overnight. Approximately 1 mL of the resulting mixture was placed in the reservoir and introduced to the system under the same pressure conditions as pivalic anhydride without any heating. Water was introduced into the system under the same conditions used with PiA. Chirped-pulse spectra were collected from 6-9 GHz with 250,000 averaged free induction decays. Numerous *a*-type K_p = 0, 1, and 2 transitions present in this region of the chirped-pulse spectra were fit together and subsequently used to find the remaining 70 transitions split into two distinct states of both *a* and *b*-type transitions. Two states were also observed for the D_2O complex but not for the DHO complex as expected. The relative signal intensity between states again showed an approximate 3:1 ratio for both the PiTFAA–H_2O and PiTFAA–D_2O complexes. The observed $9_{2\,8} \leftarrow 8_{2\,7}$ transitions for the PiA and PiTFAA H_2O and D_2O complexes are shown in Figure 4.1. Note that the aforementioned 3:1 ratio between states is warped in Figure 4.1 as the intensity is in the squared representation and proximity to cavity tuning frequencies impacts line intensity. Table 4.3 shows the assigned spectroscopic constants for all PiTFAA monohydrate isotopologues and states. Assigned transitions, frequencies, and residuals for all three measured monohydrates and their isotopologues are included in Appendix D.

(see Figure 4.1 and Table 4.3 on the following pages)

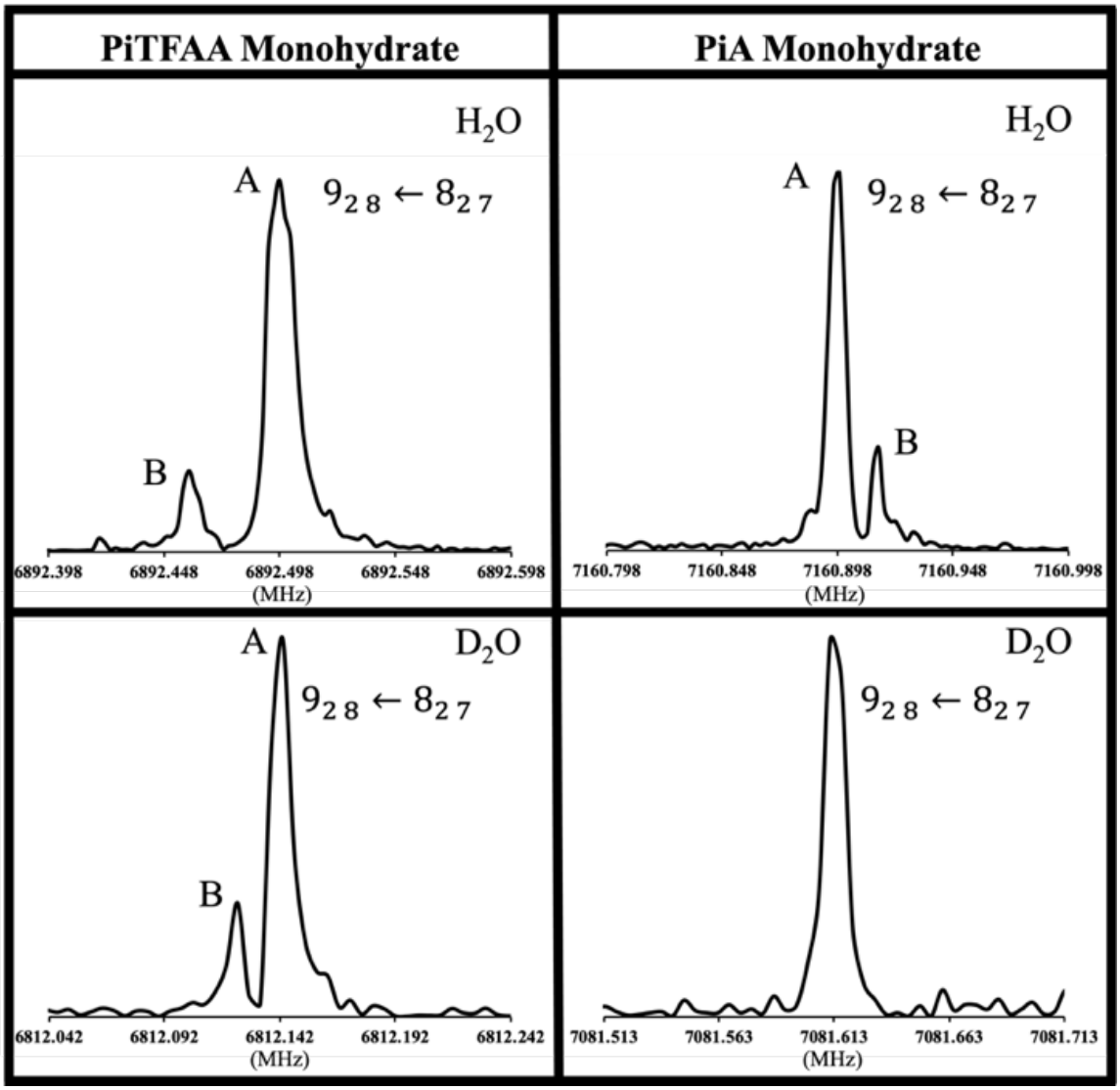

Figure 4.1 Excerpts of Various Monohydrate Cavity Spectra
200 kHz sections of cavity spectra for the $9_{2\,8} \leftarrow 8_{2\,7}$ transition of PiTFAA–H_2O, PiTFAA-D_2O, PiA–H_2O, and PiA–D_2O. The observed water tunneling states are labelled A and B, but no states were observed for PiA–D_2O. Note that The splitting between the PiTFAA–H_2O states are twice as large as the PiTFAA–D_2O isotopologue (which was true for all transitions in the PiTFAA monohydrate spectrum), and the PiA–H_2O splitting is much smaller than the PiTFAA–H_2O splitting. Assuming the D_2O decrease in splitting between water tunneling states observed for PiTFAA is true for PiA, it is possible that the PiA–D_2O states were not resolvable given the smaller splitting between the water tunneling states of the PiA monohydrates.

Table 4.3 Spectroscopic Constants of the PiTFAA Monohydrate[a]

	PiTFAA-H_2O: State A	*PiTFAA-H_2O: State B*	*PiTFAA-DOH*	*PiTFAA-D_2O: State A*	*PiTFAA-D_2O: State B*
A (MHz)	1017.21048(24)	1017.2221(27)	1002.5104(14)	977.5360(12)	977.5303(19)
B (MHz)	414.94690(15)	414.959623(76)	414.73946(14)	413.438665(59)	413.437079(88)
C (MHz)	358.321562(89)	358.31070(10)	356.284532(68)	352.521556(56)	352.52093(10)
Δ_J (kHz)	0.01524(57)	0.01761(59)	0.01454(42)	0.01633(38)	0.01695(48)
Δ_{JK} (kHz)	0.2259(32)	0.2297(74)	0.2288(84)	0.2374(32)	0.2386(69)
Δ_K (kHz)	0.1114(51)	0.133(48)	[0.1114]	[0.1114]	[0.133]
δ_J (kHz)	-0.00124(32)	-	-0.00129(27)	[-0.00124]	-
δ_K (kHz)	0.067(13)	0.136(15)	0.083(10)	0.1147(80)	[0.136]
N	41 (39)[b]	29 (27)[b]	21	30	18
no. of a-type	29	21	17	25	17
no. of b-type	12	8	4	5	1
RMS (kHz)	1.8	1.8	0.5	1.0	1.3

(a) Distortion constants in square brackets are fixed to those of the parent.
(b) Numbers in parenthesis denotes number of distinct frequencies

Computational Methods and Results

The structures of the TFAA–H_2O, PiA–H_2O, and two conformers of PiTFAA–H_2O were predicted with the Gaussian16 suite of programs[28] using B3LYP, M06-2X, and MP2 calculations, each with 6-311++G(d,p), 6-311++G(2d,2p), and 6-311++G(3d,3p) basis sets. The MP2/6-311++G(3d,3p) optimization for PiA–H_2O was the only calculation that was unable to complete despite multiple attempts with several extended days of run time. The structures of TFAA–H_2O, PiA–H_2O, and both conformers of PiTFAA–H_2O are shown and labelled in Figure 4.2. Dashed lines are included to highlight the hydrogen bonding and nucleophilic association interaction sites in each complex.

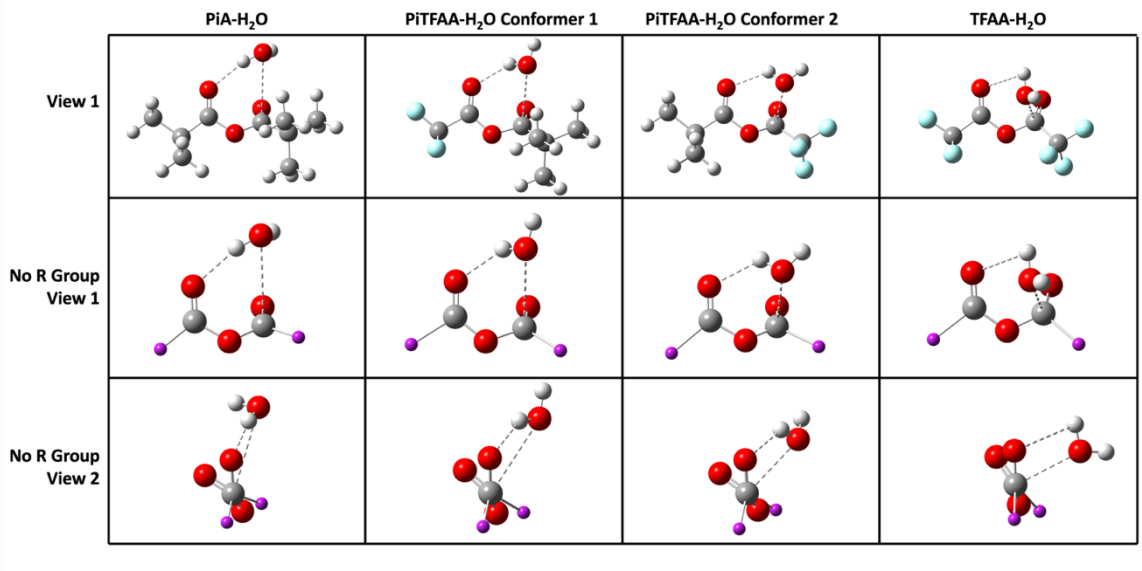

Figure 4.2 Computational Structures of Carboxylic Anhydride Monohydrates
Predicted monohydrate structures from MP2/6-311++G(d,p) calculations whose rotational constants were overall closest to the averaged constants. Both conformers of PiTFAA–H_2O are shown here, but only one spectrum was observed. Dashed lines indicate hydrogen bonds and nucleophilic association of the water molecule with the electrophilic carbonyl carbon. See the text for a discussion regarding the relative importance of these two interactions in each of the structures. The complexes in View 1 are aligned relative to the plane of the leftmost carbonyl. View 2 is aligned through the two carbonyl carbons. Decluttered views of the monohydrate structures are shown below with the R groups removed to highlight how water is oriented relative to the O=C–O–C=O backbone.

The rotational constants averaged across all calculations are compared to the observed rotational constants of the anhydride monohydrates in Table 4.4. The variation in predicted rotational constants between the used computational levels is shown for each monohydrate in Figure 4.3. Note that both conformers are included for PiTFAA–H_2O. The Cartesian coordinates of the anhydride monohydrate structures predicted with MP2/6-311++G(d,p) calculations (the closest constants to the averaged rotational constants overall) are included in Appendix D. Anecdotally, the structures of these anhydrides change very little upon water complexation relative to the structures of their free monomers.

Table 4.4 Comparison of Experimental and Average Predicted Rotational Constants

		Experimental	*Average Computational*[a]	*% Diff.*
TFAA–H_2O	*A* (MHz)	1154.259850(88)	1176 (±40)	1.78
	B (MHz)	397.74570(14)	398 (±2)	0.03
	C (MHz)	366.55343(13)	369 (±5)	0.61
PiA–H_2O	*A* (MHz)	974.02978(27)	992 (±50)	1.80
	B (MHz)	436.558625(28)	441 (±10)	0.97
	C (MHz)	370.190169(28)	376 (±13)	1.44
PiTFAA–H_2O: Conformer 1	*A* (MHz)	1017.21048(24)	1033 (±51)	1.59
	B (MHz)	414.94690(15)	414 (±3)	0.02
	C (MHz)	358.321562(89)	361 (±8)	0.62
PiTFAA–H_2O: Conformer 2	*A* (MHz)	1017.21048(24)	1128(±45)	10.86
	B (MHz)	414.94690(15)	416 (±2)	0.23
	C (MHz)	358.321562(89)	377 (±6)	5.09

(a) Numbers in parenthesis are standard deviations. See Figure 4.3 for a graphical representation of the total variance in predicted rotational constants across the methods used.

Relative total energy and zero point corrected (ZPE) energies were calculated for both PiTFAA conformers, though the identity of the minimum energy conformer is inconclusive across the calculations applied in this study. B3LYP and MP2 calculations predict Conformer 1 to be lower in energy, while M06-2X predict Conformer 2 to be lower in energy. However, all calculations agree that both conformers are relatively close in energy being within only 1 kcal/mol of each other. A summary of these results is presented in Table 4.5.

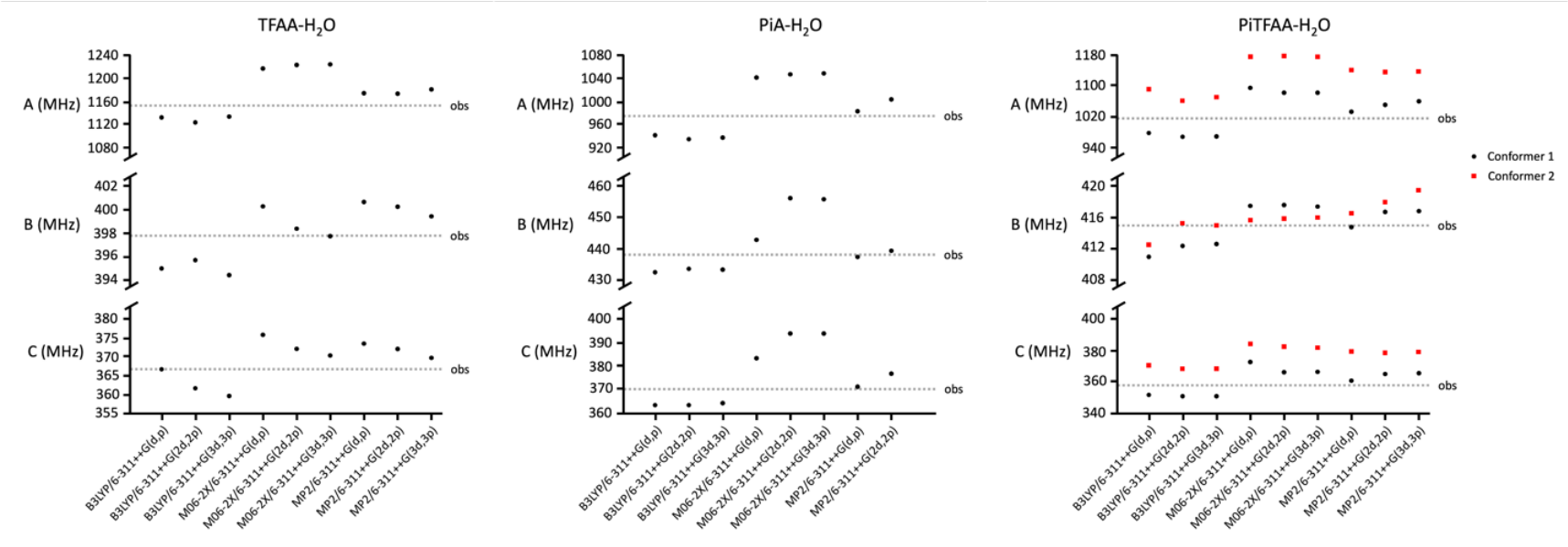

Figure 4.3 Variance in Rotational Constants Predicted with Different Methods

A comparison of the rotational constants predicted from each computational method for each anhydride respectively. The observed constants are represented by the dotted lines. Note that both conformers of PiTFAA–H_2O are included.

Table 4.5 Comparison of the Energies for the Two Conformers of PiTFAA–H_2O

		Conformer 1		Conformer 2	
		Rel. Energy (kcal/mol)	*Rel. ZPE*[a] (kcal/mol)	*Rel. Energy* (kcal/mol)	*Rel. ZPE*[a] (kcal/mol)
B3LYP	*6-311++G(d,p)*	0.000	0.000	0.606	0.739
	6-311++G(2d,2p)	0.000	0.000	0.553	0.699
	6-311++G(3d,3p)	0.000	0.000	0.447	0.641
M06-2X	*6-311++G(d,p)*	0.676	0.504	0.000	0.000
	6-311++G(2d,2p)	0.641	0.478	0.000	0.000
	6-311++G(3d,3p)	0.625	0.511	0.000	0.000
MP2	*6-311++G(d,p)*	0.000	0.000	0.023	0.213
	6-311++G(2d,2p)	0.000	0.000	0.105	0.386
	6-311++G(3d,3p)	0.000	0.000	0.070	0.328

(a) ZPE stands for Zero Point corrected Energy

As previously mentioned, D_2O and DHO isotopologues were observed for each of the anhydrides. In order to determine whether the C=O···DOH or C=O···HOD isotopologue was observed, the averaged rotational constants were scaled for both isotopologues and compared to the corresponding observed constants as shown in Table 4.6. Note that the DOH isotopologue features hydrogen bonding with the deuterium and the HOD features hydrogen bonding with the hydrogen. The results in Table 4.6 would indicate that the DOH isotopologue was observed for each anhydride monohydrate based on very slightly better agreement between predicted and observed constants. This result is generally expected for DOH vs. HOD isotopologues.

Table 4.6 Comparison of DOH and HOD Monohydrate Rotational Constants

			C=O---DOH		C=O---HOD	
		Experimental (MHz)	*Predicted*[a] *(MHz)*	*% Diff.*	*Predicted*[a] *(MHz)*	*% Diff.*
TFAA	*A*	1132.72180(38)	1132.115	0.05	1131.069	0.15
	B	397.48644(32)	397.443	0.01	365.931	0.39
	C	364.05003(26)	364.259	-0.06	364.212	-0.04
PiTFAA Conf 1	*A*	1002.5104(14)	1002.459	0.01	993.195	0.93
	B	414.73946(14)	414.750	0.00	413.566	0.28
	C	356.284532(68)	356.140	0.04	354.514	0.50
PiA	*A*	962.1560(18)	960.858	0.13	956.569	0.58
	B	436.48724(11)	436.395	0.02	435.259	0.28
	C	368.590488(73)	368.217	0.10	366.819	0.48

(a) The predicted rotational constants in this table are the isotopologue rotational constants averaged across the used computational methods scaled by the ratio between the parent observed and averaged rotational constants shown in Table 4.4

Discussion

The *t*-butyl and trifluoromethyl anhydride R groups in this study have been specifically chosen due to their opposite electronic character for the purpose of studying their impact on anhydride-water complexation. A *t*-butyl group is electron donating which should increase the hydrogen bonding ability of an attached carbonyl oxygen as well as stabilize the partial positive charge on the carbonyl carbon thereby decreasing its relative electrophilicity. The highly electron withdrawing trifluoromethyl group has the exact opposite effects on an attached carbonyl by decreasing the hydrogen bonding ability of the oxygen and increasing the electrophilicity of the carbon. Therefore, PiA is expected to show strong hydrogen bonding and poor nucleophilic association, while TFAA is expected to show poor hydrogen bonding and strong nucleophilic association. The mixed anhydride, PiTFAA, features both R groups which sets up an interesting competition between the possible intermolecular interactions with water. Note also that these carboxylic anhydrides do not contain hydrogen bond donor sites.

In order to determine which intermolecular interaction is dominant in these water complexes, two sets of structural parameters have been used to gauge the prominence of both types of interaction. As shown in Figure 4.4, the degree of nucleophilic association has been gauged by the distance between water's oxygen and the carbonyl's carbon (r_{NA}) as well as the angle of nucleophilic attack (ϕ_{NA}). Note that the Bürgi-Dunitz trajectory defines the ideal ϕ_{NA} value as 107°.[29] For hydrogen bonding, the distance (r_{HB}) and angle (ϕ_{HB}) of the hydrogen bond have been used for the degree of the hydrogen bonding interaction. Table 4.7 shows these structural parameters averaged across each of the computational methods used.

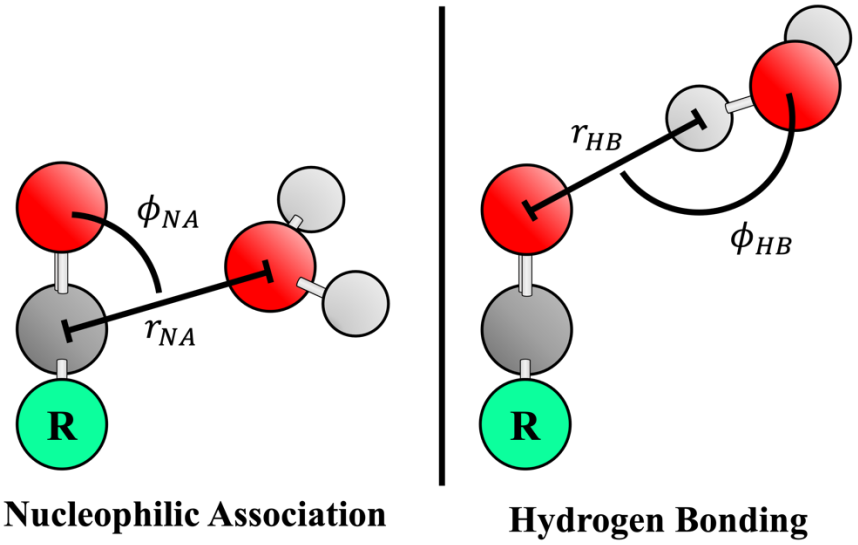

Figure 4.4 Structural Parameters of Intermolecular Interaction
Pictural representations of the parameters used to gauge the relative strength of the nucleophilic association and hydrogen bonding intermolecular interactions in the anhydride monohydrates.

Table 4.7 Hydrogen Bonding and Nucleophilic Association Structural Parameters[a]

	PiA–H_2O	PiTFAA–H_2O Conformer 1	PiTFAA–H_2O Conformer 2	TFAA–H_2O
r_{HB} (Å)	2.00	2.07	2.12	2.63
ϕ_{HB}(deg)	164.5°	150.7°	138.4°	99.3°
r_{NA} (Å)	3.16	3.09	2.71	2.65
ϕ_{NA}(deg)	79.1°	82.5°	96.0°	98.7°

(a) Values in this table are the averaged values across all used levels of theory

Beginning with PiA–H_2O, we see that it has the shortest and most linear hydrogen bond with r_{HB} and ϕ_{HB} values of 2.00 Å and 164.5° respectively. Conversely, PiA–H_2O has the largest r_{NA} (3.16 Å) and the furthest ϕ_{NA} from the ideal Bürgi-Dunitz trajectory value of 107°. These results indicate that the PiA–H_2O is bound primarily by hydrogen bonding with minimal nucleophilic association as expected. Moving to TFAA–H_2O, we see that it has the worst hydrogen bond (r_{HB} = 2.63 Å and ϕ_{HB} = 99.3°), but the shortest r_{NA} (2.65 Å) and a ϕ_{NA} value of 98.7° which is the closest angle to 107° of the anhydride monohydrates in this study. Therefore, we conclude that the TFAA–H_2O complex is dominated by the nucleophilic association interaction and displays little to no hydrogen bonding as expected.

This competition between hydrogen bonding and nucleophilic association is particularly pronounced in the mixed anhydride and is likely the cause of the ambiguity among theoretical methods in Table 4.5 as to which conformer is lowest in energy.

Before analyzing the intermolecular interactions in the PiTFAA–H_2O complex, we must first investigate its two conformers whose structures are shown in Figure 4.2. In Conformer 1, water is oriented to hydrogen bond with the trifluoromethyl side carbonyl oxygen and nucleophilically associate with the *t*-butyl side carbonyl carbon. Oppositely, water hydrogen bonds with the *t*-butyl side carbonyl oxygen and nucleophilically associates with the trifluoromethyl side carbonyl carbon in Conformer 2. According to chemical intuition, we would expect the hydrogen bond and the nucleophilic association interactions to be stronger in Conformer 2 because the electron donating *t*-butyl group should increase the hydrogen bonding ability of the adjacent carbonyl oxygen and the trifluoromethyl group should increase the electrophilicity of the adjacent carbonyl carbon (as previously noted). However, the averaged structural parameters in Table 4.7 actually indicate that the hydrogen bond is stronger in Conformer 1 as it has a shorter and more linear hydrogen bond. Note also that the hydrogen bond in Conformer 1 is predicted to be slightly weaker than that of PiA–H_2O. This deviation from chemical intuition may be the result of less prominent interactions in the complex such as a possible very weak hydrogen bond between water's oxygen and a *t*-butyl methyl hydrogen. In line with chemical intuition, the nucleophilic association interaction is still predicted to be stronger in Conformer 2, though it has a slightly longer r_{NA} and the ϕ_{NA} is further from 107° than TFAA–H_2O. Therefore, it would appear that the intermolecular interactions present in PiTFAA–H_2O Conformer 1 more closely resemble those of PiA-H_2O while those in PiTFAA–H_2O Conformer 2 are more similar to those in TFAA–H_2O.

As shown in Table 4.5, there is some disagreement between computational methods as to which conformer is the global minimum. B3LYP calculations predict Conformer 1 to be lower in energy by around 0.6 kcal/mol, while M06-2X predicts Conformer 2 to be lower in energy by approximately the same. MP2 calculations predict Conformer 1 to be lower in energy by a trivial amount (~0.1 kcal/mol). Given the small conformational energy

differences, we could not definitively say which of these two conformers is the global minimum even if the computational methods were in agreement. However, a comparison of the predicted constants from both conformers to the fitted rotational constants clearly indicates that Conformer 1 was observed. As shown in Table 4.5, the percent differences between the fitted and averaged predicted rotational constants are all less than 2% for Conformer 1, while those of Conformer 2 differ more significantly overall. Additionally, the rotational constants' percent differences of the TFAA and PiA analogues are quite similar to those of Conformer 1 for *A*, *B*, and *C* respectively. This not only indicates that Conformer 1 was observed, but that the use of these averaged rotational constants is consistent for carboxylic anhydride monohydrate systems.

A second piece of evidence for the observation of Conformer 1 is the predicted dipole moments. The average predicted *a*, *b*, and *c* dipole moments of Conformer 1 are 2.25, 1.36 and 0.63 Debye respectively, while the predicted values for Conformer 2 are 3.20, 0.86, and 0.25 Debye. Both *a*- and *b*-type transitions were observed which is expected from both conformers, however the transitions from both spectral types measured were relatively similar in intensity. If Conformer 2 was observed, we would expect a more significant difference in signal intensity between the *a*-type and *b*-type transitions than what was observed. No *c*-type transitions were measured even after extensive signal averaging. It is worth noting that a significant amount of signal averaging and frequency scanning was employed in hopes of observing a second PiTFAA monohydrate conformer, but no additional peaks were discovered.

Conclusion

The microwave spectra of three carboxylic acid anhydride monohydrates as well as their D_2O and DOH isotopologues have been observed and assigned. Two water tunneling states with approximately 3:1 intensity ratios were observed for PiTFAA–H_2O, PiTFAA–D_2O, and PiA–H_2O. Two conformers were predicted for the PiTFAA monohydrate, though only one conformer was observed. While chemical intuition predicted Conformer 2 of PiTFAA–H_2O is better suited for both hydrogen bonding and nucleophilic association, the theoretical structural parameters indicate that Conformer 1 has the better hydrogen bond

(but still the lesser nucleophilic association). Upon analysis of the computed structures, it was determined that nucleophilic association was the primary intermolecular interaction in the TFAA monohydrate, while the PiA and PiTFAA monohydrates were primarily bound by hydrogen bonding.

Acknowledgements

This work was supported by the National Science Foundation (Grant No. CHE 1563324) and the Minnesota Supercomputing Institute.

Chapter 5: A Microwave and Computational Study of Pivalic Sulfuric Anhydride and the Pivalic Acid Monomer: Mechanistic Insights into the RCOOH + SO_3 Reaction

Adapted with permission from Nathan Love, Casey A. Carpenter, Anna K. Huff, Christopher J. Douglas, and K. R. Leopold.

Submitted to *J. Phys. Chem. A.*

July 11, 2022

Overview

The microwave spectrum of pivalic sulfuric anhydride, $(CH_3)_3CCOOSO_2OH$ (PivSA), has been observed by rotational spectroscopy. The compound was formed by reaction of SO_3 with $(CH_3)_3CCOOH$ (pivalic acid) in a supersonic jet in a manner analogous to that previously observed with other carboxylic acids. Computational analysis indicates that the reaction is best described as a pericyclic process coupled with a 60 degree rotation of the *t*-butyl group. Product formation can occur through either a sequential (two-step) or a concerted (one-step) pathway. The former involves an internal rotation of the *t*-butyl group through a 0.11 kcal/mol barrier followed by the pericyclic reaction that joins the moieties. The latter passes through a second order saddle point in which the internal rotation and pericyclic reaction occur simultaneously. This path is the most energetically favorable, as the zero-point corrected energy at the saddle point structure is 0.16 kcal/mol *below* that of a putative $(CH_3)_3CCOOH$-SO_3 precursor complex. Additional computational work involving a series of carboxylic acids is reported which explores the effects of gas phase acidity and basicity of the RCOOH reactant on reaction energetics. These calculations, together with prior experimental and theoretical studies of the acetic and trifluoroacetic derivatives, demonstrate that the basicity of the carbonyl oxygen, not the acidity of the COOH proton, is the important driving factor for the reaction. As a precursor to the experimental work on the title molecule, microwave spectra of the parent and OD forms of the pivalic acid monomer were recorded and are reported here as well. A convenient synthesis of SO_3 is also described.

Introduction

Previous work in our laboratory has shown that carboxylic sulfuric anhydrides (CSAs) can be readily formed through a low-to-no barrier pericyclic reaction between a carboxylic acid (RCOOH) and SO_3,[1-5] viz.,

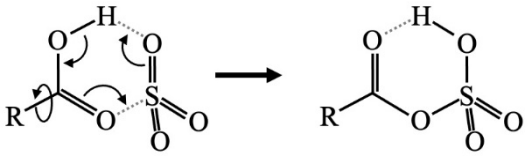

(1)

In cases where the R group of the carboxylic acid is a three-fold rotor such as in acetic or trifluoroacetic acid (R = CH_3, CF_3), the orientation of the rotor relative to the carboxyl moiety differs between that in the complex and that in the product. Thus, reaction (1) for these species is accompanied by an additional 60 degree rotation of the R group. As a result, the potential energy surfaces for these systems have both a pair of transition states corresponding to the internal rotation and the pericyclic reaction, as well as a second order saddle point corresponding to a concerted process in which the internal rotation and pericyclic reaction occur concurrently.

For most of the CSAs studied to date, the barriers to product formation relative to the putative precursor complexes are small and, in some cases, negative. For instance, the zero-point corrected barriers for R = H, *s-cis* H_2C=CH, and HC≡C are 0.26, −0.22, and 0.01 kcal/mol at the CCSD(T)/CBS(D-T)//M06-2X/6-311++G(3df,3pd) level of theory. For R = CH_3, the sequential and concerted transition state energies are 0.057 kcal/mol and −0.12 kcal/mol, respectively, at the same level of theory. In contrast, however, the zero-point corrected barriers to formation of the trifluoroacetic acid derivative, CF_3COOSO_2OH, through either the sequential or concerted pathways are considerably higher than those of the other previously studied CSAs (1.17 and 1.21 kcal/mol, respectively). This result is consistent with our experimental observation that signal strengths for trifluoroacetic sulfuric anhydride were notably lower than those for the other anhydrides studied, though dipole moment components may also have played a role. The reason for the heightened zero-point corrected barrier to the formation of the trifluoroacetic acid derivative is unclear but could be due to (i) the mass effects associated

with the 60 degree rotation of the relatively massive trifluoromethyl group and/or (ii) the electronic effects of the trifluoromethyl group on the activation barrier for the pericyclic reaction. A direct comparison between R = CH_3 and R = CF_3 does not address this question because the methyl group of acetic acid is both a light rotor and electron donating, while the CF_3 group in the trifluoroacetic acid is both more massive and highly electron withdrawing.

In this work, we report a computational and microwave study of pivalic sulfuric anhydride (PivSA) which was formed in a supersonic jet from pivalic acid, $(CH_3)_3CCOOH$, and SO_3. While the CF_3 and $C(CH_3)_3$ groups are similar in their mass distribution, they are quite different electronically, with the former being electron withdrawing and the latter being electron donating. Acetic and pivalic acids, however, are more similar in their electronic character but differ significantly in the mass of the rotor. Thus, a comparison of the reactions of SO_3 with acetic, trifluoroacetic, and pivalic acids should help to further explore the energetics of CSA formation. This goal is further supported by computations, also presented here, which explore the gas phase acidity and basicity of a series of carboxylic acids that have been observed to react with SO_3. Microwave spectra of the parent and OD forms of the pivalic acid monomer were also obtained in preparation for this work and are reported here as well, as is a convenient laboratory preparation of SO_3.

Computational Methods and Results

Geometry and frequency calculations were performed at the M06-2X/6-311++G(3df,3pd) level of theory using the Gaussian16 suite of programs.[6] The predicted structures and atomic numbering for the pivalic acid–SO_3 complex as well as that of the anhydride product are shown in Figure 5.1. Calculations were also performed on the pivalic acid monomer. Atomic Cartesian coordinates for all minimum energy structures (precursor, anhydride, and monomer) are given in Appendix E. For all species studied, the calculated minimum energies were improved with single-point CCSD(T) calculations at the M06-2X/6-311++G(3df,3pd) geometries using the complete basis set extrapolation scheme of Neese and Valeev between the ANO-pVDZ and ANO-pVTZ basis sets (CBS(D-T)).[7]

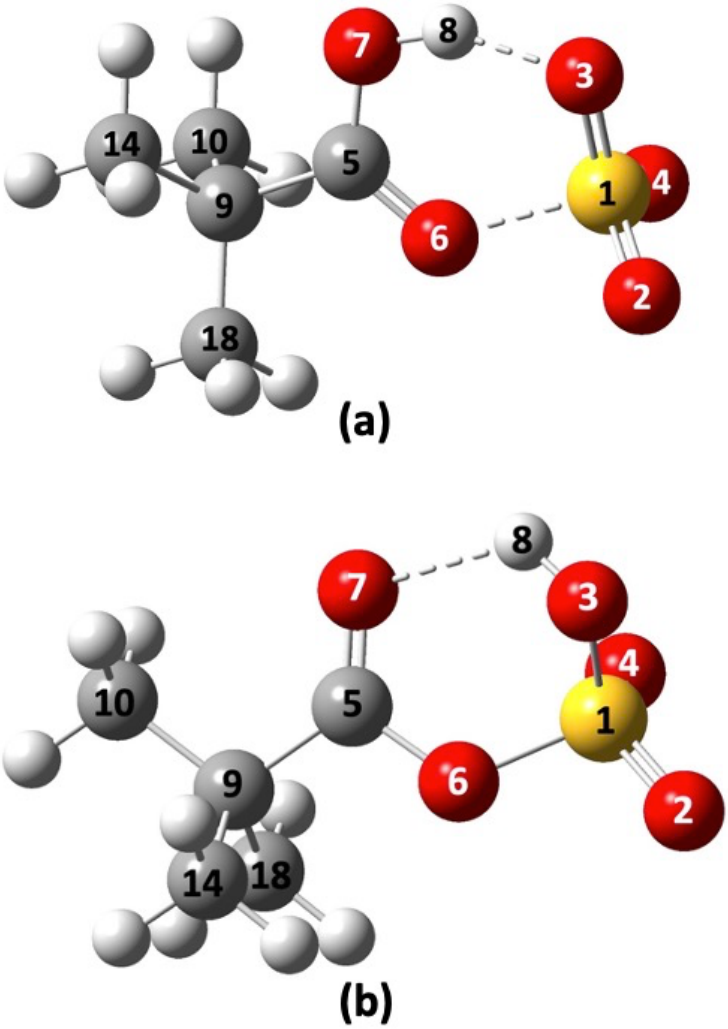

Figure 5.1 Computational Structures of PivSA and its Precursor Complex
Predicted structures of (a) the pivalic acid-SO_3 complex and (b) PivSA determined from geometry calculations at the M06-2X/6 311++G(3df,3pd) level of theory. In (a), the dotted lines represent the hydrogen bond and a nucleophilic association interaction. In (b), the dotted line represents an intramolecular hydrogen bond.

Zero-point energy corrections were applied using M06-2X/6-311++G(3df,3pd) frequencies. These levels of theory were chosen to be consistent with our previous CSA studies.[1-5] Table 5.1 summarizes the important results of the calculations and includes analogous results for the acetic and trifluoroacetic acid systems for comparison. Figure 5.2 displays the calculated energies of the precursor complex and the anhydride product (labeled I and V, respectively) relative to that of the isolated free monomers. After zero-point corrections, the precursor complex and the anhydride lie 17.1 and 20.4 kcal/mol, respectively, lower in energy than the sum of the energies of the free monomers.

Table 5.1 Theoretical Results for Pivalic Sulfuric Anhydride

	Free Acid	Precursor Complex	Anhydride
ΔE relative to free monomers (kcal/mol)			
pivalic	–	−18.6 (−17.1)	−22.1 (−20.4)
acetic	–	−17.2 (−15.7)	−20.7 (−18.9)
trifluoroacetic	–	−11.5 (−10.2)	−16.2 (−14.4)
V_3 (kcal/mol)[b]			
pivalic	0.73 (0.74)	0.11 (0.05)	1.15 (1.23)
acetic	0.44 (0.36)	0.11 (0.06)	0.65[c] (0.53)
trifluoroacetic	0.64 (0.62)	0.38 (0.35)	0.78 (0.77)
R(S1-O6) (Å)			
pivalic	–	1.903	1.621
acetic	–	1.932	1.626
trifluoroacetic	–	2.148	1.648
Overall Sequential Pathway Barrier (kcal/mol)[d]			
pivalic	–	1.67 (0.05)[e]	
acetic	–	1.89 (0.06)[e]	
trifluoroacetic	–	3.29 (1.17)	
Concerted Pathway Barrier (kcal/mol)[d]			
pivalic	–	2.08 (−0.16)	
acetic	–	2.10 (−0.12)	
trifluoroacetic	–	3.39 (1.21)	

(a) Values determined at the CCSD(T)/CBS(D-T)//M06-2X/6-311++G(3df,3pd) level of theory as described in the text. Values in parentheses include zero-point corrections using M06-2X/6-311++G(3df,3pd) frequencies. Values for the acetic and trifluoroacetic acid derivatives are from references 2, 4, and 5.
(b) V_3 is the potential barrier for internal rotation of the CX_3 group (X = H, F, or CH_3).
(c) Experimental value is 0.68932(9) kcal/mol (reference 2).
(d) The sequential pathway for the formation of PivSA proceeds through structures II and III in Figure 5.2. The concerted pathway proceeds through structure IV in Figure 5.2, which is a second order saddle point. Acetic and trifluoroacetic species proceed through analogous structures for both pathways.
(e) For the pivalic and acetic species, the 60 degree rotation transition in the sequential pathway determines the barrier after zero-point energy corrections (rather than the pericyclic transition state, which determines the barrier without zero-point corrections). Thus, the 1.67 and 1.89 kcal/mol barriers arise from the pericyclic transition state (III) without zero-point corrections. With zero-point corrections, the barrier (0.05 or 0.06 kcal/mol) is due to internal rotation. For the trifluoroacetic species, the pericyclic transition state has the highest energy, with or without zero-point corrections and determines the barrier in either case.

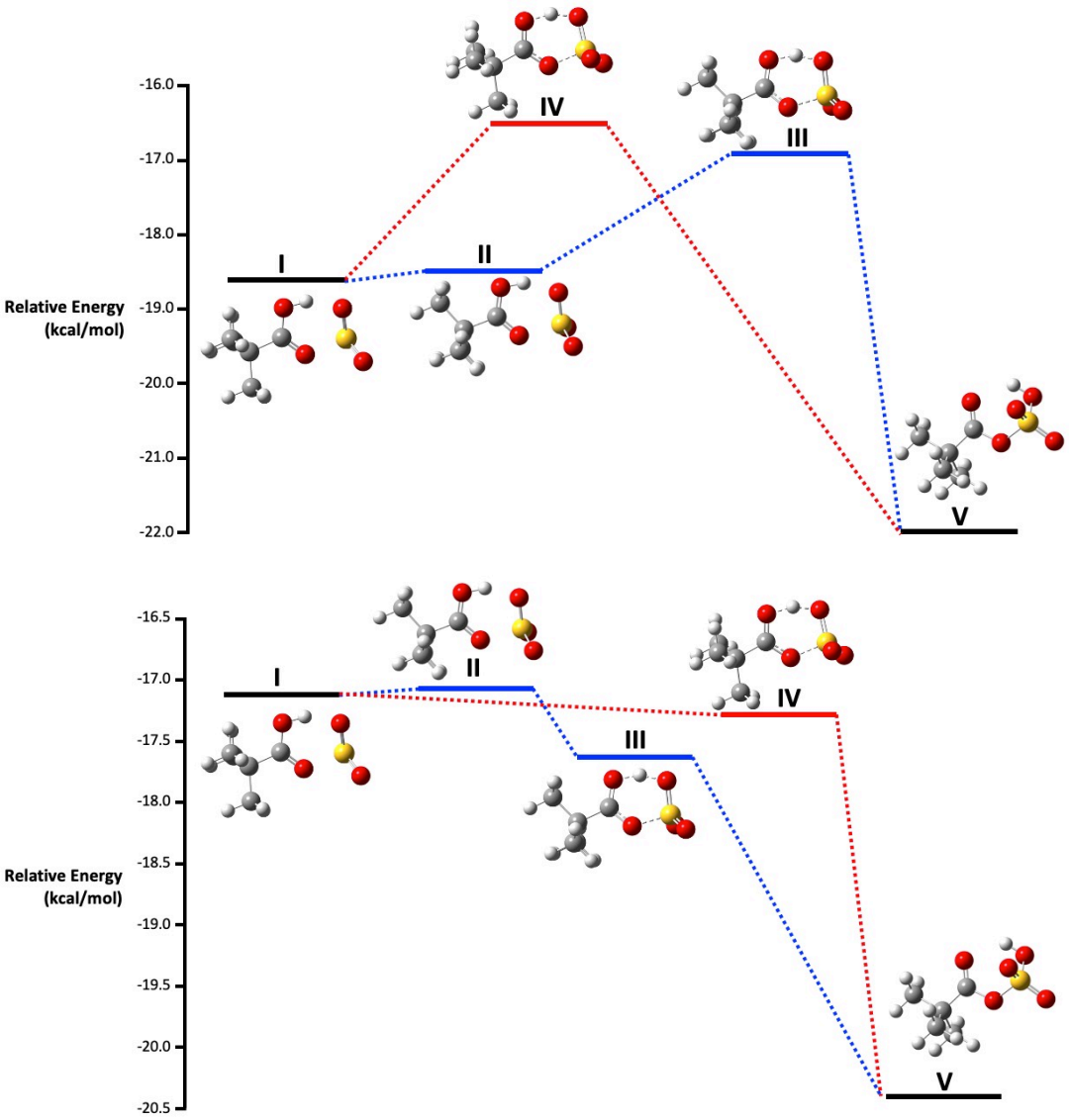

Figure 5.2 Potential Energy Surface of PivSA Formation
The potential energy surface of the formation of PivSA (V) starting from the pivalic acid-SO_3 precursor complex (I). The sequential pathway in which a 60 degree rotation of the *t*-butyl group precedes the pericyclic transition state is represented in blue and passes through structures II and III. The red pathway represents the concerted pathway in which structure IV is the second order saddle point. (a) CCSD(T)/CBS(D-T)//M06-2X/6-311++G(3df,3pd) electronic energies uncorrected for zero-point energy. The sequential and concerted barriers to formation are 1.56 and 2.08 kcal/mol respectively. (b) CCSD(T)/CBS(D-T)//M06-2X/6-311++G(3df,3pd) electronic energies corrected for zero-point energy. The sequential and concerted barriers to formation are −0.05 and −0.16 kcal/mol respectively.

Inspection of the calculated structures reveals that the transition between the precursor complex and the anhydride involves a 60 degree rotation of the *t*-butyl group. Specifically,

in both species, the in-plane methyl group is nearly eclipsed with the carbonyl oxygen, with torsional angles of 14 degrees and 4 degrees for the precursor complex and anhydride, respectively. However, since reaction (1) converts the OH oxygen to the C=O oxygen, the rotation must take place to maintain the near-eclipsed orientation. A similar rotation has been noted for the reactions with acetic[2] and trifluoroacetic[4] acids. The three-fold barrier to internal rotation of the *t*-butyl group with respect to the O7-C5-O6 plane was calculated by imposing a 60 degree rotation of the former and subsequently searching for a transition state at the M06-2X/6-311++G(3df,3pd) level. The result was the transition state shown as structure II in Figure 5.2, which, using CCSD(T) energies, lies 0.11 kcal/mol higher in energy than the minimum energy structure before zero-point corrections (0.05 kcal/mol after zero-point corrections). The 0.11 kcal/mol value is the potential barrier for internal rotation and is surprisingly lower than the corresponding value similarly determined for free pivalic acid (0.73 kcal/mol). The internal rotation barriers, V_3, are also given in Table 5.1.

After the rotation of the *t*-butyl group, the barrier for reaching the pericyclic transition state (structure III in Figure 5.2) from the internal rotation transition state was determined to be 1.56 kcal/mol (1.67 kcal/mol from the minimum energy of the precursor complex). However, after zero-point corrections, the energy of structure III is 0.52 kcal/mol *below* that of the precursor. Thus, with zero-point energy taken into account, the only barrier to product formation is the 0.05 kcal/mol due to internal rotation of the *t*-butyl group. Alternatively, a second order saddle point (IV) was found in which the internal rotation and pericyclic reaction occur simultaneously. The barrier for this concerted pathway was calculated to be 2.08 kcal/mol above that of the precursor complex without zero-point corrections, but 0.16 kcal/mol *below* that of the precursor complex when zero-point corrections are applied. Thus, after zero-point corrections, there is no barrier to product formation passing through the saddle point. These results are also shown in Figure 5.2, in which the sequential and concerted pathways are highlighted in blue and red, respectively. The barriers calculated for both pathways are summarized in Table 5.2. Cartesian coordinates for the calculated transition state and saddle point structures are also included in Appendix E.

Table 5.2. Experimental and Theoretical Properties of CSA Precursor Carboxylic Acid Monomers

	Barrier to CSA Formation[a]	Gas Phase Acidity (kcal/mol)		Gas Phase Basicity (kcal/mol)	
R Group	**(kcal/mol)**	***Calc***[b]	***Exp***	***Calc***[b]	***Exp***
CF_3[c]	1.17 (1.21)[d]	315.2	317.4(20)[e]	160.4	162.7[f]
H[g]	0.26	336.5	339.2(15)[h]	169.9	169.8[f]
C≡CH[i]	0.01	326.5		177.2	
CH_3[j]	0.057 (−0.12)[d]	339.4	341.1(20)[f]	180.4	179.9[f]
$CH{=}CH_2$ (s-trans)[k]	−0.22	336.0	337.2(28)[l]	183.7	
$CH{=}CH_2$ (s-cis)[k]	−0.33	336.3		184.6	
$C(CH_3)_3$[m]	0.05 (−0.16)[d]	336.8	338.0(20)	188.9	

(a) CCSD(T)/CBS(D-T)//M06-2X/6-311++G(3df,3pd) energies with zero-point corrections from M06-2X/6-311++G(3df,3pd) frequencies.
(b) Theoretical values obtained from M06-2X/6-311++G(3df,3pd) thermodynamic calculations as described in the text.
(c) Reference 4.
(d) Value outside of parentheses corresponds to the barrier of the sequential pathway of the CF_3, $C(CH_3)_3$, or CH_3 transition state followed by the pericyclic transition state. Value inside the parentheses corresponds to the barrier of the simultaneous pathway in which CF_3, $C(CH_3)_3$, or CH_3 rotation and the pericyclic processes occur simultaneously via a second order saddle point. Values include zero-point corrections.
(e) Reference 10.
(f) Reference 11.
(g) Reference 1.
(h) Reference 12.
(i) Reference 5.
(j) Reference 2.
(k) Reference 3.
(l) Reference 14.
(m) This work.

Because reaction (1) involves both the donation of a carbonyl oxygen lone pair and the transfer of the COOH proton to the SO_3, it is of interest to assess both the acidity of the proton and basicity of the oxygen in order to better understand the effects of the R group on the reaction energetics. The gas phase acidities and basicities are defined in terms of the free energy changes for the following reactions,[8] respectively,

$$RCOOH \rightarrow RCOO^- + H^+ \quad (2)$$

$$RCOOH + H^+ \rightarrow RCOOH_2^+ \quad (3)$$

Reaction (2) provides a measure of the ease with which a proton is donated by the carboxylic acid, with smaller values corresponding to stronger acids. Reaction (3) is a

rough gauge of the basicity of the carbonyl oxygen (though it does not rigorously measure its Lewis basicity toward SO_3). The gas phase basicity is defined as the negative of the free energy change for Reaction (3), with higher values corresponding to stronger bases. The free energy of the hydrogen cation has been calculated to be -0.010012 Hartree assuming the enthalpy as 5/2RT, a temperature of 298.15 K, and using the entropy value of 108.946 J/mol·K.[9] The free energies of the neutral, protonated, and deprotonated carboxylic acids at 298.15 K were determined in Gaussian16 from frequency calculations performed at the M06-2X/6-311++G(3df,3pd) level of theory and subsequently combined with that of the hydrogen cation to determine free energy changes for reactions (2) and (3). The gas phase acidity and basicity of other carboxylic acids observed to form CSAs are listed in Table 5.2 alongside their respective transition barriers to reaction with SO_3 determined from the CCSD(T) calculations. Experimental values are included for comparison where available.[10-14]

Experimental Methods and Results

Preparation of Sulfur Trioxide: SO_3 appears to be no longer commercially available and thus, while it is a known product of the thermal decomposition of $K_2S_2O_8$ or $K_2S_2O_7$,[15,16] the following procedure was employed to produce the compound on a scale appropriate for the experiments performed in this work. To a 1-neck 100 mL round bottom flask equipped with a stir bar and a 14/20 short-path distilling head (Thermometer joint 10/18) with a 25 mL receiving flask, was added P_2O_5 (183 mmol, 52.10 g) and fuming sulfuric acid (20% SO_3) (153 mmol, 15.00 g, 7.79 mL). The distilling flask was heated initially to 90 °C in an oil bath, then raised in 10 °C increments approximately every five minutes. The first collection of clear, colorless liquid was at an oil bath temperature of approximately 135 °C, with thermometer temperature reading approximately 45 °C. The oil bath temperature was gradually raised to 160 °C to continue collection until thermometer temperature decreased by several degrees, and the distillation was then removed from heat. Approximately 9.40 g (117 mmol, 77% yield) of colorless, liquid, sulfur trioxide were collected. A photograph of the apparatus is included in the Appendix E.

All reagents were of reagent grade and used without further purification. Distillation was carried out using flame-dried glassware under a static nitrogen atmosphere, with lightly greased joints additionally sealed with Glindemann PTFE sealing rings. Room temperature water was used in the short path condenser to prevent solid SO_3 from forming and clogging the condenser. The nitrogen line was split, with one end attached to the distilling head and the other attached to a gas inlet into a sealed, 100 ml "dead flask" also equipped with an outlet line. This line was terminated with a ~12 gauge steel needle piercing a septum-stoppered, 500 ml round bottom flask containing ~250 ml of 6 M NaOH aqueous quench solution and equipped with a gas outlet line terminating in an oil bubbler. Prior to beginning the reaction, the distilling head gas line needle was submerged in the aqueous quench so escaping SO_3 gas bubbled through. Rubber septa and Tygon laboratory tubing were used. Warning: Sulfur trioxide reacts violently with water, fumes in ambient atmosphere, degrades most materials except Teflon, and is readily carried by dynamic argon/nitrogen gas resulting in leaking of sealed joints. The freshly distilled reagent is best used immediately for desired reactions. Teflon stopcock sealed Schlenk glassware is recommended for long-term storage of SO_3, which eventually polymerizes[17] but can be liquefied by heating to 40 °C overnight. Melting of solid, polymerized, SO_3 can lead to pressure build-up and should be done in a hood with a blast-shield.

Measurement and Assignment of Microwave Spectra of the Pivalic Acid Monomer: Spectra of the pivalic acid monomer were first measured with our tandem cavity[18] and chirped-pulse[19] spectrometer, details of which have been described elsewhere.[20,21] Experimental uncertainties on measured transition frequencies are estimated to be approximately 3 kHz on the cavity system and 10 kHz on the chirped-pulse spectrometer. Pivalic acid (99% purity, purchased from Sigma-Aldrich) was introduced into the vacuum system by continuously flowing 0.6 atm of argon over a few grams of solid pivalic acid (melting point = 35 °C) to entrain its vapor in the flowing gas. The resulting pivalic acid-argon mixture was injected through a 0.016 in. hypodermic needle along the axis of a pulsed Ar expansion with a stagnation pressure of 1.0 atm. Singly deuterated pivalic acid, $(CH_3)_3CCOOD$, was synthesized according to a literature procedure.[22] The chirped-pulse spectra were initially assigned using DAPPERS,[23] and the higher sensitivity cavity

method was subsequently employed to measure lower intensity transitions for both isotopologues and resolve nuclear hyperfine splitting for OD-pivalic acid. No evidence of internal rotation was observed for either isotopologue.

Spectra were well fit using the Watson A-reduced Hamiltonian in the I^r representation[24] using Pickett's SPFIT program.[25] Only the quartic centrifugal distortion terms were required. For the OD species, deuterium quadrupole coupling constants were also included. Fitted spectroscopic constants are given in Table 5.3 and compared with calculated values. Also included in the table are calculated values of the magnitudes of the dipole moment components, μ_a, μ_b, and μ_c for the parent species. Note that there is good agreement between predicted and fitted rotational constants as highlighted by the percent differences of 1% or less for both isotopologues. Moreover, although not explicitly shown in the table, the predicted isotope shifts of *A*, *B*, and *C* for the OD species were in all within 1.1 MHz of the observed values. Tables of assigned transitions, as well as the residuals from the least squares fits, are included in Appendix E.

Measurement and Assignment of Microwave Spectra of Pivalic Sulfuric Anhydride: To observe the anhydride, SO_3 was introduced into the system by flowing 1.0 atm of argon through a stainless steel bubbler containing freshly synthesized SO_3. The resulting Ar/SO_3 mixture was pulsed into the vacuum chamber through a 0.8 mm diameter stainless steel cone nozzle. The configuration is similar to that previously described.[5] Pivalic acid was introduced in the same manner outlined above. Upon introduction of SO_3 to the system, a new set of intense transitions was immediately observable in the chirped-pulse spectrum, a portion of which is shown in Figure 5.3. After accounting for known transitions of pivalic acid and $Ar{-}SO_3$[26] this new set of transitions was readily attributed to PivSA. The predicted rotational constants were entered into DAPPERS and a fit comprised of only *a*-type transitions was quickly obtained. Based on this fit, the higher sensitivity cavity spectrometer was used to observe several *b*- and *c*-type transitions. As with the pivalic acid monomer, no evidence of internal rotation was observed. The *b*- and *c*-type spectra were significantly weaker than the *a*-types lines, but generally comparable in intensity to each other.

Table 5.3 Spectroscopic Constants of Pivalic Acid

	$(CH_3)_3CCOOH$			$(CH_3)_3CCOOD$		
	Obs. [MHz]	Calc. [MHz]	(Obs.-Calc.)[a] [MHz]	Obs. [MHz]	Calc. [MHz]	(Obs.- Calc.)[a] [MHz]
A [MHz]	3315.00358(21)	3346.7	−31.7 (-1.0%)	3300.61293(65)	3331.4	−30.8 (-0.9%)
B [MHz]	2368.64502(18)	2393.5	−24.9 (-1.0%)	2303.71608(45)	2327.5	−23.8 (-1.0 %)
C [MHz]	1991.08702(15)	2007.8	−16.7 (-0.8%)	1940.11926(44)	1955.8	−15.7 -(0.8%)
Δ_J [kHz]	0.2306(92)			0.236(21)		
Δ_{JK} [kHz]	2.3233(62)			2.139(37)		
Δ_K [kHz]	−2.204(16)			−1.995(44)		
δ_J [kHz]	0.0348(10)			0.0330(71)		
δ_K [kHz]	−5.8238(71)			−5.862(67)		
χ_{aa} [MHz]				0.2545(23)		
$(\chi_{bb}-\chi_{cc})$ [MHz]				0.0380(52)		
N[b]	41			23(65)[c]		
RMS [kHz]	3.9			2.6		
$\lvert\mu_a\rvert$ [D]		0.9				
$\lvert\mu_b\rvert$ [D]		1.5				
$\lvert\mu_c\rvert$ [D]		0.0				

(a) Observed value minus that calculated at the M06-2X/6-311++G(3df,3pd) level of theory. Number in parentheses is the (Obs. – Calc.) expressed as a percent of the observed value.

(b) Number of transitions in the least squares fit.

(c) Number in parenthesis indicates the number of deuterium hyperfine components assigned.

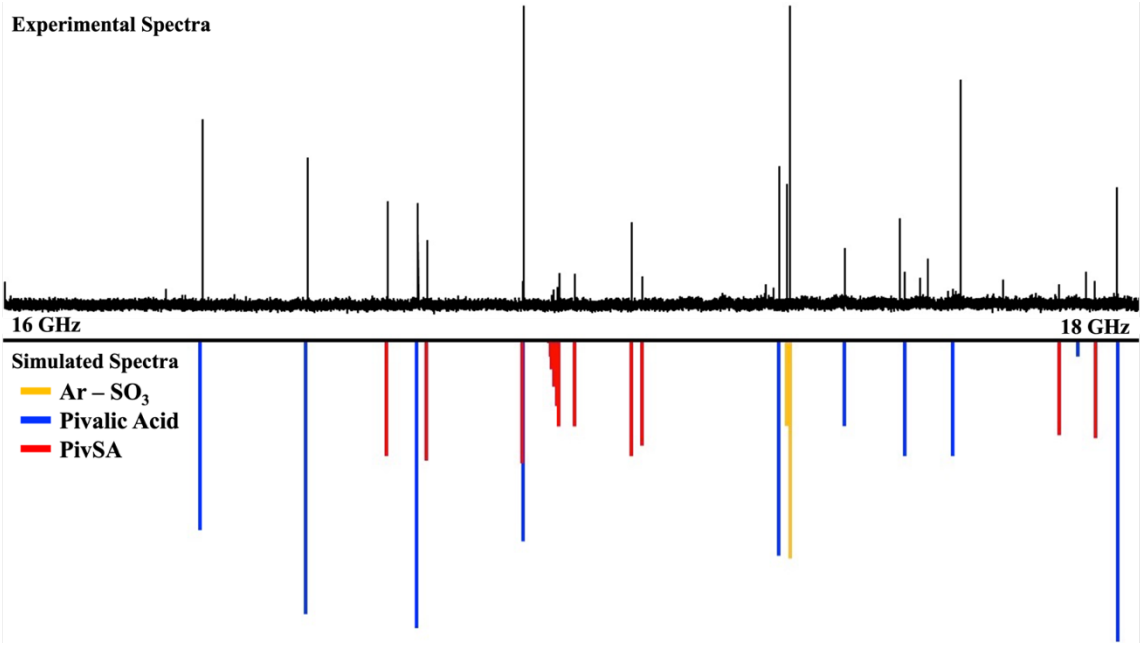

Figure 5.3 Excerpt of the PiVSA Chirped-Pulse Spectrum
The microwave chirped-pulse spectrum of a pivalic acid/SO_3/Ar mixture between 16 and 18 GHz (top), and the calculated spectra of PivSA using fitted constants (bottom). Observed transitions of Ar-SO_3 are also indicated. Note that calculated relative spectral intensities of the three species are not comparable.

The hyperfine splitting in the $(CH_3)_3CCOOD$ spectrum was too collapsed to resolve even with the higher resolution cavity spectrometer. The fitted parameters for the parent, deuterated, and naturally abundant ^{34}S isotopologues are shown in Table 5.4 and all assigned transitions are given in Appendix E. No spectra were observed that could be attributed to the pivalic acid–SO_3 complex (Figure 5.1a).

Table 5.4 Spectroscopic Constants of PivSA

	$(CH_3)_3CCOOSO_2OH$	$(CH_3)_3CCOOSO_2O\mathbf{D}$	$(CH_3)_3CCOO^{\mathbf{34}}SO_2OH$
A [MHz]	1976.53327(37)	1950.673(25)	1976.041(29)
B [MHz]	621.914269(34)	620.35633(13)	617.273994(76)
C [MHz]	589.252788(30)	585.99770(13)	585.060380(81)
Δ_J [kHz]	0.01910(18)	0.01890(40)	0.01738(49)
Δ_{JK} [kHz]	0.0741(29)	0.088(10)	0.084(14)
δ_J [kHz]	0.00115(17)	[0.00115]	[0.00115]
N^a	73	48	22
RMS [kHz]	3.9	3.4	1.3

(a) Number of transitions in the least squares fit.

Discussion

Table 5.5 compares the experimental rotational constants of the parent isotopologue with those calculated for both the anhydride and the precursor complex. It is seen from the table that the calculated constants for the former are in much better agreement with those for the latter, indicating that the observed species is indeed the anhydride. The table also gives the deuterium and ^{34}S isotope shifts in the rotational constants (which most easily enable the isotopic data to distinguish between species) and, again, it is seen that those for the anhydride are in better agreement with experiment than those for the precursor complex. The computationally determined values of the magnitudes of the dipole moment components, μ_a, μ_b, and μ_c are also included. Note that μ_b and μ_c are comparable in magnitude for the anhydride, but differ by a factor of seven for the complex. Thus, while the observation of *c*-type transitions does not rigorously distinguish the precursor from the anhydride (since $\mu_c \neq 0$ in both cases), the similar intensity of the observed *b*- and *c*-type spectra would be expected for the anhydride but not the precursor. Indeed, since the observed *b*-type transitions were themselves rather weak, the 0.1 D value of $|\mu_c|$ of the complex would not be expected to give rise to observable spectra at all. Thus, the observation of *c*-type spectra and their comparable intensities to those of the *b*-type lines further support the conclusion that the anhydride is the species that was observed.

The S1-O6 bond in the precursor complex has a calculated bond length of 1.903 Å (Table 5.1). This is somewhat longer than the S-O(H) single bond in H_2SO_4, 1.574(10) Å,[27] but considerably shorter than the 2.432(3) Å intermolecular sulfur-oxygen bond in $SO_3\cdots OH_2$.[28] Thus, as we have noted for other carboxylic sulfuric anhydrides,[5] the precursor complex is best described as containing a partially formed dative bond of the kind that has been discussed at great length previously.[29,30] Moreover, the −18.6 kcal/mol binding energy of the precursor complex is larger than that of a typical van der Waals interaction but indeed comparable to that of a partially formed dative bond. In contrast, the S1-O6 bond length in the anhydride, 1.621 Å, is almost identical to the S−O(H) bond in sulfuric acid, indicating that it is an “ordinary” covalent single bond. Correspondingly, the −22.1 kcal/mol binding energy reflects further advancement of the sulfur-oxygen partial bond in the precursor complex upon anhydride formation. The significant variation

Table 5.5 Calculated Constants for the Anhydride and Precursor Complex and Comparison with Observed Values

		Anhydride		Precursor	
	Observed	Calculated[a]	(Obs.-Calc.)[b]	Calculated[a]	(Obs.-Calc.)[b]
A [MHz]	1976.53327(37)	1990.5	−14.0 (−0.7%)	2002.3	−25.8 (−1%)
B [MHz]	621.914269(34)	625.8	−3.9 (−0.6%)	580.7	41.3 (7%)
C [MHz]	589.252788(30)	592.8	−3.5 (−0.6%)	551.6	37.6 (6%)
$\lvert\mu_a\rvert$ [D]					
$\lvert\mu_b\rvert$ [D]					
$\lvert\mu_c\rvert$ [D]					
$(CH_3)_3CCOOSO_2OD$					
ΔA [MHz]	−25.86027	−27.1	1.2 (5%)	-23.8	−2.0 (−8%)
ΔB [MHz]	−1.55794	−1.8	0.2 (13%)	-0.1	−1.5 (−94%)
ΔC [MHz]	−3.25509	−3.5	0.2 (7%)	-1.9	−1.4 (−42%)
$(CH_3)_3CCOO^{34}SO_2OH$					
ΔA [MHz]	−0.49227	−0.4	−0.05 (-9%)	−0.1	−0.4 (−80%)
ΔB [MHz]	−4.64027	−4.7	0.03 (0.6%)	−5.1	0.4 (9%)
ΔC [MHz]	−4.19241	−4.2	−0.01 (-0.3%)	−4. 6	0.4 (9%)

(a) Theoretical constants are from M06-2X/6-311++G(3df,3pd) calculations.

(b) Numbers in parentheses are the percent error in the calculation, i.e., 100×(obs.-calc.)/|obs|. The absolute value is taken in the denominator so that a positive percent error on the isotope shifts indicates that the magnitude of the calculated shift exceeds that of the observed shift (both of which are negative).

in the internal rotation barrier of the *t*-butyl group may, in part, reflect changes in electronic structure that accompany the progression from separated monomers to partially bound complex to a *bone fide* chemically bonded molecule.

As noted above and diagrammed in Figure 5.2, the energy barrier starting from the precursor complex is 1.67 kcal/mol for the sequential pathway. This arises from a small (0.11 kcal/mol) internal rotation barrier of the *t*-butyl group followed by an additional 1.56 kcal/mol needed to reach the pericyclic transition state. However, with zero-point energy corrections, the energy of the pericyclic transition state falls *below* that of the precursor complex. This indicates that the only barrier for the sequential process is the small energy associated with the internal rotation. For the concerted pathway, the second order saddle point lies 2.08 kcal/mol higher in energy than the precursor complex without zero-point corrections but is brought to 0.16 kcal/mol *lower* in energy when zero-point corrections are applied. Thus, passing through the saddle point (which incorporates the internal rotation) has no barrier after zero-point corrections and thus represents the most energetically favorable pathway to the product.

It is of interest to compare these results with those for the trifluoroacetic sulfuric anhydride which, as noted in the Introduction, was considerably more difficult to observe than either the pivalic or acetic derivatives. Table 5.1, which also includes analogous results for the acetic acid reaction, shows that, in contrast to the pivalic acid reaction, both the sequential and concerted processes for trifluoroacetic acid have positive barriers whether or not zero-point energy corrections are included. Indeed, it is seen that, of the three systems, the trifluoroacetic acid reaction is the only one for which the pericyclic transition state represents the activation barrier, even after zero-point corrections. It is interesting to note that the moment of inertia of the CF_3 group about its pseudo-C_3 axis (88 amu·Å^2) is similar to that of the *t*-butyl group in PivSA (111 amu·Å^2). However, the internal rotation barrier in the precursor complex is somewhat larger for trifluoroacetic acid (0.38 kcal/mol vs. 0.11 kcal/mol for pivalic acid). Since it is not necessarily clear whether these differences play a significant role in the difference between their respective reactions with SO_3, a simple comparison of pivalic and trifluoracetic acids is inconclusive. However, as also

seen in Table 5.1, the barriers for both the sequential and concerted pathways in the acetic acid reaction, for which the moment of inertia of the rotor is only ~3 amu·Å^2, are very similar to those of the pivalic acid reaction, even after zero-point energy is taken into account. Since methyl and *t*-butyl groups are both electron releasing while the trifluoromethyl group is electron withdrawing, this suggests that the electronic character of the R group influences the overall barriers to product formation and that the requisite internal rotation plays less of a role. Zero-point energy is a crucial factor but has a much more significant effect on the pericyclic transition states than it does on the internal rotation barriers. In light of these observations, the remaining focus of the discussion will be on the impact of electronic properties of the R group of the carboxylic acid on the reaction energetics.

Although in previous work we have loosely described reaction (1) as a cycloaddition, it more closely resembles a pericyclic hetero-ene reaction, as there is a net gain of one sigma bond and a net loss of one pi bond.[31] Such an identification allows for further depth of understanding of the reaction mechanism. Figure 5.4 depicts the rearrangement of electrons and bonds that occurs when the reaction takes place for any carboxylic acid (i.e., any R group).

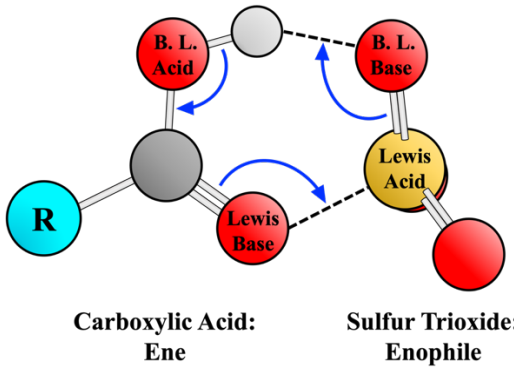

Figure 5.4 Hetero-ene Transition State for RCOOH + SO_3
The structure of a generalized hetero-ene transition state between a carboxylic acid as the ene and SO_3 as the enophile. The blue arrows highlight the movement of electrons that occurs in the hetero-ene transition state. As a part of the hetero-ene reaction, the carboxylic acid behaves simultaneously as a Brønsted-Lowry acid and Lewis base. Accordingly, the hydroxyl oxygen which acts as the Brønsted-Lowry acid is labeled "B.L. Acid" and the sulfur oxygen which acts as the Brønsted-Lowry base is labeled "B.L. Base". The sulfur atom is labeled as "Lewis Acid" and the carbonyl oxygen is labeled as "Lewis Base".

It can be seen from the figure that the carboxylic acid simultaneously behaves as both a Brønsted-Lowry acid by donating a proton to an SO_3 oxygen, and a Lewis base by donating electrons to the electrophilic SO_3 sulfur. In general, electron withdrawing R groups are expected to increase the relative Brønsted-Lowry acidity and decrease the relative Lewis basicity of carboxylic acids, while electron donating R groups have the opposite effects. Thus, electronic effects related to R set up a competition between factors that influence the energetics of the hetero-ene transition state.

The calculated acidities and basicities in Table 5.2 provide rough quantitative measures that help elucidate the relative importance of these two conflicting effects. From the table, it is seen that the barrier to CSA formation is largest when the gas phase acidity value of the carboxylic acid is smallest (i.e., the acid is strongest). In other words, stronger Brønsted-Lowry acids, such as trifluoroacetic acid, do not necessarily correspond to lower activation barriers. This trend would indicate that the ability of a carboxylic acid to behave as a proton donor is relatively unimportant to the hetero-ene transition state. In contrast, the CSA formation barrier appears to decrease as the gas phase basicity of the carboxylic acid increases. These results suggest, therefore, that the hetero-ene reaction to form a CSA is driven primarily by the ability of a carboxylic acid to donate a lone electron pair to the sulfur. The energies of the anhydride products relative to those of the free monomers follow the same trend, with the magnitude of ΔE in Table 5.1 ordered such that $R = CF_3 < CH_3 < C(CH_3)_3$.

Conclusion

Microwave spectra of the pivalic acid monomer and its reaction product with SO_3 (pivalic sulfuric anhydride, PivSA) have been measured and assigned. Sequential and concerted reaction pathways involving a 60 degree rotation of the carboxylic R group and a hetero-ene transition state were determined computationally for the formation of PivSA from the pivalic acid – SO_3 precursor complex. Pivalic acid was specifically chosen for this study due to the similar mass distribution and dissimilar electronic effects of its *t*-butyl R group compared with those of a trifluoromethyl group. A comparison between PivSA and its acetic and trifluoroacetic acid analogs shows that the 60 degree rotation of the *t*-butyl or

CF_3 group that accompanies product formation minimally impacts the reaction energetics, whereas the electronic effects related to the carboxylic R group drive the barrier height and the overall energy change for the reaction. The impact of electronic effects on the hetero-ene transition state has been further examined through the use of gas phase acidity and basicity calculations which show the reaction is more favorable for carboxylic acids that are weaker Brønsted-Lowry acids and stronger Lewis bases. In other words, the basicity of the carbonyl oxygen is more important than the acidity of the COOH group. Additionally, a convenient medium-to-large scale synthesis of SO_3 has been documented, as the compound has become more difficult to obtain commercially.

Acknowledgements

This work was supported by the National Science Foundation (Grant No. CHE 1953528) and the Minnesota Supercomputing Institute.

Chapter 6: Proton Transfer in a Bare Superacid–Amine Complex: A Microwave and Computational Study of Trimethylammonium Triflate

Adapted with permission from Nathan Love, Anna K. Huff and K. R. Leopold.
J. Phys. Chem. A. **2021**, *125*, pp. 5061-5068.

Overview

The complex formed from trimethylamine ($(CH_3)_3N$) and trifluoromethanesulfonic acid (triflic acid, CF_3SO_3H) has been observed by Fourier transform microwave spectroscopy in a supersonic jet. Spectroscopic data, most notably ^{14}N nuclear quadrupole coupling constants, are combined with computational results at several levels of theory to unambiguously demonstrate complete or near-complete proton transfer from the triflic acid to the trimethylamine upon complexation. Thus, the system is best regarded as a trimethylammonium triflate ion pair in the gas phase. The formation of an isolated ion pair in a 1:1 complex of a Brønsted acid and base is unusual and likely arises due to the strong acidity of triflic acid. Simple energetic arguments based on proton affinities and the Coulomb interaction energy can be used to rationalize this result.

Introduction

Proton transfer is a simple and ubiquitous chemical reaction whose influence spans industrial to atmospheric to biological chemistry. Most proton transfer events in these arenas occur in the solution phase, and an interesting question concerns the role of solvation in facilitating the process. Cluster science has long sought to examine this question in the context of small molecular clusters, whose "solvation numbers" range from zero to "several". The majority of these studies indicate that for Brønsted acid–base pairs that readily undergo proton transfer under bulk conditions the corresponding bare molecular complexes fail to do so and are best described as hydrogen-bonded systems.[1]

Numerous techniques have been brought to bear on the question of proton transfer in isolated acid–base complexes, with amine–hydrogen halide systems playing a prototypical role. These include, but are not limited to, early cluster beam experiments,[2,3] negative ion photoelectron spectroscopy,[4,5] and numerous *ab initio* and density functional theory studies.[6-16] Most closely related to this work is a classic series of microwave studies by Legon and co-workers which has brought into particularly sharp focus the differences between proton transfer in clusters and condensed phase.[17] Using amine–hydrogen halide complexes as prototypes, these workers used indicators such as ^{14}N nuclear quadrupole coupling and centrifugal distortion constants to assess whether the $R_3NH^+X^-$ ion pair exists in an isolated complex. The quadrupole coupling tensor depends on the electric field gradient at the nucleus arising from all extra-nuclear charges and is therefore acutely sensitive to the electronic environment at the ^{14}N nucleus. Because the electronic environment at the nitrogen nucleus becomes more symmetrical when R_3N is transformed into R_3NH^+, the quadrupole coupling constants tend toward zero, rendering them useful probes of proton transfer. While the bulk phase reaction of $R_3N(g)$ and HX readily form crystalline $R_3NH^+X^-(s)$, complexes involving NH_3 were found to be hydrogen-bonded systems, e.g., $H_3N\cdots HX$. For trimethylamine, only the strongest acids, HBr and HI, formed complexes which were best described as ion pairs. The effect of adding one HF molecule to the gas phase $H_3N\cdots HF$ complex to form $H_3N\cdots(HF)_2$ has also been explored by rotational spectroscopy, with the result that the added HF drives the system in the direction of proton transfer but does not induce gas phase ion pair formation.[18]

Collectively, these results speak to the importance of both acid strength and local environment in determining whether or not proton transfer will take place.

Microwave studies involving complexes of HNO_3 with NH_3[19] and trimethylamine[20] (TMA = $(CH_3)_3N$) have also been reported. For these systems, the degree of proton transfer was again gauged by differences in the $H^{14}NO_3$ nuclear quadrupole tensor upon complexation with the result that in the TMA complex the proton transfer is ~62% complete. The ^{14}N coupling tensor for the TMA, however, suggests a degree of proton transfer of only 31%, underscoring that the "degree" of proton transfer is defined only by the method used to measure it. Nevertheless, various measures of proton transfer, including bond distance and calculated infrared frequencies, paint a similar picture. Hydrated complexes of other strong acids, e.g., HNO_3–$(H_2O)_{n=1-3}$,[21-23] HCl–$(H_2O)_{n=1,2}$,[24,25] $(HCl)_2$–H_2O,[26] HBr–$(H_2O)_{n=1,2}$,[27,28] and HI–H_2O,[29] have also been studied by microwave methods with an eye toward exploring the effect of hydration and microsolvation on proton transfer. A more extensive set of references, including those to both calculations and other types of experiments, may be found in reference 1.

In this paper, we further explore the influence of acidity on proton transfer in the gas phase. To do so, we report a microwave and computational study of the complex formed from TMA and the "superacid" triflic acid (trifluoromethanesulfonic acid, CF_3SO_3H). Superacids are compounds with a higher (more negative) Hammett acidity function (H_0)[30] than pure sulfuric acid ($H_0 = -12$) or for which the chemical potential of the acidic proton is greater than that of pure sulfuric acid.[31-33] Triflic acid is one of the most readily available superacids, with reports of its H_0 value in the −13.7 to −14.1 range,[32,34] thus making it about 100 times more acidic than sulfuric acid.[34] Though highly corrosive, it is a relatively safe superacid to work with and finds numerous applications in synthetic chemistry.[32,35]

Experimental Methods and Results

Spectra were taken on a pulsed-nozzle Fourier transform microwave spectrometer[36,37] with broadband (chirped-pulse)[38] and high-resolution (cavity)[39] capabilities. Transitions in the broadband and high-resolution systems were measured to accuracies of 12 and 3 kHz, respectively. To prepare the complex, a 0.5% mixture of TMA in argon was pulsed into

the system at a stagnation pressure of 1.0 atm through a 0.8 mm diameter stainless steel cone nozzle. Triflic acid was introduced into the system by entraining the acid vapor in a 0.6 atm argon flow over an ~1.5 mL sample contained in a reservoir a short distance away from the nozzle. The resulting triflic acid/Ar mixture was then injected into the expanding gas plume through a 0.016 in. ID stainless steel needle that was inserted into the cone nozzle, as described previously.[40,41] The formation of the trimethylammonium triflate ion pair occurred during the on-the-fly mixing of the triflic acid/Ar and TMA/Ar gas mixtures, as evidenced by the resulting spectra and by the formation of small, yellowish crystals around the end of the stainless steel needle.

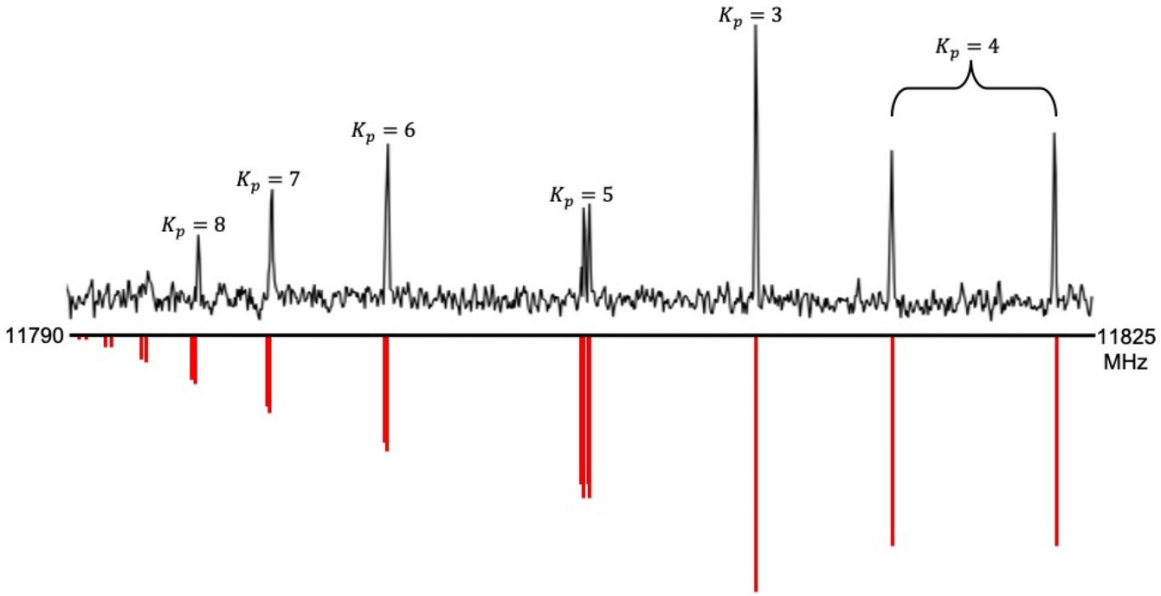

Figure 6.1 Excerpt of the $(CH_3)_3NH^+ \cdot OSO_2CF_3$ Chirped-Pulse Rotational Spectrum
A portion of the chirped-pulse microwave spectrum of trimethylammonium triflate resulting from the average of 40,000 free induction decay signals, each collected for 20 μs. The final fitted hyperfine frequencies are shown below as a stick spectrum. The transitions are all members of a pair of $J = 12 \leftarrow 11$ *a*-type transitions with the same K_p value (e.g., $12_{5,7} \leftarrow 11_{5,6}$ and $12_{5,8} \leftarrow 11_{5,7}$) whose splitting decreases as K_p increases. For K_p = 6–8, the two transitions are near perfectly overlapped. For K_p values in the 3–5 range, the individual transitions are resolvable with the chirped-pulse method. The second member of the $K_p = 3$ pair appears at a frequency higher than 11825 MHz.

A broadband spectrum was initially collected in 3 GHz segments between 6 and 18 GHz. A portion of the spectrum is shown in Figure 6.1. Because of the small ^{14}N nuclear hyperfine constants and the relatively high J levels accessed, the nuclear hyperfine structure was not resolvable at this stage, but a preliminary analysis using approximate line centers was, nevertheless, possible. Initial assignments were readily obtained in under

3 min using the DAPPERS package[42] which was able to assign and fit 26 R-branch *a*-type transitions with $K_p \leq 2$ between $J = 6$ and 16 by using a semirigid rotor Hamiltonian. The resulting constants were highly predictive of the remaining 419 *a*- and *b*-type rotation-hyperfine transitions that were subsequently observed and measured with the cavity system. The *a*-type transitions were typically ~20–30 times stronger than the *b*-type lines. A few searches were conducted for predicted *c*-type transitions, but none were observed. However, this was expected given the small value of μ_c (0.2 D, see next section) and the signal-to-noise ratios obtained for the *a*- and *b*-type lines. A representative cavity spectrum with resolved ^{14}N hyperfine structure is shown in Figure 6.2.

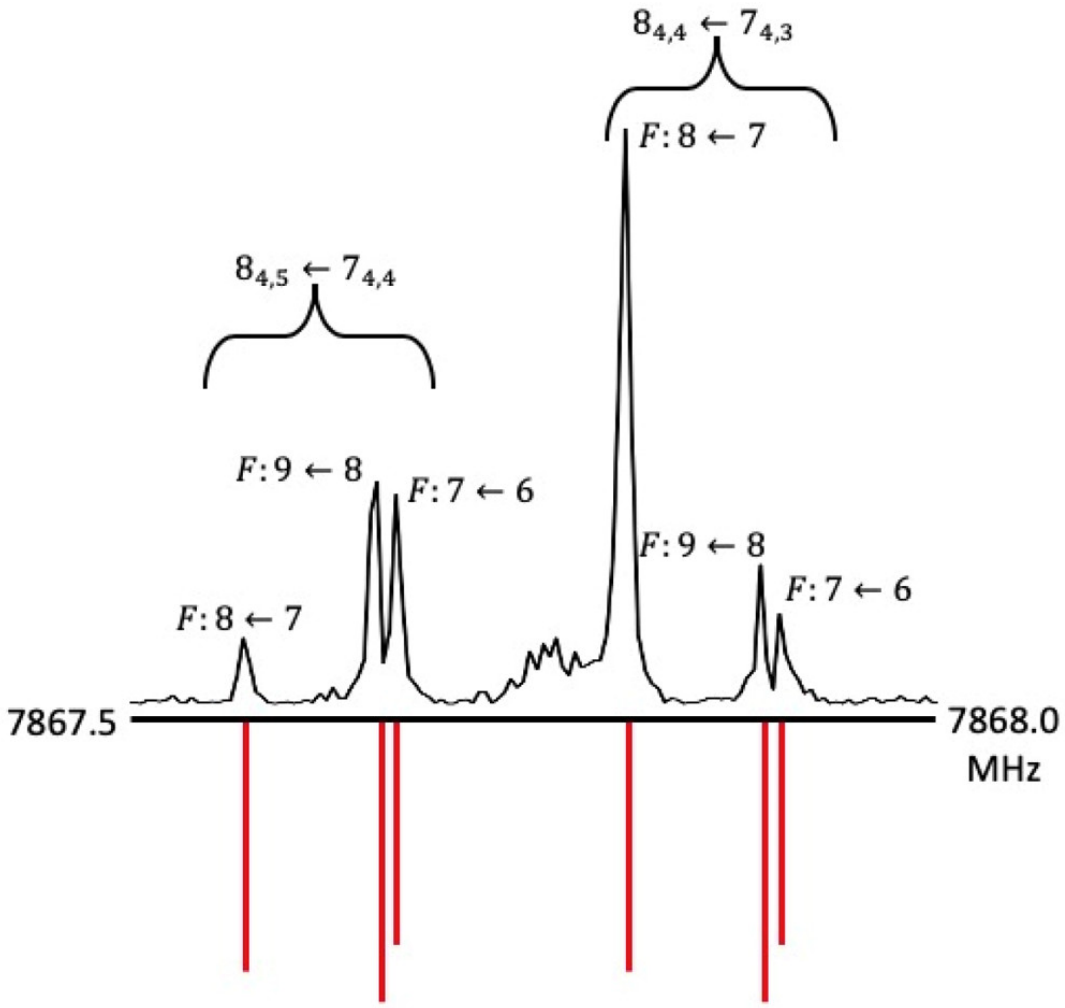

Figure 6.2 Excerpt of the $(CH_3)_3NH^+ \cdot OSO_2CF_3$ Cavity Rotation Spectrum
Cavity spectrum of resolved hyperfine components of a pair of high-K_p transitions resulting from the average of 400 free induction decay signals each collected for 205.5 μs. The stick spectrum shown below represents the frequencies obtained from the final fit.

The observed frequencies were fit to a Watson A-reduced Hamiltonian, and the resulting rotational, distortion, and ^{14}N hyperfine constants are given in Table 6.1. Their predicted values at the MP2/6-311++G(df,pd) level of theory are also included in the table. Further details of the calculations and a more complete set of computational results are presented below.

Table 6.1 Experimental and Computational Results for Trimethylammonium Triflate

	Experimental	*MP2/6-311++G(df,pd)*	
A (MHz)	1358.28926(38)	1358	0.02%
B (MHz)	513.700508(88)	517	-0.64%
C (MHz)	468.210731(85)	471	-0.60%
Δ_J (kHz)	0.05857(49)		
Δ_{JK} (kHz)	-0.0885(27)		
Δ_K (kHz)	0.379(16)		
δ_J (kHz)	0.01087(36)		
δ_K (kHz)	0.100(30)		
χ_{aa} (MHz)	-1.5170(15)	-1.56	-2.8%
χ_{bb} (MHz)	0.8047(16)	0.83	-3.1%
χ_{cc} (MHz)	0.7123(17)	0.74	-3.9%
N^a	419 (246)		
no. of *a*-type	365 (109)[b]		
no. of *b*-type	54 (17)[b]		
RMS (kHz)	2.6		

(a) Number of transitions in the least-squares fit. Number in parentheses denotes the number of distinct frequencies.

(b) Number of transitions of the indicated type, including hyperfine components. The number in parentheses is the number of distinct rotational transitions.

Computational Methods and Results

B3LYP, M06-2X, and MP2 geometry optimization and frequency calculations were performed with varying basis sets for the trimethylammonium triflate complex, triflic acid, and trimethylamine. All calculations were performed by using Gaussian16.[43] A comparison of the results of these calculations, both with each other and with the available experimental data, is shown in Table 6.2.

Table 6.2 Computational Results for Trimethylammonium Triflate

	B3LYP	M06-2X	MP2	Observed[a]
	6-311++G(d,p)	6-311++G(d,p)	6-311++G(d,p)	
	6-311++G(df,pd)	6-311++G(df,pd)	6-311++G(df,pd)	
A (MHz)	1356	1352	1346	1358
	1357	1352	1358	
B (MHz)	479	518	509	514
	481	521	517	
C (MHz)	440	470	464	468
	442	473	471	
R(N–H) (Å)[b]	1.08	1.08	1.08	
	1.08	1.08	1.09	
R(O–H) (Å)[c]	1.54	1.51	1.49	
	1.53	1.50	1.46	
∠(N–H–O) (deg)	178.9	178.6	178.5	
	179.3	178.8	176.9	
ρ_{PT} (Å)	0.51	0.48	0.47	
	0.50	0.48	0.43	
Δ*E* (kcal/mol)	–26.7	–32.1	–31.7	
	–26.1	–31.4	–31.4	
ΔE_{ZP} (kcal/mol)	–23.8	–29.7	–29.0	
	–23.2	–29.0	–29.1	
χ_{aa} (MHz)	–1.49	–1.33	–1.46	–1.5170(15)
	–1.54	–1.36	–1.56	
χ_{bb} (MHz)	0.87	0.74	0.791	0.8047(19)
	0.89	0.74	0.83	
χ_{cc} (MHz)	0.62	0.59	0.67	0.7124(19)
	0.65	0.63	0.74	
μ_a (D)	10.6	10.1	10.2	
	10.6	10.0	9.9	
μ_b (D)	3.9	3.9	3.8	
	3.9	4.0	3.5	
μ_c (D)	0.2	0.2	0.2	
	0.2	0.2	0.2	
μ_T (D)[d]	11.3	10.8	10.9	
	11.3	10.8	10.5	

(a) Values expressing the full measurement accuracy are given in Table 6.1.
(b) The calculated distance in TMAH+ at the MP2/6-311++G(df,pd) level is 1.024 Å.
(c) The calculated distance in free triflic acid at the MP2/6-311++G(df,pd) level is 0.967 Å.
(d) Total dipole moment = $\sqrt{\mu_a^2 + \mu_b^2 + \mu_c^2}$.

The method/basis set in best agreement with *A* and *B* rotational constants was MP2/6-311++G(df,pd), which produced values accurate to 0 and 3 MHz, respectively. For the *C* rotational constant, the M06-2X/6-311++G(d,p) level/basis set performed slightly better than MP2/6-311++G(df,pd), with the two methods reproducing the experimental value to within 2 and 3 MHz, respectively. Note that, overall, both methods outperformed the B3LYP calculations. While both the MP2 and M06-2X results are in reasonable agreement with experiment, the MP2/6-311++G(df,pd) calculations are, for the most part, in somewhat better agreement with observed values. Therefore, this was the method chosen for further computational analysis in this work. The *a*, *b*, and *c* dipole moments calculated at the MP2/6-311++G(df,pd) are 10.6, 3.9, and 0.2 D, respectively, and the nuclear quadrupole coupling constants, χ_{aa}, χ_{bb}, and χ_{cc}, are within 4% of the observed values. The optimized structure is shown in Figure 6.3, and the Cartesian coordinates for this predicted structure are included in Appendix F.

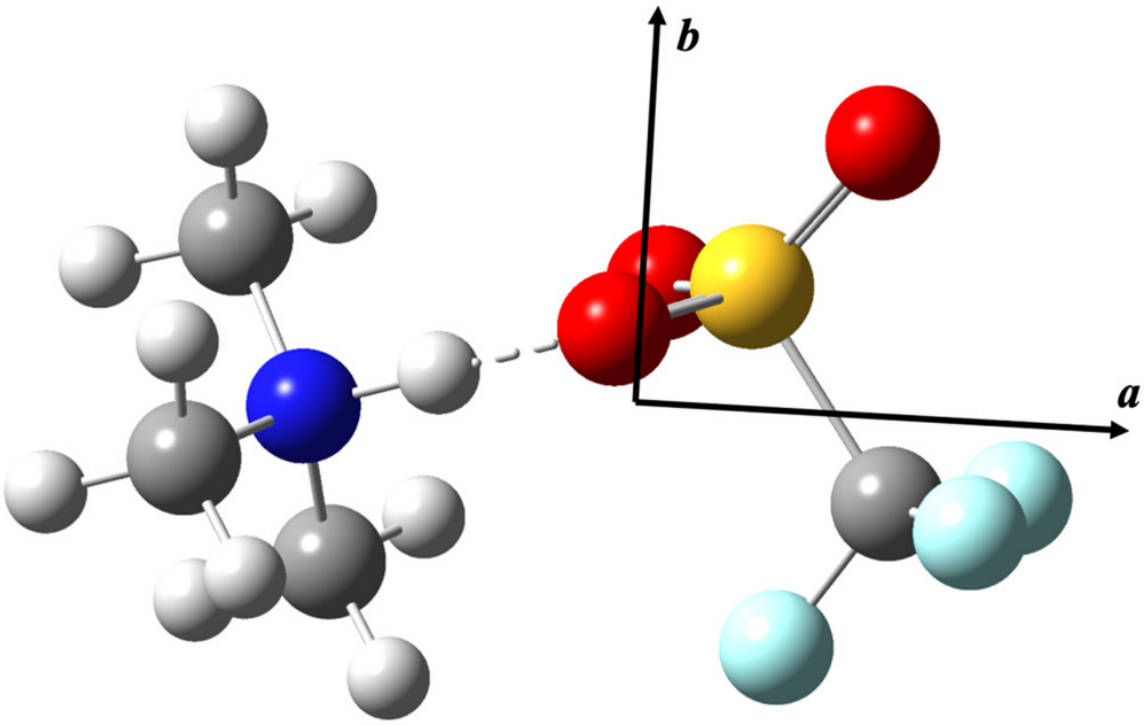

Figure 6.3 Computational Structure of Trimethylammonium Triflate
Optimized structure of trimethylammonium triflate obtained with MP2/6-311++G(df,pd) calculations. The orientation of the *a*- and *b*-inertial axes is shown. The *a*- and *b*-axes are in the plane of the page, and the origin is drawn at the center of mass of the complex.

The binding energy for the complex at the MP2/6-311++G(df,pd) level was determined to be −31.4 kcal/mol (−29.1 kcal/mol after zero-point energy corrections). A one-dimensional potential was also calculated by fixing the N–H distance at a series of values and reoptimizing the energy with respect to all remaining structural parameters. The resulting potential function is shown in Figure 6.4. Figure 6.5 shows an electrostatic potential map on the electron density surface, where red regions represent more negative charge and blue represent regions represent more positive charge.

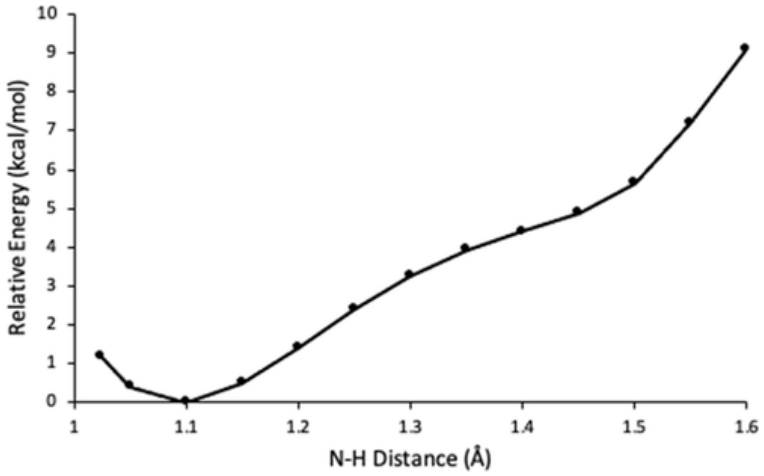

Figure 6.4 Energy of Proton Transfer between TMA and Triflic Acid
Energy of the $CF_3SO_3H–N(CH_3)_3$ complex at a series of fixed N–H distances, calculated at the MP2/6-311++G(df,pd) level of theory. At each point on the curve, all other structural parameters have been optimized.

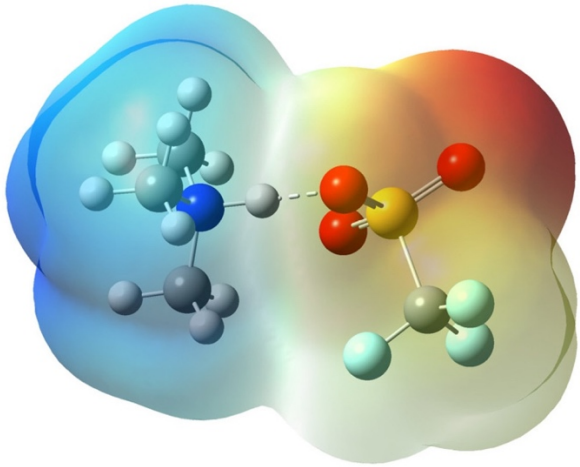

Figure 6.5 Electrostatic Potential Map of Trimethylammonium Triflate
Optimized structure of trimethylammonium triflate obtained with MP2/6-311++G(df,pd) calculations, with an electrostatic potential map on the electron density surface. Regions in red indicate negative charge, and regions in blue indicate positive charge. The isovalue in the plot is 0.0004 au.

Finally, as noted above, the ^{14}N nuclear quadrupole coupling tensor depends on the electric field gradient at the nitrogen nucleus due to extranuclear charges, and thus the measured quadrupole coupling constants were expected to be sensitive to the location of the proton in the complex. Thus, χ_{aa}, χ_{bb}, and χ_{cc} were calculated at the MP2/6-311++G(df,pd) level at each of the N–H distances represented in Figure 6.4. Figure 6.6 shows the resulting values. The experimental hyperfine constants are indicated by squares that have been placed at the nitrogen–hydrogen distance obtained from the fully optimized structure (1.093 Å) and are seen to be in excellent agreement with those calculated at that distance.

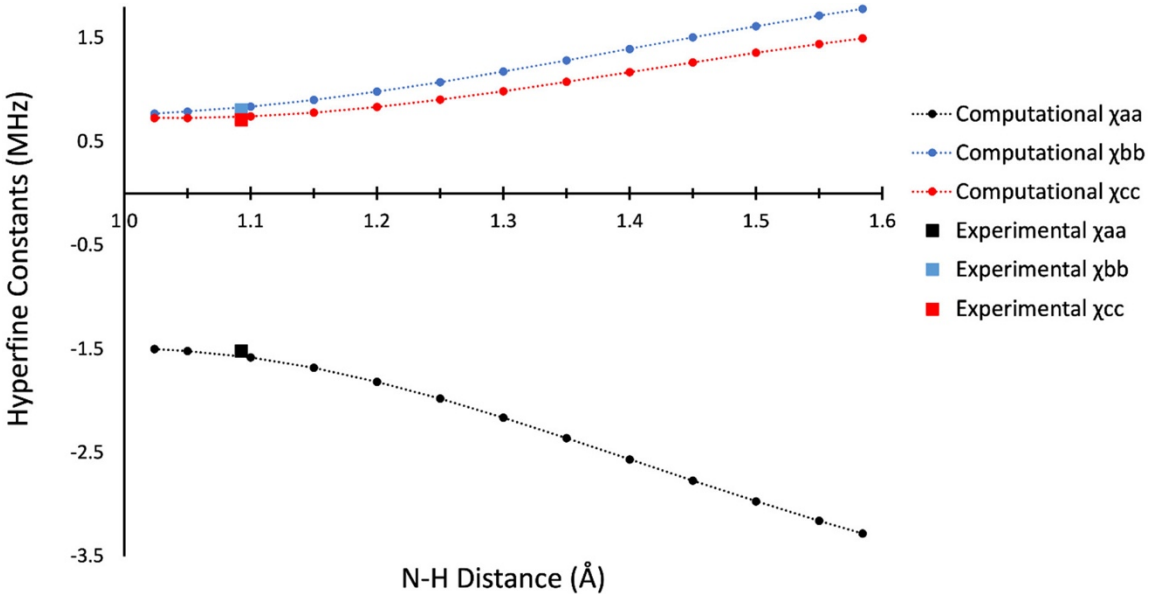

Figure 6.6 Change of Hyperfine Constants with Variable N-H Distance
A plot showing the predicted ^{14}N hyperfine constants at fixed N–H interatomic distances along the proton transfer coordinate with all remaining coordinates optimized. All values are from MP2/6-311++G(df,pd) calculations. The square points represent the experimentally determined hyperfine constants. These points are placed at an N–H interatomic distance of 1.093 Å, which is that obtained from the fully optimized structure at the same level of theory.

Discussion

The body of both experimental and theoretical evidence obtained in this work indicates that the complex formed from triflic acid and trimethylamine in a cold supersonic jet is best described as a trimethylammonium triflate ion pair, $(CH_3)_3NH^+\cdots O_3SCF_3^-$. As described below, the strongest experimental evidence comes from the observed nuclear

quadrupole coupling constants, while the computational results provide both supporting and independent information.

If the complex were weakly bound, the standard approach to interpreting the observed nuclear quadrupole coupling constants would involve examination of the projections of the coupling constants of free TMA (assumed to be unperturbed upon complexation) onto the inertial axis system of the complex. However, projection of the known quadrupole coupling tensor of free TMA[44] onto the inertial axis system of the calculated structure gives a predicted value of χ_{aa} equal to −3.30 MHz, quite different from the observed value of −1.517 MHz. Likewise, for $(\chi_{bb} - \chi_{cc})$, the projected value is 0.65 MHz, which also differs significantly from the observed value of 0.092 MHz. These results suggest substantial electronic rearrangement of the TMA unit upon complexation but, taken alone, do not necessarily indicate that proton transfer is the cause. In this regard, we note that projecting the theoretical quadrupole coupling tensor for $TMAH^+$ previously obtained at the B3LYP/6-311++G(3df,2p) level of theory[45] also gives poor agreement with the observed coupling constants of the complex, with projected values of χ_{aa} and $(\chi_{bb} - \chi_{cc})$ equal to −0.159 and 0.031 MHz, respectively. In this case, however, polarization and charge transfer, which are not accounted for in an analysis based on projection, are expected to be especially important. Overall, it is apparent that a simple analysis based on projecting free, unperturbed monomer values of the ^{14}N coupling constants is not a good way to proceed and needs to be replaced with comparisons based on full electronic structure calculations which automatically incorporate the full range of physical effects that can influence the electric field gradient at the ^{14}N nucleus.

As noted above, Figure 6.6 shows that the observed values of χ_{aa}, χ_{bb}, and χ_{cc} are in excellent agreement with those calculated at an N–H distance of 1.093 Å. Moreover, it is clear that any significantly different choice of the distance would yield poorer agreement between the observed and calculated values. Because the sum of covalent radii[46] for nitrogen and hydrogen is 1.03 Å, this provides strong evidence that the observed coupling constants reflect complete or near-complete transfer of the triflic acid proton to the trimethylamine. Indeed, the N–H distance calculated at the MP2/6-311++G(df,pd) level

for $TMAH^+$ is 1.02 Å, indicating that the calculated value in the complex (1.09 Å) is quite close to that in the trimethylammonium cation. Complementing this viewpoint is the calculated O–H bond distance, which increases from 0.97 Å in free triflic acid to 1.459 Å in the complex (again with the MP2/6-311++G(df,pd) level/basis), the latter being much too long to imply the retention of a covalent O–H interaction in the adduct. Interestingly, while the location of the potential energy minimum at 1.093 Å is clear in Figure 6.4, the curve shows a slight inflection at long distances (∼1.5 Å), which is perhaps reasonably regarded as a vestige of a minimum at the hydrogen-bonded geometry.

Inferences based on bond lengths can be further developed through use of the "proton transfer parameter", ρ_{PT}, which was first defined by Kurnig and Scheiner[47] for the study of amine–hydrogen halide complexes and later adapted in the study of HNO_3 complexes.[20,22,23] For the triflic acid–TMA system, the definition takes the form

$$\rho_{PT} = \left(r_{OH}^{complex} - r_{OH}^{free}\right) - \left(r_{NH}^{complex} - r_{NH}^{free}\right)$$

Here, $r_{OH}^{complex}$ and $r_{HN}^{complex}$ represent interatomic distances from the predicted complex structure, r_{OH}^{free} represents the O–H interatomic distance for free triflic acid, and r_{HN}^{free} represents the N–H interatomic distance in $TMAH^+$. For a hydrogen-bonded complex, the first term is negligible and the second term is positive, giving ρ_{PT} a negative value. When proton transfer has taken place, the first term is positive and the second term is negligible, giving ρ_{PT} a positive value. Values of ρ_{PT} calculated are included in Table 6.2, where it may be seen that all levels of theory employed concur with the conclusion that proton transfer has taken place upon formation of the complex.

In addition, albeit less direct, evidence for proton transfer comes from the calculated dipole moment of the complex. At the MP2/6-311++G(df,pd) level of theory, the total dipole moment, μ_T, is 10.5 D (Table 6.2). This exceeds the sum of the calculated dipole moments of free TMA (0.9 D) and triflic acid (2.7 D) by 6.9 D, thus further indicating substantial charge separation upon complex formation. Such a separation is consistent with the visual representation of the charge distribution provided by the electrostatic potential map shown

in Figure 6.5. There, it may be seen that the proton lies in the electropositive region of the complex which clearly resembles a $TMAH^+$ cation.

Finally, simple energetic arguments make it possible to understand why triflic acid and trimethylamine would form an ion pair in the gas phase without the assistance of a microsolvent. These arguments are similar to those applied to amine–hydrogen halide[17] and nitric acid–water complexes.[1] From measured proton affinities,[48] we have

$$CF_3SO_3H \rightarrow H^+ + CF_3SO_3^- \quad \Delta H = 305\ kcal/mol$$
$$TMA + H^+ \rightarrow TMAH^+ \quad \Delta H = -227\ kcal/\text{mol}$$

Thus, the transfer of a proton from triflic acid to TMA to form $TMAH^+$ and $CF_3SO_3^-$ at infinite separation is endothermic by 78.2 kcal/mol. This endothermicity is offset, however, by the Coulomb energy associated with bringing the ions to their distance in the complex. There is, of course, some ambiguity in the choice of that distance, as the ions are not point charges. However, if we estimate it to be roughly the nitrogen–sulfur distance calculated from the Cartesian coordinates provided in Appendix F (3.356 Å), then the Coulomb energy ($q_1q_2/4\pi\varepsilon_0 r$, where q_1 and q_2 are unit charges of opposite sign and r is the distance) has a value of −99 kcal/mol. This brings the overall reaction energy to −21 kcal/mol, indicating an energetic favorability for transfer of the proton. Note that if, instead of using the nitrogen–sulfur distance, we distribute the negative charge of the $CF_3SO_3^-$ moiety equally among the three oxygens (which bear the negative formal charge of the anion) and retain a unit positive charge on the nitrogen (since it bears the positive formal charge of the $TMAH^+$ cation), the sum of the resulting Coulomb energies is −104 kcal/mol. This value is probably somewhat better than the −99 kcal/mol based on the N–S distance and brings the net interaction energy to −26 kcal/mol. Fortunately, the two methods of calculation are similar enough to provide some confidence that the result is not wildly dependent on the chosen distance. A pictorial representation of the energetics is shown in Figure 6.7.

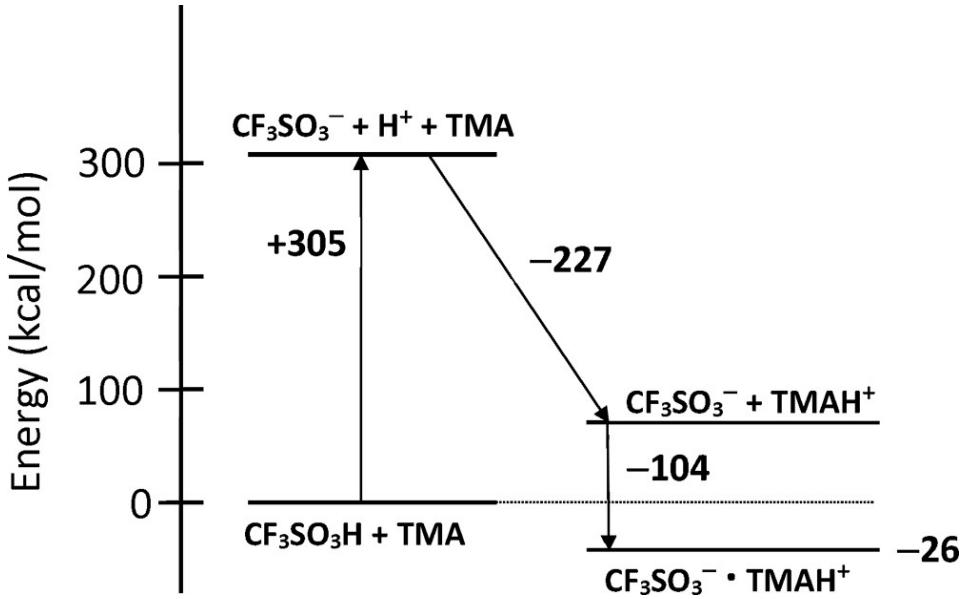

Figure 6.7 Ionization Energy Diagram
Energy diagram depicting the ionization of triflic acid (+305 kcal/mol), proton attachment to TMA (−227 kcal/mol), and the Coulomb energy, $q_1q_2/4\pi\varepsilon_0 r$ (−104 kcal/mol), combining to place the energy of the ion pair at 26 kcal/mol below that of the separated triflic acid and TMA. The first two steps are based on experimental proton affinity values. The third step is approximate, as described in the text. The energy of the final ion pair computed at the MP2/6-311++G(df,pd) level of theory is −31.4 kcal/mol. See the text for a discussion.

The energy change for complex formation of ∼−26 kcal/mol estimated from this simple model is somewhat smaller in magnitude than the −31.4 kcal/mol computed at the MP2/6-311++G(df,pd) level of theory. A disparity is expected given the ambiguity associated with assigning a distance to ions that are not point charges and the neglect of effects such as polarization and distortion of the moieties. However, it suffices to provide an intuitive understanding of the energetics of ion pair formation in the gas phase. Note, however, that these arguments establish the stability of the ion pair relative to that of the isolated monomers but do not address the relative stabilities of the ion pair and the hydrogen-bonded form. Such a comparison is necessary to understand whether or not proton transfer should occur in the isolated complex. As seen in Figure 6.4, however, the hydrogen-bonded complex is a hypothetical species for this system, and thus its energy cannot be rigorously determined. Nevertheless, a binding energy of −26 kcal/mol (or −31.4 kcal/mol from full electronic structure calculations) is larger than that of a typical (non-proton-shared) hydrogen bond,[49] making the preference for ion pair formation entirely plausible.

Finally, it is interesting to note that the value of the deprotonation energy for triflic acid (305 kcal/mol) is significantly less than that of other common acids. For example, values for HNO_3 and HCl are 324 and 333 kcal/mol, respectively.[48] These values would not predict a decisive preference for proton transfer by the above model. Specifically, in the case of HCl, the model predicts an ion pair energy of −12 kcal/mol relative to the isolated monomers, while for HNO_3, the predicted value is −3 kcal/mol relative to the isolated monomers. The former is quite comparable to an expected hydrogen bond energy while the latter is so close to zero that even its sign is not clear. Interestingly, HNO_3–TMA showed significant changes in the ^{14}N quadrupole coupling constants which were interpreted as indicating partial, though not complete, proton transfer,[20] and HCl–TMA has been described as a proton-shared system.[17] It seems logical to conclude that the strong acidity of triflic acid and its correspondingly low deprotonation energy underlie its ability to form a bare ion pair with TMA in the gas phase.

Conclusion

The microwave spectrum of the trimethylammonium triflate ion pair has been observed by chirped-pulse and cavity Fourier transform microwave spectroscopy using on-the-fly mixing of triflic acid and trimethylamine in a supersonic jet. A computational analysis of the complex indicates the formation of an ion pair resulting from complete or near-complete proton transfer from the acid to the base. A comparison of the computed hyperfine constants at different degrees of proton transfer with their experimentally determined values confirms this prediction. Simple energetic arguments based on proton affinities and Coulomb attraction readily rationalize the spontaneous ionization observed in the cold 1:1 complex.

Acknowledgements

This work was supported by the National Science Foundation (Grants CHE 1563324 and CHE 1953528) and the Minnesota Supercomputing Institute. N.L. was supported, in part, by a Lester C. and Joan Krogh-Excellence Fellowship at the University of Minnesota.

Chapter 7: Automation of the Chirped-pulse Method and Supporting Programs

Note to the Reader

Chapter 7 focuses on the development of LabVIEW programs designed to improve efficiency and ease of data collection and averaging for the chirped-pulse method. This chapter will discuss the need for such software in the Leopold Lab, program organization, and relevant LabVIEW jargon. Lastly, operational instructions are described for future graduate students.

Background

Prior to the development of the Chip-o-matic, the broadband chirped-pulse method required manual operation which considerably limited the volume and speed at which data could be measured. The Leopold Lab's Tektronix DPO 4000 series oscilloscope could only collect 10,000 free induction decays (FIDs) before reaching a memory limit at which point the operator had to manually save the 10,000 averaged FIDs as three data file types (time domain as a .txt file and frequency domain and .txt and .spe files), transfer those files to a computer via USB, and initialize another 10,000 FID "run". The Chirp-o-matic is a LabVIEW based program that fully automates this process resulting in a more efficient and robust data collection process.

Prior to the development of the Data Averaging Suite (DAS), the chirped-pulse data sets were manually averaged using a template written by a previous Leopold Lab researcher in Microsoft Excel. Given the much larger volumes of data possible with the Chirp-o-matic, this data averaging method is no longer viable. The DAS is capable of averaging large chirped-pulse data sets in a matter of seconds while removing the risk of human error. Note that both of these programs are stored on the Leopold Lab "Hot Storage" in case of a computer catastrophe.

Chirp-o-matic

The Chirp-o-matic is written as a Virtual Instrument (VI) which is a program that models the appearance and function of a physical instrument. In the main Chirp-o-matic VI there are approximately 20 sub-VIs which are subroutines with inputs and outputs that are packaged as a unit and perform specific tasks. The sub-VIs are organized into three sequence frames which consecutively run their respective segments of code before moving to the next frame or ending the program. The operation of each frame is described here in detail.

The first sequence frame contains only one sub-VI which prompts the user to input relevant experimental parameters. Logged parameters include sample identity, pulsing pressure, microwave frequency region, and the digital delay between molecular pulse and measurement. A miscellaneous parameter entry section is also included when necessary (this is often where flow line backing pressures and reservoir temperatures are recorded). The logged parameters are then compiled into a file basename that is used later by the program for saving multiple file types. Lastly, the file basename is displayed to the user for confirmation before moving on to the second frame.

The second frame collects two pieces of information that are important for the operation of the third frame. First, the user is prompted for the number of runs (1 run = 10,000 FIDs) to be collected. The inputted value dictates the number of times the third frame will loop. Second, the user is prompted for whether or not they would like to use the "Auto Averager" function which is described later. Before entering the final frame, the user can choose to begin collection or restart at the beginning of the first sequence frame.

The third sequence frame is the largest and most complex of the frames. This stage of the program oversees communication with the oscilloscope, data transfer, auto-averaging (if selected), cloud storage, and the function of the graphical user interface. Through an LAN connection, the program initiates collection by sending the user specified experimental parameters from sequence frames 1 and 2 to the oscilloscope using coding blocks from National Instrument's DPO 4000 Series Instrument Driver.[1] Once the program has

measured 10,000 FIDs (the oscilloscope's memory limit), the program instructs the scope to Fourier transform the data and extracts the time and frequency domain intensity data. These data are combined with pre-generated reference time and frequency x-data which significantly reduced the amount of time spent between 10,000 FID acquisition runs. These data are saved as the text and spectral filetypes to the University of Minnesota cloud storage system (a.k.a. the hot storage) allowing for remote access anywhere. If the auto averager option is toggled on in frame 2, the data of a completed 10,000 FID acquisition run is automatically averaged with all previous runs and the resulting averaged data are saved alongside the completed run data. Lastly, the graphical user interface of the Chirp-o-matic displays the number of runs completed in each frequency region, progress bars for the current run and the total collection, and options to quit after the current run or immediately.

Operation of this program is fairly straightforward. The user need only open the program with LabVIEW (which is provided by the University of Minnesota), run the program by clicking the arrow button highlighted in Figure 7.1, and then follow the prompts given by the running program. It is fine to enter collection parameters before turning on the electronics of the chirped-pulse method, but the user should not start the collection until power for the low noise amplifier has been turned on.

Lastly, the program is designed in such a way that little to no errors are possible (as has been the case over the last five years). The one exception is when connection between the chirp computer and UMN servers is temporarily severed (i.e. a WIFI outage) in which case the program cannot save data directly to the UMN cloud storage. This issue is easily resolved by restarting operation of the program once connection to the servers has been restored.

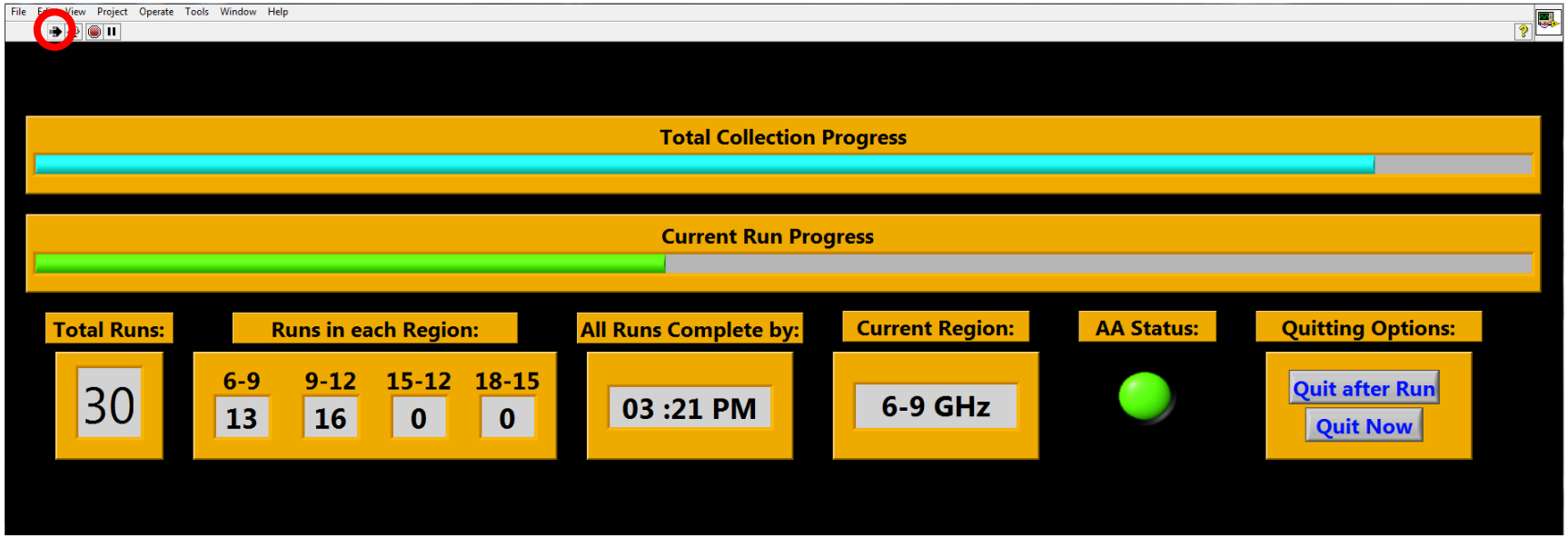

Figure 7.1 Chirp-o-matic Graphical User Interface
A screenshot of the Chirp-o-matic Graphical User Interface. The arrow that starts the program is circled in the top lefthand corner.

Data Averaging Suite

The DAS is a much simpler program than the Chirp-o-matic, but it plays an important role in averaging and splicing data together. Since its development, the DAS has most often been used simply to splice Chirp-o-matic auto-averaged spectra from different frequency regions into one larger spectral file. However, normal spectral files can also be averaged and spliced together using the DAS. The program offers two methods for selecting files: one at a time or by folder. Keywords can be used to specify which files in a selected folder will be averaged. For example, if a folder contains spectral files with data in the 6-9 and 9-12 GHz frequency regions, using the keyword "6-9" will only select files that have "6-9" in the filename. Any keyword can be used as long as it is a part of the filename. Finally, each file averaged with the DAS is tagged with the string "__AVE__" so that no files are accidently overwritten.

Similar to running the Chirp-o-matic, the user simply needs to open the DAS in LabVIEW and press the white arrow in the top left corner of the window. Instructions are included on the graphical user interface of the DAS for convenience. Operation of this program is not connected whatsoever to the chirp electronics and can be done so at any time. No errors have been encountered while using the DAS as it is a fairly straightforward program.

References

Introduction

1. Neumark, D. M. Time-Resolved Photoelectron Spectroscopy of Molecules and Clusters. *Annu. Rev. Phys. Chem.* **2001**, *52*, 8255– 8277.
2. Fennel, T.; Meiwes-Broer, K. H.; Tiggesbäumker, J.; Reinhard, P. G.; Dinh, P. M.; Suraud, E. Laser-Driven Nonlinear Cluster Dynamics. *Rev. Mod. Phys.* **2010**, *82*, 1793– 1842.
3. Häber, T.; Schmitt, U.; Suhm, M. A. FTIR-Spectroscopy of Molecular Clusters in Pulsed Supersonic Slit-Jet Expansions. *Phys. Chem. Chem. Phys.* **1999**, *1*, 5573– 5582.
4. Kulmala, M.; Petäjä, T.; Ehn, M.; Thornton, J.; Sipilä, M.; Worsnop, D. R.; Kerminen, V.- M. Chemistry of Atmospheric Nucleation: On the Recent Advances on Precursor Characterization and Atmospheric Cluster Composition in Connection with Atmospheric New Particle Formation. *Annu. Rev. Phys. Chem.* **2014**, *65*, 21– 37.
5. Asmis, K. R.; Pivonka, N. L.; Santambrogio, G.; Brummer, M.; Kaposta, C.; Neumark, D. M.; Woste, L. Gas Phase Infrared Spectrum of the Protonated Water Dimer. *Science* **2003**, *299*, 1375– 1377.
6. Bizzarri, A.; Stolte, S.; Reuss, J.; Van Duijneveldt-van De Rijdt, J. G. C. M.; Van Duijneveldt, F. B. Infrared Excitation and Dissociation of Methanol Dimers and Trimers. *Chem. Phys.* **1990**, *143*, 423– 435.
7. Huisken, F.; Stemmler, M. Infrared Photodissociation of Small Methanol Clusters. *Chem. Phys. Lett.* **1988**, *144,* 391– 395.
8. Riehn, C.; Lahmann, C.; Wassermann, B.; Brutschy, B. IR Depletion Spectroscopy. A Method for Characterizing a Microsolvation Environment. *Chem. Phys. Lett.* **1992**, *197*, 443– 450.
9. Zwier, T. S. The Spectroscopy of Solvation in Hydrogen-Bonded Aromatic Clusters. *Annu. Rev. Phys. Chem.* **1996**, *47*, 205– 241.
10. Basic, Z.; Miller, R. E. Molecular Clusters: Structure and Dynamics of Weakly Bound Systems. *J. Phys. Chem.* **1996**, *100*, 12945– 12959.
11. Strelnikov, D. V.; Link, M.; Weippert, J.; Kappes, M. M. Optical Spectroscopy of Small Carbon Clusters from Electron-Impact Fragmentation and Ionization of Fullerene-C60. *J. Phys. Chem. A.* **2019**, *123*, 5325– 5333.
12. Kraitchman, J. Determination of Molecular Structure from Microwave Spectroscopic Data. *Am. J. Phys.* **1953**, *21*, 17– 24.

13. Phillips, J. A.; Canagaratna, M.; Goodfriend, H.; Grushow, A.; Almlöf, J.; Leopold, K. R. Microwave and Ab Initio Investigation of HF-BF_3. *J. Am. Chem. Soc.* **1995**, *117*, 12549– 12556.

14. Balle, T. J.; Flygare, W. H. Fabry-Perot Cavity Pulsed Fourier Transform Microwave Spectrometer with a Pulsed Nozzle Particle Source. *Rev. Sci. Instrum.* **1981**, *52*, 33– 45.

15. Brown, G. G.; Dian, B. C.; Douglass, K. O.; Geyer, S. M.; Shipman, S. T.; Pate, B. H. A broadband Fourier Transform Microwave Spectrometer Based on Chirped Pulse Excitation. *Rev. Sci. Instrum.* **2008**, *79*, 1– 14.

16. Dewberry, C. T.; Mackenzie, R. B.; Green, S.; Leopold, K. R. 3D-Printed Slit Nozzles for Fourier Transform Microwave Spectroscopy. *Rev. Sci. Instrum.* **2015**, *86*, 065107.

17. Mackenzie, R. B.; Dewberry, C. T.; Leopold, K. R. Gas Phase Observation and Microwave Spectroscopic Characterization of Formic Sulfuric Anhydride. *Science*. **2015**. *349*, 58– 61.

18. Huff, A. K.; Mackenzie, R. B.; Smith, C. J.; Leopold K. R. Facile Formation of Acetic Sulfuric Anhydride: Microwave Spectrum, Internal Rotation, and Theoretical Calculations. *J. Phys. Chem. A* **2017**, *121*, 5659– 5664.

19. Huff, A. K.; Mackenzie, R. B.; Smith, C. J.; Leopold K. R. A Perfluorinated Carboxylic Sulfuric Anhydride: Microwave and Computational Studies of CF_3COOSO_2OH. *J. Phys. Chem. A* **2019**, *123*, 2237– 2243.

20. Smith, C. J.; Huff, A. K.; Mackenzie, R. B.; Leopold K. R. Observation of Two Conformers of Acrylic Sulfuric Anhydride by Microwave Spectroscopy. *J. Phys. Chem. A* **2017**, *121*, 9074– 9080.

21. Smith, C. J.; Huff, A. K.; Mackenzie, R. B.; Leopold K. R. Carboxylic Sulfuric Anhydrides. *J. Phys. Chem. A* **2020**, *124*, 601– 612.

22. Smith, C. J.; Huff, A. K.; Mackenzie, R. B.; Leopold K. R. Hydration of an Acid Anhydride: The Water Complex of Acetic Sulfuric Anhydride. *J. Phys. Chem. A* **2018**, *122*, 4549– 4554.

23. Love, N.; Smith, C. J.; Huff, A. K.; Leopold, K. R. A Microwave and Computational Study of Trifluoroacetic Anhydride. *J. Mol. Spectrosc.* **2019**, *365*, 111210.

24. Love N.; Huff, A. K.; Leopold, K. R. A New Program for the Assignment and Fitting of Dense Rotational Spectra Based on Spectral Progressions: Application to the Microwave Spectrum of Pivalic Anhydride. *J. Mol. Spectrosc.* **2020**, *370*, 111294.

25. Love, N.; Huff, A. K.; Leopold, K. R. Proton Transfer in a Bare Superacid-Amine Complex: A Microwave and Computational Study of Trimethylammonium Triflate. *J. Phys. Chem. A.* **2021**, *125*, 5061– 5068.

26. Sedo G.; Doran, J. L.; Leopold, K. R. Partial Proton Transfer in the Nitric Acid Trihydrate Complex. *J. Phys. Chem. A* **2009**, *113*, 11301– 11310.

27. Huff, A. K.; Love, N.; Leopold, K. R. Microwave Study of Triflic Acid Hydrates: Evidence for the Transition from Hydrogen-Bonded Clusters to a Microsolvated Ion Pair. *J. Phys. Chem. A.* **2021**, *125*, 8033– 88046.

Chapter 1

1. Mackenzie, R. B.; Dewberry, C. T.; Leopold, K. R. Gas Phase Observation and Microwave Spectroscopic Characterization of Formic Sulfuric Anhydride. *Science* **2015**, *349*, 58– 61.
2. Huff, A. K.; Mackenzie, R. B.; Smith, C. J.; Leopold K. R. Facile Formation of Acetic Sulfuric Anhydride: Microwave Spectrum, Internal Rotation, and Theoretical Calculations. *J. Phys. Chem. A* **2017**, *121*, 5659– 5664.
3. Huff, A. K.; Mackenzie, R. B.; Smith, C. J.; Leopold K. R. A Perfluorinated Carboxylic Sulfuric Anhydride: Microwave and Computational Studies of CF_3COOSO_2OH. *J. Phys. Chem. A* **2019**, *123*, 2237– 2243.
4. Smith, C. J.; Huff, A. K.; Mackenzie, R. B.; Leopold K. R. Observation of Two Conformers of Acrylic Sulfuric Anhydride by Microwave Spectroscopy. *J. Phys. Chem. A* **2017**, *121*, 9074–9080.
5. Smith, C. J.; Huff, A. K.; Mackenzie, R. B.; Leopold K. R. Carboxylic Sulfuric Anhydrides. *J. Phys. Chem. A* **2020**, *124*, 601– 612.
6. Smith, C. J.; Huff, A. K.; Mackenzie, R. B.; Leopold K. R. Hydration of an Acid Anhydride: The Water Complex of Acetic Sulfuric Anhydride. *J. Phys. Chem. A* **2018**, *122*, 4549– 4554.
7. Vaccani, S.; Bauder, A.; Günthard, Hs. H. Microwave Spectrum, Dipole Moment, and Conformation of Formic Anhydride. *Chem. Phys. Lett*. **1975**, *35*, 457– 460.
8. Vaccani, S.; Roos, U.; Bauder, A.; Günthard, Hs. H. Microwave Spectra, Substitution Structure, and Vibrational Satellites of Formic Anhydride. *Chem. Phys*. **1977**, *19*, 51– 57.
9. Alonso J. L.; Pastrana, M. R.; Pelaez, J.; Arauzo, A. Ring-bending Potential Function and Electric Dipole Moment of Maleic Anhydride. *Spectrochimica Acta.* **1983**, *39*, 215– 222.
10. Bauder, A. Microwave Spectrum of Formic Acetic Anhydride. *Mol. Phys*. **2013**, *111*, 1999– 2002.
11. Caminati, W.; Giorgini, M. G.; Ruiz-Pastrana, M.; Alonso, J. L. A Study of the Ring-Bending and Ring-Twisting Motions in Maleic Anhydride by Rotational Analysis of the Corresponding Vibrational Satellites. *Spectrochimica Acta*. **1984**, *41*, 937– 941.
12. Wu, G.; Shlykov, S.; Van Alseny, F. S.; Geise, H. J.; Sluyts, E.; Van der Veken, B. J. Formic Anhydride in the Gas Phase, Studied by Electron Diffraction and Microwave and Infrared Spectroscopy, Supplemented with Ab-Initio Calculations of Geometries and Force Fields. *J. Phys. Chem*. **1995**, *99*, 8589–8598.
13. Abdo, B. T. Molecular Structure of 3,4-difluorofuran-2,5-dione (difluoromaleic anhydride) as Determined by Electron Diffraction and Microwave Spectroscopy in the Gas Phase and by Theoretical Computations. *J. Phys. Chem. A*. **1999**, *103*, 1758– 1767.

14. Pejlovas, A. M.; Sun, M.; Kukolich, S. G. Microwave Measurements of the Spectra and Molecular Structure of Phthalic Anhydride. *J. Mol. Spectrosc*. **2014**, *299*, 43– 47.

15. McMahon, T. J.; Bailey, J. R.; Bird, R. G. Structure and Dynamics of Succinic, Methyl Succinic and Itaconic Anhydrides in the Gas-Phase. *J. Mol. Spectrosc*. **2018**, *347*, 35– 40.

16. Dewberry, C. T.; Mackenzie, R. B.; Green, S.; Leopold, K. R. 3D-Printed Slit Nozzles for Fourier Transform Microwave Spectroscopy. *Rev. Sci. Instrum*. **2015**, *86*, 065107.

17. Pickett, H. M. The Fitting and Prediction of Vibrational-Rotational Spectra with Spin Interactions. *J. Mol. Spectrosc.* **1991**, *148*, 371– 377.

18. Frisch, M. J.; Trucks, G. W.; Schlegel, H. B.; Scuseria, G. E.; Robb, M. A.; Cheeseman, J. R.; Scalmani, G.; Barone, V.; Petersson, G. A., Nakatsuji, X. L.; et al. Gaussian 16; Gaussian, Inc.: Wallingford, CT, **2016**.

19. Atkinson, S. J., Noble-Eddy, R.; Masters, S. L. Gas-Phase Structures of Ketene and Acetic Acid from Acetic Anhydride Using Very-High-Temperature Gas Electron Diffraction. *J. Phys. Chem. A*. **2016**, *120*, 2041– 2048.

20. Wollrab, J. E. Rotational Spectra and Molecular Structure. Academic Press, New York, **1967**.

21. Stolwijk, V. M.; van Eijck, B. P. Microwave Spectra and Barriers to Internal Rotation of Trifluoroacetic Acid and Trifluoroacetyl Fluoride. *J. Mol. Spectrosc*. **1985**, *113*, 196– 207.

Chapter 2

1. Brown, G. G.; Dian, B. C.; Douglass, K. O.; Geyer, S.M.; Shipman, S. T.; Pate, B. H. A Broadband Fourier Transform Microwave Spectrometer Based on Chirped Pulse Excitation. *Rev*. *Sci*. *Instrum*. **2008**, *79*, 1– 14.
2. Park, G. G.; Field, R. W. Perspective: The First Ten Years of Broadband Chirped Pulse Fourier Transform Microwave Spectroscopy. *J. Chem. Phys.* **2016**, *144*, 200901.
3. Winnewisser, B. P.; Reinstädtler, J.; Yamada, K. M. T.; Behrend, J. Interactive Loomis-Wood Assignment Programs *J. Mol. Spectrosc.* **1989**, *136,* 12– 16.
4. Moruzzi, G.; Li-Hong, X.; Lees, R. M.; Winnewasser, B. R.; Winnewasser, M. Investigation of the Ground Vibrational State of CD_3OH by a New "Ritz" Program for Direct Energy Level Fitting. *J. Mol. Spectrosc.* **1994**, *167*, 156– 175.
5. Helm, R. M.; Vogel, H. P.; Neusser, H. J. Highly Resolved UV Spectroscopy: Structure of S_1 benzonitrile and benzonitrile-argon by Correlation Automated Rotational Fitting. *Chem. Phys. Lett.* **1997**, *270,* 285– 292.
6. Hageman, J. A.; Wehrens, R.; de Gelder, R.; Meerts, L. W.; Budens, L. M. C. Direct Determination of Molecular Constants from Rovibronic Spectra with Genetic Algorithms. *J. Chem. Phys***. 2000**, *113,* 7955– 7962.
7. Meerts, L. W.; Schmitt, M.; Groenenboom, G. C. New Applications of the Genetic Algorithm for the Interpretation of High-Resolution Spectra. *Can*. *J. Chem.* **2004**, *82*, 804– 819.
8. Medvedev, I. R.; Winnewisser, M.; Winnewisser, B. P.; de Lucia, F. C.; Herbst, E. The use of CAAARS (Computer Aided Assignment of Asymmetric Rotor Spectra) in the Analysis of Rotational Spectra. *J. Mol. Struct.* **2005**, *742,* 229– 236.
9. Moruzzi, G. A Heuristic Approach to Automated Molecular Line Assignment. *J. Mol. Spectrosc.* **2005**, *229*, 19– 30.
10. Riffe, E. J.; Shipman, S. T.; Gaster, S. A.; Funderbark, C. M.; Brown, G. G. Rotational Spectrum of Eugenol as Analyzed with Double Resonance and Grid-Based Autofit. *J. Phys. Chem. A* **2019**, *123*, 1091– 1099.
11. Yeh, L.; Satterthwaite, D. P. Automated, Context-free Assignment of Asymmetric Rotor Microwave Spectra. *J. Chem. Phys.* **2019**, *150*, 204122.
12. Seifert, N. A.; Finneran, I. A.; Perez, C.; Zaleski, D. P.; Neill, J. L.; Steber, A. L.; Suenram, R. D.; Lesarri, A.; Shipman, S. T.; Pate, B. H. AUTOFIT, an Automated Fitting Tool for Broadband Rotational Spectra ,and Applications to 1-hexanal. *J. Mol. Spectrosc.* **2015**, *312*, 13– 21.
13. Wester, C. M.; Billinghusrt, B. E. Automatic Assignment and Fitting of Spectra with PGOPHER. *Phys. Chem. Chem. Phys.* **2017**, *19*, 10222– 10226.
14. Plusquellic, D. F. nist.gov/publications/user-guide-JB95exe-spectral-fitting-program-v1024-13001.

15. Kisiel, Z.; Pszczółkowski, L.; Medvedev, I.R.; Winnewisser, M.; DeLucia, F. C.; Herbst, E. Rotational Spectrum of trans-trans diethyl ether in the Ground and Three Excited Vibrational States. *J. Mol. Spectrosc.* **2005**, *233*, 231– 243.

16. Pickett, H. M. The Fitting and Prediction of Vibration-Rotation Spectra with Spin Interactions. *J. Mol. Spectrosc.* **1991**, *148*, 371– 377.

17. Cooke, S. A.; Ohring, P. Decoding Pure Rotational Molecular Spectra for Asymmetric Molecules. *J. Spectrosc.* **2012**, *2013*, 1– 10.

18. Smith, C. J.; Huff, A. K.; Mackenzie, R. B.; Leopold K. R. Carboxylic Sulfuric Anhydrides. *J. Phys. Chem. A* **2020**, *124*, 601– 612.

19. Smith, C. J.; Huff, A. K.; Mackenzie, R. B.; Leopold K. R. Hydration of an Acid Anhydride: The Water Complex of Acetic Sulfuric Anhydride. *J. Phys. Chem. A* **2018**, *122*, 4549– 4554.

20. Love, N.; Smith, C. J.; Huff, A. K.; Leopold, K. R. A Microwave and Computational Study of Trifluoroacetic Anhydride. *J. Mol. Spectrosc.* **2019**, *365*, 111210.

21. Dewberry, C. T.; Mackenzie, R. B.; Green, S.; Leopold, K. R. 3D-Printed Slit Nozzles for Fourier Transform Microwave Spectroscopy. *Rev. Sci. Instrum*. **2015**, *86*, 065107.

22. Phillips, J. A.; Canagaratna, M.; Goodfriend, H.; Grushow, A.; Almlöf, J.; Leopold, K. R. Microwave and ab Initio Investigation of HF-BF_3. *J. Am. Chem. Soc.* **1995**, *117,* 12549– 12556.

23. Huff, A. K.; Mackenzie, R. B.; Smith, C. J.; Leopold K. R. Facile Formation of Acetic Sulfuric Anhydride: Microwave Spectrum, Internal Rotation, and Theoretical Calculations. *J. Phys. Chem. A* **2017**, *121*, 5659– 5664.

24. Frisch, M. J.; Trucks, G. W.; Schlegel, H. B.; Scuseria, G. E.; Robb, M. A.; Cheeseman, J. R.; Scalmani, G.; Barone, V.; Petersson, G. A., Nakatsuji, X. L.; et al. Gaussian 16; Gaussian, Inc.: Wallingford, CT, **2016**.

25. Kraitchman, J. Determination of Molecular Structure from Microwave Spectroscopic Data. *Am. J. Phys.* **1953**, *21*, 17– 24.

26. The KRA program by Z. Kisiel, may be downloaded from www.ifpan.edu.pl/~kisiel/struct/struct.htm#kra.

27. Xie, F.; Seifert, N. A.; Matthias, H.; Javix, T.; Wolfgang, J.; Yunjie, X. The Rich Conformational Landscape of erillyl alcohol Revealed by Broadband Rotational Spectroscopy and Theoretical Modelling. *Phys. Chem. Chem. Phys.* **2019**, *21*, 15408– 15416.

28. Higgins, P. M.; Esselman, B. J.; Zdanovskaia, M. A.; Woods, R. C.; McMahon, R. J. Millimeter-wave Spectroscopy of the Chlorine Isotopologues of chloropyrazine and Twenty-Two of their Vibrationally Excited States. *J. Mol. Spectrosc.* **2019**, *364*, 111179–1–15.

29. Esselman, B. J.; Zdanovskaia, M. A.; Woods, R. C.; McMahon, R. J. Millimeter-wave Spectroscopy of the Chlorine Isotopologues of 2-chloropyridine and Twenty-Three of their Vibrationally Excited States. *J. Mol. Spectrosc.* **2019**, *364*, 111206.

30. Marshall, M. D.; Leung, H. O.; Wang, K.; Acha, M. D. Microwave Spectrum and Molecular Structure of the Chiral Tagging Candidate, 3,3,3-trifluoro-1,2-epoxypropane and its Complex with the Argon Atom. *J. Phys. Chem. A.* **2018**, *122*, 4670– 4680.
31. Vaccani, S.; Roos, U.; Bauder, A.; Günthard, Hs. H. Microwave Spectra, Substitution Structure, and Vibrational Satellites of Formic Anhydride. *Chem. Phys*. **1977**, *19*, 51– 57.
32. Vaccani, S.; Bauder, A.; Günthard, Hs. H. Microwave Spectrum, Dipole Moment, and Conformation of Formic Anhydride. *Chem. Phys. Lett*. **1975**, *35*, 457– 460.
33. Bauder, A. Microwave Spectrum of Formic Acetic Anhydride. *Mol. Phys*. **2013**, *111*, 1999– 2002.

Chapter 3

1. Boogaard, A.; Geise, H. J.; Mijlhoff, F. C. An Electron Diffraction Investigation of the Molecular Structure of Formic Anhydride. *J. Mol. Struct.* **1972**, *13*, 53– 58.
2. Vaccani, S.; Roos, U.; Bauder, A.; Gunthard, H. H. Microwave Spectra, Substitution Structure and Vibrational Satellites of Formic Anhydride. *Chem. Phys*. **1977**, *19*, 51– 57.
3. Vledder, H. J.; Mijlhoff, F. C.; Leyte, J. C. Vibrational Structure and Normal Coordinate Analysis of Formic Acetic Anhydride. *J. Mol. Struct*. **1971**, *10*, 57– 73.
4. Wu, G.; Shlykov, S.; Alsenoy, C. Van; Geise, H. J. Formic Acetic Anhydride in the Gas Phase, Studied by Electron Diffraction and Infrared Spectroscopy , Supplemented with Ab-Initio Calculations of Geometries and Force Fields. *J. Phys. Chem.* **1996**, *100*, 11620– 11629.
5. Bauder, A. Microwave Spectrum of Formic Acetic Anhydride. *Mol. Phys*. **2013**, *111*, 1999– 2002.
6. Vledder, H. J.; Van Kleef, F. S. M.; Mijlhoff, F. C.; Leyte, J. C. Vibrational Spectra, Nomral Coordinate Analysis, and Conformation of Acetic Anhydride. *J. Mol. Struct.* **1971**, *10*, 189– 202.
7. Wu, G.; Alsenoy, C. Van; Geise, H. J. Acetic Anhydride in the Gas Phase , Studied by Electron Diffraction and Infrared Spectroscopy , Supplemented With Ab Initio Calculations of Geometries and Force Fields. *J. Phys. Chem.* **2000**, *104*, 1576– 1587.
8. Love, N.; Smith, C. J.; Huff, A. K.; Leopold, K. R. A Microwave and Computational Study of Trifluoroacetic Anhydride. *J. Mol. Spectrosc.* **2019**, *365*, 111210.
9. Love, N.; Huff, A. K.; Leopold, K. R. A New Program for the Assignment and Fitting of Dense Rotational Spectra Based on Spectral Progressions: Application to the Microwave Spectrum of Pivalic Anhydride. *J. Mol. Spectrosc.* **2020**, *370*, 111294.
10. Alonso, J. L.; Pastrana, M. R.; Pelaez, J.; Arauzo, A. Ring-Bending Potential Function and Electric Dipole Moment of Maleic Anhydride. *Spectrochem. Acta* **1983**, *39*, 215– 222.
11. Pejlovas, A. M.; Sun, M.; Kukolich, S. G. Microwave Measurements of the Spectra and Molecular Structure for Phthalic Anhydride. *J. Mol. Spectrosc.* **2014**, *299*, 43– 47.
12. Montiel-Smith, S.; Meza-Reyes, S.; Viñas-Bravo, O.; Fernández-Herrera, M. A.; Martínez-Pascual, R.; Sandoval-Ramírez, J.; Fuente, A.; Reyes, M.; Ruiz, J. A. In Situ Preparation of Mixed Anhydrides Containing the Trifluoroacetyl Moiety. Application to the Esterification of Cholesterol and Phenol. *ARKIVOC* **2005**, 127– 135.
13. Bourne, B. E. J.; Stacey, M.; Tatlow, J. C. Studies of Trifluoroacetic Acid. Part XII.* Acyl Trifluoroacetates and their Reactions. *J. Chem. Soc.* **1954**, 2006–2012.

14. Dewberry, C. T.; Mackenzie, R. B.; Green, S.; Leopold, K. R. 3D-Printed Slit Nozzles for Fourier Transform Microwave Spectroscopy. *Rev. Sci. Instrum.* **2015**, *86*, 065107.

15. Phillips, J. A.; Canagaratna, M.; Goodfriend, H.; Grushow, A.; Almlöf, J.; Leopold, K. R. Microwave and Ab Initio Investigation of HF-BF_3. *J. Am. Chem. Soc.* **1995**, *117*, 12549– 12556.

16. Pickett, H. M. The Fitting and Prediction of Vibration-Rotation Spectra with Spin Interactions. *J. Mol. Spectrosc.* **1991**, *148*, 371– 377.

17. Hartwig, H.; Dreizler, H. The Microwave Spectrum of Trans-2,3-Dimethyloxirane in Torsional Excited States. *Z. Naturforsch., A Phys. Sci.* **1996**, *51*, 923– 932.

18. Hansen, N.; Mäder, H.; Bruhn, T. A Molecular Beam Fourier Transform Microwave Study of 0-Tolunitrile: N Nuclear Quadrupole Coupling and Methyl Internal Rotation Effects A Molecular Beam Fourier Transform Microwave Study of o-Tolunitrile: ^{14}N Nuclear Quadrupole Coupling and Methyl Inte. *Mol. Phys.* **2009**, *97*, 587– 595.

19. Herbers, S.; Vinh, H.; Nguyen, L. Next Level Achievement of the XIAM Code in Modeling the Microwave Spectrum of m -Methylanisole. *J. Mol. Spectrosc.* **2020**, *370*, 111289.

20. Kraitchman, J. Determination of Molecular Structure from Microwave Spectroscopic Data. *Am. J. Phys.* **1953**, *21*, 17– 24.

21. The KRA program by Z. Kisiel, may be downloaded from www.ifpan.edu.pl/~kisiel/struct/struct.htm#kra.

22. Frisch, M. J.; Trucks, G. W.; Schlegel, H. B.; Scuseria, G. E.; Robb, M. A.; Cheeseman, J. R.; Scalmani, G.; Barone, V.; Petersson, G. A.; Nakatsuji, X. L.; *Gaussian 16*; Gaussian, Inc.: Wallingford, CT, 2016.

23. Krisher, L. C.; Saegebarth, E. Microwave Spectrum of Acetic Acid , CH_3COOH and CD_3COOH. *J. Chem. Phys.* **1970**, *54*, 4553– 4558.

24. Huff, A. K.; Mackenzie, R. B.; Smith, C. J.; Leopold, K. R. Facile Formation of Acetic Sulfuric Anhydride: Microwave Spectrum, Internal Rotation, and Theoretical Calculations. *J. Phys. Chem. A* **2017**, *121*, 5659– 5664.

25. Jabri, A.; Van, V.; Lam, V.; Stahl, W.; Kleiner, I. Probing the Methyl Torsional Barriers of the E and Z Isomers of Butadienyl Acetate by Microwave Spectroscopy. *ChemPhysChem* **2016**, *17*, 2660– 2665.

26. Erickson, J. A.; Mcloughlin, J. I. Hydrogen Bond Donor Properties of the Difluoromethyl Group. *J. Org. Chem.* **1995**, *60*, 1626– 1631.

27. Van, V.; Nguyen, T.; Stahl, W.; Vinh, H.; Nguyen, L.; Kleiner, I. Coupled Large Amplitude Motions : The Effects of Two Methyl Internal Rotations and ^{14}N Quadrupole Coupling in 4, 5-Dimethylthiazole Investigated by Microwave Spectroscopy. *J. Mol. Struct.* **2020**, *1207*, 127787.

28. Tudoire, M.; Kleiner, I.; Hougen, J. T.; Melandri, S.; Sutikdja, L. W.; Stahl, W. A Fitting Program for Molecules with Two Inequivalent Methyl Tops and a Plane of Symmetry at Equilibrium : Application to New Microwave and Millimeter-Wave Measurements of Methyl Acetate. *J. Mol. Spectrosc.* **2011**, *269*, 211– 225.

Chapter 4

1. Legon, A. C. The Nature of Ammonium and Methylammonium Halides in the Vapor Phase: Hydrogen Bonding versus Proton Transfer. *Chem. Soc. Rev.* **1993**, *22* (3), 153– 163.
2. Hunt, S. W.; Higgins, K. J.; Craddock, M. B.; Brauer, C. S.; Leopold, K. R. Influence of a Polar Near Neighbor on Incipient Proton Transfer in a Strongly Hydrogen Bonded Complex. *J. Am. Chem. Soc.* **2003**, *125*, 13850– 13860.
3. Ott, M. E.; Leopold, K. R. A Microwave Study of the Ammonia - Nitric Acid Complex. *J. Phys. Chem. A* **1999**, *103*, 1322– 1328.
4. Sedo, G.; Leopold, K. R. Partial Proton Transfer in a Molecular Complex: Assessments from Both the Donor and Acceptor Points of View. *J. Phys. Chem. A* **2011**, *115*, 1787– 1794.
5. Love, N.; Huff, A. K.; Leopold, K. R. Proton Transfer in a Bare Superacid-Amine Complex: A Microwave and Computational Study of Trimethylammonium Triflate. *J. Phys. Chem. A.* **2021**, *125*, 5061– 5068.
6. Huff, A. K.; Love, N.; Leopold, K. R. Microwave Study of Triflic Acid Hydrates: Evidence for the Transition from Hydrogen-Bonded Clusters to a Microsolvated Ion Pair. *J. Phys. Chem. A.* **2021**, *125*, 8033– 88046.
7. Canagaratna, M.; Phillips, J. A.; Ott, M. E.; Leopold, K. R. The Nitric Acid – Water Complex: Microwave Spectrum, Structure, and Tunneling. *J. Phys. Chem. A* **1998**, *102*, 1489– 1497.
8. Ouyang, B.; Starkey, T. G.; Howard, B. J. High-Resolution Microwave Studies of Ring-Structured Complexes between Trifluoroacetic Acid and Water. *J. Phys. Chem. A.* **2007**, *111*, 6165– 6175.
9. Craddock, M. B.; Brauer, C. S.; Leopold, K. R. Microwave Spectrum, Structure, and Internal Dynamics of the Nitric Acid Dihydrate Complex. *J. Phys. Chem. A* **2008**, *112*, 488– 496.
10. Sedo, G.; Doran, J. L.; Leopold, K. R. Partial Proton Transfer in the Nitric Acid Trihydrate Complex. *J. Phys. Chem. A* **2009**, *113*, 11301– 11310.
11. Kisiel, Z.; Białkowska-Jaworska, E.; Pszczółkowski, L.; Milet, A.; Struniewicz, C.; Moszynski, R.; Sadlej, J. Structure and Properties of the Weakly Bound Trimer $(H_2O)_2\cdots HCl$ Observed by Rotational Spectroscopy. *J. Chem. Phys.* **2000**, *112*, 5767– 5776.
12. Kisiel, Z.; Lesarri, A.; Neill, J. L.; Muckle, M. T.; Pate, B. H. Structure and Properties of the $(HCl)_2\cdots H_2O$ Cluster Observed by Chirped-Pulse Fourier Transform Microwave Spectroscopy. *Phys. Chem. Chem. Phys.* **2011**, *13*, 13912– 13919.

13. Legon, A. C.; Suckley, A. P. Bromine Nuclear Quadrupole and Hydrogen - Bromine Nuclear Spin – Nuclear Spin Coupling in the Rotational Spectrum of $H_2O\cdots HBr$. *Chem. Phys. Lett.* **1988**, *150*, 153– 158.

14. Kisiel, Z.; Pietrewicz, B. A.; Desyatnyk, O.; Pszczółkowski, L.; Struniewicz, I.; Sadlej, J. Structure and Properties of the Weakly Bound Cyclic Trimer $(H_2O)_2\cdots HBr$ Observed by Rotational Spectroscopy. *J. Chem. Phys.* **2003**, *119*, 5907– 5917.

15. McIntosh, A.; Walther, T.; Lucchese, R. R.; Bevan, J. W.; Suenram, R. D.; Legon, A. C. The Microwave Spectrum and Ground-State Structure of $H_2O\cdots HI$. *Chem. Phys. Lett.* **1999**, *314*, 57– 64.

16. Smith, C. J.; Huff, A. K.; Mackenzie, R. B.; Leopold K. R. Hydration of an Acid Anhydride: The Water Complex of Acetic Sulfuric Anhydride. *J. Phys. Chem. A* **2018**, *122*, 4549– 4554.

17. Mackenzie, R. B.; Dewberry, C. T.; Leopold, K. R. Gas Phase Observation and Microwave Spectroscopic Characterization of Formic Sulfuric Anhydride. *Science*. **2015**. *349*, 58– 61.

18. Huff, A. K.; Mackenzie, R. B.; Smith, C. J.; Leopold, K. R. Facile Formation of Acetic Sulfuric Anhydride: Microwave Spectrum, Internal Rotation, and Theoretical Calculations. *J. Phys. Chem. A* **2017**, *121*, 5659– 5664.

19. Smith, C. J.; Huff, A. K.; Mackenzie, R. B.; Leopold K. R. Observation of Two Conformers of Acrylic Sulfuric Anhydride by Microwave Spectroscopy. *J. Phys. Chem. A* **2017**, *121*, 9074– 9080.

20. Huff, A. K.; Mackenzie, R. B.; Smith, C. J.; Leopold K. R. A Perfluorinated Carboxylic Sulfuric Anhydride: Microwave and Computational Studies of CF_3COOSO_2OH. *J. Phys. Chem. A* **2019**, *123*, 2237– 2243.

21. Smith, C. J.; Huff, A. K.; Mackenzie, R. B.; Leopold K. R. Carboxylic Sulfuric Anhydrides. *J. Phys. Chem. A* **2020**, *124*, 601– 612.

22. Brown, G. G.; Dian, B. C.; Douglass, K. O.; Geyer, S. M.; Shipman, S. T.; Pate, B. H. A Broadband Fourier Transform Microwave Spectrometer Based on Chirped Pulse Excitation. *Rev. Sci. Instrum.* **2008**, *79*, 053103.

23. Balle, T. J.; Flygare, W. H. Fabry-Perot Cavity Pulsed Fourier Transform Microwave Spectrometer with a Pulsed Nozzle Particle Source. *Rev. Sci. Instrum.* **1981**, *52*, 33– 45.

24. Phillips, J. A.; Canagaratna, M.; Goodfriend, H.; Grushow, A.; Almlöf, J.; Leopold, K. R. Microwave and Ab Initio Investigation of $HF\text{-}BF_3$. *J. Am. Chem. Soc.* **1995**, *117*, 12549– 12556.

25. Dewberry, C. T.; Mackenzie, R. B.; Green, S.; Leopold, K. R. 3D-Printed Slit Nozzles for Fourier Transform Microwave Spectroscopy. *Rev. Sci. Instrum.* **2015**, *86*, 065107.

26. Love, N.; Huff, A. K.; Leopold, K. R. A New Program for the Assignment and Fitting of Dense Rotational Spectra Based on Spectral Progressions: Application to the Microwave Spectrum of Pivalic Anhydride. *J. Mol. Spectrosc.* **2020**, *370*, 111294.

27. Montiel-Smith, S.; Meza-Reyes, S.; Viñas-Bravo, O.; Fernández-Herrera, M. A.; Martínez-Pascual, R.; Sandoval-Ramírez, J.; Fuente, A.; Reyes, M.; Ruiz, J. A. In Situ Preparation of Mixed Anhydrides Containing the Trifluoroacetyl Moiety. Application to the Esterification of Cholesterol and Phenol. *ARKIVOC* **2005**, 127– 135.

28. Frisch, M. J.; Trucks, G. W.; Schlegel, H. B.; Scuseria, G. E.; Robb, M. A.; Cheeseman, J. R.; Scalmani, G.; Barone, V.; Petersson, G. A.; Nakatsuji, X. L.; *Gaussian 16*; Gaussian, Inc.: Wallingford, CT, 2016.

29. Bürgi, H. B.; Dunitz, J. D.; Lehn, J. M.; Wipff, G. Stereochemistry of Reaction Paths at Carbonyl Centres. *Tetrahedron* **1974**, *30*, 1563– 1572.

Chapter 5

1. Mackenzie, R. B.; Dewberry, C. T.; Leopold, K. R. Gas Phase Observation and Microwave Spectroscopic Characterization of Formic Sulfuric Anhydride. *Science*. **2015**. *349*, 58– 61.
2. Huff, A. K.; Mackenzie, R. B.; Smith, C. J.; Leopold, K. R. Facile Formation of Acetic Sulfuric Anhydride: Microwave Spectrum, Internal Rotation, and Theoretical Calculations. *J. Phys. Chem. A* **2017**, *121*, 5659– 5664.
3. Smith, C. J.; Huff, A. K.; Mackenzie, R. B.; Leopold K. R. Observation of Two Conformers of Acrylic Sulfuric Anhydride by Microwave Spectroscopy. *J. Phys. Chem. A* **2017**, *121*, 9074– 9080.
4. Huff, A. K.; Mackenzie, R. B.; Smith, C. J.; Leopold K. R. A Perfluorinated Carboxylic Sulfuric Anhydride: Microwave and Computational Studies of CF_3COOSO_2OH. *J. Phys. Chem. A* **2019**, *123*, 2237– 2243.
5. Smith, C. J.; Huff, A. K.; Mackenzie, R. B.; Leopold K. R. Carboxylic Sulfuric Anhydrides. *J. Phys. Chem. A* **2020**, *124*, 601– 612.
6. Frisch, M. J.; Trucks, G. W.; Schlegel, H. B.; Scuseria, G. E.; Robb, M. A.; Cheeseman, J. R.; Scalmani, G.; Barone, V.; Petersson, G. A.; Nakatsuji, X. L.; *Gaussian 16*; Gaussian, Inc.: Wallingford, CT, 2016.
7. Neese, F.; Valeev, E. F. Revisiting the Atomic Natural Orbital Approach for Basis Sets: Robust Systematic Basis Sets for Explicitly Correlated and Conventional Correlated Ab Initio Methods. *J. Chem*. *Theory Comput*. **2011**, *7*, 33– 43.
8. Lias, S. G., Bartmess, J. E., Liebman, J. F., Holmes, J. L., Levin, R. D., Mallard, W. G., Eds.; Ion Energetics Data. In *NIST Chemistry WebBook*; NIST Standard Reference Data Base, Number 69; National Institute of Standards and Technology: Gaithersburg, MD, http://webbook.nist.gov (retrieved March 19, 2021).
9. Chase, M.W., Jr. NIST-JANAF Thermochemical Tables, Fourth Ed., *J. Phys. Chem*. *Ref. Data Monograph 9*, **1998**, 1-1951.
10. Caldwell, G.; Renneboog, R.; Kebarle, P. Gas Phase Acidities of Aliphatic Carboxylic Acids, Based on Measurements of Proton Transfer Equilibria. *Can. J. Chem*. **1989**, *67*, 611.
11. Hunter, E. P. L.; Lias, S. G.; Hunter, E. P. L.; Lias, S. G. Evaluated Gas Phase Basicities and Proton Affinities of Molecules: An Update. *J. Phys. Chem. Ref. Data* **1998**, *27*, 413– 656.
12. Kim, E.H.; Bradforth, S.E.; Arnold, D.W.; Metz, R.B.; Neumark, D.M. Study of HCO_2 and DCO_2 by Negative Ion Photoelectron Spectroscopy, *J. Chem. Phys*. **1995**, *103*, 7801– 7814.

13. Jinfeng, C.; Topsom, R.D.; Headley, A.D.; Koppel, I.; Mishima, M.; Taft, R.W.; Veji, S. Acidities of Substituted Acetic Acids, *J. Mol. Struct*. **1988**, *168*, 141– 146.

14. Graul, S.T.; Schnute, M.E.; Squires, R.R. Gas Phase Acidities of Carboxylic Acids and Alcohols from Collision-Induced Dissociation of Dimer Cluster Ions, *Int. J. Mass Spectrom. Ion Proc.* **1990**, *96*, 181– 198. (Conformer not specified.)

15. De Vries, K.J.; Gellings, P.J. The Thermal Decomposition of Potassium and Sodium-Pyrosulfate, *J. Inorg. Nucl. Chem*. **1969**, *31*, 1307– 1313.

16. Barbooti, M.M.; Jasim, F. On the Thermal Decomposition of Alkali Persulfates by Derivatograph. *Thermochimica Acta* **1976**, *16*, 402– 406.

17. Greenwood, N.N.; Earnshaw, A. Chemistry of the Elements, *Pergamon Press: Oxford*, **1984**.

18. Balle, T. J.; Flygare, W. H. Fabry-Perot Cavity Pulsed Fourier Transform Microwave Spectrometer with a Pulsed Nozzle Particle Source. *Rev. Sci. Instrum.* **1981**, *52*, 33– 45.

19. Brown, G. G.; Dian, B. C.; Douglass, K. O.; Geyer, S. M.; Shipman, S. T.; Pate, B. H. A Broadband Fourier Transform Microwave Spectrometer Based on Chirped Pulse Excitation. *Rev. Sci. Instrum.* **2008**, *79*, 053103.

20. Phillips, J. A.; Canagaratna, M.; Goodfriend, H.; Grushow, A.; Almlöf, J.; Leopold, K. R. Microwave and Ab Initio Investigation of HF-BF_3. *J. Am. Chem. Soc.* **1995**, *117*, 12549– 12556.

21. Dewberry, C. T.; Mackenzie, R. B.; Green, S.; Leopold, K. R. 3D-Printed Slit Nozzles for Fourier Transform Microwave Spectroscopy. *Rev. Sci. Instrum.* **2015**, *86*, 065107.

22. Ji, P.; Zhang, Y.; Dong, Y.; Huang, H.; Wei, Y.; Wang, W. Synthesis of Enantioenriched α - Deuterated α - Amino Acids Enabled by an Organophotocatalytic Radical Approach. *Org. Lett*. **2020**, *22*, 1557– 1562.

23. Love, N.; Huff, A. K.; Leopold, K. R. A New Program for the Assignment and Fitting of Dense Rotational Spectra Based on Spectral Progressions: Application to the Microwave Spectrum of Pivalic Anhydride. *J. Mol. Spectrosc.* **2020**, *370*, 111294.

24. Watson, J.K.G. Aspects of Quartic and Sextic Centrifugal Effects on Rotational Energy Levels, in Vibrational Spectra and Structure, Durig, J.R. *(Ed.)Elsevier Scientific Publishing, Amsterdam*, **1977**, pp. 1– 89.

25. Pickett, H. M. The Fitting and Prediction of Vibration-Rotation Spectra with Spin Interactions. *J. Mol. Spectrosc.* **1991**, *148*, 371– 377.

26. Bowen, K.H.; Leopold, K.R.; Chance, K.V.; Klemperer, W. Weakly Bound Complexes of Sulfur Trioxide: The Structure of $ArSO_3$ and the Dipole Moment of N_2SO_3, *J. Chem. Phys*. **1980**, *73*, 137– 141.

27. Kuckzkowski, R. L.; Suenram, R. D.; Lovas, F. J. Microwave Spectrum, Structure, and Dipole Moment of Sulfuric Acid, *J. Am. Chem. Soc.* **1981**, 2561– 2566.

28. Phillips, J.A.; Canagaratna, M.; Goodfriend, H.; Leopold, K.R. Microwave Detection of a Key Intermediate in the Formation of Atmospheric Sulfuric Acid: The Structure of $H_2O{-}SO_3$, *J. Phys. Chem*. **1995**, *99*, 501– 504.

29. Leopold, K.R.; Canagaratna, M.; Phillips, J.A. Partially Bonded Molecules from the Solid State to the Stratosphere, *Acc. Chem. Res*. **1997**, 30, 57– 64.

30. Leopold, K.R., Partially Bonded Molecules and Their Transition to the Crystalline State, in Advances in Molecular Structure Research; Hargittai, M., Hargittai, I. *Eds: JAI Press Greenwich, CT* **1996**, Vol. 2, pp.103– 127.

31. Hoffmann, H.M.R. The Ene Reaction, *Angew. Chem. Internat. Edit*. **1969**, *8*, 556– 577.

Chapter 6

1. Leopold, K. R. Hydrated Acid Clusters. *Annu. Rev. Phys. Chem.* **2011**, *62*, 327–349.
2. Cheung, J. T.; Dixon, D. A.; Herschbach, D. R. Cluster Beam Chemistry: Adducts of Hydrogen Halides with Ammonia Clusters. *J. Phys. Chem.* **1988**, *92*, 2536– 2541.
3. Breen, J. J.; Kilgore, S.; Wei, S.; Tzeng, W.-B.; Keesee, R. G.; Castleman, A. W., Jr. Reactions of Hydrogen Halides with Clusters of Ammonia Molecules. *J. Phys. Chem.* **1989**, *93*, 7703– 7707.
4. Eustis, S. N.; Radisic, D.; Bowen, K. H.; Bachorz, R. A.; Haranczyk, M.; Schenter, G. K.; Gutowski, M. Electron-Driven Acid-Base Chemistry: Proton Transfer from Hydrogen Chloride to Ammonia. *Science* **2008**, *319*, 936– 939.
5. Eustis, S. N.; Whiteside, A.; Wang, D.; Gutowski, M.; Bowen, K. H. Ammonia Hydrogen Bromide and Ammonia Hydrogen Iodide Complexes: Anion Photoelectron and Ab Initio Studies. *J. Phys. Chem. A* **2010**, *114*, 1357– 1363.
6. Del Bene, J. E.; Jordan, M. J. T. What a Difference a Decade Makes: Progress in Ab Initio Studies of the Hydrogen Bond. *J. Mol. Struct.: THEOCHEM* **2001**, *573*, 11– 23.
7. Jordan, M. J. T.; Del Bene, J. E. Unraveling Environmental Effects on Hydrogen-Bonded Complexes: Matrix Effects on the Structures and Proton-Stretching Frequencies of Hydrogen Halide Complexes with Ammonia and Trimethylamine. *J. Am. Chem. Soc.* **2000**, *122*, 2101– 2115.
8. Brauer, C. S.; Craddock, M. B.; Kilian, J.; Grumstrup, E. M.; Orilall, M. C.; Mo, Y.; Gao, J.; Leopold, K. R. Amine Hydrogen Halide Complexes: Experimental Dipole Moments and a Theoretical Decomposition of Dipole Moments and Bond Energies. *J. Phys. Chem. A* **2006**, *110*, 10025– 10034.
9. Barnes, A. J.; Latajka, Z.; Biczysko, M. Proton Transfer in Strongly Hydrogen-Bonded Molecular Complexes: Matrix Effects. *J. Mol. Struct.* **2002**, *614*, 11– 21.
10. Scheiner, S. *Hydrogen Bonding: A Theoretical Perspective*; Oxford University Press: New York, 1997.
11. *Theoretical Treatments of Hydrogen Bonding*; Hadži, Ed.; John Wiley and Sons: Chichester, UK, 1997.
12. *Proton Transfer in Hydrogen-Bonded Systems*; Bountis, T., Ed.; NATO ASI Series, B: Physics Vol. 291; Plenum: New York, 1992.
13. Latajka, Z.; Scheiner, S.; Ratajczak, H. The Proton Position in Amine-HX (X = Br, I) Complexes. *Chem. Phys.* **1992**, *166*, 85– 96.
14. Mulliken, R. S.; Person, W. B. *Molecular Complexes. A Lecture and Reprint Volume*; Wiley-Interscience: New York, 1969.

15. Mulliken, R. S. Molecular Compounds and Their Spectra. III. The Interaction of Electron Donors and Acceptors. *J. Phys. Chem.* **1952**, *56*, 801.

16. Coulson, C. A. *Valence*; Oxford University Press: Glasgow, 1952.

17. Legon, A. C. The Nature of Ammonium and Methylammonium Halides in the Vapor Phase: Hydrogen Bonding versus Proton Transfer. *Chem. Soc. Rev.* **1993**, *22* (3), 153– 163.

18. Hunt, S. W.; Higgins, K. J.; Craddock, M. B.; Brauer, C. S.; Leopold, K. R. Influence of a Polar Near Neighbor on Incipient Proton Transfer in a Strongly Hydrogen Bonded Complex. *J. Am. Chem. Soc.* **2003**, *125*, 13850– 13860.

19. Ott, M. E.; Leopold, K. R. A Microwave Study of the Ammonia - Nitric Acid Complex. *J. Phys. Chem. A* **1999**, *103*, 1322– 1328.

20. Sedo, G.; Leopold, K. R. Partial Proton Transfer in a Molecular Complex: Assessments from Both the Donor and Acceptor Points of View. *J. Phys. Chem. A* **2011**, *115*, 1787– 1794.

21. Canagaratna, M.; Phillips, J. A.; Ott, M. E.; Leopold, K. R. The Nitric Acid – Water Complex: Microwave Spectrum, Structure, and Tunneling. *J. Phys. Chem. A* **1998**, *102*, 1489– 1497.

22. Craddock, M. B.; Brauer, C. S.; Leopold, K. R. Microwave Spectrum, Structure, and Internal Dynamics of the Nitric Acid Dihydrate Complex. *J. Phys. Chem. A* **2008**, *112*, 488– 496.

23. Sedo, G.; Doran, J. L.; Leopold, K. R. Partial Proton Transfer in the Nitric Acid Trihydrate Complex. *J. Phys. Chem. A* **2009**, *113*, 11301– 11310.

24. Kisiel, Z.; Pietrewicz, B. A.; Fowler, P. W.; Legon, A. C.; Steiner, E. Rotational Spectra of the Less Common Isotopomers, Electric Dipole Moment, and the Double Minimum Inversion Potential of $H_2O\cdots HCl$. *J. Phys. Chem. A* **2000**, *104*, 6970– 6978.

25. Kisiel, Z.; Białkowska-Jaworska, E.; Pszczółkowski, L.; Milet, A.; Struniewicz, C.; Moszynski, R.; Sadlej, J. Structure and Properties of the Weakly Bound Trimer $(H_2O)_2\cdots HCl$ Observed by Rotational Spectroscopy. *J. Chem. Phys.* **2000**, *112*, 5767– 5776.

26. Kisiel, Z.; Lesarri, A.; Neill, J. L.; Muckle, M. T.; Pate, B. H. Structure and Properties of the $(HCl)_2\cdots H_2O$ Cluster Observed by Chirped-Pulse Fourier Transform Microwave Spectroscopy. *Phys. Chem. Chem. Phys.* **2011**, *13*, 13912– 13919.

27. Legon, A. C.; Suckley, A. P. Bromine Nuclear Quadrupole and Hydrogen - Bromine Nuclear Spin – Nuclear Spin Coupling in the Rotational Spectrum of $H_2O\cdots HBr$. *Chem. Phys. Lett.* **1988**, *150*, 153– 158.

28. Kisiel, Z.; Pietrewicz, B. A.; Desyatnyk, O.; Pszczółkowski, L.; Struniewicz, I.; Sadlej, J. Structure and Properties of the Weakly Bound Cyclic Trimer $(H_2O)_2\cdots HBr$ Observed by Rotational Spectroscopy. *J. Chem. Phys.* **2003**, *119*, 5907– 5917.

29. McIntosh, A.; Walther, T.; Lucchese, R. R.; Bevan, J. W.; Suenram, R. D.; Legon, A. C. The Microwave Spectrum and Ground-State Structure of $H_2O\cdots HI$. *Chem. Phys. Lett.* **1999**, *314*, 57– 64.

30. Hammett, L. P.; Deyrup, A. J. A Series of Simple Basic Indicators. I. The Acidity Functions of Mixtures of Sulfuric and Perchloric Acids with Water. *J. Am. Chem. Soc.* **1932**, *54*, 2721– 2739.

31. Himmel, D.; Goll, S. K.; Leito, I.; Krossing, I. A Unified PH Scale for All Phases. *Angew. Chem., Int. Ed.* **2010**, *49*, 6885– 6888.

32. Kazakova, A. N.; Vasilyev, A. V. Trifluoromethanesulfonic Acid in Organic Synthesis. *Russ. J. Org. Chem.* **2017**, *53*, 485– 509.

33. Olah, G. A.; Prakash, G. K. S.; Sommer, J. Superacids. *Science* **1979**, *206* (4414), 13– 20.

34. Saito, S.; Saito, S.; Ohwada, T.; Shudo, K. The Hammett Acidity Function H_o of Trifluoromethanesulfonic Acid – Trifluoroacetic Acid and Related Acid Systems. A Versatile Nonaqueous Acid System. *Chem. Pharm. Bull.* **1991**, *39*, 2718– 2720.

35. Howells, R. D.; Mc Cown, J. D. Trifluoromethanesulfonic Acid and Derivatives. *Chem. Rev.* **1977**, *77*, 69– 92.

36. Phillips, J. A.; Canagaratna, M.; Goodfriend, H.; Grushow, A.; Almlöf, J.; Leopold, K. R. Microwave and Ab Initio Investigation of HF-BF_3. *J. Am. Chem. Soc.* **1995**, *117*, 12549– 12556.

37. Dewberry, C. T.; Mackenzie, R. B.; Green, S.; Leopold, K. R. 3D-Printed Slit Nozzles for Fourier Transform Microwave Spectroscopy. *Rev. Sci. Instrum.* **2015**, *86*, 065107.

38. Brown, G. G.; Dian, B. C.; Douglass, K. O.; Geyer, S. M.; Shipman, S. T.; Pate, B. H. A Broadband Fourier Transform Microwave Spectrometer Based on Chirped Pulse Excitation. *Rev. Sci. Instrum.* **2008**, *79*, 053103.

39. Balle, T. J.; Flygare, W. H. Fabry-Perot Cavity Pulsed Fourier Transform Microwave Spectrometer with a Pulsed Nozzle Particle Source. *Rev. Sci. Instrum.* **1981**, *52*, 33– 45.

40. Canagaratna, M.; Phillips, J. A.; Goodfriend, H.; Leopold, K. R. Structure and Bonding of the Sulfamic Acid Zwitterion: Microwave Spectrum of $^{+}H_3N\cdot SO_3^{-}$. *J. Am. Chem. Soc.* **1996**, *118*, 5290– 5295.

41. Huff, A. K.; Mackenzie, R. B.; Smith, C. J.; Leopold, K. R. Facile Formation of Acetic Sulfuric Anhydride: Microwave Spectrum, Internal Rotation, and Theoretical Calculations. *J. Phys. Chem. A* **2017**, *121*, 5659– 5664.

42. Love, N.; Huff, A. K.; Leopold, K. R. A New Program for the Assignment and Fitting of Dense Rotational Spectra Based on Spectral Progressions: Application to the Microwave Spectrum of Pivalic Anhydride. *J. Mol. Spectrosc.* **2020**, *370*, 111294.

43. Frisch, M. J.; Trucks, G. W.; Schlegel, H. B.; Scuseria, G. E.; Robb, M. A.; Cheeseman, J. R.; Scalmani, G.; Barone, V.; Petersson, G. A.; Nakatsuji, X. L.; *Gaussian 16*; Gaussian, Inc.: Wallingford, CT, 2016.

44. Rego, C. A.; Batten, R. C.; Legon, A. C. The Properties of the Hydrogen-Bonded Dimer $(CH_3)_3N\cdots HCN$ from an Investigation of its Rotational Spectrum. *J. Chem. Phys.* **1988**, *89*, 696– 702.

45. Domene, C. P.; Fowler, P. W.; Legon, A. C. ^{14}N Electric Field Gradient in Trimethylamine Complexes as a Diagnostic for Formation of Ion Pairs. *Chem. Phys. Lett.* **1999**, *309*, 463– 470.

46. Pyykkö, P. Additive Covalent Radii for Single-, Double-, and Triple-Bonded Molecules and Tetrahedrally Bonded Crystals: A Summary. *J. Phys. Chem. A* **2015**, *119*, 2326– 2337.

47. Kurnig, I. J.; Scheiner, S. Ab Initio Investigation of the Structure of Hydrogen Halide-Amine Complexes in the Gas Phase and in a Polarizable Medium. *Int. J. Quantum Chem.* **1987**, *32*, 47– 56.

48. Lias, S. G., Bartmess, J. E., Liebman, J. F., Holmes, J. L., Levin, R. D., Mallard, W. G., Eds.; Ion Energetics Data. In *NIST Chemistry WebBook*; NIST Standard Reference Data Base, Number 69; National Institute of Standards and Technology: Gaithersburg, MD, http://webbook.nist.gov (retrieved March 19, 2021).

49. For example, in $HNO_3–(H_2O)_n$ complexes, each hydrogen bond has been estimated to contribute −10 kcal/mol to the overall binding energy of the complex. (1) In $H_3N–HF$, the calculated binding energy is −12.9 kcal/mol (−12.3 kcal/mol with counterpoise correction). (18)

Chapter 7

1. http://sine.ni.com/apps/utf8/niid_web_display.download_page?p_id_guid=6E23DB10D9FC2B05E04400144FB7D21D

Appendix G

1. Huff, A. K.; Love, N.; Leopold, K. R. Microwave Study of Triflic Acid Hydrates: Evidence for the Transition from Hydrogen-Bonded Clusters to a Microsolvated Ion Pair. *J. Phys. Chem. A.* **2021**, *125*, 8033– 88046.
2. Legon, A. C. The Nature of Ammonium and Methylammonium Halides in the Vapor Phase: Hydrogen Bonding versus Proton Transfer. *Chem. Soc. Rev.* **1993**, *22*, 153– 163.
3. Love, N.; Huff, A. K.; Leopold, K. R. Proton Transfer in a Bare Superacid-Amine Complex: A Microwave and Computational Study of Trimethylammonium Triflate. *J. Phys. Chem. A.* **2021**, *125*, 5061– 5068.
4. Sedo, G.; Leopold, K. R. Partial Proton Transfer in a Molecular Complex: Assessments from Both the Donor and Acceptor Points of View. *J. Phys. Chem. A* **2011**, *115*, 1787– 1794.
5. Robert, T.; Magna, L.; Hélène, O. B.; Gilbert, B. A Comparison of the Acidity Levels in Room-Temperature Ionic Liquids. *J. Electrochem. Soc.* **2009**, *156*, F115– F121.
6. Balle, T. J.; Flygare, W. H. Fabry-Perot Cavity Pulsed Fourier Transform Microwave Spectrometer with a Pulsed Nozzle Particle Source. *Rev. Sci. Instrum.* **1981**, *52*, 33– 45.
7. Brown, G. G.; Dian, B. C.; Douglass, K. O.; Geyer, S. M.; Shipman, S. T.; Pate, B. H. A broadband Fourier Transform Microwave Spectrometer Based on Chirped Pulse Excitation. *Rev. Sci. Instrum.* **2008**, *79*, 1– 14.
8. Phillips, J. A.; Canagaratna, M.; Goodfriend, H.; Grushow, A.; Almlöf, J.; Leopold, K. R. Microwave and Ab Initio Investigation of HF-BF_3. *J. Am. Chem. Soc.* **1995**, *117*, 12549– 12556.
9. Dewberry, C. T.; Mackenzie, R. B.; Green, S.; Leopold, K. R. 3D-Printed Slit Nozzles for Fourier Transform Microwave Spectroscopy. *Rev. Sci. Instrum.* **2015**, *86*, 065107.
10. Frisch, M. J.; Trucks, G. W.; Schlegel, H. B.; Scuseria, G. E.; Robb, M. A.; Cheeseman, J. R.; Scalmani, G.; Barone, V.; Petersson, G. A., Nakatsuji, X. L.; et al. Gaussian 16; Gaussian, Inc.: Wallingford, CT, **2016**.

Appendices

Appendix A: Supplementary Material for Chapter 1

Table A.1 Observed Transitions of TFAA

J'	K_a'	K_c'	J''	K_a''	K_c''	Obs. Frequency (MHz)	Obs. - Calc. (MHz)
4	4	1	5	3	2	4539.172*	-0.004
4	4	0	5	3	3	4539.432*	-0.004
7	5	3	8	4	4	4545.907*	-0.006
7	5	2	8	4	5	4545.961*	-0.002
10	6	5	11	5	6	4551.477*	0.002
10	6	4	11	5	7	4551.477*	-0.006
13	7	7	14	6	8	4556.283*	0.001
13	7	6	14	6	9	4556.283*	0.000
16	8	9	17	7	10	4560.579*	0.011
16	8	8	17	7	11	4560.579*	0.011
6	5	2	7	4	3	5367.402*	-0.005
6	5	1	7	4	4	5367.417*	-0.007
9	6	4	10	5	5	5373.794*	0.001
9	6	3	10	5	6	5373.794*	-0.002
12	7	6	13	6	7	5379.275*	-0.005
12	7	5	13	6	8	5379.275*	-0.005
15	8	8	16	7	9	5384.122*	-0.002
15	8	7	16	7	10	5384.122*	-0.002
9	3	6	9	2	7	6015.345	-0.001
8	3	5	8	2	6	6068.621	-0.002
14	2	12	13	3	11	6084.150	-0.005
3	2	2	2	1	1	6107.617*	-0.003
7	3	4	7	2	5	6107.635*	0.001
16	2	15	16	1	16	6116.652	0.008
6	3	3	6	2	4	6134.534	-0.001
5	3	2	5	2	3	6151.768	-0.008
3	3	0	3	2	1	6166.920	-0.010
3	3	1	3	2	2	6170.495	0.009
4	3	2	4	2	3	6172.436	-0.001
5	3	3	5	2	4	6176.372	-0.002
6	3	4	6	2	5	6183.241	-0.005
5	5	1	6	4	2	6188.174*	-0.005

* Denotes transitions measured with the cavity method

Table A.1 Observed Transitions of TFAA (cont'd)

J'	K_a'	K_c'	J''	K_a''	K_c''	Obs. Frequency (MHz)	Obs. - Calc. (MHz)
5	5	0	6	4	3	6188.174*	-0.010
7	3	5	7	2	6	6194.133	-0.010
8	6	3	9	5	4	6195.380*	-0.009
8	6	2	9	5	5	6195.380*	-0.010
11	7	5	12	6	6	6201.574*	-0.007
11	7	4	12	6	7	6201.574*	-0.007
14	8	7	15	7	8	6207.013*	-0.004
14	8	6	15	7	9	6207.013*	-0.004
8	3	6	8	2	7	6210.257	-0.011
17	9	9	18	8	10	6211.888*	0.003
17	9	8	18	8	11	6211.888*	0.003
9	3	7	9	2	8	6232.908	-0.004
10	3	8	10	2	9	6263.420	-0.001
11	3	9	11	2	10	6303.161	-0.007
11	1	10	10	2	9	6352.056	0.001
12	3	10	12	2	11	6353.513	-0.003
13	3	11	13	2	12	6415.786	-0.007
14	3	12	14	2	13	6491.261	0.000
7	1	7	6	0	6	6517.638	-0.004
9	0	9	8	1	8	6559.718	-0.004
15	3	13	15	2	14	6581.085	-0.004
16	3	14	16	2	15	6686.325	-0.006
17	3	15	17	2	16	6807.905	0.002
4	2	3	3	1	2	6875.108	-0.002
18	3	16	18	2	17	6946.561	-0.009
7	6	2	8	5	3	7016.370*	-0.009
7	6	1	8	5	4	7016.370*	-0.009
10	7	4	11	6	5	7023.262*	-0.009
10	7	3	11	6	6	7023.262*	-0.009
13	8	6	14	7	7	7029.310*	-0.005
13	8	5	14	7	8	7029.310*	-0.005
19	2	18	19	1	19	7056.857	0.016
8	1	8	7	0	7	7225.416	0.002
20	3	18	20	2	19	7277.398	0.002

* Denotes transitions measured with the cavity method

Table A.1 Observed Transitions of TFAA (cont'd)

J'	K_a'	K_c'	J''	K_a''	K_c''	Obs. Frequency (MHz)	Obs. - Calc. (MHz)
12	1	11	11	2	10	7341.556	0.013
10	0	10	9	1	9	7444.416	0.002
5	2	4	4	1	3	7625.437	-0.004
21	4	17	21	3	18	7823.676	0.008
23	3	21	23	2	22	7910.840	0.001
9	1	9	8	0	8	7929.168	0.001
20	4	16	20	3	17	7973.908	-0.002
5	2	3	4	1	4	7992.883	-0.001
19	4	15	19	3	16	8106.259	0.004
18	4	14	18	3	15	8219.997	0.007
17	4	13	17	3	14	8315.435	-0.002
11	0	11	10	1	10	8322.426	0.004
13	1	12	12	2	11	8337.328	0.004
6	2	5	5	1	4	8358.778	0.001
16	4	12	16	3	13	8393.726	0.003
15	4	11	15	3	12	8456.549	0.015
14	4	10	14	3	11	8505.855	-0.004
13	4	9	13	3	10	8543.787	0.004
12	4	8	12	3	9	8572.327	0.001
11	4	7	11	3	8	8593.344	0.003
10	4	6	10	3	7	8608.455	0.000
14	4	11	14	3	12	8611.575	-0.001
15	4	12	15	3	13	8611.867	0.007
13	4	10	13	3	11	8613.377	-0.001
16	4	13	16	3	14	8615.205	0.008
12	4	9	12	3	10	8616.449	0.000
9	4	5	9	3	6	8619.043	-0.003
11	4	8	11	3	9	8620.132	0.003
17	4	14	17	3	15	8622.690*	0.000
10	4	7	10	3	8	8623.914	0.004
8	4	4	8	3	5	8626.250*	0.000
3	3	1	2	2	0	8626.754	-0.005
9	4	6	9	3	7	8627.434*	0.001
3	3	0	2	2	1	8627.482*	0.001
8	4	5	8	3	6	8630.465	-0.006
7	4	3	7	3	4	8630.982	0.000

* Denotes transitions measured with the cavity method

Table A.1 Observed Transitions of TFAA (cont'd)

J'	K_a'	K_c'	J''	K_a''	K_c''	Obs. Frequency (MHz)	Obs. - Calc. (MHz)
10	1	10	9	0	9	8632.034	-0.001
7	4	4	7	3	5	8632.919	0.009
6	4	2	6	3	3	8633.958	0.002
6	4	3	6	3	4	8634.730*	-0.001
18	4	15	18	3	16	8635.557*	-0.001
5	4	1	5	3	2	8635.723*	0.000
5	4	2	5	3	3	8635.982*	0.000
4	4	0	4	3	1	8636.695*	0.000
4	4	1	4	3	2	8636.760*	0.000
20	4	17	20	3	18	8682.740	-0.001
24	4	21	24	3	22	8901.915	-0.006
6	2	4	5	1	5	8921.978	-0.004
7	2	6	6	1	5	9075.396	0.000
17	2	15	16	3	14	9168.556	0.004
12	0	12	11	1	11	9191.962	-0.005
11	1	11	10	0	10	9336.930	0.001
4	3	2	3	2	1	9444.297	0.001
4	3	1	3	2	2	9447.921	-0.006
8	2	7	7	1	6	9775.705	0.000
7	2	5	6	1	6	9882.632	-0.001
12	1	12	11	0	11	10046.306	0.001
13	0	13	12	1	12	10052.002	-0.002
5	3	3	4	2	2	10259.078	-0.002
5	3	2	4	2	3	10270.022	0.001
15	1	14	14	2	13	10337.605	0.001
9	2	8	8	1	7	10460.276	-0.003
13	1	13	12	0	12	10761.993	-0.001
8	2	6	7	1	7	10879.089	0.002
21	5	16	21	4	17	10891.433	-0.003
14	0	14	13	1	13	10902.178	-0.003
23	5	19	23	4	20	10958.521	0.009
19	5	14	19	4	15	10972.013	0.005
22	5	18	22	4	19	10972.456	0.008
18	5	13	18	4	14	11001.131	-0.007
20	5	16	20	4	17	11002.314	0.004
17	5	12	17	4	13	11024.549	0.007

* Denotes transitions measured with the cavity method

Table A.1 Observed Transitions of TFAA (cont'd)

J'	K_a'	K_c'	J''	K_a''	K_c''	Obs. Frequency (MHz)	Obs. - Calc. (MHz)
18	5	14	18	4	15	11030.899	0.011
16	5	12	16	4	13	11055.242	-0.004
15	5	10	15	4	11	11058.145	0.003
15	5	11	15	4	12	11065.399	-0.003
6	3	4	5	2	3	11069.146	0.003
14	5	9	14	4	10	11069.922	0.011
14	5	10	14	4	11	11074.149	0.001
13	5	8	13	4	9	11079.148	0.002
13	5	9	13	4	10	11081.512	-0.004
12	5	7	12	4	8	11086.321	-0.003
12	5	8	12	4	9	11087.586	0.001
11	5	6	11	4	7	11091.831	-0.003
11	5	7	11	4	8	11092.468	0.000
6	3	3	5	2	4	11094.776	-0.003
10	5	5	10	4	6	11095.995	-0.004
10	5	6	10	4	7	11096.292	-0.004
9	5	4	9	4	5	11099.083	-0.001
9	5	5	9	4	6	11099.197	-0.015
8	5	3	8	4	4	11101.310*	-0.001
8	5	4	8	4	5	11101.361*	0.001
7	5	2	7	4	3	11102.863*	-0.002
7	5	3	7	4	4	11102.883*	0.002
6	5	1	6	4	2	11103.903	0.000
6	5	2	6	4	3	11103.892	-0.016
5	5	0	5	4	1	11104.558	0.000
5	5	1	5	4	2	11104.558	0.000
10	2	9	9	1	8	11129.892	0.001
19	2	17	18	3	16	11307.805	0.004
16	1	15	15	2	14	11336.325	0.004
14	1	14	13	0	13	11485.139	0.000
15	0	15	14	1	14	11742.718	0.002
11	2	10	10	1	9	11785.563	0.006
7	3	5	6	2	4	11872.066	0.005
4	4	1	3	3	0	11914.128*	0.002
4	4	0	3	3	1	11914.134*	-0.001
9	2	7	8	1	8	11915.618	0.005

* Denotes transitions measured with the cavity method

Table A.1 Observed Transitions of TFAA (cont'd)

J'	K_a'	K_c'	J''	K_a''	K_c''	Obs. Frequency (MHz)	Obs. - Calc. (MHz)
7	3	4	6	2	5	11923.497	0.002
15	1	15	14	0	14	12216.216	-0.003
17	1	16	16	2	15	12329.951	-0.001
12	2	11	11	1	10	12428.569	-0.005
16	0	16	15	1	15	12574.242	-0.005
8	3	6	7	2	5	12665.038	-0.008
5	4	2	4	3	1	12733.241*	0.000
5	4	1	4	3	2	12733.309*	0.002
8	3	5	7	2	6	12757.767	-0.003
16	1	16	15	0	15	12955.164	-0.006
10	2	8	9	1	9	12996.197	0.001
18	1	17	17	2	16	13315.399	0.002
17	0	17	16	1	16	13397.663	-0.001
9	3	7	8	2	6	13445.107	-0.004
23	6	17	23	5	18	13445.387	0.010
23	6	18	23	5	19	13457.202	0.009
21	6	16	21	5	17	13490.695	-0.003
20	6	14	20	5	15	13501.607	0.000
20	6	15	20	5	16	13504.647	0.009
19	6	13	19	5	14	13515.001	0.015
19	6	14	19	5	15	13516.821	0.002
18	6	12	18	5	13	13526.277	0.000
18	6	13	18	5	14	13527.364	0.010
17	6	11	17	5	12	13535.756	-0.002
17	6	12	17	5	13	13536.375	0.005
16	6	10	16	5	11	13543.666	-0.002
16	6	11	16	5	12	13543.999	-0.004
15	6	9	15	5	10	13550.213	-0.001
15	6	10	15	5	11	13550.391	0.001
6	4	3	5	3	2	13552.092	-0.005
6	4	2	5	3	3	13552.357	-0.004
14	6	8	14	5	9	13555.580*	0.001
14	6	9	14	5	10	13555.664*	-0.003
13	6	8	13	5	9	13559.958	-0.009
12	6	6	12	5	7	13563.400	0.003
12	6	7	12	5	8	13563.400	-0.016

* Denotes transitions measured with the cavity method

Table A.1 Observed Transitions of TFAA (cont'd)

J'	K_a'	K_c'	J''	K_a''	K_c''	Obs. Frequency (MHz)	Obs. - Calc. (MHz)
11	6	5	11	5	6	13566.118	-0.007
11	6	6	11	5	7	13566.135	0.002
10	6	4	10	5	5	13568.221	-0.005
10	6	5	10	5	6	13568.221	-0.008
9	6	3	9	5	4	13569.797	-0.010
9	6	4	9	5	5	13569.797	-0.011
8	6	2	8	5	3	13570.954	-0.008
8	6	3	8	5	4	13570.954	-0.008
7	6	1	7	5	2	13571.766	-0.010
7	6	2	7	5	3	13571.766	-0.010
6	6	0	6	5	1	13572.313	-0.012
6	6	1	6	5	2	13572.313	-0.012
9	3	6	8	2	7	13599.541	-0.001
14	2	13	13	1	12	13683.464	-0.001
17	1	17	16	0	16	13701.520	-0.006
11	2	9	10	1	10	14124.245	0.001
10	3	8	9	2	7	14209.274	-0.006
18	0	18	17	1	17	14213.975	-0.002
19	1	18	18	2	17	14289.796	0.009
15	2	14	14	1	13	14299.622	0.004
7	4	4	6	3	3	14370.432	-0.004
7	4	3	6	3	4	14371.227	-0.004
10	3	7	9	2	8	14451.116	-0.002
18	1	18	17	0	17	14454.562	-0.009
16	2	15	15	1	14	14911.664	0.000
11	3	9	10	2	8	14954.844	-0.006
19	0	19	18	1	18	15024.220	0.006
8	4	5	7	3	4	15187.880	-0.004
8	4	4	7	3	5	15189.874	-0.004
5	5	1	4	4	0	15201.103	-0.002
19	1	19	18	0	18	15213.469	-0.003
20	1	19	19	2	18	15250.677	-0.004
12	2	10	11	1	11	15302.362	-0.003
11	3	8	10	2	9	15315.197	-0.010
17	2	16	16	1	15	15522.523	0.001
12	3	10	11	2	9	15679.616	-0.001

Table A.1 Observed Transitions of TFAA (cont'd)

J'	K_a'	K_c'	J''	K_a''	K_c''	Obs. Frequency (MHz)	Obs. - Calc. (MHz)
20	0	20	19	1	19	15829.353	0.002
20	1	20	19	0	19	15977.370	-0.002
21	7	15	21	6	16	15990.947	0.005
9	4	6	8	3	5	16003.918	-0.003
9	4	5	8	3	6	16008.315	-0.005
18	7	11	18	6	12	16013.429	0.014
18	7	12	18	6	13	16013.429	-0.010
17	7	10	17	6	11	16018.866	0.002
17	7	11	17	6	12	16018.866	-0.010
6	5	2	5	4	1	16020.274	-0.008
16	7	9	16	6	10	16023.448	-0.003
16	7	10	16	6	11	16023.448	-0.009
15	7	8	15	6	9	16027.275	0.001
15	7	9	15	6	10	16027.275	-0.002
14	7	7	14	6	8	16030.424	-0.002
14	7	8	14	6	9	16030.424	-0.003
13	7	6	13	6	7	16032.993	0.002
13	7	7	13	6	8	16032.993	0.002
12	7	5	12	6	6	16035.045	-0.002
12	7	6	12	6	7	16035.045	-0.002
11	7	4	11	6	5	16036.666	-0.002
11	7	5	11	6	6	16036.666	-0.002
10	7	3	10	6	4	16037.916	-0.005
10	7	4	10	6	5	16037.916	-0.005
9	7	2	9	6	3	16038.861	-0.005
9	7	3	9	6	4	16038.861	-0.005
8	7	1	8	6	2	16039.554	-0.005
8	7	2	8	6	3	16039.554	-0.005
7	7	0	7	6	1	16040.041	-0.009
7	7	1	7	6	2	16040.041	-0.009
18	2	17	17	1	16	16135.277	0.004
12	3	9	11	2	10	16194.932	-0.007
21	1	20	20	2	19	16196.239	0.004
13	3	11	12	2	10	16382.061	0.000
13	2	11	12	1	12	16532.234	-0.010
21	0	21	20	1	20	16630.271	-0.002

Table A.1 Observed Transitions of TFAA (cont'd)

J'	K_a'	K_c'	J''	K_a''	K_c''	Obs. Frequency (MHz)	Obs. - Calc. (MHz)
19	2	18	18	1	17	16752.994	-0.004
10	4	7	9	3	6	16817.844	0.000
10	4	6	9	3	7	16826.666	0.005
7	5	3	6	4	2	16839.354	-0.007
7	5	2	6	4	3	16839.354	-0.011
14	3	12	13	2	11	17061.424	0.000
13	3	10	12	2	11	17093.879	-0.001
20	2	19	19	1	18	17378.591	0.003
22	1	22	21	0	21	17516.971	-0.006
11	4	8	10	3	7	17628.725	-0.004
11	4	7	10	3	8	17645.123	-0.003
8	5	3	7	4	4	17658.268	-0.011
8	5	4	7	4	3	17658.268	0.006
15	3	13	14	2	12	17717.704	0.011

Table A.2 Coordinates of TFAA Minimum

Cartesian coordinates [in Å] of the minimum energy structure of trifluoroacetic anhydride from M06-2X/6-311++G(3df) calculations.

	X	Y	Z
C	1.166548	-0.670692	0.220750
O	1.276605	-1.782400	0.583573
O	-0.000001	0.007954	0.000033
C	-1.166542	-0.670690	-0.220732
O	-1.276587	-1.782392	-0.583578
C	-2.343512	0.292912	0.046434
C	2.343509	0.292915	-0.046438
F	-2.318981	0.689210	1.312568
F	-3.484216	-0.314710	-0.194517
F	-2.245424	1.361374	-0.732595
F	2.318934	0.689236	-1.312564
F	2.245449	1.361364	0.732614
F	3.484222	-0.314710	0.194461

Appendix B: Supplementary Material for Chapter 2

Table B.1 Observed Transitions of Parent PiA

J'	K_a'	K_c'	J''	K_a''	K_c''	Obs. Frequency (MHz)	Obs. - Calc. (MHz)
6	1	6	5	0	5	6194.871	-0.001
10	1	9	9	2	8	6278.807	0.006
8	0	8	7	1	7	6307.198	0.004
4	2	3	3	1	2	6715.722	-0.002
4	2	2	3	1	3	6853.770	-0.005
14	2	13	13	3	10	6944.797	0.002
7	1	7	6	0	6	7016.331	-0.002
9	0	9	8	1	8	7253.941*	0.003
11	1	10	10	2	9	7280.090	0.003
16	4	12	16	3	13	7399.949	-0.001
15	4	11	15	3	12	7426.995	0.005
14	4	10	14	3	11	7448.111	-0.002
13	4	9	13	3	10	7464.349	0.004
12	4	8	12	3	9	7476.605	-0.002
17	4	14	17	3	15	7482.901	-0.008
16	4	13	16	3	14	7483.254	-0.004
18	4	15	18	3	16	7484.274	-0.003
15	4	12	15	3	13	7484.809	-0.003
11	4	7	11	3	8	7485.694	-0.004
14	4	11	14	3	12	7487.125	-0.007
19	4	16	19	3	17	7487.939	-0.003
13	4	10	13	3	11	7489.853	-0.001
10	4	6	10	3	7	7492.301	0.001
12	4	9	12	3	10	7492.687	-0.003
11	4	8	11	3	9	7495.416	-0.002
9	4	5	9	3	6	7496.982	-0.001
10	4	7	10	3	8	7497.885	-0.003
9	4	6	9	3	7	7500.003	-0.004
8	4	4	8	3	5	7500.210	-0.003
8	4	5	8	3	6	7501.729	-0.003
7	4	3	7	3	4	7502.367	-0.001
7	4	4	7	3	5	7503.057	-0.003
6	4	2	6	3	3	7503.744	-0.001
6	4	3	6	3	4	7504.022	-0.002
5	4	1	5	3	2	7504.577*	-0.003

* Denotes transitions measured with the cavity method

Table B.1 Observed Transitions of Parent PiA (cont'd)

J'	K_a'	K_c'	J''	K_a''	K_c''	Obs. Frequency (MHz)	Obs. - Calc. (MHz)
5	4	2	5	3	3	7504.673*	0.000
4	4	0	4	3	1	7505.058	0.009
14	2	12	13	3	11	7530.393	0.005
5	2	4	4	1	3	7562.719	-0.002
17	3	15	16	4	12	7685.714	0.007
15	2	14	14	3	11	7777.893	0.009
5	2	3	4	1	4	7796.200	-0.001
17	3	14	16	4	13	7811.409	0.006
8	1	8	7	0	7	7831.593	0.002
3	3	1	2	2	0	8035.208	-0.005
3	3	0	2	2	1	8035.558	-0.002
10	0	10	9	1	9	8200.567	0.001
12	1	11	11	2	10	8288.674	0.004
6	2	5	5	1	4	8398.699	0.000
15	2	13	14	3	12	8529.571	-0.003
9	1	9	8	0	8	8642.273	0.004
18	3	15	17	4	14	8751.169	0.007
6	2	4	5	1	5	8754.792	0.001
4	3	2	3	2	1	8925.882	0.000
4	3	1	3	2	2	8927.621	0.000
11	0	11	10	1	10	9145.355	-0.001
7	2	6	6	1	5	9223.772	-0.004
13	1	12	12	2	11	9303.664	0.004
10	1	10	9	0	9	9450.101	-0.001
16	2	14	15	3	13	9543.432	-0.009
21	5	16	21	4	17	9557.316	0.002
20	5	15	20	4	16	9575.423	-0.007
21	5	17	21	4	18	9584.077	-0.008
19	5	14	19	4	15	9590.391	0.005
20	5	16	20	4	17	9593.823	-0.007
18	5	13	18	4	14	9602.688*	0.000
19	5	15	19	4	16	9602.769*	0.000
18	5	14	18	4	15	9610.824	-0.007
17	5	12	17	4	13	9612.765	0.001
17	5	13	17	4	14	9617.985	0.000
16	5	11	16	4	12	9620.980	0.002

* Denotes transitions measured with the cavity method

Table B.1 Observed Transitions of Parent PiA (cont'd)

J'	K_a'	K_c'	J''	K_a''	K_c''	Obs. Frequency (MHz)	Obs. - Calc. (MHz)
16	5	12	16	4	13	9624.227	-0.004
15	5	10	15	4	11	9627.635	0.001
15	5	11	15	4	12	9629.593	-0.004
14	5	9	14	4	10	9632.990	0.001
14	5	10	14	4	11	9634.127	-0.003
13	5	8	13	4	9	9637.253	-0.005
13	5	9	13	4	10	9637.890	-0.005
12	5	7	12	4	8	9640.620	-0.004
12	5	8	12	4	9	9640.957	-0.006
11	5	6	11	4	7	9643.237	-0.006
11	5	7	11	4	8	9643.402	-0.009
10	5	5	10	4	6	9645.245*	0.001
10	5	6	10	4	7	9645.322*	-0.001
9	5	4	9	4	5	9646.734*	-0.009
9	5	5	9	4	6	9646.786*	0.009
8	5	3	8	4	4	9647.838	0.003
7	5	2	7	4	3	9648.605	-0.002
7	5	3	7	4	4	9648.605	-0.007
6	5	1	6	4	2	9649.126	-0.004
6	5	2	6	4	3	9649.126	-0.005
5	5	0	5	4	1	9649.463	-0.003
5	5	1	5	4	2	9649.463	-0.003
7	2	5	6	1	6	9731.547	-0.001
5	3	3	4	2	2	9815.229	-0.001
5	3	2	4	2	3	9820.465	-0.001
8	2	7	7	1	6	10038.123	-0.005
12	0	12	11	1	11	10086.792	0.006
11	1	11	10	0	10	10256.851	-0.002
14	1	13	13	2	12	10324.022	0.003
6	3	4	5	2	3	10702.306	-0.001
6	3	3	5	2	4	10714.564	-0.004
8	2	6	7	1	7	10728.697	-0.003
9	2	8	8	1	7	10841.996	0.001
13	0	13	12	1	12	11023.613	0.001
12	1	12	11	0	11	11064.212	0.000
4	4	1	3	3	0	11071.240	-0.001

* Denotes transitions measured with the cavity method

Table B.1 Observed Transitions of Parent PiA (cont'd)

J'	K_a'	K_c'	J''	K_a''	K_c''	Obs. Frequency (MHz)	Obs. - Calc. (MHz)
4	4	0	3	3	1	11071.240	-0.004
15	1	14	14	2	13	11348.553	0.007
7	3	5	6	2	4	11585.928	-0.003
7	3	4	6	2	5	11610.528	-0.003
18	2	16	17	3	15	11613.075	0.002
10	2	9	9	1	8	11635.693	-0.002
9	2	7	8	1	8	11748.619	0.000
21	6	15	21	5	16	11752.271	-0.001
20	6	14	20	5	15	11759.619	0.003
20	6	15	20	5	16	11760.224	-0.005
19	6	13	19	5	14	11765.913	0.002
17	6	11	17	5	12	11775.819	-0.004
17	6	12	17	5	13	11775.945	-0.002
14	6	8	14	5	9	11785.451	-0.004
13	6	7	13	5	8	11787.597	0.002
13	6	8	13	5	9	11787.597	-0.006
12	6	6	12	5	7	11789.316	0.001
12	6	7	12	5	8	11789.316	-0.002
11	6	5	11	5	6	11790.675	0.000
11	6	6	11	5	7	11790.675	-0.002
10	6	4	10	5	5	11791.731	-0.001
10	6	5	10	5	6	11791.731	-0.002
9	6	3	9	5	4	11792.534	0.000
9	6	4	9	5	5	11792.534	0.000
8	6	2	8	5	3	11793.128	-0.001
8	6	3	8	5	4	11793.128	-0.001
7	6	1	7	5	2	11793.554	0.000
7	6	2	7	5	3	11793.554	0.000
6	6	0	6	5	1	11793.847	-0.001
6	6	1	6	5	2	11793.847	-0.001
13	1	13	12	0	12	11873.694	0.001
14	0	14	13	1	13	11954.930	0.000
5	4	2	4	3	1	11962.663*	0.001
5	4	1	4	3	2	11962.685*	-0.001
16	1	15	15	2	14	12375.882	-0.001
11	2	10	10	1	9	12419.637	-0.005

* Denotes transitions measured with the cavity method

Table B.1 Observed Transitions of Parent PiA (cont'd)

J'	K_a'	K_c'	J''	K_a''	K_c''	Obs. Frequency (MHz)	Obs. - Calc. (MHz)
8	3	6	7	2	5	12464.700	-0.007
8	3	5	7	2	6	12509.084	-0.009
14	1	14	13	0	13	12686.548	-0.003
10	2	8	9	1	9	12793.701	-0.007
6	4	3	5	3	2	12853.963*	-0.001
6	4	2	5	3	3	12854.060*	0.002
15	0	15	14	1	14	12880.183	-0.003
12	2	11	11	1	10	13194.352	-0.005
9	3	7	8	2	6	13337.066	-0.003
17	1	16	16	2	15	13404.516	-0.002
9	3	6	8	2	7	13411.127	-0.009
15	1	15	14	0	14	13503.719	-0.002
7	4	4	6	3	3	13745.031	-0.004
7	4	3	6	3	4	13745.314	-0.004
16	0	16	15	1	15	13799.159	0.000
11	2	9	10	1	10	13866.270	-0.002
20	7	13	20	6	14	13917.846	-0.001
19	7	12	19	6	13	13921.531	-0.004
18	7	11	18	6	12	13924.706	0.001
18	7	12	18	6	13	13924.706	-0.002
17	7	10	17	6	11	13927.405	-0.004
17	7	11	17	6	12	13927.405	-0.005
16	7	9	16	6	10	13929.693	-0.003
16	7	10	16	6	11	13929.693	-0.004
15	7	8	15	6	9	13931.612	-0.001
15	7	9	15	6	10	13931.612	-0.002
14	7	7	14	6	8	13933.200	-0.004
14	7	8	14	6	9	13933.200	-0.004
13	7	6	13	6	7	13934.505	-0.002
13	7	7	13	6	8	13934.505	-0.002
12	7	5	12	6	6	13935.559	-0.003
12	7	6	12	6	7	13935.559	-0.003
11	7	4	11	6	5	13936.400	-0.002
11	7	5	11	6	6	13936.400	-0.002
10	7	3	10	6	4	13937.058	-0.002
10	7	4	10	6	5	13937.058	-0.002

* Denotes transitions measured with the cavity method

Table B.1 Observed Transitions of Parent PiA (cont'd)

J'	K_a'	K_c'	J''	K_a''	K_c''	Obs. Frequency (MHz)	Obs. - Calc. (MHz)
9	7	2	9	6	3	13937.561	-0.004
9	7	3	9	6	4	13937.561	-0.004
8	7	1	8	6	2	13937.940	-0.004
8	7	2	8	6	3	13937.940	-0.004
7	7	0	7	6	1	13938.216	-0.004
7	7	1	7	6	2	13938.216	-0.004
13	2	12	12	1	11	13960.486	-0.004
5	5	1	4	4	0	14107.075	-0.005
5	5	0	4	4	1	14107.075	-0.005
10	3	8	9	2	7	14201.357	-0.004
10	3	7	9	2	8	14317.699	-0.008
16	1	16	15	0	15	14325.802	-0.001
18	1	17	17	2	16	14432.811	-0.002
8	4	5	7	3	4	14635.711	-0.005
8	4	4	7	3	5	14636.423	-0.004
17	0	17	16	1	16	14711.915	0.000
14	2	13	13	1	12	14718.831	-0.002
12	2	10	11	1	11	14968.396	-0.004
6	5	2	5	4	1	14998.512	-0.004
6	5	1	5	4	2	14998.512	-0.004
11	3	9	10	2	8	15055.902	-0.006
17	1	17	16	0	16	15153.077	-0.002
11	3	8	10	2	9	15230.013	-0.009
19	1	18	18	2	17	15459.039	-0.002
15	2	14	14	1	13	15470.331	-0.002
9	4	6	8	3	5	15525.788	-0.005
9	4	5	8	3	6	15527.355	-0.004
18	0	18	17	1	17	15618.732	-0.002
7	5	3	6	4	2	15889.894	-0.007
7	5	2	6	4	3	15889.894	-0.008
22	2	20	21	3	19	15892.284	0.006
12	3	10	11	2	9	15899.127	-0.006
18	1	18	17	0	17	15985.556	0.000
24	8	16	24	7	17	16055.436	0.004
24	8	17	24	7	18	16055.436	0.002
23	8	15	23	7	16	16059.548	-0.004
23	8	16	23	7	17	16059.548	-0.005

Table B.1 Observed Transitions of Parent PiA (cont'd)

J'	K_a'	K_c'	J''	K_a''	K_c''	Obs. Frequency (MHz)	Obs. - Calc. (MHz)
21	8	13	21	7	14	16066.378	-0.002
21	8	14	21	7	15	16066.378	-0.003
20	8	12	20	7	13	16069.169	0.000
20	8	13	20	7	14	16069.169	0.000
19	8	11	19	7	12	16071.592	0.003
19	8	12	19	7	13	16071.592	0.003
18	8	10	18	7	11	16073.679	0.002
18	8	11	18	7	12	16073.679	0.002
17	8	9	17	7	10	16075.468	0.004
17	8	10	17	7	11	16075.468	0.004
16	8	8	16	7	9	16076.983	0.000
16	8	9	16	7	10	16076.983	0.000
15	8	7	15	7	8	16078.263	0.001
15	8	8	15	7	9	16078.263	0.001
14	8	6	14	7	7	16079.325	-0.003
14	8	7	14	7	8	16079.325	-0.003
13	8	5	13	7	6	16080.206	-0.002
13	8	6	13	7	7	16080.206	-0.002
12	8	4	12	7	5	16080.925	0.000
12	8	5	12	7	6	16080.925	0.000
11	8	3	11	7	4	16081.502	0.000
11	8	4	11	7	5	16081.502	0.000
10	8	2	10	7	3	16081.958	0.000
10	8	3	10	7	4	16081.958	0.000
9	8	1	9	7	2	16082.316	0.002
9	8	2	9	7	3	16082.316	0.002
8	8	0	8	7	1	16082.588	0.002
8	8	1	8	7	2	16082.588	0.002
13	2	11	12	1	12	16101.842	-0.006
12	3	9	11	2	10	16149.479	-0.006
16	2	15	15	1	14	16216.113	0.002
10	4	7	9	3	6	16414.974	-0.006
10	4	6	9	3	7	16418.114	-0.005
20	1	19	19	2	18	16481.451	0.000
19	0	19	18	1	18	16520.052	-0.001
13	3	11	12	2	10	16729.648	-0.006
8	5	4	7	4	3	16781.195	-0.003

Table B.1 Observed Transitions of Parent PiA (cont'd)

J'	K_a'	K_c'	J''	K_a''	K_c''	Obs. Frequency (MHz)	Obs. - Calc. (MHz)
8	5	3	7	4	4	16781.195	-0.008
19	1	19	18	0	18	16823.036	0.004
17	2	16	16	1	15	16957.447	-0.003
13	3	10	12	2	11	17077.691	-0.007
6	6	0	5	5	1	17142.893	-0.005
6	6	1	5	5	0	17142.893	-0.005
14	2	12	13	1	13	17267.951	-0.012
11	4	8	10	3	7	17302.905	-0.003
11	4	7	10	3	8	17308.742	-0.005
20	0	20	19	1	19	17416.402	0.004
14	3	12	13	2	11	17546.373	-0.005
20	1	20	19	0	19	17665.152	-0.001
9	5	5	8	4	4	17672.357	0.000
18	2	17	17	1	16	17695.801	-0.001
10	5	6	9	4	5	18563.320†	-0.001
8	6	3	7	5	2	18925.718†	0.000
8	6	2	7	5	3	18925.718†	0.000
13	4	10	12	3	9	19072.976†	-0.005
9	6	4	8	5	3	19817.058†	0.002
9	6	3	8	5	4	19817.058†	0.002

† Denotes transition with frequencies calculated from measured sideband peaks

Table B.2 Observed Transitions of ^{13}C6/^{13}C19 PiA

J'	K_a'	K_c'	J''	K_a''	K_c''	Obs. Frequency (MHz)	Obs. - Calc. (MHz)
7	0	7	6	1	6	5327.447*	0.002
7	3	4	7	2	5	5340.838*	0.001
5	1	5	4	0	4	5346.603*	0.000
6	3	3	6	2	4	5353.825*	-0.001
7	3	5	7	2	6	5382.198*	-0.002
6	1	6	5	0	5	6171.715*	0.005
8	0	8	7	1	7	6267.758*	0.001
7	1	7	6	0	6	6989.208*	-0.001
9	0	9	8	1	8	7209.839*	-0.001
8	1	8	7	0	7	7800.508*	-0.002
3	3	1	2	2	0	8031.266*	-0.001
3	3	0	2	2	1	8031.607*	0.000
10	0	0	9	1	9	8151.900*	0.001
9	1	9	8	0	8	8607.203*	-0.004
4	3	2	3	2	1	8917.455*	0.001
4	3	1	3	2	2	8919.157*	-0.002
10	1	0	9	0	9	9411.008*	0.000
11	1	1	10	0	0	10213.655*	0.001
4	4	1	3	3	0	11066.615*	0.004
4	4	0	3	3	1	11066.615*	0.001
5	4	2	4	3	1	11953.534*	-0.001
5	4	1	4	3	2	11953.559*	0.001
5	5	1	4	4	0	14101.766	-0.002
5	5	0	4	4	1	14101.766	-0.002
6	5	2	5	4	1	14988.698	-0.009
6	5	1	5	4	2	14988.698	-0.009
7	5	3	6	4	2	15875.587	-0.009
7	5	2	6	4	3	15875.587	-0.010
6	6	1	5	5	0	17136.903	-0.003
6	6	0	5	5	1	17136.903	-0.003

* Denotes transitions measured with the cavity method

Table B.3 Observed Transitions of ^{13}C7/^{13}C20 PiA

J'	K_a'	K_c'	J''	K_a''	K_c''	Obs. Frequency (MHz)	Obs. - Calc. (MHz)
7	0	7	6	1	6	5282.884*	0.002
5	1	5	4	0	4	5320.933*	0.000
7	3	4	7	2	5	5348.924*	0.003
6	3	3	6	2	4	5361.548*	-0.003
5	3	2	5	2	3	5369.571*	0.000
8	0	8	7	1	7	6216.937*	0.000
9	0	9	8	1	8	7152.857*	0.002
3	3	1	2	2	0	8020.944*	0.000
3	3	0	2	2	1	8021.274*	0.000
9	1	9	8	0	8	8561.403*	0.000
4	3	2	3	2	1	8901.293*	0.001
4	3	1	3	2	2	8902.949*	0.000
10	1	10	9	0	9	9360.108*	0.000
5	3	3	4	2	2	9780.381*	0.000
5	3	2	4	2	3	9785.366*	-0.002
11	1	11	10	0	10	10157.556*	0.000
4	4	1	3	3	0	11053.327*	0.001
4	4	0	3	3	1	11053.327*	-0.002
5	4	2	4	3	1	11934.386*	-0.004
5	4	1	4	3	2	11934.415*	0.004

* Denotes transitions measured with the cavity method

Table B.4 Observed Transitions of ^{13}C11/^{13}C24 PiA

J'	K_a'	K_c'	J''	K_a''	K_c''	Obs. Frequency (MHz)	Obs. - Calc. (MHz)
5	1	5	4	0	4	5321.290*	0.003
8	3	6	8	2	7	5325.553*	0.000
9	3	7	9	2	8	5337.543*	0.000
7	0	7	6	1	6	5339.567*	0.000
10	3	8	10	2	9	5353.781*	-0.002
6	1	6	5	0	5	6142.923*	-0.006
8	0	8	7	1	7	6279.831*	0.000
7	1	7	6	0	6	6956.831*	0.001
9	0	9	8	1	8	7221.483*	-0.001
3	3	1	2	2	0	7961.814*	-0.001
3	3	0	2	2	1	7962.193*	0.003
4	3	2	3	2	1	8846.888*	0.003
4	3	1	3	2	2	8848.763*	-0.001
5	3	3	4	2	2	9730.526*	0.001
5	3	2	4	2	3	9736.186*	0.000
4	4	1	3	3	0	10969.618*	0.001
4	4	0	3	3	1	10969.618*	-0.003
5	4	2	4	3	1	11855.497*	-0.003
5	4	1	4	3	2	11855.527*	0.001
5	1	5	4	0	4	5321.290*	0.003

* Denotes transitions measured with the cavity method

Table B.5 Observed Transitions of ^{13}C15/^{13}C28 PiA

J'	K_a'	K_c'	J''	K_a''	K_c''	Obs. Frequency (MHz)	Obs. - Calc. MHz)
7	0	7	6	1	6	5322.873*	-0.001
7	3	5	7	2	6	5324.104*	0.000
8	3	6	8	2	7	5331.209*	-0.002
5	1	5	4	0	4	5336.909*	0.000
9	3	7	9	2	8	5341.253*	0.000
10	3	8	10	2	9	5354.878*	0.000
6	1	6	5	0	5	6163.624*	-0.002
8	0	8	7	1	7	6260.286*	-0.002
7	1	7	6	0	6	6982.974*	-0.001
9	0	9	8	1	8	7199.666*	-0.004
3	3	1	2	2	0	7970.629*	0.000
3	3	0	2	2	1	7970.941*	0.001
10	0	10	9	1	9	8139.340*	0.001
4	3	2	3	2	1	8855.708*	0.000
4	3	1	3	2	2	8857.272*	0.000
5	3	3	4	2	2	9739.596*	-0.001
5	3	2	4	2	3	9744.303*	-0.002
4	4	1	3	3	0	10981.931*	-0.003
4	4	0	3	3	1	10981.931*	-0.006
5	4	2	4	3	1	11867.685*	-0.003
5	4	1	4	3	2	11867.709*	0.001
6	4	3	5	3	2	12753.334*	-0.001
6	4	2	5	3	3	12753.419*	0.003

* Denotes transitions measured with the cavity method

Table B.6 Observed Transitions of ^{13}C=O PiA

J'	K_a'	K_c'	J''	K_a''	K_c''	Obs. Frequency (MHz)	Obs. - Calc. (MHz)
6	3	3	6	2	4	5339.354*	0.001
5	3	2	5	2	3	5347.761*	0.001
7	0	7	6	1	6	5355.080*	-0.004
4	3	2	4	2	3	5357.747*	-0.002
5	1	5	4	0	4	5359.340*	0.001
6	3	4	6	2	5	5362.968*	0.000
7	3	5	7	2	6	5368.263*	-0.001
8	0	8	7	1	7	6298.963*	-0.002
9	0	9	8	1	8	7244.545*	0.001
3	3	1	2	2	0	8027.232*	-0.003
3	3	0	2	2	1	8027.581*	0.000
9	1	9	8	0	8	8631.539*	-0.001
4	3	2	3	2	1	8916.783*	0.001
4	3	1	3	2	2	8918.523*	0.003
10	1	10	9	0	9	9438.308*	-0.001
5	3	3	4	2	2	9805.008*	0.000
5	3	2	4	2	3	9810.242*	0.001
11	1	11	10	0	10	10244.004*	0.005
4	4	1	3	3	0	11060.300*	0.002
4	4	0	3	3	1	11060.300*	-0.001
5	4	2	4	3	1	11950.595*	-0.001
5	4	1	4	3	2	11950.621*	0.001

* Denotes transitions measured with the cavity method

Table B.7 Observed Transitions of C=^{18}O PiA

J'	K_a'	K_c'	J''	K_a''	K_c''	Obs. Frequency (MHz)	Obs. - Calc. (MHz)
3	3	1	2	2	0	7894.860*	0.000
3	3	0	2	2	1	7895.250*	-0.001
4	4	1	3	3	0	10875.634*	0.003
4	4	0	3	3	1	10875.634*	-0.001
5	4	2	4	3	1	11762.785*	-0.002
5	4	1	4	3	2	11762.818*	0.002
5	5	1	4	4	0	13856.187*	-0.003
5	5	0	4	4	1	13856.187*	-0.003
6	5	2	5	4	1	14743.362*	-0.003
6	5	1	5	4	2	14743.362*	-0.003
7	5	3	6	4	2	15630.486*	0.002
7	5	2	6	4	3	15630.486*	0.000
8	5	4	7	4	3	16517.507*	0.002
8	5	3	7	4	4	16517.507*	-0.004
6	6	1	5	5	0	16836.729*	0.001
6	6	0	5	5	1	16836.729*	0.001

* Denotes transitions measured with the cavity method

Table B.8 Observed Transitions of Bridge ^{18}O PiA

J'	K_a'	K_c'	J''	K_a''	K_c''	Obs. Frequency (MHz)	Obs. - Calc. MHz)
4	4	1	3	3	0	11066.999*	0.002
4	4	0	3	3	1	11066.999*	-0.002
5	4	2	4	3	1	11958.423*	-0.006
5	4	1	4	3	2	11958.459*	0.003
6	4	3	5	3	2	12849.736*	0.000
6	4	2	5	3	3	12849.841*	-0.001

* Denotes transitions measured with the cavity method

Table B.9 Coordinates of PiA Minimum

Cartesian coordinates [in Å] of the minimum energy structure of pivalic anhydride from M06-2X/6-311++G(3df,3pd) calculations.

	X	Y	Z
C	1.139643	0.447793	-0.350513
O	1.081827	1.473542	-0.945815
O	0.000006	-0.251592	0.000086
C	-1.139670	0.447812	0.350550
O	-1.081902	1.473599	0.945789
C	2.395336	-0.279465	0.086978
C	3.606942	0.456156	-0.474714
H	4.517959	-0.048517	-0.154611
H	3.581241	0.474228	-1.563094
H	3.633132	1.485848	-0.123948
C	2.359500	-1.725369	-0.420841
H	3.273835	-2.232039	-0.112574
H	1.509335	-2.267248	-0.011949
H	2.303997	-1.757553	-1.509016
C	2.421453	-0.264103	1.621889
H	3.331645	-0.754062	1.967277
H	2.414571	0.757000	2.002330
H	1.564996	-0.794467	2.034422
C	-2.395324	-0.279482	-0.086990
C	-3.606978	0.456180	0.474544
H	-4.517968	-0.048520	0.154403
H	-3.581370	0.474336	1.562925
H	-3.633140	1.485844	0.123696
C	-2.359525	-1.725347	0.420945
H	-1.509322	-2.267254	0.012169
H	-2.304118	-1.757446	1.509127
H	-3.273831	-2.232044	0.112637
C	-2.421310	-0.264238	-1.621903
H	-3.331472	-0.754226	-1.967331
H	-2.414394	0.756835	-2.002423
H	-1.564817	-0.794635	-2.034323

Appendix C: Supplementary Material for Chapter 3

Table C.1 Observed Transitions of Parent PiTFAA

J'	K_a'	K_c'	J''	K_a''	K_c''	Obs. Frequency (MHz)	Obs. - Calc. (MHz)
7	2	5	6	2	4	6010.239	-0.004
15	3	13	15	2	14	6059.149	-0.001
3	2	1	2	1	2	6065.662	0.002
7	1	6	6	1	5	6077.055	-0.001
8	1	8	7	1	7	6720.133	0.000
7	1	7	6	0	6	6768.393	0.003
4	2	3	3	1	2	6792.408	-0.003
8	0	8	7	0	7	6800.036	0.002
11	1	10	10	2	9	6814.186	-0.004
8	2	7	7	2	6	6835.208	0.000
8	4	5	7	4	4	6844.954*	-0.001
8	4	4	7	4	3	6844.974*	0.001
8	3	6	7	3	5	6846.805	0.003
8	3	5	7	3	4	6848.254	0.001
8	2	6	7	2	5	6876.587	0.003
9	0	9	8	1	8	6908.338	-0.003
8	1	7	7	1	6	6942.337	0.000
4	2	2	3	1	3	6967.770	0.001
21	4	17	21	3	18	7493.616	0.001
8	1	8	7	0	7	7530.234	0.010
9	1	9	8	1	8	7557.391	0.002
5	2	4	4	1	3	7591.575	-0.001
9	0	9	8	0	8	7638.531	0.001
9	2	8	8	2	7	7687.447	0.000
19	4	15	19	3	16	7697.802	-0.008
9	7	3	8	7	2	7698.522	0.009
9	7	2	8	7	1	7698.522	0.009
9	6	4	8	6	3	7699.030	0.002
9	6	3	8	6	2	7699.030	0.002
9	5	5	8	5	4	7699.875	0.006
9	5	4	8	5	3	7699.875	0.005
9	4	6	8	4	5	7701.423*	0.002
9	4	5	8	4	4	7701.464*	0.000
9	3	7	8	3	6	7703.773	0.001
9	3	6	8	3	5	7706.427	0.002

* Denotes transitions measured with the cavity method

Table C.1 Observed Transitions of Parent PiTFAA (cont'd)

J'	K_a'	K_c'	J''	K_a''	K_c''	Obs. Frequency (MHz)	Obs. - Calc. (MHz)
9	2	7	8	2	6	7745.473	0.003
18	4	14	18	3	15	7777.575	0.004
15	2	13	14	3	12	7801.918	-0.004
9	1	8	8	1	7	7806.352	0.004
12	1	11	11	2	10	7812.930	0.000
10	0	10	9	1	9	7824.786	0.000
17	4	13	17	3	14	7843.562	-0.006
5	2	3	4	1	4	7888.851	-0.001
16	4	12	16	3	13	7897.138	-0.002
15	4	11	15	3	12	7939.822	-0.001
14	4	10	14	3	11	7973.206	0.000
13	4	9	13	3	10	7998.843	0.006
12	4	8	12	3	9	8018.145	0.004
11	4	7	11	3	8	8032.391	0.000
15	4	12	15	3	13	8038.662	0.008
16	4	13	16	3	14	8038.834	-0.006
14	4	11	14	3	12	8040.166	-0.002
17	4	14	17	3	15	8041.462	0.002
12	4	9	12	3	10	8045.906	0.001
18	4	15	18	3	16	8047.344	0.001
11	4	8	11	3	9	8049.206	-0.001
10	4	7	10	3	8	8052.358	-0.006
8	4	4	8	3	5	8054.897	0.010
9	4	6	9	3	7	8055.185	0.010
9	1	9	8	0	8	8287.583	0.004
6	2	5	5	1	4	8376.854	0.001
10	1	10	9	1	9	8393.822	0.003
10	0	10	9	0	9	8473.838	0.003
10	2	9	9	2	8	8538.932	0.001
10	8	2	9	8	1	8553.756	-0.005
10	8	3	9	8	2	8553.756	-0.005
10	7	3	9	7	2	8554.227	0.000
10	7	4	9	7	3	8554.227	0.000
10	6	4	9	6	3	8554.928	0.002
10	6	5	9	6	4	8554.928	0.002
10	5	6	9	5	5	8556.076	0.005
10	5	5	9	5	4	8556.076	0.004

Table C.1 Observed Transitions of Parent PiTFAA (cont'd)

J'	K_a'	K_c'	J''	K_a''	K_c''	Obs. Frequency (MHz)	Obs. - Calc. (MHz)
10	4	7	9	4	6	8558.179*	0.000
10	4	6	9	4	5	8558.272*	0.000
10	3	8	9	3	7	8560.994	0.004
10	3	7	9	3	6	8565.521	0.001
10	2	8	9	2	7	8616.767	0.003
10	1	9	9	1	8	8668.861	0.003
11	0	11	10	1	10	8737.147	0.004
13	1	12	12	2	11	8818.295	-0.010
6	2	4	5	1	5	8831.420	0.004
10	1	10	9	0	9	9042.872	0.004
7	2	6	6	1	5	9148.435	0.005
4	3	2	3	2	1	9178.885	0.005
4	3	1	3	2	2	9181.459	-0.005
11	1	11	10	1	10	9229.403	0.001
11	0	11	10	0	10	9306.174	-0.001
11	2	10	10	2	9	9389.581	0.000
11	9	2	10	9	1	9408.994	-0.001
11	8	3	10	8	2	9409.434	0.000
11	8	4	10	8	3	9409.434	0.000
11	7	4	10	7	3	9410.044	-0.001
11	7	5	10	7	4	9410.044	-0.001
11	6	5	10	6	4	9410.966	0.002
11	6	6	10	6	5	9410.966	0.002
11	5	7	10	5	6	9412.484	0.002
11	5	6	10	5	5	9412.484	0.000
11	4	8	10	4	7	9415.253	-0.001
11	4	7	10	4	6	9415.438	-0.003
11	3	9	10	3	8	9418.411	0.000
11	3	8	10	3	7	9425.729	-0.001
11	2	9	10	2	8	9490.143	0.000
11	1	10	10	1	9	9529.609	0.001
12	0	12	11	1	11	9643.675	-0.002
7	2	5	6	1	6	9798.362*	0.000
11	1	11	10	0	10	9798.435*	0.000
14	1	13	13	2	12	9828.649	-0.001
8	2	7	7	1	6	9906.589	0.006
5	3	3	4	2	2	10031.054	-0.002

* Denotes transitions measured with the cavity method

Table C.1 Observed Transitions of Parent PiTFAA (cont'd)

J'	K_a'	K_c'	J''	K_a''	K_c''	Obs. Frequency (MHz)	Obs. - Calc. (MHz)
5	3	2	4	2	3	10038.844	0.004
12	1	12	11	1	11	10064.143	0.004
12	0	12	11	0	11	10135.939	0.001
12	2	11	11	2	10	10239.325	0.002
12	9	3	11	9	2	10264.638	0.003
12	9	4	11	9	3	10264.638	0.003
12	8	4	11	8	3	10265.196	0.003
12	8	5	11	8	4	10265.196	0.003
12	7	5	11	7	4	10265.983	0.006
12	7	6	11	7	5	10265.983	0.006
12	6	6	11	6	5	10267.162	0.002
12	6	7	11	6	6	10267.162	0.002
12	5	8	11	5	7	10269.126	0.004
12	5	7	11	5	6	10269.126	-0.002
12	4	9	11	4	8	10272.674	0.004
12	4	8	11	4	7	10273.022	0.004
12	3	10	11	3	9	10275.974	0.002
12	3	9	11	3	8	10287.273	0.005
18	5	13	18	4	14	10294.552	0.006
17	5	12	17	4	13	10310.310	0.004
18	5	14	18	4	15	10310.980	-0.006
17	5	13	17	4	14	10320.875	0.006
16	5	11	16	4	12	10323.026	0.003
16	5	12	16	4	13	10329.619	0.002
15	5	10	15	4	11	10333.238	0.008
15	5	11	15	4	12	10337.215	0.000
14	5	9	14	4	10	10341.367	-0.001
14	5	10	14	4	11	10343.693	0.003
13	5	8	13	4	9	10347.812	0.008
13	5	9	13	4	10	10349.100	-0.001
12	5	8	12	4	9	10353.526	-0.005
11	5	6	11	4	7	10356.741	0.009
11	5	7	11	4	8	10357.079	0.000
10	5	5	10	4	6	10359.684	-0.005
8	5	3	8	4	4	10363.483*	-0.001
8	5	4	8	4	5	10363.512*	0.001
7	5	2	7	4	3	10364.611	0.009

* Denotes transitions measured with the cavity method

Table C.1 Observed Transitions of Parent PiTFAA (cont'd)

J'	K_a'	K_c'	J''	K_a''	K_c''	Obs. Frequency (MHz)	Obs. - Calc. (MHz)
7	5	3	7	4	4	10364.611	0.000
12	2	10	11	2	9	10365.121	0.003
6	5	1	6	4	2	10365.361	0.008
6	5	2	6	4	3	10365.361	0.005
5	5	0	5	4	1	10365.831	0.002
5	5	1	5	4	2	10365.831	0.001
12	1	11	11	1	10	10388.322	0.002
13	0	13	12	1	12	10543.157	0.001
12	1	12	11	0	11	10556.402	0.003
9	2	8	8	1	7	10651.697	0.003
8	2	6	7	1	7	10792.864	0.002
15	1	14	14	2	13	10842.067	-0.001
6	3	4	5	2	3	10879.871	0.004
13	1	13	12	1	12	10898.044*	-0.001
6	3	3	5	2	4	10898.100*	0.001
13	0	13	12	0	12	10963.623	0.005
13	2	12	12	2	11	11088.087	0.000
13	10	3	12	10	2	11119.814	-0.008
13	9	4	12	9	3	11120.347	0.001
13	9	5	12	9	4	11120.347	0.001
13	8	5	12	8	4	11121.047	0.002
13	8	6	12	8	5	11121.047	0.002
13	7	6	12	7	5	11122.035	0.005
13	7	7	12	7	6	11122.035	0.005
13	6	8	12	6	7	11123.530	0.003
13	6	7	12	6	6	11123.530	0.002
13	5	8	12	5	7	11126.024	0.000
13	4	10	12	4	9	11130.444	0.001
13	4	9	12	4	8	11131.065	0.003
13	3	11	12	3	10	11133.593	0.003
13	3	10	12	3	9	11150.366	0.000
13	2	11	12	2	10	11241.087	0.000
13	1	12	12	1	11	11244.701	0.004
13	1	13	12	0	12	11318.513	0.006
10	2	9	9	1	8	11384.279	0.004
14	0	14	13	1	13	11434.869	0.004
4	4	1	3	3	0	11483.938	0.008

* Denotes transitions measured with the cavity method

Table C.1 Observed Transitions of Parent PiTFAA (cont'd)

J'	K_a'	K_c'	J''	K_a''	K_c''	Obs. Frequency (MHz)	Obs. - Calc. (MHz)
4	4	0	3	3	1	11483.938	0.003
7	3	5	6	2	4	11723.570	0.002
14	1	14	13	1	13	11731.154	0.005
7	3	4	6	2	5	11760.156	0.006
14	0	14	13	0	13	11789.758	0.003
9	2	7	8	1	8	11818.200	0.000
14	2	13	13	2	12	11935.813	0.002
14	9	5	13	9	4	11976.142	0.005
14	9	6	13	9	5	11976.142	0.005
14	8	6	13	8	5	11977.000	0.003
14	8	7	13	8	6	11977.000	0.003
14	7	7	13	7	6	11978.224	0.006
14	7	8	13	7	7	11978.224	0.006
14	6	9	13	6	8	11980.082	0.003
14	6	8	13	6	7	11980.082	0.003
14	5	10	13	5	9	11983.173*	-0.002
14	5	9	13	5	8	11983.199*	0.001
14	4	11	13	4	10	11988.591	0.005
14	4	10	13	4	9	11989.638	0.004
14	3	12	13	3	11	11991.175	0.001
14	3	11	13	3	10	12015.266	0.003
14	1	14	13	0	13	12086.035	-0.004
14	1	13	13	1	12	12098.432	-0.001
11	2	10	10	1	9	12104.995	-0.003
14	2	12	13	2	11	12117.392	-0.002
15	0	15	14	1	14	12318.574	-0.003
5	4	2	4	3	1	12339.190*	0.000
5	4	1	4	3	2	12339.232*	0.001
8	3	6	7	2	5	12560.123	-0.003
15	1	15	14	1	14	12563.492	-0.003
23	6	17	23	5	18	12580.160	0.000
22	6	17	22	5	18	12598.896	0.005
15	0	15	14	0	14	12614.859	-0.003
8	3	5	7	2	6	12626.109	-0.002
19	6	13	19	5	14	12628.489	-0.001
17	6	12	17	5	13	12643.483	0.006
16	6	10	16	5	11	12648.818	0.006

* Denotes transitions measured with the cavity method

Table C.1 Observed Transitions of Parent PiTFAA (cont'd)

J'	K_a'	K_c'	J''	K_a''	K_c''	Obs. Frequency (MHz)	Obs. - Calc. (MHz)
15	6	9	15	5	10	12653.485*	0.000
15	6	10	15	5	11	12653.567*	-0.003
13	6	7	13	5	8	12660.444*	0.000
13	6	8	13	5	9	12660.465*	0.001
12	6	6	12	5	7	12662.944	0.003
12	6	7	12	5	8	12662.944	-0.006
11	6	5	11	5	6	12664.908	0.000
11	6	6	11	5	7	12664.908	-0.004
10	6	4	10	5	5	12666.429	0.001
10	6	5	10	5	6	12666.429	0.000
9	6	3	9	5	4	12667.568	-0.006
9	6	4	9	5	5	12667.568	-0.007
8	6	2	8	5	3	12668.411	-0.005
8	6	3	8	5	4	12668.411	-0.005
7	6	1	7	5	2	12669.007	-0.006
7	6	2	7	5	3	12669.007	-0.006
6	6	0	6	5	1	12669.413	-0.004
6	6	1	6	5	2	12669.413	-0.004
15	2	14	14	2	13	12782.438	0.001
12	2	11	11	1	10	12814.714	0.002
15	12	3	14	12	2	12830.142	0.003
15	11	4	14	11	3	12830.634	0.004
15	11	5	14	11	4	12830.634	0.004
15	10	5	14	10	4	12831.234	-0.001
15	10	6	14	10	5	12831.234	-0.001
15	9	6	14	9	5	12832.008	-0.004
15	9	7	14	9	6	12832.008	-0.004
15	8	7	14	8	6	12833.059	0.001
15	8	8	14	8	7	12833.059	0.001
15	7	8	14	7	7	12834.551	0.001
15	7	9	14	7	8	12834.551	0.001
15	6	10	14	6	9	12836.831	0.001
15	6	9	14	6	8	12836.831	0.000
15	5	11	14	5	10	12840.628*	-0.001
15	5	10	14	5	9	12840.671*	0.000
15	4	12	14	4	11	12847.102	-0.001
15	3	13	14	3	12	12848.614	-0.004

* Denotes transitions measured with the cavity method

Table C.1 Observed Transitions of Parent PiTFAA (cont'd)

J'	K_a'	K_c'	J''	K_a''	K_c''	Obs. Frequency (MHz)	Obs. - Calc. (MHz)
15	4	11	14	4	10	12848.806	-0.004
15	1	15	14	0	14	12859.780	-0.001
17	1	16	16	2	15	12869.476	-0.001
10	2	8	9	1	9	12877.567	-0.007
15	3	12	14	3	11	12882.194	0.001
15	1	14	14	1	13	12949.229	0.000
15	2	13	14	2	12	12993.397	0.000
6	4	3	5	3	2	13194.269*	-0.002
6	4	2	5	3	3	13194.436*	0.001
16	0	16	15	1	15	13194.469*	0.001
9	3	7	8	2	6	13387.315	0.001
16	1	16	15	1	15	13395.130	-0.004
16	0	16	15	0	15	13439.385	-0.001
9	3	6	8	2	7	13497.328	0.000
13	2	12	12	1	11	13514.481	0.001
16	2	15	15	2	14	13627.917	-0.001
16	1	16	15	0	15	13640.051	-0.001
16	12	4	15	12	3	13685.752	0.005
16	12	5	15	12	4	13685.752	0.005
16	11	5	15	11	4	13686.328	0.000
16	11	6	15	11	5	13686.328	0.000
16	10	6	15	10	5	13687.045	-0.003
16	10	7	15	10	6	13687.045	-0.003
16	9	7	15	9	6	13687.979	0.002
16	9	8	15	9	7	13687.979	0.002
16	8	8	15	8	7	13689.238	0.003
16	8	9	15	8	8	13689.238	0.003
16	7	9	15	7	8	13691.036	0.000
16	7	10	15	7	9	13691.036	0.000
16	6	11	15	6	10	13693.799	0.003
16	6	10	15	6	9	13693.799	0.001
16	5	12	15	5	11	13698.393*	0.000
16	5	11	15	5	10	13698.470*	0.000
16	3	14	15	3	13	13705.804	-0.001
16	4	13	15	4	12	13705.993	0.001
16	4	12	15	4	11	13708.680	0.002
16	3	13	15	3	12	13751.359	0.000

* Denotes transitions measured with the cavity method

Table C.1 Observed Transitions of Parent PiTFAA (cont'd)

J'	K_a'	K_c'	J''	K_a''	K_c''	Obs. Frequency (MHz)	Obs. - Calc. (MHz)
16	1	15	15	1	14	13796.807	-0.002
16	2	14	15	2	13	13868.513	0.002
18	1	17	17	2	16	13878.797	0.008
11	2	9	10	1	10	13973.900	0.001
7	4	4	6	3	3	14048.991	-0.005
7	4	3	6	3	4	14049.497	0.007
17	0	17	16	1	16	14063.007	-0.002
10	3	8	9	2	7	14202.836	0.002
14	2	13	13	1	12	14205.595	0.002
17	1	17	16	1	16	14226.122	0.000
17	0	17	16	0	16	14263.676	0.001
10	3	7	9	2	8	14375.401	0.001
17	1	17	16	0	16	14426.792	0.004
17	2	16	16	2	15	14472.217	0.002
17	14	3	16	14	2	14540.346	-0.006
17	13	4	16	13	3	14540.844	0.004
17	12	5	16	12	4	14541.402	-0.004
17	11	6	16	11	5	14542.089	0.001
17	11	7	16	11	6	14542.089	0.001
17	10	7	16	10	6	14542.939	0.002
17	10	8	16	10	7	14542.939	0.002
17	9	8	16	9	7	14544.044	0.006
17	9	9	16	9	8	14544.044	0.006
17	8	9	16	8	8	14545.536	0.000
17	8	10	16	8	9	14545.536	0.000
17	7	10	16	7	9	14547.686	0.000
17	7	11	16	7	10	14547.686	0.000
17	6	12	16	6	11	14550.994	0.003
17	6	11	16	6	10	14550.994	0.000
17	5	13	16	5	12	14556.486*	-0.001
17	5	12	16	5	11	14556.623*	0.001
17	3	15	16	3	14	14562.616	0.000
17	4	14	16	4	13	14565.238	0.002
17	4	13	16	4	12	14569.343	0.004
17	3	14	16	3	13	14622.915	0.002
17	1	16	16	1	15	14640.953	-0.001
5	5	0	4	4	1	14642.843	0.003

* Denotes transitions measured with the cavity method

Table C.1 Observed Transitions of Parent PiTFAA (cont'd)

J'	K_a'	K_c'	J''	K_a''	K_c''	Obs. Frequency (MHz)	Obs. - Calc. (MHz)
5	5	1	4	4	0	14642.843	0.003
17	2	15	16	2	14	14742.235	0.002
19	1	18	18	2	17	14882.001	0.002
15	2	14	14	1	13	14889.596	-0.001
18	0	18	17	1	17	14924.865	0.003
19	7	13	19	6	14	14949.066	-0.008
18	7	11	18	6	12	14953.669	0.003
18	7	12	18	6	13	14953.669	-0.007
17	7	10	17	6	11	14957.595	0.007
17	7	11	17	6	12	14957.595	0.002
16	7	9	16	6	10	14960.889	-0.006
16	7	10	16	6	11	14960.889	-0.008
15	7	9	15	6	10	14963.667	0.009
14	7	7	14	6	8	14965.934	-0.004
14	7	8	14	6	9	14965.934	-0.004
13	7	6	13	6	7	14967.799	0.000
13	7	7	13	6	8	14967.799	0.000
12	7	5	12	6	6	14969.294	-0.002
12	7	6	12	6	7	14969.294	-0.002
11	7	4	11	6	5	14970.479	-0.001
11	7	5	11	6	6	14970.479	-0.001
10	7	3	10	6	4	14971.395	-0.003
10	7	4	10	6	5	14971.395	-0.003
9	7	2	9	6	3	14972.101	0.005
9	7	3	9	6	4	14972.101	0.005
8	7	1	8	6	2	14972.608	-0.003
8	7	2	8	6	3	14972.608	-0.003
11	3	9	10	2	8	15004.481	0.000
18	1	18	17	1	17	15056.520	-0.003
18	0	18	17	0	17	15087.968	-0.007
18	1	18	17	0	17	15219.636	0.000
11	3	8	10	2	9	15262.199	0.000
18	2	17	17	2	16	15315.295	-0.005
18	11	7	17	11	6	15397.914	0.000
18	11	8	17	11	7	15397.914	0.000
18	10	8	17	10	7	15398.906	-0.001
18	10	9	17	10	8	15398.906	-0.001
18	9	9	17	9	8	15400.200	-0.003

Table C.1 Observed Transitions of Parent PiTFAA (cont'd)

J'	K_a'	K_c'	J''	K_a''	K_c''	Obs. Frequency (MHz)	Obs. - Calc. (MHz)
18	9	10	17	9	9	15400.200	-0.003
18	8	10	17	8	9	15401.966	-0.003
18	8	11	17	8	10	15401.966	-0.003
18	7	12	17	7	11	15404.512	-0.001
18	7	11	17	7	10	15404.512	-0.001
18	6	13	17	6	12	15408.432	0.003
18	6	12	17	6	11	15408.432	-0.002
18	5	14	17	5	13	15414.929	0.000
18	5	13	17	5	12	15415.155	-0.002
18	3	16	17	3	15	15418.924	-0.004
18	4	15	17	4	14	15424.808	-0.003
18	4	14	17	4	13	15430.917	0.000
18	1	17	17	1	16	15481.524	-0.003
18	3	15	17	3	14	15496.914	0.000
6	5	2	5	4	1	15498.141	0.004
6	5	1	5	4	2	15498.141	0.004
16	2	15	15	1	14	15568.284	-0.002
18	2	16	17	2	15	15614.140	-0.001
9	4	6	8	3	5	15756.274	-0.008
9	4	5	8	3	6	15759.021	0.004
19	0	19	18	1	18	15780.784	0.001
12	3	10	11	2	9	15790.312	0.002
20	1	19	19	2	18	15876.857	-0.004
19	1	19	18	1	18	15886.401	0.001
19	0	19	18	0	18	15912.442	-0.003
19	1	19	18	0	18	16018.060	-0.001
19	2	18	18	2	17	16157.159	0.000
12	3	9	11	2	10	16159.886	-0.001
17	2	16	16	1	15	16243.694	0.002
19	10	9	18	10	8	16254.964	0.000
19	10	10	18	10	9	16254.964	0.000
19	9	10	18	9	9	16256.477	0.002
19	9	11	18	9	10	16256.477	0.002
19	8	12	18	8	11	16258.544	0.003
19	8	11	18	8	10	16258.544	0.003
19	7	13	18	7	12	16261.524	-0.001
19	7	12	18	7	11	16261.524	-0.001
19	6	14	18	6	13	16266.130	0.003

Table C.1 Observed Transitions of Parent PiTFAA (cont'd)

J'	K_a'	K_c'	J''	K_a''	K_c''	Obs. Frequency (MHz)	Obs. - Calc. (MHz)
19	6	13	18	6	12	16266.130	-0.006
19	5	15	18	5	14	16273.732	-0.002
19	5	14	18	5	13	16274.106	-0.001
19	3	17	18	3	16	16274.614	-0.002
19	4	16	18	4	15	16284.680	-0.001
13	2	11	12	1	12	16286.560	-0.002
19	4	15	18	4	14	16293.548	0.001
19	1	18	18	1	17	16318.512	0.002
7	5	3	6	4	2	16353.366	0.005
7	5	2	6	4	3	16353.366	0.003
19	3	16	18	3	15	16373.305	-0.002
19	2	17	18	2	16	16483.885	0.001
13	3	11	12	2	10	16558.781	0.000
10	4	7	9	3	6	16608.031	-0.005
10	4	6	9	3	7	16613.526	0.009
20	0	20	19	1	19	16631.553	-0.003
20	1	20	19	1	19	16715.814	-0.001
20	0	20	19	0	19	16737.172	-0.001
20	1	20	19	0	19	16821.434	0.002
21	1	20	20	2	19	16861.394	0.000
18	2	17	17	1	16	16918.039	0.001
20	2	19	19	2	18	16997.789	0.000
13	3	10	12	2	11	17070.927	-0.004
20	12	8	19	12	7	17108.729	0.002
20	12	9	19	12	8	17108.729	0.002
20	11	9	19	11	8	17109.781	0.000
20	11	10	19	11	9	17109.781	0.000
20	10	10	19	10	9	17111.116	0.003
20	10	11	19	10	10	17111.116	0.003
20	9	11	19	9	10	17112.866	0.004
20	9	12	19	9	11	17112.866	0.004
20	8	12	19	8	11	17115.265	0.003
20	8	13	19	8	12	17115.265	0.003
20	7	14	19	7	13	17118.734	0.000
20	7	13	19	7	12	17118.734	-0.001
20	6	14	19	6	13	17124.108	-0.006
20	3	18	19	3	17	17129.563	0.001
20	5	16	19	5	15	17132.920	0.004

Table C.1 Observed Transitions of Parent PiTFAA (cont'd)

J'	K_a'	K_c'	J''	K_a''	K_c''	Obs. Frequency (MHz)	Obs. - Calc. (MHz)
20	5	15	19	5	14	17133.513	0.003
20	4	17	19	4	16	17144.797	0.001
20	1	19	19	1	18	17152.021	0.001
20	4	16	19	4	15	17157.392	0.003
8	5	4	7	4	3	17208.464	0.007
8	5	3	7	4	4	17208.464	-0.002
25	8	17	25	7	18	17231.038	0.002
24	8	16	24	7	17	17237.803	0.010
24	8	17	24	7	18	17237.803	0.002
23	8	16	23	7	17	17243.782	0.006
22	8	14	22	7	15	17249.032	-0.002
22	8	15	22	7	16	17249.032	-0.004
20	3	17	19	3	16	17251.891	-0.001
21	8	13	21	7	14	17253.641	-0.003
21	8	14	21	7	15	17253.641	-0.004
20	8	12	20	7	13	17257.652	-0.005
20	8	13	20	7	14	17257.652	-0.005
19	8	11	19	7	12	17261.134	0.005
19	8	12	19	7	13	17261.134	0.005
18	8	10	18	7	11	17264.112	-0.002
18	8	11	18	7	12	17264.112	-0.002
17	8	9	17	7	10	17266.653	-0.005
17	8	10	17	7	11	17266.653	-0.005
16	8	8	16	7	9	17268.808	0.000
16	8	9	16	7	10	17268.808	0.000
15	8	7	15	7	8	17270.608	-0.001
15	8	8	15	7	9	17270.608	-0.001
14	8	6	14	7	7	17272.108	0.007
14	8	7	14	7	8	17272.108	0.007
13	8	5	13	7	6	17273.321	-0.001
13	8	6	13	7	7	17273.321	-0.001
12	8	4	12	7	5	17274.306	-0.002
12	8	5	12	7	6	17274.306	-0.002
11	8	3	11	7	4	17275.090	-0.002
11	8	4	11	7	5	17275.090	-0.002
9	8	1	9	7	2	17276.178	0.007
14	3	12	13	2	11	17308.871	0.002
20	2	18	19	2	17	17351.163	-0.001

Table C.1 Observed Transitions of Parent PiTFAA (cont'd)

J'	K_a'	K_c'	J''	K_a''	K_c''	Obs. Frequency (MHz)	Obs. - Calc. (MHz)
11	4	8	10	3	7	17457.764	-0.006
11	4	7	10	3	8	17467.975	0.007
21	0	21	20	1	20	17477.930	-0.006
21	1	21	20	1	20	17544.831	0.003
21	0	21	20	0	20	17562.193	-0.003
19	2	18	18	1	17	17593.667	-0.002
21	1	21	20	0	20	17629.089	0.001
6	6	0	5	5	1	17801.726	0.002
6	6	1	5	5	0	17801.726	0.002
22	1	21	21	2	20	17834.015	0.001
21	2	20	20	2	19	17837.196	-0.004
21	10	11	20	10	10	17967.361	0.004
21	10	12	20	10	11	17967.361	0.004
21	9	12	20	9	11	17969.369	-0.001
21	9	13	20	9	12	17969.369	-0.001
21	8	13	20	8	12	17972.139	0.000
21	8	14	20	8	13	17972.139	0.000
21	7	15	20	7	14	17976.154	0.003
21	7	14	20	7	13	17976.154	0.002
21	3	19	20	3	18	17983.648	0.000
21	5	17	20	5	16	17992.487	0.001
21	5	16	20	5	15	17993.414	0.005
14	3	11	13	2	12	17998.106	-0.001
22	1	22	21	0	21	18440.393†	0.005
7	6	1	6	5	2	18657.026†	0.006
7	6	2	6	5	1	18657.026†	0.006

† Denotes transition with frequencies calculated from measured sideband peaks

Table C.2 Observed Transitions of ^{13}C1 PiTFAA

J'	K_a'	K_c'	J''	K_a''	K_c''	Obs. Frequency (MHz)	Obs. - Calc. (MHz)
7	1	7	6	1	6	5876.653*	0.000
7	0	7	6	0	6	5952.922*	0.002
7	2	6	6	2	5	5977.013*	-0.001
7	3	5	6	3	4	5984.861*	-0.001
7	2	5	6	2	4	6005.081*	0.001
7	1	6	6	1	5	6071.905*	0.001
8	1	8	7	1	7	6713.918*	0.001
7	1	7	6	0	6	6761.083*	0.001
8	0	8	7	0	7	6793.848*	-0.002
8	2	7	7	2	6	6829.168*	0.001
8	4	5	7	4	4	6838.955*	-0.001
8	4	4	7	4	3	6838.974*	0.000
8	2	6	7	2	5	6870.712*	-0.001
9	0	9	8	1	8	6903.302*	0.000
8	1	7	7	1	6	6936.436*	0.000
9	1	9	8	1	8	7550.387*	0.000
9	0	9	8	0	8	7631.532*	0.000
9	2	8	8	2	7	7680.642*	-0.001
9	4	6	8	4	5	7694.677*	0.001
9	4	5	8	4	4	7694.720*	0.000
9	2	7	8	2	6	7738.898*	0.000
9	1	8	8	1	7	7799.693*	0.000
10	0	10	9	1	9	7818.930*	0.000

* Denotes transitions measured with the cavity method

Table C.3 Observed Transitions of ^{13}C4 PiTFAA

J'	K_a'	K_c'	J''	K_a''	K_c''	Obs. Frequency (MHz)	Obs. - Calc. (MHz)
7	1	7	6	1	6	5872.021*	0.001
7	0	7	6	0	6	5948.167*	-0.001
7	2	6	6	2	5	5972.150*	0.001
7	5	3	6	5	2	5977.861*	0.000
7	5	2	6	5	1	5977.861*	0.000
7	2	5	6	2	4	6000.083*	0.000
7	1	6	6	1	5	6066.833*	-0.001
8	1	8	7	1	7	6708.632*	0.000
7	1	7	6	0	6	6757.314*	0.001
8	0	8	7	0	7	6788.461*	0.000
8	2	7	7	2	6	6823.615*	0.000
8	5	4	7	5	3	6832.260*	0.002
8	5	3	7	5	2	6832.260*	0.002
8	2	6	7	2	5	6864.968*	0.000
8	1	7	7	1	6	6930.657*	0.001
8	1	8	7	0	7	7517.777*	0.000
9	1	9	8	1	8	7544.453*	0.000
9	0	9	8	0	8	7625.517*	-0.001
9	2	8	8	2	7	7674.406*	0.000
9	4	6	8	4	5	7688.372*	-0.001
9	4	5	8	4	4	7688.414*	-0.002
9	2	7	8	2	6	7732.396*	0.000
9	1	8	8	1	7	7793.210*	0.001
10	0	10	9	1	9	7811.135*	0.002

* Denotes transitions measured with the cavity method

Table C.4 Observed Transitions of ^{13}C6 PiTFAA

J'	K_a'	K_c'	J''	K_a''	K_c''	Obs. Frequency (MHz)	Obs. - Calc. (MHz)
7	1	7	6	1	6	5851.035*	0.000
7	0	7	6	0	6	5926.770*	-0.001
8	0	8	7	1	7	5949.716*	-0.001
7	2	6	6	2	5	5950.300*	0.000
6	1	6	5	0	5	5976.505*	0.001
7	2	5	6	2	4	5977.708*	0.000
7	1	6	6	1	5	6044.228*	0.000
8	1	8	7	1	7	6684.689*	0.000
7	1	7	6	0	6	6741.226*	-0.001
8	0	8	7	0	7	6764.174*	0.000
8	2	7	7	2	6	6798.679*	0.001
8	2	6	7	2	5	6839.262*	0.000
9	0	9	8	1	8	6863.416*	0.000
8	1	7	7	1	6	6904.879*	0.000
9	1	9	8	1	8	7517.566*	0.001
9	0	9	8	0	8	7598.387*	-0.001
9	2	8	8	2	7	7646.393*	0.000
9	2	7	8	2	6	7703.326*	0.000
9	1	8	8	1	7	7764.289*	0.000

* Denotes transitions measured with the cavity method

Table C.5 Observed Transitions of ^{13}C7 PiTFAA

J'	K_a'	K_c'	J''	K_a''	K_c''	Obs. Frequency (MHz)	Obs. - Calc. (MHz)
7	1	7	6	1	6	5858.041*	0.001
7	0	7	6	0	6	5933.853*	0.000
7	2	6	6	2	5	5957.453*	-0.001
7	2	5	6	2	4	5984.944*	-0.001
7	1	6	6	1	5	6051.513*	0.000
8	1	8	7	1	7	6692.689*	0.000
7	1	7	6	0	6	6747.722*	0.001
8	0	8	7	0	7	6772.244*	0.002
8	2	7	7	2	6	6806.848*	-0.001
8	2	6	7	2	5	6847.555*	0.001
8	1	7	7	1	6	6913.198*	0.002
8	1	8	7	0	7	7506.556*	-0.001
9	1	9	8	1	8	7526.559*	0.001
9	0	9	8	0	8	7607.436*	0.002
9	2	8	8	2	7	7655.579*	-0.001
9	4	6	8	4	5	7669.322*	0.001
9	4	5	8	4	4	7669.361*	-0.002
9	3	6	8	3	5	7674.227*	0.000
9	2	7	8	2	6	7712.680*	0.001
9	1	8	8	1	7	7773.633*	0.000
10	0	10	9	1	9	7786.030*	0.000

* Denotes transitions measured with the cavity method

Table C.6 Observed Transitions of ^{13}C11 PiTFAA

J'	K_a'	K_c'	J''	K_a''	K_c''	Obs. Frequency (MHz)	Obs. - Calc. (MHz)
7	1	7	6	1	6	5810.983*	0.000
7	0	7	6	0	6	5885.985*	0.000
7	2	6	6	2	5	5908.825*	0.001
7	2	5	6	2	4	5935.425*	0.000
7	1	6	6	1	5	6001.487*	0.000
8	1	8	7	1	7	6638.978*	0.000
7	1	7	6	0	6	6706.981*	-0.001
8	0	8	7	0	7	6717.818*	-0.001
8	2	7	7	2	6	6751.327*	0.000
8	4	5	7	4	4	6760.592*	-0.002
8	4	4	7	4	3	6760.612*	0.002
8	3	5	7	3	4	6763.713*	0.002
8	2	6	7	2	5	6790.732*	0.000
9	0	9	8	1	8	6804.379*	-0.004
8	1	7	7	1	6	6856.123*	0.001
8	1	8	7	0	7	7459.973*	-0.002
9	1	9	8	1	8	7466.217*	0.002
9	0	9	8	0	8	7546.538*	-0.001
9	2	8	8	2	7	7593.187*	0.000
9	4	6	8	4	5	7606.475*	0.001
9	4	5	8	4	4	7606.513*	0.000
9	2	7	8	2	6	7648.496*	0.000
9	1	8	8	1	7	7709.557*	0.000

* Denotes transitions measured with the cavity method

Table C.7 Observed Transitions of ^{13}C15 PiTFAA

J'	K_a'	K_c'	J''	K_a''	K_c''	Obs. Frequency (MHz)	Obs. - Calc. (MHz)
7	1	7	6	1	6	5849.768*	0.000
7	0	7	6	0	6	5923.566*	0.000
7	2	6	6	2	5	5945.951*	0.000
6	1	6	5	0	5	5967.656*	-0.005
7	2	5	6	2	4	5972.023*	0.000
7	1	6	6	1	5	6037.062*	0.001
8	1	8	7	1	7	6683.345*	0.000
7	1	7	6	0	6	6734.163*	0.001
8	0	8	7	0	7	6760.943*	-0.003
8	2	7	7	2	6	6793.789*	0.000
8	2	6	7	2	5	6832.417*	0.003
9	0	9	8	1	8	6862.272*	0.000
8	1	7	7	1	6	6896.833*	0.000
9	1	9	8	1	8	7516.175*	-0.004
9	0	9	8	0	8	7595.271*	0.003
9	2	8	8	2	7	7640.995*	-0.003
9	2	7	8	2	6	7695.219*	0.002
9	1	8	8	1	7	7755.428*	-0.001

* Denotes transitions measured with the cavity method

Table C.8 Observed Transitions of ^{13}C19 PiTFAA

J'	K_a'	K_c'	J''	K_a''	K_c''	Obs. Frequency (MHz)	Obs. - Calc. (MHz)
7	1	7	6	1	6	5842.162*	0.000
7	0	7	6	0	6	5919.082*	0.000
7	2	6	6	2	5	5944.168*	-0.001
6	1	6	5	0	5	5949.595*	0.002
7	2	5	6	2	4	5973.396*	0.001
7	1	6	6	1	5	6040.471*	0.000
8	1	8	7	1	7	6674.413*	0.001
8	0	8	7	0	7	6754.814*	0.000
8	2	7	7	2	6	6791.559*	0.000
8	3	5	7	3	4	6805.239*	0.001
8	2	6	7	2	5	6834.793*	0.000
8	1	7	7	1	6	6900.382*	-0.001
8	1	8	7	0	7	7466.963*	-0.001
9	1	9	8	1	8	7505.840*	0.000
9	0	9	8	0	8	7587.202*	0.000
9	2	8	8	2	7	7638.242*	0.000
9	4	6	8	4	5	7652.872*	0.002
9	4	5	8	4	4	7652.917*	-0.001
9	3	7	8	3	6	7655.292*	-0.001
9	2	7	8	2	6	7698.810*	0.000
9	1	8	8	1	7	7758.959*	0.000

* Denotes transitions measured with the cavity method

Table C.9 Observed Transitions of ^{18}O2 PiTFAA

J'	K_a'	K_c'	J''	K_a''	K_c''	Obs. Frequency (MHz)	Obs. - Calc. (MHz)
7	1	7	6	1	6	5851.080*	-0.001
7	0	7	6	0	6	5929.255*	0.002
6	1	6	5	0	5	5935.160*	0.000
7	1	6	6	1	5	6055.150*	0.000
8	1	8	7	1	7	6684.443*	-0.001
8	0	8	7	0	7	6765.767*	-0.001
8	2	7	7	2	6	6805.159*	0.001
8	2	6	7	2	5	6851.526*	-0.002
9	0	9	8	1	8	6912.410*	0.000
9	1	9	8	1	8	7516.935*	0.001
9	0	9	8	0	8	7598.757*	-0.005
9	2	8	8	2	7	7653.368*	-0.006

* Denotes transitions measured with the cavity method

Table C.10 Observed Transitions of ^{18}O5 PiTFAA

J'	K_a'	K_c'	J''	K_a''	K_c''	Obs. Frequency (MHz)	Obs. - Calc. (MHz)
7	1	7	6	1	6	5841.777*	-0.001
7	0	7	6	0	6	5919.635*	-0.002
7	2	6	6	2	5	5946.223*	0.000
7	2	5	6	2	4	5977.204*	0.001
7	1	6	6	1	5	6044.613*	0.003
8	1	8	7	1	7	6673.841*	0.000
8	0	8	7	0	7	6754.906*	0.003
8	1	7	7	1	6	6904.910*	-0.003
8	1	8	7	0	7	7444.418*	0.000
9	0	9	8	0	8	7586.681*	0.000
9	2	8	8	2	7	7640.622*	0.000

* Denotes transitions measured with the cavity method

Table C.11 Observed Transitions of Parent BTFAA

J'	K_a'	K_c'	J''	K_a''	K_c''	Obs. Frequency (MHz)	Obs. - Calc. (MHz)
11	1	11	10	1	10	6009.518	0.002
12	3	10	12	2	11	6013.472	-0.006
10	1	10	9	0	9	6067.597	0.008
13	3	11	13	2	12	6073.467	0.004
11	0	11	10	0	10	6088.809	0.001
17	2	16	17	1	17	6094.603	0.003
14	3	12	14	2	13	6146.120	-0.010
5	2	4	4	1	3	6165.814	0.002
12	0	12	11	1	11	6186.583	-0.002
11	2	10	10	2	9	6197.590	0.002
11	9	2	10	9	1	6224.157	-0.001
11	9	3	10	9	2	6224.157	-0.001
11	8	3	10	8	2	6224.679	0.001
11	8	4	10	8	3	6224.679	0.001
11	7	4	10	7	3	6225.439	-0.001
11	7	5	10	7	4	6225.439	-0.001
11	6	5	10	6	4	6226.628	0.001
11	6	6	10	6	5	6226.628	0.001
11	5	7	10	5	6	6228.637	0.006
11	5	6	10	5	5	6228.637	0.001
11	4	8	10	4	7	6232.309	0.003
11	4	7	10	4	6	6232.647	0.004
11	3	9	10	3	8	6235.896	0.000
11	3	8	10	3	7	6247.270	0.004
11	2	9	10	2	8	6329.457	0.001
11	1	10	10	1	9	6358.213	-0.001
18	2	17	18	1	18	6394.074	-0.001
17	3	15	17	2	16	6450.800	0.009
5	2	3	4	1	4	6517.086	-0.001
11	1	11	10	0	10	6524.717	0.002
12	1	12	11	1	11	6550.319	0.002
18	3	16	18	2	17	6584.113	-0.002
12	0	12	11	0	11	6622.495	0.003
6	2	5	5	1	4	6649.532	0.000
19	3	17	19	2	18	6734.395	0.008
12	2	11	11	2	10	6755.831	0.002
12	10	2	11	10	1	6789.907	0.010

Table C.11 Observed Transitions of Parent BTFAA (cont'd)

J'	K_a'	K_c'	J''	K_a''	K_c''	Obs. Frequency (MHz)	Obs. - Calc. (MHz)
12	10	3	11	10	2	6789.907	0.010
13	0	13	12	1	12	6790.430	-0.005
12	8	4	11	8	3	6791.053	0.001
12	8	5	11	8	4	6791.053	0.001
12	7	5	11	7	4	6792.043	0.001
12	7	6	11	7	5	6792.043	0.001
12	6	7	11	6	6	6793.586	0.005
12	6	6	11	6	5	6793.586	0.005
12	5	8	11	5	7	6796.192	0.010
12	5	7	11	5	6	6796.192	-0.001
12	4	9	11	4	8	6800.873	0.002
12	4	8	11	4	7	6801.501	0.001
12	3	10	11	3	9	6804.342	0.003
12	3	9	11	3	8	6821.845	0.002
12	2	10	11	2	9	6919.260	0.002
12	1	11	11	1	10	6925.604	-0.001
12	1	12	11	0	11	6986.224	0.000
13	1	13	12	1	12	7090.112	0.003
7	2	6	6	1	5	7117.285	-0.001
13	0	13	12	0	12	7154.169	0.003
6	2	4	5	1	5	7188.052	-0.002
13	2	12	12	2	11	7312.772	0.001
13	9	4	12	9	3	7356.706	0.006
13	9	5	12	9	4	7356.706	0.006
13	8	5	12	8	4	7357.558	0.003
13	8	6	12	8	5	7357.558	0.003
13	7	6	12	7	5	7358.814	0.002
13	7	7	12	7	6	7358.814	0.002
13	6	8	12	6	7	7360.772	0.002
13	6	7	12	6	6	7360.772	0.002
13	5	9	12	5	8	7364.085	0.010
13	4	10	12	4	9	7369.908	0.004
13	4	9	12	4	8	7371.020	0.003
13	3	11	12	3	10	7372.758	0.002
14	0	14	13	1	13	7384.862	0.002
16	1	15	15	2	14	7390.160	0.003
13	3	10	12	3	9	7398.657	0.001

Table C.11 Observed Transitions of Parent BTFAA (cont'd)

J'	K_a'	K_c'	J''	K_a''	K_c''	Obs. Frequency (MHz)	Obs. - Calc. (MHz)
13	1	13	12	0	12	7453.842	0.001
13	1	12	12	1	11	7489.719	0.003
13	2	11	12	2	10	7509.578	0.001
20	4	16	20	3	17	7529.486	0.004
3	3	0	2	2	1	7533.669	-0.012
8	2	7	7	1	6	7569.473	0.003
14	1	14	13	1	13	7628.951	0.003
14	0	14	13	0	13	7684.536	0.003
18	4	14	18	3	15	7766.794	0.012
17	4	13	17	3	14	7859.005	-0.010
14	2	13	13	2	12	7868.338	0.002
7	2	5	6	1	6	7889.293	0.003
14	10	4	13	10	3	7922.366	-0.002
14	10	5	13	10	4	7922.366	-0.002
14	9	5	13	9	4	7923.130	0.001
14	9	6	13	9	5	7923.130	0.001
14	8	6	13	8	5	7924.203	0.004
14	8	7	13	8	6	7924.203	0.004
14	7	7	13	7	6	7925.769	0.002
14	7	8	13	7	7	7925.769	0.002
14	6	9	13	6	8	7928.216	0.003
14	6	8	13	6	7	7928.216	0.002
14	1	14	13	0	13	7928.626	0.004
16	4	12	16	3	13	7934.729	-0.009
14	4	11	13	4	10	7939.414	0.002
14	3	12	13	3	11	7941.005	0.003
14	4	10	13	4	9	7941.296	0.001
15	0	15	14	1	14	7970.102	0.000
14	3	11	13	3	10	7978.024	0.005
15	4	11	15	3	12	7995.527	-0.002
9	2	8	8	1	7	8006.645	0.004
14	4	10	14	3	11	8043.285	-0.001
14	1	13	13	1	12	8050.149	0.006
13	4	9	13	3	10	8080.009	-0.001
4	3	2	3	2	1	8097.130	0.000
14	2	12	13	2	11	8099.541	0.002
4	3	1	3	2	2	8100.638	0.004

Table C.11 Observed Transitions of Parent BTFAA (cont'd)

J'	K_a'	K_c'	J''	K_a''	K_c''	Obs. Frequency (MHz)	Obs. - Calc. (MHz)
12	4	8	12	3	9	8107.649	0.002
17	1	16	16	2	15	8121.130	0.000
11	4	7	11	3	8	8127.996	0.005
10	4	6	10	3	7	8142.616	0.001
14	4	11	14	3	12	8146.181	0.010
15	4	12	15	3	13	8146.640	0.003
13	4	10	13	3	11	8147.764	0.003
16	4	13	16	3	14	8150.097	0.001
12	4	9	12	3	10	8150.618	0.006
9	4	5	9	3	6	8152.859	0.003
11	4	8	11	3	9	8154.081	0.001
17	4	14	17	3	15	8157.618*	0.000
10	4	7	10	3	8	8157.669*	-0.001
8	4	4	8	3	5	8159.827	0.008
9	4	6	9	3	7	8161.034	0.006
8	4	5	8	3	6	8163.930	-0.001
7	4	3	7	3	4	8164.394	0.007
7	4	4	7	3	5	8166.264	-0.001
15	1	15	14	1	14	8166.909	0.005
6	4	2	6	3	3	8167.258	0.004
6	4	3	6	3	4	8168.008	-0.001
5	4	1	5	3	2	8168.960	0.005
5	4	2	5	3	3	8169.206	-0.002
4	4	0	4	3	1	8169.887	-0.001
18	4	15	18	3	16	8170.388	0.005
19	4	16	19	3	17	8189.654	-0.004
15	0	15	14	0	14	8214.195	0.004
20	4	17	20	3	18	8216.771	-0.002
21	2	19	20	3	18	8396.442	0.002
15	1	15	14	0	14	8410.999	0.006
15	2	14	14	2	13	8422.466	0.006
10	2	9	9	1	8	8429.556	0.005
15	9	6	14	9	5	8489.687	0.009
15	9	7	14	9	6	8489.687	0.009
15	8	7	14	8	6	8490.998	0.006
15	8	8	14	8	7	8490.998	0.006

* Denotes transitions measured with the cavity method

Table C.11 Observed Transitions of Parent BTFAA (cont'd)

J'	K_a'	K_c'	J''	K_a''	K_c''	Obs. Frequency (MHz)	Obs. - Calc. (MHz)
15	7	8	14	7	7	8492.924	0.003
15	7	9	14	7	8	8492.924	0.003
15	6	10	14	6	9	8495.931	0.001
15	6	9	14	6	8	8495.931	-0.001
15	5	11	14	5	10	8500.995*	-0.001
15	5	10	14	5	9	8501.084*	-0.001
15	3	13	14	3	12	8508.925	0.001
15	4	12	14	4	11	8509.392	0.002
15	4	11	14	4	10	8512.450	-0.002
16	0	16	15	1	15	8546.800	0.001
15	3	12	14	3	11	8560.210	0.000
15	1	14	14	1	13	8606.519	0.004
8	2	6	7	1	7	8624.888	0.006
11	1	10	10	0	10	8658.481*	0.001
5	3	3	4	2	2	8658.625	0.005
5	3	2	4	2	3	8669.185	0.006
15	2	13	14	2	12	8688.359	0.002
16	1	16	15	1	15	8704.061	0.003
16	0	16	15	0	15	8743.604	0.004
11	2	10	10	1	9	8839.188	0.003
18	1	17	17	2	16	8844.038	0.008
16	1	16	15	0	15	8900.864	0.005
16	2	15	15	2	14	8975.099	0.005
16	7	10	15	7	9	9060.288	-0.001
16	7	9	15	7	8	9060.288	-0.001
16	5	12	15	5	11	9070.071	-0.006
16	5	11	15	5	10	9070.238	0.000
16	3	14	15	3	13	9076.360	0.003
16	4	13	15	4	12	9079.819	0.001
16	4	12	15	4	11	9084.630	0.001
17	0	17	16	1	16	9115.823	0.007
16	3	13	15	3	12	9145.425	0.004
16	1	15	15	1	14	9158.546	0.003
6	3	4	5	2	3	9215.558	0.001
12	2	11	11	1	10	9236.804	0.003
6	3	3	5	2	4	9240.292	-0.006

* Denotes transitions measured with the cavity method

Table C.11 Observed Transitions of Parent BTFAA (cont'd)

J'	K_a'	K_c'	J''	K_a''	K_c''	Obs. Frequency (MHz)	Obs. - Calc. (MHz)
17	1	17	16	1	16	9240.489	-0.004
17	0	17	16	0	16	9273.077	0.001
16	2	14	15	2	13	9275.361	0.001
17	1	17	16	0	16	9397.754	0.002
9	2	7	8	1	8	9398.921	-0.002
12	1	11	11	0	11	9495.278*	0.001
17	2	16	16	2	15	9526.205	0.002
19	1	18	18	2	17	9556.125	-0.004
17	9	8	16	9	7	9623.166	0.003
17	9	9	16	9	8	9623.166	0.003
13	2	12	12	1	11	9623.969	0.003
17	8	9	16	8	8	9625.076	0.001
17	8	10	16	8	9	9625.076	0.001
17	7	11	16	7	10	9627.885	0.001
17	7	10	16	7	9	9627.885	0.001
17	6	12	16	6	11	9632.277	0.007
17	6	11	16	6	10	9632.277	0.001
17	5	13	16	5	12	9639.608	0.005
17	5	12	16	5	11	9639.884	0.000
17	3	15	16	3	14	9643.139	0.002
17	4	14	16	4	13	9650.664	0.005
17	4	13	16	4	12	9657.993	0.001
18	0	18	17	1	17	9678.133	0.001
17	1	16	16	1	15	9706.068	0.001
17	3	14	16	3	13	9733.715	0.001
7	3	5	6	2	4	9765.604	0.001
18	1	18	17	1	17	9776.299	0.003
18	0	18	17	0	17	9802.813	0.005
7	3	4	6	2	5	9815.243	0.002
17	2	15	16	2	14	9859.995	0.002
18	1	18	17	0	17	9900.970	-0.003
14	2	13	13	1	12	10002.580	-0.005
18	2	17	17	2	16	10075.776	0.005
18	9	9	17	9	8	10190.123	0.007
18	9	10	17	9	9	10190.123	0.007
18	8	10	17	8	9	10192.385	0.000

* Denotes transitions measured with the cavity method

Table C.11 Observed Transitions of Parent BTFAA (cont'd)

J'	K_a'	K_c'	J''	K_a''	K_c''	Obs. Frequency (MHz)	Obs. - Calc. (MHz)
18	8	11	17	8	10	10192.385	0.000
18	7	12	17	7	11	10195.722	0.001
18	7	11	17	7	10	10195.722	0.001
18	6	13	17	6	12	10200.939	0.007
18	6	12	17	6	11	10200.939	-0.005
18	3	16	17	3	15	10209.100	0.004
18	5	14	17	5	13	10209.599	0.003
18	5	13	17	5	12	10210.076	0.006
10	2	8	9	1	9	10215.215	-0.003
18	4	15	17	4	14	10221.864	0.004
18	4	14	17	4	13	10232.740	0.004
19	0	19	18	1	18	10234.729	-0.001
18	1	17	17	1	16	10249.105	0.002
20	1	19	19	2	18	10255.136	0.004
8	3	6	7	2	5	10306.075	0.001
19	1	19	18	1	18	10311.552	0.001
18	3	15	17	3	14	10324.972	0.002
19	0	19	18	0	18	10332.897	0.003
13	1	12	12	0	12	10362.501*	-0.001
8	3	5	7	2	6	10395.560	0.005
19	1	19	18	0	18	10409.717	0.001
4	4	1	3	3	0	10433.492	0.002
4	4	0	3	3	1	10433.492	-0.007
18	2	16	17	2	15	10441.808	0.004
17	5	13	17	4	14	10445.953	0.002
16	5	12	16	4	13	10457.010	0.004
15	5	10	15	4	11	10459.608	0.003
14	5	9	14	4	10	10470.971	-0.001
14	5	10	14	4	11	10475.141	0.001
13	5	8	13	4	9	10479.888	0.005
13	5	9	13	4	10	10482.217	0.002
12	5	7	12	4	8	10486.806	0.003
12	5	8	12	4	9	10488.044	0.000
11	5	6	11	4	7	10492.114	0.005
11	5	7	11	4	8	10492.745	0.012
10	5	5	10	4	6	10496.119	0.002

* Denotes transitions measured with the cavity method

Table C.11 Observed Transitions of Parent BTFAA (cont'd)

J'	K_a'	K_c'	J''	K_a''	K_c''	Obs. Frequency (MHz)	Obs. - Calc. (MHz)
10	5	6	10	4	7	10496.408	0.000
9	5	5	9	4	6	10499.208	0.002
7	5	2	7	4	3	10502.717	0.011
7	5	3	7	4	4	10502.717	-0.005
6	5	1	6	4	2	10503.703	0.005
6	5	2	6	4	3	10503.703	0.000
5	5	0	5	4	1	10504.327	0.005
5	5	1	5	4	2	10504.327	0.005
19	2	18	18	2	17	10623.803	0.002
16	2	15	15	1	14	10743.483	0.002
19	9	10	18	9	9	10757.227	0.006
19	9	11	18	9	10	10757.227	0.006
19	8	11	18	8	10	10759.887	-0.003
19	8	12	18	8	11	10759.887	-0.003
19	7	13	18	7	12	10763.821	0.005
19	7	12	18	7	11	10763.821	0.004
19	6	13	18	6	12	10769.965	-0.007
19	3	17	18	3	16	10774.074	0.002
19	5	15	18	5	14	10780.079	0.004
19	5	14	18	5	13	10780.852	0.004
36	5	32	36	4	33	10780.852	0.010
20	0	20	19	1	19	10786.547	0.007
19	1	18	18	1	17	10787.876	0.005
19	4	16	18	4	15	10793.352	0.004
19	4	15	18	4	14	10809.087	0.003
9	3	7	8	2	6	10834.093	-0.004
20	1	20	19	1	19	10846.342	0.003
20	0	20	19	0	19	10863.369	0.007
19	3	16	18	3	15	10918.855	0.001
20	1	20	19	0	19	10923.164	0.003
9	3	6	8	2	7	10983.119	0.006
5	4	2	4	3	1	10999.172	0.009
19	2	17	18	2	16	11020.401	0.003
11	2	9	10	1	10	11077.008	0.001
17	2	16	16	1	15	11111.149	0.008
20	2	19	19	2	18	11170.318	0.005
20	1	19	19	1	18	11322.808	0.004

Table C.11 Observed Transitions of Parent BTFAA (cont'd)

J'	K_a'	K_c'	J''	K_a''	K_c''	Obs. Frequency (MHz)	Obs. - Calc. (MHz)
20	9	11	19	9	10	11324.489	0.002
20	9	12	19	9	11	11324.489	0.002
20	8	12	19	8	11	11327.602	0.002
20	8	13	19	8	12	11327.602	0.002
20	7	14	19	7	13	11332.189	0.006
20	7	13	19	7	12	11332.189	0.005
21	0	21	20	1	20	11334.402	-0.002
20	3	18	19	3	17	11337.924	0.005
10	3	8	9	2	7	11346.824	0.001
20	5	16	19	5	15	11351.055	0.005
20	5	15	19	5	14	11352.282	0.002
20	4	17	19	4	16	11365.037	0.005
21	1	21	20	1	20	11380.731	0.000
20	4	16	19	4	15	11387.286	0.000
21	0	21	20	0	20	11394.203	0.001
21	1	21	20	0	20	11440.532	0.003
18	2	17	17	1	16	11480.846	0.001
20	3	17	19	3	16	11514.811	-0.004
6	4	3	5	3	2	11564.588	0.003
6	4	2	5	3	3	11564.845	0.002
10	3	7	9	2	8	11580.153	0.006
20	2	18	19	2	17	11595.429	0.005
22	1	21	21	2	20	11607.714	0.000
21	2	20	20	2	19	11715.354	0.006
11	3	9	10	2	8	11841.675	0.005
21	1	20	20	1	19	11854.520	0.006
22	0	22	21	1	21	11879.062	0.008
21	10	11	20	10	10	11889.361	0.003
21	10	12	20	10	11	11889.361	0.003
21	8	13	20	8	12	11895.531	0.003
21	8	14	20	8	13	11895.531	0.004
21	3	19	20	3	18	11900.496	0.004
21	7	15	20	7	14	11900.842	0.005
21	7	14	20	7	13	11900.842	0.004
22	1	22	21	1	21	11914.795	0.002
21	5	17	20	5	16	11922.539	0.009
22	0	22	21	0	21	11925.385	0.004

Table C.11 Observed Transitions of Parent BTFAA (cont'd)

J'	K_a'	K_c'	J''	K_a''	K_c''	Obs. Frequency (MHz)	Obs. - Calc. (MHz)
21	4	18	20	4	17	11936.803	0.002
22	1	22	21	0	21	11961.122	0.002
21	3	18	20	3	17	12112.109	-0.001
21	2	19	20	2	18	12166.548	0.003
11	3	8	10	2	9	12189.282	0.004
20	2	19	19	1	18	12237.981	-0.003
22	2	21	21	2	20	12258.965	0.001
12	3	10	11	2	9	12316.552	-0.001
22	1	21	21	1	20	12383.726	-0.001
23	0	23	22	1	22	12421.117	0.000
23	1	23	22	1	22	12448.585	0.002
22	10	12	21	10	11	12456.588	0.001
22	10	13	21	10	12	12456.588	0.001
23	0	23	22	0	22	12456.853	-0.003
22	9	13	21	9	12	12459.535	0.000
22	9	14	21	9	13	12459.535	0.000
22	3	20	21	3	19	12461.674	0.003
22	8	14	21	8	13	12463.680	-0.002
22	8	15	21	8	14	12463.680	-0.002
22	7	16	21	7	15	12469.793	-0.001
22	7	15	21	7	14	12469.793	-0.004
22	6	17	21	6	16	12479.340	0.002
22	5	18	21	5	17	12494.514	0.002
22	5	17	21	5	16	12497.401	-0.002
22	4	19	21	4	18	12508.524	-0.001
22	4	18	21	4	17	12550.334	-0.008
8	4	5	7	3	4	12693.562	-0.011
8	4	4	7	3	5	12695.516	0.000
22	3	19	21	3	18	12709.867	0.000
22	2	20	21	2	19	12733.440	0.000
13	3	11	12	2	10	12770.050	0.000
23	2	22	22	2	21	12801.230	-0.003
12	3	9	11	2	10	12813.529	-0.003
12	6	6	12	5	7	12830.115	0.007
12	6	7	12	5	8	12830.115	-0.012
11	6	5	11	5	6	12832.722	0.003
11	6	6	11	5	7	12832.722	-0.005

Table C.11 Observed Transitions of Parent BTFAA (cont'd)

J'	K_a'	K_c'	J''	K_a''	K_c''	Obs. Frequency (MHz)	Obs. - Calc. (MHz)
10	6	4	10	5	5	12834.727	-0.001
10	6	5	10	5	6	12834.727	-0.004
9	6	3	9	5	4	12836.235	-0.001
9	6	4	9	5	5	12836.235	-0.002
8	6	2	8	5	3	12837.331	-0.004
8	6	3	8	5	4	12837.331	-0.005
7	6	1	7	5	2	12838.109	0.001
7	6	2	7	5	3	12838.109	0.001
23	1	22	22	1	21	12911.201	-0.001
13	2	11	12	1	12	12946.009	-0.001
24	0	24	23	1	23	12961.105	-0.012
24	1	24	23	1	23	12982.151	-0.002
24	0	24	23	0	23	12988.581	-0.002
24	1	24	23	0	23	13009.619	0.000
23	3	21	22	3	20	13021.346	-0.001
23	10	13	22	10	12	13023.963	-0.002
23	10	14	22	10	13	13023.963	-0.002
23	9	14	22	9	13	13027.334	0.000
23	9	15	22	9	14	13027.334	0.000
23	8	16	22	8	15	13032.080	0.005
23	8	15	22	8	14	13032.080	0.005
23	7	17	22	7	16	13039.078	0.010
23	7	16	22	7	15	13039.078	0.005
23	6	18	22	6	17	13049.977	-0.002
23	6	17	22	6	16	13050.164	-0.003
23	5	19	22	5	18	13067.000	0.010
23	5	18	22	5	17	13071.283	0.001
23	4	20	22	4	19	13080.067	0.003
23	4	19	22	4	18	13135.747	0.003
14	3	12	13	2	11	13201.476	0.001
9	4	6	8	3	5	13256.264	-0.007
9	4	5	8	3	6	13260.563	0.005
23	2	21	22	2	20	13295.806	0.004
23	3	20	22	3	19	13307.168	-0.001
5	5	1	4	4	0	13333.597	0.001
5	5	0	4	4	1	13333.597	0.000
24	2	23	23	2	22	13342.243	0.001

Table C.11 Observed Transitions of Parent BTFAA (cont'd)

J'	K_a'	K_c'	J''	K_a''	K_c''	Obs. Frequency (MHz)	Obs. - Calc. (MHz)
24	1	23	23	1	22	13437.644	-0.002
23	2	22	22	1	21	13452.481	-0.002
13	3	10	12	2	11	13456.355	-0.004
25	1	25	24	1	24	13515.543	0.000
25	0	25	24	0	24	13520.522	0.004
24	3	22	23	3	21	13579.424	-0.006
24	10	14	23	10	13	13591.492	-0.007
24	10	15	23	10	14	13591.492	-0.007
24	9	15	23	9	14	13595.328	-0.001
24	9	16	23	9	15	13595.328	-0.001
24	7	18	23	7	17	13608.684	0.008
24	7	17	23	7	16	13608.684	-0.001
15	3	13	14	2	12	13610.867	0.006
24	6	19	23	6	18	13621.074	-0.001
24	6	18	23	6	17	13621.364	-0.011
24	5	20	23	5	19	13639.934	-0.005
24	5	19	23	5	18	13646.186	-0.006
24	4	21	23	4	20	13651.258	-0.002
24	4	20	23	4	19	13724.052	0.003
10	4	7	9	3	6	13816.920	-0.001
10	4	6	9	3	7	13825.517	0.002
24	2	22	23	2	21	13853.366	0.000
25	2	24	24	2	23	13882.090	0.001
24	2	23	23	1	22	13883.522	-0.003
6	5	2	5	4	1	13899.333	0.001
6	5	1	5	4	2	13899.333	0.000
24	3	21	23	3	20	13903.123	0.001
14	2	12	13	1	13	13955.430	-0.010
25	1	24	24	1	23	13963.666	0.000
16	3	14	15	2	13	13998.862	0.000
26	1	26	25	1	25	14048.791	0.001
26	0	26	25	0	25	14052.626	0.004
14	3	11	13	2	12	14121.600	-0.007
25	3	23	24	3	22	14135.847	-0.004
25	9	16	24	9	15	14163.526	-0.001
25	9	17	24	9	16	14163.526	-0.001
25	8	18	24	8	17	14169.619	-0.007

Table C.11 Observed Transitions of Parent BTFAA (cont'd)

J'	K_a'	K_c'	J''	K_a''	K_c''	Obs. Frequency (MHz)	Obs. - Calc. (MHz)
25	8	17	24	8	16	14169.619	-0.008
25	7	19	24	7	18	14178.638	0.005
25	7	18	24	7	17	14178.638	-0.011
25	6	20	24	6	19	14192.644	0.003
25	6	19	24	6	18	14193.115	0.003
25	4	22	24	4	21	14221.952	0.001
25	5	20	24	5	19	14222.268	-0.007
25	4	21	24	4	20	14315.404	-0.005
17	3	15	16	2	14	14366.643	0.003
11	4	8	10	3	7	14374.626	0.001
11	4	7	10	3	8	14390.610	0.002
25	2	23	24	2	22	14405.935	0.002
26	2	25	25	2	24	14420.876	0.002
7	5	3	6	4	2	14464.984	0.007
7	5	2	6	4	3	14464.984	0.003
26	1	25	25	1	24	14489.728	0.004
25	3	22	24	3	21	14496.923	0.000
27	1	27	26	1	26	14581.921	-0.001
27	0	27	26	0	26	14584.856	-0.009
26	3	24	25	3	23	14690.561	0.000
18	3	16	17	2	15	14715.747	0.006
26	10	16	25	10	15	14727.071	0.006
26	10	17	25	10	16	14727.071	0.006
26	9	17	25	9	16	14731.931	-0.008
26	9	18	25	9	17	14731.931	-0.008
26	8	19	25	8	18	14738.812	0.005
26	8	18	25	8	17	14738.812	0.004
26	6	21	25	6	20	14764.706	0.012
26	6	20	25	6	19	14765.425	0.005
26	5	22	25	5	21	14787.115	0.001
26	4	23	25	4	22	14791.958	-0.007
26	5	21	25	5	20	14799.698	0.001
15	3	12	14	2	13	14813.480	-0.001
26	4	22	25	4	21	14909.855	0.000
12	4	9	11	3	8	14928.232	0.002
12	4	8	11	3	9	14956.210	-0.002
27	2	26	26	2	25	14958.697	-0.009

Table C.11 Observed Transitions of Parent BTFAA (cont'd)

J'	K_a'	K_c'	J''	K_a''	K_c''	Obs. Frequency (MHz)	Obs. - Calc. (MHz)
8	5	4	7	4	3	15030.456	0.004
15	7	8	15	6	9	15160.714	0.012
15	7	9	15	6	10	15160.714	0.010
14	7	7	14	6	8	15163.711	-0.001
14	7	8	14	6	9	15163.711	-0.003
13	7	6	13	6	7	15166.159	0.001
13	7	7	13	6	8	15166.159	0.000
12	7	5	12	6	6	15168.119	0.003
12	7	6	12	6	7	15168.119	0.002
11	7	4	11	6	5	15169.655	-0.002
11	7	5	11	6	6	15169.655	-0.002
10	7	3	10	6	4	15170.839	-0.004
10	7	4	10	6	5	15170.839	-0.004
8	7	1	8	6	2	15172.380	-0.005
8	7	2	8	6	3	15172.380	-0.005
13	4	10	12	3	9	15476.292	0.000
13	4	9	12	3	10	15522.883	-0.007
16	3	13	15	2	14	15536.436	-0.005
29	0	29	28	0	28	15649.653	0.000
28	4	25	27	4	24	15929.287	-0.004
14	4	11	13	3	10	16017.042	-0.006
14	4	10	13	3	11	16091.429	-0.001
6	6	0	5	5	1	16233.636	0.000
6	6	1	5	5	0	16233.636	0.000
15	4	12	14	3	11	16548.419	0.000
15	4	11	14	3	12	16662.878	-0.002
7	6	1	6	5	2	16799.390	0.004
7	6	2	6	5	1	16799.390	0.004
16	4	13	15	3	12	17068.034	0.007
16	4	12	15	3	13	17238.588	0.003
8	6	3	7	5	2	17365.081	-0.001
8	6	2	7	5	3	17365.081	-0.001
13	8	5	13	7	6	17502.971	0.000
13	8	6	13	7	7	17502.971	0.000
17	4	14	16	3	13	17573.273	0.008
13	5	9	12	4	8	17850.851	-0.008
13	5	8	12	4	9	17852.163	0.002

Table C.11 Observed Transitions of Parent BTFAA (cont'd)

J'	K_a'	K_c'	J''	K_a''	K_c''	Obs. Frequency (MHz)	Obs. - Calc. (MHz)
9	6	4	8	5	3	17930.678	-0.001
9	6	3	8	5	4	17930.678	-0.001

Table C.12 Observed Transitions of ^{13}C4 BTFAA

J'	K_a'	K_c'	J''	K_a''	K_c''	Obs. Frequency (MHz)	Obs. - Calc. (MHz)
10	1	10	9	1	9	5464.323*	0.001
10	0	10	9	0	9	5548.902*	0.001
10	2	8	9	2	7	5739.234*	-0.001
10	1	9	9	1	8	5785.609*	-0.001
11	1	11	10	1	10	6005.797*	0.001
11	2	10	10	2	9	6194.533*	-0.001
11	1	10	10	1	9	6355.534*	0.000
12	1	12	11	1	11	6546.218*	0.001
12	0	12	11	0	11	6618.082*	-0.001
12	2	11	11	2	10	6752.446*	0.001
13	0	13	12	1	12	6789.642*	-0.001
12	2	10	11	2	9	6917.193*	0.000
12	1	11	11	1	10	6922.557*	0.001
12	1	12	11	0	11	6977.756*	-0.001
13	1	13	12	1	12	7085.623*	-0.001
13	0	13	12	0	12	7149.318*	0.000
14	0	14	13	1	13	7383.286*	0.003
13	1	13	12	0	12	7445.300*	0.002
14	1	14	13	0	13	7920.057*	0.002
15	0	15	14	1	14	7967.733*	0.002

* Denotes transitions measured with the cavity method

Table C.13 Observed Transitions of ATFAA

J'	K_a'	K_c'	J''	K_a''	K_c''	Sym	Obs. Frequency (MHz)	Obs. - Calc. (MHz)
4	2	3	4	1	4	E	6009.318	0.007
4	2	3	4	1	4	A	6018.391	0.004
4	0	4	3	0	3	E	6196.590	0.003
4	0	4	3	0	3	A	6196.688	-0.012
5	2	4	5	1	5	E	6218.762	-0.007
4	2	3	3	2	2	A	6220.248	0.000
5	2	4	5	1	5	A	6223.675	0.004
5	0	5	4	1	4	A	6224.831	0.001
4	2	3	3	2	2	E	6226.255	0.009
4	2	2	3	2	1	E	6239.594	-0.003
4	2	2	3	2	1	A	6245.808	0.001
3	1	3	2	0	2	E	6298.037	-0.003
3	1	3	2	0	2	A	6298.429	0.003
7	1	6	6	2	5	A	6338.712	0.002
7	1	6	6	2	5	E	6341.075	0.000
4	1	3	3	1	2	E	6376.962	-0.004
4	1	3	3	1	2	A	6377.183	-0.002
6	2	5	6	1	6	E	6468.666	-0.003
6	2	5	6	1	6	A	6471.617	0.008
7	2	6	7	1	7	E	6760.573	-0.002
7	2	6	7	1	7	A	6762.651	-0.003
8	2	7	8	1	8	E	7095.312	0.002
8	2	7	8	1	8	A	7097.025	-0.001
15	3	12	15	2	13	A	7434.107	0.006
9	2	8	9	1	9	E	7473.003	-0.003
9	2	8	9	1	9	A	7474.620	0.009
4	1	4	3	0	3	E	7698.762	-0.001
4	1	4	3	0	3	A	7699.033	0.001
5	0	5	4	0	4	E	7727.039	0.007
5	0	5	4	0	4	A	7727.151	-0.011
5	2	4	4	2	3	A	7772.085	-0.001
5	2	4	4	2	3	E	7776.236	0.001
5	3	3	4	3	2	A	7786.095	0.002
5	3	2	4	3	1	A	7787.175	0.000
5	2	3	4	2	2	E	7818.314	-0.001

Table C.13 Observed Transitions of ATFAA (cont'd)

J'	K_a'	K_c'	J''	K_a''	K_c''	Sym	Obs. Frequency (MHz)	Obs. - Calc. (MHz)
5	2	3	4	2	2	A	7822.735	0.002
10	2	9	10	1	10	E	7893.228	0.001
10	2	9	10	1	10	A	7894.882	0.006
13	3	10	13	2	11	A	7898.553	-0.006
5	1	4	4	1	3	E	7966.079	0.000
5	1	4	4	1	3	A	7966.298	0.003
12	3	9	12	2	10	A	8156.395	-0.001
12	3	9	12	2	10	E	8159.145	0.001
8	1	7	7	2	6	A	8176.616	0.007
8	1	7	7	2	6	E	8177.880	0.002
11	2	10	11	1	11	E	8355.002	0.004
11	2	10	11	1	11	A	8356.813	0.004
11	3	8	11	2	9	A	8408.937	0.011
11	3	8	11	2	9	E	8413.726	0.005
10	3	7	10	2	8	E	8650.231	-0.002
2	2	1	1	1	0	A	8684.331	0.002
2	2	0	1	1	1	A	8767.020	0.004
9	3	6	9	2	7	A	8844.907	-0.002
12	2	11	12	1	12	E	8856.813	0.013
9	3	6	9	2	7	E	8858.189	-0.006
12	2	11	12	1	12	A	8858.884	-0.010
11	2	9	10	3	8	A	8897.114	0.006
8	3	5	8	2	6	A	9011.233	0.002
8	3	5	8	2	6	E	9030.065	0.001
5	1	5	4	0	4	E	9068.953	0.000
5	1	5	4	0	4	A	9069.131	-0.003
6	1	6	5	1	5	A	9073.833	-0.011
7	3	4	7	2	5	A	9139.010	0.005
7	3	4	7	2	5	E	9162.010	-0.007
6	3	3	6	2	4	A	9230.341	0.003
6	0	6	5	0	5	E	9246.000	0.003
6	0	6	5	0	5	A	9246.146	0.007
6	3	3	6	2	4	E	9255.219	0.004
5	3	2	5	2	3	A	9290.376	0.004
5	3	2	5	2	3	E	9314.567	0.000

Table C.13 Observed Transitions of ATFAA (cont'd)

J'	K_a'	K_c'	J''	K_a''	K_c''	Sym	Obs. Frequency (MHz)	Obs. - Calc. (MHz)
6	2	5	5	2	4	A	9321.781	0.000
6	2	5	5	2	4	E	9323.697	0.003
4	3	1	4	2	2	A	9325.930	0.001
3	3	1	3	2	2	E	9340.645	0.009
3	3	0	3	2	1	A	9344.199	-0.001
6	3	4	5	3	3	A	9346.066	0.003
4	3	1	4	2	2	E	9346.393	0.003
6	3	3	5	3	2	A	9348.938	-0.003
5	3	3	5	2	4	E	9351.956	0.000
3	3	1	3	2	2	A	9356.984	-0.006
3	3	0	3	2	1	E	9358.719	-0.002
4	3	2	4	2	3	A	9363.969	0.000
5	3	3	5	2	4	A	9377.979	0.003
6	3	4	6	2	5	A	9402.257	-0.001
6	2	4	5	2	3	E	9406.734	0.001
6	2	4	5	2	3	A	9408.975	0.000
7	3	5	7	2	6	E	9415.632	0.003
7	3	5	7	2	6	A	9440.439	-0.004
8	3	6	8	2	7	E	9475.791	-0.003
8	3	6	8	2	7	A	9496.409	-0.003
6	1	5	5	1	4	E	9551.416	-0.002
6	1	5	5	1	4	A	9551.656	0.001
9	3	7	9	2	8	E	9559.107	0.001
9	3	7	9	2	8	A	9574.157	-0.002
7	0	7	6	1	6	E	9582.965	0.002
7	0	7	6	1	6	A	9583.157	0.001
10	3	8	10	2	9	E	9667.659	0.003
10	3	8	10	2	9	A	9677.646	0.000
11	3	9	11	2	10	E	9804.135	-0.003
11	3	9	11	2	10	A	9810.671	-0.003
9	1	8	8	2	7	A	10037.599	-0.001
9	1	8	8	2	7	E	10038.243	-0.002
3	2	2	2	1	1	A	10159.771	-0.001
13	3	11	13	2	12	A	10178.998	-0.001
5	1	4	4	0	4	A	10269.419	0.004

Table C.13 Observed Transitions of ATFAA (cont'd)

J'	K_a'	K_c'	J''	K_a''	K_c''	Sym	Obs. Frequency (MHz)	Obs. - Calc. (MHz)
3	2	1	2	1	2	A	10412.958	0.000
14	3	12	14	2	13	A	10420.029	-0.003
7	0	7	6	0	6	E	10752.687	0.005
7	0	7	6	0	6	A	10752.828	-0.006
7	2	6	6	2	5	A	10868.918	0.002
7	2	6	6	2	5	E	10869.717	0.000
7	5	3	6	5	2	A	10897.909	-0.003
7	5	2	6	5	1	A	10897.909	-0.004
7	3	5	6	3	4	A	10907.106	0.004
7	3	5	6	3	4	E	10909.785	0.004
7	3	4	6	3	3	E	10910.494	0.000
7	3	4	6	3	3	A	10913.552	0.002
7	2	5	6	2	4	E	11003.695	0.003
7	2	5	6	2	4	A	11004.883	-0.001
7	1	6	6	1	5	E	11131.961	0.001
7	1	6	6	1	5	A	11132.230	0.004
8	0	8	7	1	7	E	11252.587	0.002
8	0	8	7	1	7	A	11252.883	0.002
4	2	3	3	1	2	E	11585.422	0.003
4	2	3	3	1	2	A	11594.787	0.004
4	2	2	3	1	2	E	11640.899	0.002
4	2	2	3	1	3	A	12113.818	-0.005
4	2	2	3	1	3	E	12121.851	0.000
8	0	8	7	0	7	E	12247.436	0.004
8	0	8	7	0	7	A	12247.592	-0.004
8	2	7	7	2	6	A	12413.084	-0.002
8	2	7	7	2	6	E	12413.384	-0.003
8	3	6	7	3	5	A	12469.055	0.000
8	3	6	7	3	5	E	12473.547	-0.004
8	3	5	7	3	4	E	12476.930	-0.006
8	3	5	7	3	4	A	12481.867	-0.002
8	2	6	7	2	5	E	12608.887	-0.001
8	2	6	7	2	5	A	12609.643	0.000
8	1	7	7	1	6	E	12706.518	-0.002
8	1	7	7	1	6	A	12706.815	-0.001

Table C.13 Observed Transitions of ATFAA (cont'd)

J'	K_a'	K_c'	J''	K_a''	K_c''	Sym	Obs. Frequency (MHz)	Obs. - Calc. (MHz)
12	4	8	12	3	9	A	12821.477	0.000
9	0	9	8	1	8	E	12905.695	-0.002
9	0	9	8	1	8	A	12906.112	-0.001
11	4	7	11	3	8	A	12911.562	0.002
11	4	7	11	3	8	E	12941.937	0.004
5	2	4	4	1	3	E	12984.699	0.011
5	2	4	4	1	3	A	12989.682	-0.002
10	4	6	10	3	7	E	13004.319	0.001
9	4	5	9	3	6	A	13020.903	-0.003
10	4	7	10	3	8	E	13029.061	-0.006
9	4	6	9	3	7	E	13040.453	-0.003
9	4	5	9	3	6	E	13044.572	-0.007
8	4	4	8	3	5	A	13050.878	-0.003
12	4	9	12	3	10	A	13054.611	-0.004
11	4	8	11	3	9	A	13055.004	-0.005
10	4	7	10	3	8	A	13059.756	-0.005
13	4	10	13	3	11	A	13061.345	0.003
7	4	4	7	3	5	E	13064.627	-0.004
9	4	6	9	3	7	A	13066.655	0.000
8	4	4	8	3	5	E	13069.055	0.005
7	4	3	7	3	4	A	13070.176	0.000
6	4	3	6	3	4	E	13072.930	-0.004
8	4	5	8	3	6	A	13074.038	-0.003
7	4	4	7	3	5	A	13080.800	-0.005
4	4	1	4	3	2	E	13081.481	-0.006
6	4	2	6	3	3	A	13082.041	0.006
7	4	3	7	3	4	E	13083.798	-0.001
5	4	1	5	3	2	A	13088.927	0.012
5	4	2	5	3	3	A	13090.349	-0.002
6	4	2	6	3	3	E	13092.866	0.004
5	4	1	5	3	2	E	13098.363	-0.010
4	4	0	4	3	1	E	13101.530	-0.001
9	0	9	8	0	8	A	13731.945	0.000
5	2	4	4	1	4	A	13790.474	0.001
5	2	3	4	1	4	A	13879.517	-0.004

Table C.13 Observed Transitions of ATFAA (cont'd)

J'	K_a'	K_c'	J''	K_a''	K_c''	Sym	Obs. Frequency (MHz)	Obs. - Calc. (MHz)
5	2	3	4	1	4	E	13883.101	-0.003
3	3	1	2	2	1	E	14011.437	-0.002
3	3	1	2	2	0	A	14021.105	-0.004
3	3	0	2	2	1	A	14023.736	0.003
9	4	5	8	4	4	A	14024.941	0.000
3	3	0	2	2	0	E	14031.411	-0.003
9	3	7	8	3	6	A	14031.653	0.003
9	3	7	8	3	6	E	14037.276	0.001
9	3	6	8	3	5	E	14048.794	0.000
9	3	6	8	3	5	A	14054.914	-0.002
9	2	7	8	2	6	E	14220.663	-0.001
9	2	7	8	2	6	A	14221.239	0.001
9	1	8	8	1	7	E	14273.754	0.001
9	1	8	8	1	7	A	14274.077	0.001
9	1	8	8	1	7	A	14274.077	0.001
6	2	5	5	1	4	E	14342.304	0.001
6	2	5	5	1	4	A	14345.171	0.000
9	1	9	8	0	8	A	14402.154	0.003
9	1	9	8	0	8	E	14402.332	-0.001
6	2	4	5	1	4	A	14521.410	-0.002
10	0	10	9	1	9	E	14537.477	-0.006
10	0	10	9	1	9	A	14538.059	0.002
10	0	10	9	0	9	E	15208.050	-0.002
10	0	10	9	0	9	A	15208.262	-0.001
6	2	5	5	1	5	A	15545.448	-0.005
10	7	4	9	7	3	A	15568.346	0.003
10	7	3	9	7	2	A	15568.346	0.003
4	3	2	3	2	1	A	15571.372	-0.003
4	3	1	3	2	2	A	15584.579	0.001
4	3	1	3	2	1	E	15585.990	0.003
10	4	7	9	4	6	A	15587.602	-0.004
10	4	6	9	4	5	A	15589.064	-0.001
10	3	8	9	3	7	A	15594.504	0.003
10	3	8	9	3	7	E	15599.493	0.001
10	3	7	9	3	6	E	15628.289	0.001

Table C.13 Observed Transitions of ATFAA (cont'd)

J'	K_a'	K_c'	J''	K_a''	K_c''	Sym	Obs. Frequency (MHz)	Obs. - Calc. (MHz)
10	3	7	9	3	6	A	15633.840	0.000
7	2	6	6	1	5	E	15660.598	-0.004
7	2	6	6	1	5	A	15662.430	-0.002
12	1	11	11	2	10	E	15698.421	-0.001
12	1	11	11	2	10	A	15698.686	-0.002
6	2	4	5	1	5	A	15721.692	-0.002
6	2	4	5	1	5	E	15723.058	-0.003
10	1	10	9	0	9	A	15740.955	0.000
10	1	10	9	0	9	E	15741.291	0.001
10	1	9	9	1	8	E	15832.185	-0.001
10	1	9	9	1	8	A	15832.528	-0.002
10	2	8	9	2	7	E	15836.247	-0.002
10	2	8	9	2	7	A	15836.753	-0.003
8	1	7	7	0	7	E	15933.285	-0.015
8	1	7	7	0	7	A	15933.982	0.004
7	2	5	6	1	5	A	15974.635	-0.005
7	2	5	6	1	5	E	15975.176	0.001
11	0	11	10	1	10	E	16145.741	-0.002
11	0	11	10	1	10	A	16146.556	0.007
11	0	11	10	0	10	E	16678.978	-0.003
11	0	11	10	0	10	A	16679.241	0.000
14	5	9	14	4	10	A	16698.059	-0.001
14	5	10	14	4	11	E	16707.828	0.007
14	5	9	14	4	10	E	16720.295	-0.001
14	5	10	14	4	11	A	16733.240	-0.007
13	5	9	13	4	10	E	16735.738	-0.004
13	5	8	13	4	9	A	16736.311	0.005
12	5	8	12	4	9	E	16759.107	-0.002
12	5	7	12	4	8	A	16765.159	0.001
12	5	8	12	4	9	A	16775.771	-0.002
11	5	7	11	4	8	E	16777.801	0.000
12	5	7	12	4	8	E	16778.588	0.003
11	5	6	11	4	7	A	16786.722	-0.007
11	5	7	11	4	8	A	16792.085	-0.002
10	5	6	10	4	7	E	16792.266	0.001

Table C.13 Observed Transitions of ATFAA (cont'd)

J'	K_a'	K_c'	J''	K_a''	K_c''	Sym	Obs. Frequency (MHz)	Obs. - Calc. (MHz)
11	5	6	11	4	7	E	16797.754	-0.006
10	5	5	10	4	6	A	16802.679	0.013
9	5	5	9	4	6	E	16803.138	0.004
10	5	6	10	4	7	A	16805.185	-0.001
8	5	4	8	4	5	E	16811.053	0.001
10	5	5	10	4	6	E	16812.320	0.000
9	5	5	9	4	6	A	16815.334	-0.008
7	5	3	7	4	4	E	16816.615	0.002
6	5	2	6	4	3	E	16820.345	0.001
8	5	3	8	4	4	A	16822.513	0.013
5	5	1	5	4	2	E	16822.698	-0.003
8	5	4	8	4	5	A	16822.919	-0.002
9	5	4	9	4	5	E	16823.187	0.001
8	5	3	8	4	4	E	16831.089	0.003
7	5	2	7	4	3	E	16836.631	-0.001
6	5	1	6	4	2	E	16840.357	0.004
5	5	0	5	4	1	E	16842.708	0.003
8	2	7	7	1	6	E	16942.033	0.005
8	2	7	7	1	6	A	16943.292	0.000
11	2	10	10	2	9	A	17024.093	-0.003
11	1	11	10	0	10	A	17094.858	0.003
11	1	11	10	0	10	E	17095.418	0.002
5	3	3	4	2	2	A	17111.661	0.000
5	3	2	4	2	2	A	17113.106	0.001
5	3	3	4	2	3	E	17128.189	-0.002
11	6	5	10	6	4	A	17131.721	0.005
11	6	6	10	6	5	A	17131.721	0.005
5	3	2	4	2	2	E	17132.883	0.001
5	3	3	4	2	3	A	17150.073	0.011
5	3	2	4	2	3	A	17151.509	0.003
11	4	8	10	4	7	A	17152.369	-0.003
11	4	7	10	4	6	A	17155.273	-0.002
11	3	9	10	3	8	A	17157.125	0.001
11	3	9	10	3	8	E	17160.433	0.002
11	3	8	10	3	7	E	17215.911	0.001

Table C.13 Observed Transitions of ATFAA (cont'd)

J'	K_a'	K_c'	J''	K_a''	K_c''	Sym	Obs. Frequency (MHz)	Obs. - Calc. (MHz)
11	3	8	10	3	7	A	17219.844	-0.002
11	1	10	10	1	9	A	17380.638	0.000
11	2	9	10	2	8	E	17452.425	0.003
11	2	9	10	2	8	A	17452.916	0.004
13	1	12	12	2	11	E	17585.602	0.001
13	1	12	12	2	11	A	17586.037	-0.005
7	2	5	6	1	6	A	17652.732	-0.001
7	2	5	6	1	6	E	17652.956	-0.003
12	0	12	11	1	11	E	17730.554	-0.005
12	0	12	11	1	11	A	17731.722	0.003

Table C.14 Observed Transitions of APiA

J'	K_a'	K_c'	J''	K_a''	K_c''	Sym	Obs. Frequency (MHz)	Obs. - Calc. (MHz)
3	1	3	2	0	2	E	6299.091	-0.001
3	1	3	2	0	2	A	6301.224	-0.004
5	0	5	4	1	4	A	6814.468	-0.003
5	0	5	4	1	4	E	6814.947	0.001
9	3	6	9	2	7	A	7578.793	-0.002
8	3	5	8	2	6	A	7691.208	0.003
7	3	4	7	2	5	A	7775.894	0.009
4	1	4	3	0	3	E	7816.833	0.000
4	1	4	3	0	3	A	7818.220	0.004
7	3	4	7	2	5	E	7832.631	-0.006
6	3	3	6	2	4	A	7835.518	-0.005
5	3	2	5	2	3	A	7874.314	-0.001
5	3	3	5	2	4	E	7883.407	-0.009
4	3	2	4	2	3	E	7884.224	-0.006
6	3	3	6	2	4	E	7887.150	0.002
6	3	4	6	2	5	E	7889.905	0.000
4	3	1	4	2	2	A	7897.142	0.009
3	3	0	3	2	1	A	7908.813	0.002
7	3	5	7	2	6	E	7909.337	-0.002
4	3	2	4	2	3	A	7921.415	0.002

Table C.14 Observed Transitions of APiA (cont'd)

J'	K_a'	K_c'	J''	K_a''	K_c''	Sym	Obs. Frequency (MHz)	Obs. - Calc. (MHz)
4	3	1	4	2	2	E	7929.922	-0.001
5	3	3	5	2	4	A	7930.373	0.003
3	3	0	3	2	1	E	7934.848	0.003
8	3	6	8	2	7	E	7944.791	0.010
6	3	4	6	2	5	A	7945.940	-0.001
7	3	5	7	2	6	A	7970.504	-0.007
2	2	1	1	1	0	A	7982.736	0.005
8	3	6	8	2	7	A	8006.662	0.002
2	2	0	1	1	1	A	8043.172	0.002
9	3	7	9	2	8	A	8057.079	-0.010
11	3	9	11	2	10	E	8169.832	0.008
6	0	6	5	1	5	E	8543.441	0.005
6	0	6	5	1	5	A	8543.600	-0.001
5	1	5	4	0	4	E	9310.949	0.003
5	1	5	4	0	4	A	9311.859	0.001
3	2	2	2	1	1	A	9555.188	0.002
3	2	1	2	1	2	A	9739.769	-0.003
7	0	7	6	1	6	E	10274.979	-0.002
7	0	7	6	1	6	A	10275.710	0.001
6	1	6	5	0	5	E	10786.171	0.005
6	1	6	5	0	5	A	10786.691	0.001
7	4	3	7	3	4	E	11089.459	0.001
6	4	2	6	3	3	E	11095.003	-0.005
4	2	3	3	1	2	A	11097.987	0.000
5	4	1	5	3	2	E	11098.481	0.003
4	4	0	4	3	1	E	11100.487	-0.002
4	2	2	3	1	3	A	11475.258	0.004
8	0	8	7	1	7	A	12004.389	-0.002
7	1	7	6	0	6	E	12248.113	0.006
5	2	4	4	1	3	A	12611.321	-0.001
3	3	1	2	2	1	E	12783.256	-0.003
3	3	1	2	2	0	A	12809.129	-0.003
3	3	0	2	2	1	A	12810.795	-0.003
3	3	0	2	2	0	E	12831.826	-0.002
5	2	3	4	1	4	A	13256.007	-0.004

Table C.14 Observed Transitions of APiA (cont'd)

J'	K_a'	K_c'	J''	K_a''	K_c''	Sym	Obs. Frequency (MHz)	Obs. - Calc. (MHz)
5	2	3	4	1	4	E	13282.871	0.004
8	1	8	7	0	7	A	13702.630	-0.004
8	1	8	7	0	7	E	13702.966	-0.005
9	0	9	8	1	8	E	13721.918	-0.002
9	0	9	8	1	8	A	13723.986	0.001
6	2	5	5	1	4	A	14095.603	-0.002
8	5	3	8	4	4	A	14237.668	-0.007
8	5	4	8	4	5	A	14237.878	0.002
5	5	0	5	4	1	A	14245.238	0.005
5	5	1	5	4	2	A	14245.238	0.002
8	5	3	8	4	4	E	14258.100	0.001
7	5	2	7	4	3	E	14261.644	0.002
6	5	1	6	4	2	E	14264.025	0.000
5	5	0	5	4	1	E	14265.543	0.007
4	3	2	3	2	1	A	14437.015	0.000
4	3	1	3	2	2	A	14445.394	0.000
6	2	4	5	1	5	A	15089.681	-0.004
6	2	4	5	1	5	E	15106.091	0.000
9	1	9	8	0	8	A	15156.050	-0.005
9	1	9	8	0	8	E	15157.018	-0.001
10	0	10	9	1	9	E	15427.070	-0.001
10	0	10	9	1	9	A	15430.136	-0.002
7	2	6	6	1	5	E	15538.522	-0.005
7	2	6	6	1	5	A	15551.542	0.003
5	3	3	4	2	3	E	16045.782	-0.002
5	3	3	4	2	2	A	16058.536	0.000
5	3	2	4	2	3	A	16083.811	-0.002
5	3	2	4	2	2	E	16091.393	-0.004
10	1	10	9	0	9	A	16614.077	-0.003
10	1	10	9	0	9	E	16615.946	0.002
12	1	11	11	2	10	A	16823.509	-0.002
12	1	11	11	2	10	E	16824.460	-0.002
8	2	7	7	1	6	E	16971.503	0.003
8	2	7	7	1	6	A	16980.200	0.008
7	2	5	6	1	6	A	16984.661	0.002

Table C.14 Observed Transitions of APiA (cont'd)

J'	K_a'	K_c'	J''	K_a''	K_c''	Sym	Obs. Frequency (MHz)	Obs. - Calc. (MHz)
7	2	5	6	1	6	E	16993.684	0.006
11	0	11	10	1	10	E	17115.632	0.002
11	0	11	10	1	10	A	17120.141	0.007
9	6	3	9	5	4	A	17405.197	0.001
9	6	4	9	5	5	A	17405.197	-0.004
8	6	2	8	5	3	A	17407.878	-0.001
8	6	3	8	5	4	A	17407.878	-0.003
7	6	1	7	5	2	A	17409.777	0.002
7	6	2	7	5	3	A	17409.777	0.002
4	4	1	3	3	1	E	17579.959	-0.007
4	4	0	3	3	0	E	17628.472	0.000
6	3	4	5	2	3	A	17669.218	0.003
6	3	4	5	2	4	E	17679.499	0.001
6	3	3	5	2	3	E	17712.839	-0.001
6	3	3	5	2	4	A	17728.458	0.002

Table C.15 Observed Transitions of ADFAA

J'	K_a'	K_c'	J''	K_a''	K_c''	Sym	Obs. Frequency (MHz)	Obs. - Calc. (MHz)
3	1	3	2	1	2	A	6217.827	-0.001
3	1	3	2	1	2	E	6219.480	-0.003
3	0	3	2	0	2	E	6456.012	-0.002
3	0	3	2	0	2	A	6456.425	0.001
3	2	2	2	2	1	A	6517.147	0.000
3	2	2	2	2	1	E	6540.171	0.001
3	2	1	2	2	0	E	6554.752	0.000
3	2	1	2	2	0	A	6577.876	-0.003
3	1	2	2	1	1	E	6795.563	0.001
3	1	2	2	1	1	A	6797.243	-0.001
4	0	4	3	1	3	A	7230.242	-0.004
4	0	4	3	1	3	E	7231.675	0.000
6	2	5	6	1	6	A	7590.316	-0.004
3	1	3	2	0	2	E	7765.149	0.009
3	1	3	2	0	2	A	7767.784	0.007
4	1	4	3	1	3	A	8274.215	0.002
4	1	4	3	1	3	E	8275.073	0.001
7	2	6	7	1	7	E	8293.377	0.004
6	3	3	6	2	4	A	8489.146	0.012
4	0	4	3	0	3	E	8540.802	0.001
4	0	4	3	0	3	A	8541.601	0.002
6	3	3	6	2	4	E	8576.873	-0.009
4	2	3	3	2	2	A	8677.560	0.002
4	2	3	3	2	2	E	8704.945	0.005
4	3	2	3	3	1	A	8718.017	0.000
4	3	1	3	3	0	E	8720.044	0.002
4	3	2	3	3	1	E	8720.378	0.004
4	3	1	3	3	0	A	8722.581	0.002
4	2	2	3	2	1	E	8797.982	0.005
4	1	3	3	1	2	E	9042.450	0.000
4	1	3	3	1	2	A	9043.218	0.001
6	3	4	6	2	5	A	9385.712	0.006
5	0	5	4	1	4	E	9535.561	-0.009
5	0	5	4	1	4	A	9536.486	-0.003
4	1	4	3	0	3	E	9584.201	0.003

Table C.15 Observed Transitions of ADFAA (cont'd)

J'	K_a'	K_c'	J''	K_a''	K_c''	Sym	Obs. Frequency (MHz)	Obs. - Calc. (MHz)
4	1	4	3	0	3	A	9585.567	0.001
2	2	1	1	1	0	A	9722.174	0.001
2	2	0	1	1	0	E	9803.995	0.002
2	2	1	1	1	1	E	9841.329	0.000
2	2	0	1	1	1	A	9930.912	0.003
5	1	5	4	1	4	A	10318.795	0.000
5	1	5	4	1	4	E	10319.761	0.001
5	0	5	4	0	4	E	10578.968	0.001
5	0	5	4	0	4	A	10580.460	0.004
5	2	4	4	2	3	A	10827.781	0.002
5	2	4	4	2	3	E	10843.023	0.004
5	4	1	4	4	0	E	10895.752	0.006
5	4	2	4	4	1	A	10895.896	0.008
5	3	3	4	3	2	A	10907.012	0.004
5	3	2	4	3	1	A	10922.836	0.000
5	2	3	4	2	2	E	11093.651	0.006
5	2	3	4	2	2	A	11108.943	0.004
5	1	4	4	1	3	E	11269.383	0.004
5	1	4	4	1	3	A	11269.914	0.002
5	1	5	4	0	4	A	11362.765	0.003
5	1	5	4	0	4	E	11363.162	0.004
3	2	2	2	1	1	E	11637.322	0.000
3	2	2	2	1	1	A	11701.154	0.004
6	0	6	5	1	5	E	11792.020	-0.007
6	0	6	5	1	5	A	11796.633	0.003
3	2	2	2	1	2	E	12224.010	-0.005
3	2	2	2	1	2	A	12281.325	-0.009
6	1	6	5	1	5	A	12350.954	-0.004
6	1	6	5	1	5	E	12352.745	-0.002
3	2	1	2	1	2	A	12357.400	-0.007
3	2	1	2	1	2	E	12413.429	0.011
7	4	3	7	3	4	A	12565.065	-0.008
6	0	6	5	0	5	E	12576.216	-0.002
6	0	6	5	0	5	A	12578.936	-0.001
6	4	3	6	3	4	E	12643.025	-0.002

Table C.15 Observed Transitions of ADFAA (cont'd)

J'	K_a'	K_c'	J''	K_a''	K_c''	Sym	Obs. Frequency (MHz)	Obs. - Calc. (MHz)
5	4	2	5	3	3	E	12673.190	0.000
7	4	4	7	3	5	A	12713.508	-0.001
5	4	1	5	3	2	A	12714.994	-0.001
6	4	2	6	3	3	E	12723.777	-0.005
5	4	2	5	3	3	A	12735.869	0.004
4	4	0	4	3	1	E	12778.873	-0.006
6	2	5	5	2	4	A	12965.440	-0.003
6	2	5	5	2	4	E	12971.988	-0.002
6	5	1	5	5	0	E	13072.279	-0.004
6	4	3	5	4	2	A	13085.934	0.000
6	4	2	5	4	1	E	13086.114	-0.003
6	4	3	5	4	2	E	13086.617	0.000
6	4	2	5	4	1	A	13087.059	-0.001
6	3	4	5	3	3	A	13098.761	-0.002
6	3	4	5	3	3	E	13116.780	0.000
6	3	3	5	3	2	E	13122.104	0.000
6	1	6	5	0	5	A	13133.265	0.000
6	1	6	5	0	5	E	13136.941	0.003
6	3	3	5	3	2	A	13140.286	-0.003
6	2	4	5	2	3	E	13412.997	0.002
6	2	4	5	2	3	A	13419.571	-0.002
6	1	5	5	1	4	E	13469.189	-0.002
6	1	5	5	1	4	A	13469.738	0.002
4	2	3	3	1	2	E	13546.699	-0.001
4	2	3	3	1	2	A	13581.464	0.000
4	2	2	3	1	2	A	13805.428	0.003
4	2	2	3	1	2	E	13829.137	-0.003
7	0	7	6	1	6	E	13985.408	0.001
7	0	7	6	1	6	A	13996.747	0.002
5	1	4	4	0	4	A	14242.476	-0.007
5	1	4	4	0	4	E	14242.931	0.005
7	1	7	6	1	6	A	14371.159	-0.001
7	1	7	6	1	6	E	14374.861	-0.003
7	0	7	6	0	6	E	14546.127	-0.001
7	0	7	6	0	6	A	14551.074	0.001

Table C.15 Observed Transitions of ADFAA (cont'd)

J'	K_a'	K_c'	J''	K_a''	K_c''	Sym	Obs. Frequency (MHz)	Obs. - Calc. (MHz)
8	1	7	7	2	6	A	14707.174	-0.005
4	2	3	3	1	3	E	14709.480	0.008
4	2	3	3	1	3	A	14741.068	0.004
7	1	7	6	0	6	A	14925.490	0.002
7	1	7	6	0	6	E	14935.587	0.003
4	2	2	3	1	3	A	14965.028	0.002
4	2	2	3	1	3	E	14991.913	0.001
7	2	6	6	2	5	A	15088.431	-0.002
7	2	6	6	2	5	E	15091.331	-0.005
7	6	1	6	6	0	E	15249.111	0.001
7	5	2	6	5	1	E	15260.632	-0.002
7	4	4	6	4	3	A	15281.364	-0.003
7	4	3	6	4	2	E	15282.712	-0.005
7	4	4	6	4	3	E	15283.474	-0.002
7	4	3	6	4	2	A	15285.086	-0.003
7	3	5	6	3	4	A	15290.891	-0.003
7	3	5	6	3	4	E	15319.817	-0.001
5	2	4	4	1	3	E	15347.266	-0.003
7	3	4	6	3	3	E	15352.740	-0.001
5	2	4	4	1	3	A	15366.028	0.002
7	3	4	6	3	3	A	15381.782	0.000
3	3	1	2	2	1	E	15592.956	-0.003
7	1	6	6	1	5	E	15633.165	-0.003
7	1	6	6	1	5	A	15633.885	-0.001
3	3	1	2	2	1	A	15649.838	-0.008
3	3	0	2	2	1	A	15650.606	-0.003
3	3	0	2	2	0	E	15679.249	-0.001
7	2	5	6	2	4	E	15737.183	-0.001
7	2	5	6	2	4	A	15740.124	-0.003
5	2	3	4	1	3	A	15871.143	-0.004
5	2	3	4	1	3	E	15880.332	-0.003
8	0	8	7	1	7	E	16113.531	-0.006
8	0	8	7	1	7	A	16137.383	-0.001
8	1	8	7	1	7	A	16380.699	-0.002
8	1	8	7	1	7	E	16388.014	-0.006

Table C.15 Observed Transitions of ADFAA (cont'd)

J'	K_a'	K_c'	J''	K_a''	K_c''	Sym	Obs. Frequency (MHz)	Obs. - Calc. (MHz)
6	5	1	6	4	2	E	16408.280	0.009
8	0	8	7	0	7	E	16502.997	0.003
8	0	8	7	0	7	A	16511.796	-0.002
8	1	8	7	0	7	A	16755.110	-0.006
8	1	8	7	0	7	E	16777.472	-0.004
6	2	5	5	1	4	E	17049.877	-0.003
6	2	5	5	1	4	A	17061.553	-0.004
6	1	5	5	0	5	A	17131.762	-0.002
8	2	7	7	2	6	A	17195.034	-0.003
8	2	7	7	2	6	E	17196.454	-0.001
5	2	4	4	1	4	A	17294.637	0.007
8	6	2	7	6	1	E	17436.239	0.000
8	5	3	7	5	2	E	17453.470	0.001
8	5	4	7	5	3	A	17453.803	-0.003
8	3	6	7	3	5	A	17480.188	0.001
8	4	5	7	4	4	A	17482.351	0.006
8	4	4	7	4	3	E	17486.831	0.001
8	4	5	7	4	4	E	17487.722	0.001
8	4	4	7	4	3	A	17492.456	0.001
8	3	6	7	3	5	E	17509.484	0.001
8	3	5	7	3	4	E	17624.792	0.005
8	3	5	7	3	4	A	17654.118	0.003
8	1	7	7	1	6	E	17752.492	-0.002
8	1	7	7	1	6	A	17753.546	-0.001
4	3	2	3	2	2	E	17773.165	0.002
4	3	2	3	2	1	A	17774.642	-0.001
4	3	1	3	2	1	A	17779.966	-0.002
5	2	3	4	1	4	A	17799.754	0.002
5	2	3	4	1	4	E	17810.485	-0.001
5	2	3	4	1	4	E	17810.485	-0.001
4	3	1	3	2	1	E	17844.544	0.004
4	3	1	3	2	2	A	17856.041	0.000
9	0	9	8	0	8	E	18457.004†	0.009
9	0	9	8	0	8	A	18471.274†	0.005

† Denotes transition with frequencies calculated from measured sideband peaks

Table C.15 Observed Transitions of ADFAA (cont'd)

J'	K_a'	K_c'	J''	K_a''	K_c''	Sym	Obs. Frequency (MHz)	Obs. - Calc. (MHz)
9	1	9	8	0	8	A	18624.696†	-0.001
9	2	8	8	2	7	A	19284.133†	0.007
9	2	8	8	2	7	E	19285.006†	0.004
9	3	7	8	3	6	A	19662.975†	0.005

† Denotes transition with frequencies calculated from measured sideband peaks

Table C.16 Observed Transitions of Acetic Anhydride

J'	K_a'	K_c'	J''	K_a''	K_c''	Sym	Obs. Frequency (MHz)	Obs. - Calc. (MHz)
3	1	3	3	0	3	AA	3009.287	0.017
3	1	3	3	0	3	EE_j	3014.726	0.052
2	0	2	1	1	0	AE	3082.881	0.059
2	1	2	2	0	2	AE	3113.782	0.017
2	0	2	1	1	0	E_iE	3131.831	0.022
2	1	2	2	0	2	E_iE	3141.744	-0.014
2	0	2	1	1	0	EA	3172.095	-0.106
2	1	2	2	0	2	EA	3173.617	-0.040
1	1	1	1	0	1	AE	3193.243	0.038
1	1	1	1	0	1	E_iE	3234.421	-0.009
2	1	2	2	0	2	AA	3260.492	0.014
2	1	2	2	0	2	EE_j	3260.520	0.032
1	1	1	1	0	1	EA	3275.933	-0.106
2	0	2	1	1	0	EE_j	3297.193	-0.006
2	0	2	1	1	0	AA	3310.994	0.000
1	1	1	1	0	1	EE_j	3427.553	0.025
1	1	1	1	0	1	AA	3436.892	0.011
1	0	1	0	0	0	AE	3465.709	-0.003
1	0	1	0	0	0	EA	3467.141	-0.006
1	0	1	0	0	0	EE_j	3467.600	0.005
1	0	1	0	0	0	E_iE	3468.122	0.009
1	0	1	0	0	0	AA	3469.255	-0.006
2	0	2	1	1	1	AA	3494.468	0.004
2	0	2	1	1	1	EE_j	3500.691	-0.014
2	0	2	1	1	1	EA	3651.088	0.113

Table C.16 Observed Transitions of Acetic Anhydride (cont'd)

J'	K_a'	K_c'	J''	K_a''	K_c''	Sym	Obs. Frequency (MHz)	Obs. - Calc. (MHz)
2	0	2	1	1	1	E_iE	3694.618	0.009
2	0	2	1	1	1	AE	3731.545	-0.032
3	0	3	2	1	1	AE	6425.045	0.041
3	0	3	2	1	1	E_iE	6468.107	0.031
3	0	3	2	1	1	EA	6496.644	-0.041
3	0	3	2	1	1	EE_j	6559.152	-0.015
3	0	3	2	1	1	AA	6568.231	-0.001
1	1	1	0	0	0	AE	6658.953	0.036
1	1	1	0	0	0	E_iE	6702.532	-0.011
1	1	1	0	0	0	EA	6743.064	-0.122
2	1	2	1	1	1	AA	6754.948	0.006
2	1	2	1	1	1	EE_j	6761.194	0.001
2	1	2	1	1	1	EA	6824.702	0.070
2	1	2	1	1	1	E_iE	6836.378	0.011
2	1	2	1	1	1	AE	6845.323	-0.019
1	1	1	0	0	0	EE_j	6895.125	0.002
1	1	1	0	0	0	AA	6906.144	0.003
2	0	2	1	0	1	AE	6924.789	0.007
2	0	2	1	0	1	EA	6927.013	-0.001
2	0	2	1	0	1	EE_j	6928.226	-0.008
2	0	2	1	0	1	E_iE	6929.051	0.012
2	0	2	1	0	1	AA	6931.348	0.003
2	1	1	1	1	0	AE	7028.314	0.010
2	1	1	1	1	0	E_iE	7039.348	0.004
2	1	1	1	1	0	EA	7047.793	-0.060
1	1	0	0	0	0	AA	7089.619	0.008
1	1	0	0	0	0	EE_j	7098.634	0.005
2	1	1	1	1	0	EE_j	7112.996	-0.010
2	1	1	1	1	0	AA	7121.901	-0.004
3	0	3	2	1	2	EA	7198.719	0.039
1	1	0	0	0	0	EA	7222.067	0.107
1	1	0	0	0	0	E_iE	7265.339	-0.004
1	1	0	0	0	0	AE	7307.623	-0.049
7	2	6	7	1	6	E_iE	7829.598	-0.007

Table C.16 Observed Transitions of Acetic Anhydride (cont'd)

J'	K_a'	K_c'	J''	K_a''	K_c''	Sym	Obs. Frequency (MHz)	Obs. - Calc. (MHz)
7	2	6	7	1	6	AA	8125.002	0.003
6	2	5	6	1	5	E_iE	8326.331	0.031
6	2	5	6	1	5	AA	8718.451	0.024
5	2	4	5	1	4	E_iE	8754.824	0.038
5	2	4	5	1	4	EA	8857.342	0.272
4	2	3	4	1	3	AE	9016.702	-0.127
4	2	3	4	1	3	E_iE	9123.091	0.013
5	2	4	5	1	4	EE_j	9214.818	-0.171
4	2	3	4	1	3	EA	9228.755	0.069
5	2	4	5	1	4	AA	9239.544	0.033
3	2	2	3	1	2	E_iE	9423.761	0.004
2	2	1	2	1	1	AE	9508.406	0.085
3	2	2	3	1	2	EA	9533.674	-0.111
4	0	4	3	1	2	AE	9603.751	0.035
4	2	3	4	1	3	EE_j	9631.434	-0.161
2	2	1	2	1	1	E_iE	9633.916	-0.013
4	0	4	3	1	2	E_iE	9638.219	0.016
4	0	4	3	1	2	EA	9656.068	-0.001
4	2	3	4	1	3	AA	9681.529	0.028
4	0	4	3	1	2	EE_j	9687.369	-0.003
4	0	4	3	1	2	AA	9695.861	0.005
3	2	2	3	1	2	EE_j	9964.400	-0.075
2	1	2	1	0	1	AE	10038.555	0.008
3	2	2	3	1	2	AA	10039.646	0.026
2	1	2	1	0	1	E_iE	10070.790	-0.007
2	1	2	1	0	1	EA	10100.634	-0.037
3	1	3	2	1	2	AA	10127.938	0.003
3	1	3	2	1	2	EE_j	10129.166	0.005
3	1	3	2	1	2	EA	10163.552	0.048
3	1	3	2	1	2	E_iE	10173.591	-0.002
3	1	3	2	1	2	AE	10182.835	-0.004
2	1	2	1	0	1	EE_j	10188.742	0.021
2	2	1	2	1	1	EE_j	10220.056	0.014
2	2	1	2	1	1	AA	10310.625	0.027

Table C.16 Observed Transitions of Acetic Anhydride (cont'd)

J'	K_a'	K_c'	J''	K_a''	K_c''	Sym	Obs. Frequency (MHz)	Obs. - Calc. (MHz)
3	0	3	2	0	2	AE	10370.493	0.007
3	0	3	2	0	2	EA	10372.335	-0.002
3	0	3	2	0	2	EE_j	10374.964	-0.010
3	0	3	2	0	2	E_iE	10375.625	0.014
3	0	3	2	0	2	AA	10379.146	0.004
3	2	2	2	2	1	AA	10407.285	-0.002
3	2	1	2	2	0	AA	10435.745	-0.002
3	1	2	2	1	1	AE	10617.508	0.015
3	1	2	2	1	1	AE	10617.511	0.018
3	1	2	2	1	1	E_iE	10630.827	0.018
3	1	2	2	1	1	E_iE	10630.831	0.022
3	1	2	2	1	1	EA	10636.658	-0.044
3	1	2	2	1	1	EA	10636.658	-0.044
3	1	2	2	1	1	EE_j	10672.892	-0.023
3	1	2	2	1	1	EE_j	10672.894	-0.021
3	1	2	2	1	1	AA	10678.262	-0.004
2	1	1	1	0	1	AA	10742.261	0.005
2	1	1	1	0	1	EE_j	10744.044	0.003
2	1	1	1	0	1	EA	10802.713	0.047
2	1	1	1	0	1	E_iE	10836.570	-0.004
2	2	0	2	1	2	AA	10868.175	0.013
4	0	4	3	1	3	AE	10870.089	0.002
2	1	1	1	0	1	AE	10870.236	-0.028
2	2	0	2	1	2	EE_j	10954.224	-0.245
3	2	1	3	1	3	AA	11175.985	0.011
3	2	1	3	1	3	EE_j	11245.761	0.108
2	2	0	2	1	2	E_iE	11461.314	-0.027
3	2	1	3	1	3	EA	11592.527	0.061
4	2	2	4	1	4	AA	11621.629	-0.005
4	2	2	4	1	4	EE_j	11664.536	0.170
3	2	1	3	1	3	E_iE	11707.606	-0.055
4	2	2	4	1	4	E_iE	12095.127	-0.066
4	2	2	4	1	4	AE	12195.693	0.018
5	2	3	5	1	5	AA	12233.382	-0.011

Table C.16 Observed Transitions of Acetic Anhydride (cont'd)

J'	K_a'	K_c'	J''	K_a''	K_c''	Sym	Obs. Frequency (MHz)	Obs. - Calc. (MHz)
5	2	3	5	1	5	EE_j	12248.398	0.135
5	0	5	4	1	3	AE	12606.603	0.020
5	2	3	5	1	5	E_iE	12632.443	-0.063
5	0	5	4	1	3	E_iE	12632.987	-0.018
5	0	5	4	1	3	EA	12644.160	0.006
5	0	5	4	1	3	EE_j	12665.308	0.022
5	0	5	4	1	3	AA	12672.830	0.010
5	2	3	5	1	5	AE	12726.796	0.119
6	2	4	6	1	6	EE_j	13036.331	0.033
6	2	4	6	1	6	AA	13042.931	-0.021
3	1	3	2	0	2	AE	13296.614	0.010
3	1	3	2	0	2	E_iE	13315.336	-0.015
3	1	3	2	0	2	EA	13337.159	-0.003
6	2	4	6	1	6	E_iE	13348.219	-0.025
3	1	3	2	0	2	AA	13388.423	0.010
3	1	3	2	0	2	EE_j	13389.685	0.036
4	1	4	3	1	3	AA	13495.789	0.002
4	1	4	3	1	3	EE_j	13496.075	0.007
4	1	4	3	1	3	EA	13513.898	0.030
4	1	4	3	1	3	E_iE	13517.962	-0.009
4	1	4	3	1	3	AE	13522.008	0.008
4	0	4	3	0	3	EA	13796.096	0.010
4	0	4	3	0	3	AE	13796.213	0.008
4	0	4	3	0	3	E_iE	13800.951	0.015
4	0	4	3	0	3	EE_j	13801.120	0.000
4	0	4	3	0	3	AA	13805.892	0.002
4	2	3	3	2	2	AA	13870.743	-0.005
4	3	2	3	3	1	AA	13889.277	-0.016
4	2	3	3	2	2	EE_j	13889.921	-0.127
4	3	1	3	3	0	AA	13890.308	-0.019
4	2	3	3	2	2	EA	13899.012	0.155
4	2	3	3	2	2	AE	13900.714	-0.110
4	2	2	3	2	1	AE	13901.544	0.095
4	2	2	3	2	1	EA	13902.019	-0.169

Table C.16 Observed Transitions of Acetic Anhydride (cont'd)

J'	K_a'	K_c'	J''	K_a''	K_c''	Sym	Obs. Frequency (MHz)	Obs. - Calc. (MHz)
4	2	3	3	2	2	E_iE	13903.585	0.043
4	2	2	3	2	1	E_iE	13905.484	-0.020
4	2	2	3	2	1	EE_j	13914.849	0.067
4	2	2	3	2	1	AA	13941.439	-0.008
7	2	5	7	1	7	EE_j	14056.799	-0.078
7	2	5	7	1	7	AA	14081.938	0.011
4	1	3	3	1	2	AE	14193.185	-0.003
4	1	3	3	1	2	EA	14203.926	-0.030
4	1	3	3	1	2	E_iE	14204.247	0.026
4	1	3	3	1	2	EE_j	14222.890	-0.037
4	1	3	3	1	2	AA	14228.863	-0.004
7	2	5	7	1	7	E_iE	14287.864	0.068
3	1	2	2	0	2	EE_j	14488.710	-0.012
3	1	2	2	0	2	AA	14489.173	-0.004
3	1	2	2	0	2	EA	14512.354	0.000
3	1	2	2	0	2	E_iE	14538.349	0.005
3	1	2	2	0	2	AE	14562.954	-0.021
6	0	6	5	1	4	AE	15426.677	0.012
6	0	6	5	1	4	E_iE	15442.197	-0.082
6	0	6	5	1	4	EA	15447.566	0.013
6	0	6	5	1	4	EE_j	15471.627	0.072
6	0	6	5	1	4	AA	15476.710	0.005
7	1	6	6	2	4	AA	15617.981	0.010
4	1	4	3	0	3	AE	16448.129	0.011
4	1	4	3	0	3	E_iE	16457.679	-0.032
4	1	4	3	0	3	AA	16505.074	0.017
4	1	4	3	0	3	EE_j	16510.797	0.054
8	3	6	8	2	6	AA	16644.275	-0.020
5	1	5	4	1	4	AA	16857.159	-0.007
5	1	5	4	1	4	EE_j	16857.547	0.009
5	1	5	4	1	4	AE	16868.815	0.012
5	1	5	4	1	4	E_iE	16869.033	-0.017
5	1	5	4	1	4	EA	16869.842	0.009
7	3	5	7	2	5	AA	17019.135	-0.007

Table C.16 Observed Transitions of Acetic Anhydride (cont'd)

J'	K_a'	K_c'	J''	K_a''	K_c''	Sym	Obs. Frequency (MHz)	Obs. - Calc. (MHz)
2	2	1	1	1	1	AE	17185.383	0.004
5	0	5	4	0	4	EA	17192.030	-0.011
5	0	5	4	0	4	AE	17196.050	-0.005
5	0	5	4	0	4	E_iE	17199.018	-0.005
5	0	5	4	0	4	EE_j	17200.836	-0.005
5	0	5	4	0	4	AA	17205.830	-0.001
2	2	1	1	1	1	E_iE	17236.061	-0.012
2	2	1	1	1	1	EA	17279.437	-0.122
6	3	4	6	2	4	AA	17284.559	-0.001
5	2	4	4	2	3	AA	17329.377	-0.004
5	2	4	4	2	3	EE_j	17347.262	-0.054
5	3	2	4	3	1	E_iE	17365.774	-0.046
5	3	3	4	3	2	AA	17366.989	-0.020
5	3	3	4	3	2	E_iE	17367.490	0.078
5	3	2	4	3	1	AA	17370.612	-0.010
5	2	4	4	2	3	EA	17380.920	0.184
5	2	4	4	2	3	AE	17385.989	-0.131
5	2	4	4	2	3	E_iE	17388.309	0.056
5	2	3	4	2	2	AE	17399.916	0.111
5	2	3	4	2	2	EA	17403.198	-0.207
5	2	3	4	2	2	E_iE	17406.350	-0.012
2	2	1	1	1	0	AA	17432.518	0.015
2	2	0	1	1	0	AA	17439.657	0.022
5	2	3	4	2	2	EE_j	17441.417	-0.019
5	3	3	5	2	3	AA	17457.733	0.008
5	2	3	4	2	2	AA	17468.913	-0.012
2	2	0	1	1	0	EE_j	17512.198	0.042
2	2	1	1	1	1	EE_j	17536.550	-0.004
4	3	2	4	2	2	AA	17559.655	0.013
3	3	1	3	2	1	AA	17611.819	0.024
2	2	1	1	1	1	AA	17615.989	0.016
3	3	0	3	2	2	AA	17647.574	0.016
4	3	1	4	2	3	AA	17667.143	0.006
2	2	0	1	1	0	EA	17684.667	0.080

Table C.16 Observed Transitions of Acetic Anhydride (cont'd)

J'	K_a'	K_c'	J''	K_a''	K_c''	Sym	Obs. Frequency (MHz)	Obs. - Calc. (MHz)
5	3	2	5	2	4	AA	17708.373	-0.006
2	2	0	1	1	0	E_iE	17734.875	-0.033
5	1	4	4	1	3	AE	17745.907	0.002
5	1	4	4	1	3	EA	17752.342	-0.010
5	1	4	4	1	3	E_iE	17756.588	0.043
5	1	4	4	1	3	EE_j	17763.877	-0.045
5	1	4	4	1	3	AA	17771.372	0.002
2	2	0	1	1	0	AE	17778.366	-0.067
6	3	3	6	2	5	AA	17783.402	-0.026
7	3	4	7	2	6	AA	17907.777	-0.023
4	1	3	3	0	3	EE_j	18336.648†	-0.027
4	1	3	3	0	3	AA	18338.904†	0.003
4	1	3	3	0	3	EA	18343.962†	-0.010
4	1	3	3	0	3	E_iE	18366.986†	0.032
4	1	3	3	0	3	AE	18385.661†	-0.016

† Denotes transition with frequencies calculated from measured sideband peaks

Table C.17 Observed Transitions of D6 Acetic Anhydride

J'	K_a'	K_c'	J''	K_a''	K_c''	Sym	Obs. Frequency (MHz)	Obs. - Calc. (MHz)
2	1	2	1	1	1	AA	5922.191	0.007
2	0	2	1	0	1	EA	6074.574	-0.003
2	0	2	1	0	1	EE_j	6074.705	0.003
2	0	2	1	0	1	E_iE	6074.955	0.004
2	0	2	1	0	1	AA	6075.085	0.003
1	1	0	0	0	0	EA	6192.897	-0.001
1	1	0	0	0	0	EE_j	6193.450	-0.015
1	1	0	0	0	0	AA	6193.651	0.000
1	1	0	0	0	0	E_iE	6194.677	-0.004
1	1	0	0	0	0	AE	6196.050	-0.003
2	1	1	1	1	0	AE	6236.239	0.009
2	1	1	1	1	0	E_iE	6237.951	0.013
2	1	1	1	1	0	EE_j	6239.449	-0.018
2	1	1	1	1	0	AA	6240.190	0.011
7	2	6	7	1	6	EA	7082.107	0.016
7	2	6	7	1	6	EE_j	7090.003	-0.002
6	2	5	6	1	5	AE	7589.698	-0.034
6	2	5	6	1	5	E_iE	7590.735	0.000
6	2	5	6	1	5	EA	7594.619	0.021
6	2	5	6	1	5	AA	7602.198	0.012
6	2	5	6	1	5	EE_j	7603.607	-0.001
5	2	4	5	1	4	AE	8033.950	-0.039
5	2	4	5	1	4	E_iE	8037.827	0.000
5	2	4	5	1	4	EA	8043.029	0.025
5	2	4	5	1	4	AA	8053.811	0.010
5	2	4	5	1	4	EE_j	8054.355	-0.006
4	2	3	4	1	3	AE	8403.380	-0.032
4	2	3	4	1	3	E_iE	8411.319	-0.015
4	2	3	4	1	3	EA	8419.532	0.024
4	2	3	4	1	3	EE_j	8436.149	0.002
4	2	3	4	1	3	AA	8436.858	0.007
4	0	4	3	1	2	AA	8523.980	0.001
4	0	4	3	1	2	EE_j	8524.037	-0.008
4	0	4	3	1	2	E_iE	8525.167	-0.002

Table C.17 Observed Transitions of D6 Acetic Anhydride (cont'd)

J'	K_a'	K_c'	J''	K_a''	K_c''	Sym	Obs. Frequency (MHz)	Obs. - Calc. (MHz)
3	2	2	3	1	2	AE	8696.589	-0.007
3	2	2	3	1	2	E_iE	8707.463	-0.014
3	2	2	3	1	2	EA	8718.538	0.011
3	2	2	3	1	2	AA	8747.220	0.008
3	1	3	2	1	2	EE_j	8879.207	0.000
3	1	3	2	1	2	EA	8879.312	0.003
3	1	3	2	1	2	AA	8879.416	0.001
3	1	3	2	1	2	E_iE	8879.767	-0.006
3	1	3	2	1	2	AE	8879.819	-0.001
3	0	3	2	0	2	EA	9096.468	-0.006
3	0	3	2	0	2	EE_j	9096.679	-0.004
3	0	3	2	0	2	E_iE	9096.996	0.001
3	0	3	2	0	2	AA	9097.209	0.001
3	1	2	2	1	1	AE	9354.453	0.005
3	1	2	2	1	1	EA	9354.961	-0.002
3	1	2	2	1	1	EE_j	9355.401	-0.004
3	1	2	2	1	1	E_iE	9355.601	0.004
3	1	2	2	1	1	AA	9356.293	-0.004
2	1	1	1	0	1	EA	9390.772	-0.011
2	1	1	1	0	1	AE	9391.921	0.008
2	1	1	1	0	1	E_iE	9392.044	-0.003
2	1	1	1	0	1	EE_j	9392.477	-0.018
2	1	1	1	0	1	AA	9393.200	0.006
3	2	1	3	1	3	AA	9731.750	0.004
3	2	1	3	1	3	EE_j	9734.453	-0.022
3	2	1	3	1	3	EA	9746.788	-0.001
3	2	1	3	1	3	E_iE	9758.548	-0.028
3	2	1	3	1	3	AE	9768.736	0.015
4	2	2	4	1	4	AA	10117.534	0.007
4	2	2	4	1	4	EA	10121.056	-0.017
4	2	2	4	1	4	E_iE	10130.184	-0.016
4	2	2	4	1	4	AE	10137.236	0.030
5	2	3	5	1	5	EA	10643.568	-0.014
5	2	3	5	1	5	EE_j	10644.967	-0.047
5	2	3	5	1	5	AA	10646.876	-0.003

Table C.17 Observed Transitions of D6 Acetic Anhydride (cont'd)

J'	K_a'	K_c'	J''	K_a''	K_c''	Sym	Obs. Frequency (MHz)	Obs. - Calc. (MHz)
5	2	3	5	1	5	AE	10652.766	0.050
5	0	5	4	1	3	AA	11138.555	-0.008
5	0	5	4	1	3	EE_j	11139.109	-0.007
5	0	5	4	1	3	E_iE	11139.754	0.007
5	0	5	4	1	3	AE	11140.099	-0.009
5	0	5	4	1	3	EA	11140.508	0.018
4	1	4	3	1	3	EA	11831.809	0.002
4	1	4	3	1	3	EE_j	11831.929	0.003
4	1	4	3	1	3	AE	11831.974	0.000
4	1	4	3	1	3	E_iE	11832.173	-0.007
4	1	4	3	1	3	AA	11832.217	0.001
4	0	4	3	0	3	EA	12100.246	0.005
4	0	4	3	0	3	EE_j	12100.553	-0.006
4	0	4	3	0	3	E_iE	12100.868	0.001
4	0	4	3	0	3	AA	12101.176	-0.004
4	2	3	3	2	2	AA	12157.073	-0.005
4	2	3	3	2	2	EE_j	12158.686	-0.010
4	2	3	3	2	2	EA	12166.949	0.005
4	2	3	3	2	2	E_iE	12170.865	-0.002
4	2	3	3	2	2	AE	12172.567	-0.017
4	2	2	3	2	1	AE	12200.479	0.020
4	2	2	3	2	1	E_iE	12203.803	-0.001
4	2	2	3	2	1	EA	12206.073	-0.018
4	2	2	3	2	1	EE_j	12214.748	0.000
4	2	2	3	2	1	AA	12217.994	-0.003
4	1	3	3	1	2	AE	12465.773	0.005
4	1	3	3	1	2	EA	12465.957	-0.007
4	1	3	3	1	2	EE_j	12466.293	-0.003
4	1	3	3	1	2	E_iE	12467.011	0.001
4	1	3	3	1	2	AA	12467.436	-0.003
3	1	2	2	0	2	EA	12671.141	-0.028
3	1	2	2	0	2	E_iE	12672.699	0.005
3	1	2	2	0	2	EE_j	12673.201	0.004
3	1	2	2	0	2	AA	12674.408	-0.001
6	0	6	5	1	4	AA	13603.491	-0.003

Table C.17 Observed Transitions of D6 Acetic Anhydride (cont'd)

J'	K_a'	K_c'	J''	K_a''	K_c''	Sym	Obs. Frequency (MHz)	Obs. - Calc. (MHz)
6	0	6	5	1	4	E_iE	13604.491	0.012
6	0	6	5	1	4	EE_j	13604.786	-0.016
6	0	6	5	1	4	AE	13605.674	-0.023
6	0	6	5	1	4	EA	13605.906	0.028
4	1	4	3	0	3	AA	14455.552	0.002
5	1	5	4	1	4	EE_j	14779.100	0.007
5	1	5	4	1	4	E_iE	14779.219	-0.006
5	1	5	4	1	4	AA	14779.435	0.000
6	3	4	6	2	4	AA	15058.515	0.000
5	0	5	4	0	4	EA	15080.938	0.030
5	0	5	4	0	4	EE_j	15081.357	-0.010
5	0	5	4	0	4	E_iE	15081.592	0.004
5	0	5	4	0	4	AA	15082.015	-0.009
2	2	1	1	1	0	AE	15156.159	0.009
2	2	1	1	1	0	E_iE	15169.820	0.017
2	2	1	1	1	0	EA	15181.887	-0.007
5	2	4	4	2	3	EE_j	15188.412	0.001
5	2	4	4	2	3	EA	15193.352	-0.005
5	2	4	4	2	3	E_iE	15197.690	-0.007
5	2	4	4	2	3	AE	15200.332	-0.008
5	3	3	5	2	3	AA	15207.844	0.002
2	2	1	1	1	0	EE_j	15212.791	0.019
5	3	3	4	3	2	AA	15220.908	0.008
5	3	2	4	3	1	AA	15223.981	-0.011
2	2	0	1	1	0	AA	15228.380	0.001
2	2	0	1	1	0	EE_j	15236.230	-0.016
2	2	0	1	1	0	EA	15250.671	0.011
2	2	0	1	1	0	E_iE	15261.153	-0.001
2	2	0	1	1	0	AE	15270.094	-0.006
5	2	3	4	2	2	AE	15294.414	0.006
4	3	2	4	2	2	AA	15295.729	0.001
5	2	3	4	2	2	E_iE	15299.155	0.007
5	2	3	4	2	2	EA	15301.380	0.001
5	2	3	4	2	2	EE_j	15306.803	-0.008
5	2	3	4	2	2	AA	15308.781	-0.006

Table C.17 Observed Transitions of D6 Acetic Anhydride (cont'd)

J'	K_a'	K_c'	J''	K_a''	K_c''	Sym	Obs. Frequency (MHz)	Obs. - Calc. (MHz)
2	2	1	1	1	1	AE	15324.965	0.011
2	2	1	1	1	1	E_iE	15335.308	0.014
3	3	1	3	2	1	AA	15340.709	-0.006
2	2	1	1	1	1	EA	15344.391	-0.006
3	3	0	3	2	2	AA	15371.524	-0.005
2	2	1	1	1	1	EE_j	15371.985	0.021
2	2	1	1	1	1	AA	15381.222	-0.002
2	2	0	1	1	1	AA	15387.380	0.011
4	3	1	4	2	3	AA	15388.347	0.001
2	2	0	1	1	1	EE_j	15395.431	-0.007
2	2	0	1	1	1	EA	15413.180	0.017
5	3	2	5	2	4	AA	15423.799	-0.001
2	2	0	1	1	1	E_iE	15426.633	-0.011
2	2	0	1	1	1	AE	15438.894	-0.010
6	3	3	6	2	5	AA	15488.328	-0.006
5	1	4	4	1	3	EE_j	15570.194	-0.003
5	1	4	4	1	3	E_iE	15571.204	0.001
5	1	4	4	1	3	AA	15571.592	0.003
7	3	4	7	2	6	AA	15595.296	0.012
4	1	3	3	0	3	EA	16040.635	-0.024
4	1	3	3	0	3	AE	16041.137	0.039
4	1	3	3	0	3	E_iE	16042.720	0.012
4	1	3	3	0	3	EE_j	16042.818	0.008
4	1	3	3	0	3	AA	16044.639	-0.001
5	1	5	4	0	4	AA	17133.797	-0.008
6	1	6	5	1	5	AE	17719.455	-0.007
6	1	6	5	1	5	EA	17719.527	-0.003
6	1	6	5	1	5	E_iE	17719.820	-0.048
6	1	6	5	1	5	EE_j	17719.859	0.048
6	1	6	5	1	5	AA	17720.186	0.003

Table C.17 Observed Transitions of D6 Acetic Anhydride (cont'd)

J'	K_a'	K_c'	J''	K_a''	K_c''	Sym	Obs. Frequency (MHz)	Obs. - Calc. (MHz)
6	0	6	5	0	5	AA	18036.520†	-0.001
6	2	4	5	2	3	AA	18420.455†	0.005
3	2	2	2	1	2	AA	18580.500†	0.005
6	1	5	5	1	4	EE_j	18664.810†	0.006
6	1	5	5	1	4	E_iE	18666.017†	0.010
6	1	5	5	1	4	AA	18666.423†	0.001

† Denotes transition with frequencies calculated from measured sideband peaks

Table C.18 Coordinates of Non-planar *cis* PiTFAA M06-2X Minimum

Cartesian coordinates [in Å] of the non-planar *cis* minimum energy structure of pivalic trifluoroacetic anhydride from M06-2X/6-311++G(d,p) calculations.

	X	Y	Z
C	-0.976086	0.621652	0.249587
O	-1.042101	1.714503	0.695539
O	0.12987	-0.091726	-0.036407
C	1.363765	0.56118	-0.279116
O	1.394958	1.650928	-0.736291
C	2.517332	-0.348533	0.08129
C	-2.213248	-0.252788	-0.050597
F	-2.251208	-0.567559	-1.345773
F	-2.162578	-1.386998	0.651317
F	-3.323268	0.39121	0.264398
C	3.819481	0.373675	-0.261919
H	3.908927	1.308367	0.293963
H	4.665195	-0.267974	-0.006402
H	3.869017	0.608968	-1.326351
C	2.442765	-0.645497	1.587989
H	2.48913	0.274768	2.175141
H	1.526761	-1.180674	1.842442
H	3.294437	-1.269851	1.866761
C	2.394114	-1.654662	-0.719875
H	2.415358	-1.460998	-1.794799
H	3.241074	-2.298804	-0.473434
H	1.472746	-2.185004	-0.477505

Table C.19 Coordinates of Non-planar *cis* PiTFAA MP2 Minimum

Cartesian coordinates [in Å] of the non-planar *cis* minimum energy structure of pivalic trifluoroacetic anhydride from MP2/6-311++G(d,p) calculations.

	X	Y	Z
C	-0.945870	0.572117	0.271760
O	-0.941296	1.635218	0.824920
O	0.121765	-0.151377	-0.140730
C	1.365203	0.534254	-0.349247
O	1.389976	1.619900	-0.846242
C	2.512383	-0.339459	0.096149
C	-2.223345	-0.230925	-0.048733
F	-2.353412	-0.374787	-1.374239
F	-2.160947	-1.452205	0.501074
F	-3.298480	0.390549	0.420481
C	3.823980	0.376327	-0.230365
H	3.885895	1.339037	0.284495
H	4.663713	-0.247739	0.090654
H	3.914996	0.558811	-1.304858
C	2.383349	-0.558919	1.613456
H	2.391224	0.394412	2.152741
H	1.464206	-1.097501	1.859775
H	3.235279	-1.153917	1.958297
C	2.437943	-1.688511	-0.637934
H	2.496839	-1.549966	-1.722675
H	3.287286	-2.305195	-0.326136
H	1.513972	-2.221315	-0.401364

Table C.20 Coordinates of Non-planar *cis* BTFAA M06-2X Minimum

Cartesian coordinates [in Å] of the non-planar *cis* minimum energy structure of benzoic trifluoroacetic anhydride from M06-2X/6-311++G(d,p) calculations.

	X	Y	Z
C	1.637818	0.554744	-0.363654
O	1.868952	1.512032	-1.015558
O	0.439801	0.111862	0.071885
C	-0.657142	0.988677	0.166986
O	-0.509608	2.150247	0.350348
C	2.717218	-0.451344	0.092449
F	2.779529	-0.487171	1.423481
F	2.422728	-1.678447	-0.343358
F	3.90085	-0.10551	-0.381462
C	-1.93661	0.253513	0.063094
C	-1.989327	-1.123078	-0.159183
C	-3.111051	0.997761	0.192375
C	-3.224268	-1.752277	-0.252793
H	-1.073424	-1.691453	-0.254268
C	-4.339853	0.362446	0.097353
H	-3.040471	2.064983	0.3641
C	-4.395468	-1.011817	-0.125177
H	-3.272536	-2.820345	-0.424746
H	-5.253811	0.934883	0.195779
H	-5.356404	-1.507183	-0.199044

Table C.21 Coordinates of Non-planar *cis* BTFAA MP2 Minimum

Cartesian coordinates [in Å] of the non-planar *cis* minimum energy structure of benzoic trifluoroacetic anhydride from MP2/6-311++G(d,p) calculations.

	X	Y	Z
C	1.605355	0.487919	-0.415813
O	1.759958	1.373773	-1.205535
O	0.444264	0.071939	0.153807
C	-0.651921	0.978671	0.196134
O	-0.487972	2.152788	0.365698
C	2.737694	-0.423786	0.099652
F	2.887895	-0.264629	1.420821
F	2.447968	-1.711341	-0.137922
F	3.884915	-0.129764	-0.499446
C	-1.936240	0.254686	0.075352
C	-1.994756	-1.128558	-0.160284
C	-3.115079	1.006855	0.211005
C	-3.241146	-1.752274	-0.268782
H	-1.079854	-1.702590	-0.257219
C	-4.353383	0.372545	0.101263
H	-3.044286	2.074853	0.394132
C	-4.418999	-1.007052	-0.136543
H	-3.292540	-2.821686	-0.452346
H	-5.267062	0.950961	0.203929
H	-5.384512	-1.498280	-0.221064

Table C.22 Coordinates of Non-Planar *cis* ATFAA M06-2X Minimum

Cartesian coordinates [in Å] of the minimum energy structure of the non-planar *cis* conformer of acetic trifluoroacetic anhydride from M06-2X/6-311++G(d,p) calculations.

	X	Y	Z
C	0.119621	0.506108	-0.258226
O	0.002778	1.633706	-0.590035
O	-0.850081	-0.424812	-0.124919
C	-2.190365	-0.044648	0.101555
O	-2.47163	0.991745	0.592946
C	-3.093144	-1.156386	-0.323744
C	1.479447	-0.157643	0.051563
F	1.503042	-0.584331	1.314787
F	1.679222	-1.20729	-0.746472
F	2.464437	0.704882	-0.125755
H	-4.118356	-0.902066	-0.069729
H	-2.992775	-1.30574	-1.400126
H	-2.790334	-2.080529	0.169837

Table C.23 Coordinates of Non-Planar *cis* ATFAA M06-2X V_3 Transition State

Cartesian coordinates [in Å] of the V_3 transition state structure of the non-planar *cis* conformer of acetic trifluoroacetic anhydride from M06-2X/6-311++G(d,p) calculations.

	X	Y	Z
C	0.126576	0.514716	-0.259192
O	0.0178	1.65104	-0.560949
O	-0.849115	-0.417871	-0.167162
C	-2.182662	-0.045582	0.088155
O	-2.461218	0.992729	0.57871
C	-3.114861	-1.154709	-0.29358
C	1.479234	-0.162733	0.052003
F	1.484937	-0.615388	1.30652
F	1.683146	-1.196693	-0.764915
F	2.470616	0.698013	-0.095407
H	-3.634268	-1.489715	0.605006
H	-3.86082	-0.749696	-0.978015
H	-2.587958	-1.985384	-0.754187

Table C.24 Coordinates of Non-Planar *cis* ATFAA MP2 Minimum

Cartesian coordinates [in Å] of the minimum energy structure of the non-planar *cis* conformer of acetic trifluoroacetic anhydride from MP2/6-311++G(d,p) calculations.

	X	Y	Z
C	0.117198	0.483990	-0.290234
O	-0.021674	1.609183	-0.672985
O	-0.845829	-0.461563	-0.119581
C	-2.189128	-0.046531	0.120789
O	-2.447492	0.979646	0.671946
C	-3.111563	-1.116369	-0.373031
C	1.479908	-0.151772	0.053934
F	1.509397	-0.490982	1.349916
F	1.682206	-1.257561	-0.674209
F	2.467694	0.701707	-0.185801
H	-4.133622	-0.876584	-0.084028
H	-3.030854	-1.179848	-1.461328
H	-2.809025	-2.080252	0.041489

Table C.25 Coordinates of Non-Planar *cis* ATFAA MP2 V_3 Transition State

Cartesian coordinates [in Å] of the V_3 transition state structure of the non-planar *cis* conformer of acetic trifluoroacetic anhydride from MP2/6-311++G(d,p) calculations.

	X	Y	Z
C	0.244085	0.508135	-0.296547
O	0.156678	1.647479	-0.649026
O	-0.760767	-0.406735	-0.179158
C	-2.074883	0.040546	0.125607
O	-2.287250	1.085328	0.663053
C	-3.072013	-1.007654	-0.273909
C	1.571984	-0.190408	0.060885
F	1.554131	-0.568290	1.346551
F	1.749724	-1.281386	-0.695043
F	2.597891	0.630020	-0.127947
H	-3.787057	-0.549460	-0.961291
H	-2.593067	-1.864396	-0.743342
H	-3.619915	-1.321528	0.617420

Table C.26 Coordinates of CH_3 *trans*^{90} ATFAA M06-2X Minimum

Cartesian coordinates [in Å] of the minimum energy structure of the CH_3 *trans*^{90} conformer of acetic trifluoroacetic anhydride from M06-2X/6-311++G(d,p) calculations.

	X	Y	Z
C	-2.633160	1.055764	0.630144
H	-3.671066	0.963136	0.940638
O	-2.913610	-1.109105	-0.378913
O	-0.815301	-0.518776	0.038860
C	0.079984	0.426591	-0.249600
C	-2.215899	-0.252547	0.033236
O	-0.121846	1.517476	-0.675513
H	-1.998279	1.324728	1.474067
H	-2.540484	1.837777	-0.123970
C	1.496002	-0.114646	0.049485
F	2.407624	0.785047	-0.278317
F	1.608682	-0.383340	1.351654
F	1.728570	-1.231985	-0.632455

Table C.27 Coordinates of CH_3 *trans*^{120} ATFAA M06-2X Minimum

Cartesian coordinates [in Å] of the minimum energy structure of the CH_3 *trans*^{120} conformer of acetic trifluoroacetic anhydride from M06-2X/6-311++G(d,p) calculations.

	X	Y	Z
C	-2.675268	0.928397	0.861037
H	-3.752942	1.022514	0.758009
O	-2.835643	-0.979639	-0.611187
O	-0.808699	-0.508778	0.222459
C	0.060627	0.353279	-0.297801
C	-2.209389	-0.239784	0.056618
O	-0.186016	1.323921	-0.939621
H	-2.402898	0.774284	1.906660
H	-2.181205	1.833752	0.505564
C	1.497003	-0.087359	0.058813
F	2.377319	0.732330	-0.489256
F	1.659547	-0.066232	1.383520
F	1.731664	-1.323113	-0.372757

Table C.28 Coordinates of CH_3 *trans* ATFAA M06-2X V_3 Transition State

Cartesian coordinates [in Å] of the V_3 transition state structure of the CH_3 *trans* conformer of acetic trifluoroacetic anhydride from M06-2X/6-311++G(d,p) calculations.

	X	Y	Z
C	-2.583465	0.949464	0.670836
H	-3.246726	1.462830	-0.024055
O	-2.760437	-1.135349	-0.510870
O	-0.707657	-0.574741	0.164755
C	0.153113	0.316498	-0.322538
C	-2.104756	-0.312284	0.018817
O	-0.105480	1.285215	-0.962089
H	-3.165105	0.659393	1.548227
H	-1.774072	1.609899	0.967477
C	1.590753	-0.085875	0.071132
F	2.462799	0.753815	-0.459596
F	1.717855	-0.052058	1.399475
F	1.868305	-1.317306	-0.346046

Table C.29 Coordinates of CH_3 *trans*^{120} ATFAA MP2 Minimum

Cartesian coordinates [in Å] of the minimum energy structure of the CH_3 *trans*^{120} conformer of acetic trifluoroacetic anhydride from MP2/6-311++G(d,p) calculations.

	X	Y	Z
C	2.714136	-0.849827	0.963047
H	3.781275	-0.989280	0.796033
O	2.780608	0.900904	-0.728599
O	0.797672	0.509512	0.323499
C	-0.049545	-0.307498	-0.312699
C	2.204958	0.232229	0.067350
O	0.238677	-1.211730	-1.054731
H	2.520797	-0.573411	2.002584
H	2.174592	-1.775259	0.746787
C	-1.497366	0.070035	0.060958
F	-2.361843	-0.686748	-0.604401
F	-1.689746	-0.116284	1.375723
F	-1.741587	1.352912	-0.222179

Table C.30 Coordinates of CH_3 *trans* ATFAA MP2 V_3 Transition State

Cartesian coordinates [in Å] of the V_3 transition state structure of the CH_3 *trans* conformer of acetic trifluoroacetic anhydride from MP2/6-311++G(d,p) calculations.

	X	Y	Z
C	2.559366	-0.959280	0.710280
H	3.141255	-1.540876	-0.006638
O	2.768815	1.101834	-0.540583
O	0.699128	0.600122	0.230239
C	-0.145169	-0.261659	-0.350382
C	2.103535	0.301986	0.035964
O	0.146572	-1.175110	-1.079510
H	3.216439	-0.671448	1.535596
H	1.733760	-1.556794	1.090798
C	-1.589744	0.074156	0.071366
F	-2.456277	-0.672947	-0.602216
F	-1.738801	-0.174649	1.382254
F	-1.868868	1.361278	-0.147180

Table C.31 Coordinates of Non-Planar *cis* APiA M06-2X Minimum

Cartesian coordinates [in Å] of the minimum energy structure of the non-planar *cis* conformer of acetic pivalic anhydride from M06-2X/6-311++G(d,p) calculations.

	X	Y	Z
C	-0.305726	-0.417690	-0.380848
O	-0.156871	-1.513845	-0.813339
O	0.759045	0.477931	-0.292981
C	1.992458	0.023703	0.127911
O	2.120350	-0.929895	0.826709
C	-1.599666	0.210153	0.098677
C	-2.742015	-0.772486	-0.151413
H	-3.680206	-0.336159	0.198626
H	-2.837659	-0.999002	-1.214862
H	-2.572872	-1.711895	0.376908
C	-1.843705	1.525913	-0.654695
H	-2.780151	1.967304	-0.305396
H	-1.037110	2.238407	-0.479422
H	-1.929750	1.353255	-1.730222
C	-1.446139	0.486289	1.603670
H	-2.380538	0.902034	1.988052
H	-1.227922	-0.433282	2.151775
H	-0.645616	1.203282	1.793643
C	3.079368	0.924676	-0.375623
H	2.838077	1.962575	-0.144533
H	4.024949	0.639403	0.077388
H	3.138486	0.830760	-1.461537

Table C.32 Coordinates of Non-Planar *cis* APiA M06-2X V_3 Transition State

Cartesian coordinates [in Å] of the V_3 transition state structure of the non-planar *cis* conformer of acetic pivalic anhydride from M06-2X/6-311++G(d,p) calculations.

	X	Y	Z
C	-0.331785	-0.477048	-0.433926
O	-0.259534	-1.610080	-0.775820
O	0.782911	0.371105	-0.547183
C	1.930111	0.015230	0.110652
O	1.948128	-0.804730	0.976237
C	-1.544533	0.247514	0.110194
C	-2.731452	-0.713714	0.108724
H	-3.612934	-0.203934	0.503887
H	-2.952511	-1.060980	-0.902125
H	-2.525937	-1.589200	0.726561
C	-1.838700	1.474231	-0.766318
H	-2.711568	1.995294	-0.365927
H	-0.995605	2.165824	-0.775938
H	-2.060653	1.179119	-1.794648
C	-1.211391	0.692588	1.544165
H	-2.089371	1.175369	1.979640
H	-0.939531	-0.160978	2.169062
H	-0.386380	1.407334	1.555485
C	3.109246	0.820215	-0.357401
H	3.466925	1.427187	0.475299
H	3.906123	0.128113	-0.630095
H	2.854938	1.455594	-1.201374

Table C.33 Coordinates of Non-Planar *cis* APiA MP2 Minimum

Cartesian coordinates [in Å] of the minimum energy structure of the non-planar *cis* conformer of acetic pivalic anhydride from MP2/6-311++G(d,p) calculations.

	X	Y	Z
C	-0.303769	-0.418876	-0.368635
O	-0.142773	-1.523416	-0.810632
O	0.754199	0.500829	-0.265548
C	2.001951	0.025906	0.130610
O	2.144352	-0.955073	0.809094
C	-1.602889	0.205350	0.096988
C	-2.741718	-0.786264	-0.143122
H	-3.684518	-0.344244	0.194999
H	-2.831317	-1.031266	-1.205323
H	-2.573711	-1.717234	0.405081
C	-1.855315	1.506436	-0.680809
H	-2.805098	1.940235	-0.349921
H	-1.059129	2.234157	-0.506583
H	-1.925250	1.313567	-1.756806
C	-1.469740	0.510817	1.598322
H	-2.414523	0.926920	1.964219
H	-1.252010	-0.399487	2.167189
H	-0.674928	1.238503	1.783940
C	3.074358	0.947822	-0.375229
H	2.816203	1.983180	-0.143182
H	4.029515	0.680361	0.074773
H	3.134095	0.853437	-1.463004

Table C.34 Coordinates of Non-Planar *cis* APiA MP2 V_3 Transition State

Cartesian coordinates [in Å] of the V_3 transition state structure of the non-planar *cis* conformer of acetic pivalic anhydride from MP2/6-311++G(d,p) calculations.

	X	Y	Z
C	-0.247602	-0.449367	-0.395925
O	-0.097969	-1.539665	-0.875664
O	0.823143	0.448830	-0.245841
C	2.057860	-0.060159	0.148854
O	2.175738	-1.067184	0.793014
C	-1.542950	0.178494	0.075284
C	-2.693818	-0.785302	-0.215378
H	-3.634057	-0.340642	0.126396
H	-2.772920	-0.990281	-1.286850
H	-2.547802	-1.738062	0.300745
C	-1.764482	1.510739	-0.657899
H	-2.711733	1.947558	-0.323741
H	-0.959426	2.218755	-0.447084
H	-1.822922	1.358033	-1.741009
C	-1.425278	0.427319	1.588321
H	-2.368279	0.845110	1.956884
H	-1.229505	-0.506340	2.126486
H	-0.621750	1.134910	1.810502
C	3.151281	0.862020	-0.309268
H	2.725682	1.692440	-0.876476
H	3.705124	1.230354	0.553258
H	3.820229	0.309855	-0.975115

Table C.35 Coordinates of CH_3 *trans*^{90} APiA M06-2X Minimum

Cartesian coordinates [in Å] of the minimum energy structure of the CH_3 *trans*^{90} conformer of acetic pivalic anhydride from M06-2X/6-311++G(d,p) calculations.

	X	Y	Z
C	2.471658	-1.094352	0.591830
H	2.415656	-1.846086	-0.195169
O	2.806367	1.079420	-0.354348
O	0.700252	0.538809	0.035599
C	-0.261655	-0.396201	-0.231296
C	2.063214	0.236425	0.028206
O	-0.007679	-1.481455	-0.666010
C	-1.646277	0.150250	0.071819
C	-1.712323	0.500602	1.566715
H	-2.713356	0.868360	1.803753
H	-1.520564	-0.379058	2.186980
H	-0.988856	1.275937	1.822041
C	-2.680116	-0.919888	-0.273809
H	-3.681166	-0.537712	-0.062158
H	-2.625578	-1.191258	-1.329301
H	-2.520495	-1.825938	0.313231
C	-1.876712	1.413903	-0.771959
H	-1.811766	1.189793	-1.839385
H	-2.877265	1.801422	-0.566020
H	-1.145236	2.186379	-0.533391
H	3.496647	-1.003696	0.944327
H	1.808435	-1.407893	1.397306

Table C.36 Coordinates of CH_3 *trans* APiA M06-2X V_3 Transition State

Cartesian coordinates [in Å] of the V_3 transition state structure of the CH_3 *trans* conformer of acetic pivalic anhydride from M06-2X/6-311++G(d,p) calculations.

	X	Y	Z
C	-2.603868	0.990674	0.620907
H	-3.320988	1.446726	-0.059513
O	-2.799784	-1.118027	-0.496615
O	-0.754057	-0.570102	0.185302
C	0.160920	0.306113	-0.321217
C	-2.117144	-0.293094	0.011242
O	-0.162590	1.238071	-1.000567
C	1.575757	-0.077354	0.074173
C	1.676030	-0.050879	1.607285
H	2.697955	-0.298817	1.903483
H	1.441903	0.941937	2.000724
H	0.998491	-0.776581	2.059095
C	2.544992	0.928905	-0.543658
H	3.567918	0.661095	-0.269906
H	2.463943	0.933659	-1.631771
H	2.341440	1.940627	-0.188700
C	1.866602	-1.494020	-0.445253
H	1.775472	-1.538971	-1.533077
H	2.889524	-1.768802	-0.177233
H	1.182116	-2.222217	-0.009219
H	-3.126243	0.731556	1.544832
H	-1.799819	1.688182	0.835455

Table C.37 Coordinates of CH_3 *trans*^{90} APiA MP2 Minimum

Cartesian coordinates [in Å] of the minimum energy structure of the CH_3 *trans*^{90} conformer of acetic pivalic anhydride from MP2/6-311++G(d,p) calculations.

	X	Y	Z
C	-2.425676	1.073123	0.704480
H	-2.422839	1.863811	-0.047844
O	-2.830857	-1.018280	-0.426885
O	-0.694027	-0.579710	0.077358
C	0.251678	0.357246	-0.269340
C	-2.061747	-0.228615	0.042457
O	-0.028500	1.408200	-0.797206
C	1.643752	-0.137236	0.077371
C	1.727699	-0.328157	1.600727
H	2.740528	-0.648921	1.866943
H	1.521117	0.610584	2.127274
H	1.020549	-1.088435	1.942789
C	2.665853	0.902938	-0.382533
H	3.673486	0.551957	-0.137464
H	2.604253	1.063620	-1.462432
H	2.500143	1.864389	0.111523
C	1.893770	-1.478785	-0.630074
H	1.806564	-1.370460	-1.716510
H	2.909473	-1.819014	-0.401201
H	1.183751	-2.239810	-0.297934
H	-3.429148	0.971108	1.118994
H	-1.712751	1.342083	1.484780

Table C.38 Coordinates of CH_3 *trans*^{120} APiA MP2 Minimum

Cartesian coordinates [in Å] of the minimum energy structure of the CH_3 *trans*^{120} conformer of acetic pivalic anhydride from MP2/6-311++G(d,p) calculations.

	X	Y	Z
C	2.677754	-1.000747	0.608122
H	3.733971	-1.079831	0.353249
O	2.698441	1.140924	-0.530973
O	0.750072	0.468756	0.410179
C	-0.146705	-0.220089	-0.363398
C	2.120687	0.278225	0.060350
O	0.200927	-0.925800	-1.284187
C	-1.571814	0.044226	0.085944
C	-1.720115	-0.377004	1.556303
H	-2.756954	-0.219743	1.872542
H	-1.482967	-1.438822	1.687169
H	-1.065111	0.211911	2.203562
C	-2.525052	-0.764092	-0.795212
H	-3.556428	-0.572248	-0.481839
H	-2.420241	-0.484182	-1.846904
H	-2.327254	-1.836406	-0.710197
C	-1.861670	1.547120	-0.058143
H	-1.732668	1.872662	-1.095937
H	-2.898936	1.741789	0.235180
H	-1.198746	2.139239	0.577655
H	2.547738	-1.008548	1.693820
H	2.123574	-1.842687	0.187749

Table C.39 Coordinates of CH_3 *trans* APiA MP2 V_3 Transition State

Cartesian coordinates [in Å] of the V_3 transition state structure of the CH_3 *trans* conformer of acetic pivalic anhydride from MP2/6-311++G(d,p) calculations.

	X	Y	Z
C	-2.587136	0.999667	0.646872
H	-3.234358	1.513458	-0.065311
O	-2.803906	-1.098400	-0.520502
O	-0.746662	-0.590968	0.248774
C	0.150749	0.262821	-0.339953
C	-2.115582	-0.287164	0.025927
O	-0.198099	1.141979	-1.096072
C	1.572446	-0.066262	0.073948
C	1.694953	0.120892	1.594945
H	2.727306	-0.081377	1.899917
H	1.451270	1.148974	1.886009
H	1.032763	-0.563983	2.131263
C	2.529774	0.878010	-0.654134
H	3.558835	0.644197	-0.362517
H	2.439860	0.769019	-1.738481
H	2.322732	1.921738	-0.401811
C	1.878889	-1.525752	-0.297966
H	1.764879	-1.687257	-1.375240
H	2.914974	-1.754195	-0.025693
H	1.215605	-2.215686	0.229243
H	-3.182019	0.739130	1.527623
H	-1.767069	1.651821	0.939560

Table C.40 Coordinates of Non-Planar *cis* ADFAA M06-2X Minimum

Cartesian coordinates [in Å] of the minimum energy structure of the non-planar *cis* conformer of acetic difluoroacetic anhydride from M06-2X/6-311++G(d,p) calculations.

	X	Y	Z
C	-0.376792	0.627825	0.284245
O	-0.120707	1.724628	0.656264
O	0.493110	-0.397684	0.122877
C	1.856877	-0.159174	-0.112634
O	2.247365	0.848553	-0.592902
C	2.644555	-1.366727	0.283058
C	-1.801685	0.162255	-0.029354
F	-1.852415	-0.306202	-1.294340
F	-2.136801	-0.848343	0.802845
H	3.688087	-1.216312	0.020844
H	-2.506555	0.984979	0.088519
H	2.241755	-2.245370	-0.221984
H	2.540353	-1.524514	1.357843

Table C.41 Coordinates of Non-Planar *cis* ADFAA M06-2X V_3 Transition State

Cartesian coordinates [in Å] of the V_3 transition state structure of the non-planar *cis* conformer of acetic difluoroacetic anhydride from M06-2X/6-311++G(d,p) calculations.

	X	Y	Z
C	-0.385588	0.639008	0.275964
O	-0.139727	1.750892	0.606067
O	0.492375	-0.390115	0.173522
C	1.847914	-0.159833	-0.094219
O	2.234161	0.843426	-0.588821
C	2.666418	-1.360407	0.275530
C	-1.802510	0.153503	-0.042983
F	-1.830170	-0.352628	-1.294319
F	-2.142891	-0.834382	0.813527
H	3.458573	-1.036269	0.951057
H	-2.514862	0.974099	0.039505
H	3.137445	-1.745764	-0.629487
H	2.062006	-2.133225	0.741762

Table C.42 Coordinates of Non-Planar *cis* ADFAA MP2 Minimum

Cartesian coordinates [in Å] of the minimum energy structure of the non-planar *cis* conformer of acetic difluoroacetic anhydride from MP2/6-311++G(d,p) calculations.

	X	Y	Z
C	0.373161	0.592466	-0.342832
O	0.098306	1.669393	-0.798220
O	-0.488060	-0.435774	-0.099362
C	-1.857482	-0.153614	0.143386
O	-2.222324	0.870229	0.639125
C	-2.670090	-1.343212	-0.265354
C	1.801207	0.164102	-0.001665
F	1.870854	-0.163403	1.313639
F	2.136218	-0.931578	-0.730758
H	-3.707369	-1.194644	0.030750
H	2.505847	0.968730	-0.212589
H	-2.260875	-2.242666	0.199354
H	-2.599737	-1.465526	-1.349327

Table C.43 Coordinates of Non-Planar *cis* ADFAA MP2 V_3 Transition State

Cartesian coordinates [in Å] of the V_3 transition state structure of the non-planar *cis* conformer of acetic difluoroacetic anhydride from MP2/6-311++G(d,p) calculations.

	X	Y	Z
C	0.492282	0.610714	-0.320523
O	0.297198	1.730364	-0.706477
O	-0.439234	-0.380430	-0.183574
C	-1.775914	-0.041161	0.128542
O	-2.074796	0.990451	0.653507
C	-2.687666	-1.178738	-0.232524
C	1.877836	0.072554	0.038779
F	1.875249	-0.343892	1.330842
F	2.173897	-0.991939	-0.750279
H	-3.488159	-0.786194	-0.863478
H	2.637556	0.843383	-0.091968
H	-3.141224	-1.562262	0.684510
H	-2.155055	-1.975730	-0.747430

Table C.44 Coordinates of CH_3 *trans*^{90} ADFAA M06-2X Minimum

Cartesian coordinates [in Å] of the minimum energy structure of the CH_3 *trans*^{90} conformer of acetic difluoroacetic anhydride from M06-2X/6-311++G(d,p) calculations.

	X	Y	Z
C	2.365922	-1.006139	0.576563
H	2.394400	-1.673359	-0.285229
O	2.512787	1.293091	-0.109010
O	0.455053	0.484089	0.096682
C	-0.328012	-0.462448	-0.428081
C	1.866306	0.336573	0.137612
O	0.026243	-1.418544	-1.049127
C	-1.802941	-0.175766	-0.128926
H	-2.442174	-0.881491	-0.659192
H	1.705912	-1.446078	1.323911
H	3.369153	-0.875696	0.975126
F	-2.117007	1.084167	-0.481704
F	-1.997656	-0.301375	1.204220

Table C.45 Coordinates of CH_3 *trans*^{120} ADFAA M06-2X Minimum

Cartesian coordinates [in Å] of the minimum energy structure of the CH_3 *trans*^{120} conformer of acetic difluoroacetic anhydride from M06-2X/6-311++G(d,p) calculations.

	X	Y	Z
C	2.359809	-1.106844	0.618961
H	1.954941	-1.846810	-0.072864
O	2.492457	1.203678	-0.067193
O	0.449730	0.379631	0.348019
C	-0.308159	-0.254318	-0.546183
C	1.868646	0.250411	0.234650
O	0.085697	-0.886373	-1.480731
C	-1.796610	-0.096208	-0.223038
H	-2.405956	-0.501159	-1.030803
H	2.004894	-1.343895	1.623498
H	3.445962	-1.115465	0.586512
F	-2.098670	1.199926	-0.023813
F	-2.057150	-0.769310	0.922030

Table C.46 Coordinates of CH_3 *trans* ADFAA M06-2X V_3 Transition State

Cartesian coordinates [in Å] of the V_3 transition state structure of the CH_3 *trans* conformer of acetic difluoroacetic anhydride from M06-2X/6-311++G(d,p) calculations.

	X	Y	Z
C	2.307391	-1.003867	0.541126
O	3.049942	-1.307172	-0.195599
O	2.431022	1.304009	-0.111307
C	0.379010	0.503352	0.251521
O	-0.385153	-0.278614	-0.512438
C	1.790645	0.351424	0.160449
C	0.004639	-1.029445	-1.356011
F	-1.867704	-0.121007	-0.164310
F	-2.487872	-0.637623	-0.896594
H	1.524016	-1.752980	0.609454
H	2.805380	-0.901124	1.507418
H	-2.204479	1.180255	-0.110851
H	-2.071068	-0.659370	1.061156

Table C.47 Coordinates of CF_2H *trans*^{90} ADFAA M06-2X Minimum

Cartesian coordinates [in Å] of the minimum energy structure of the CF_2H *trans*^{90} conformer of acetic difluoroacetic anhydride from M06-2X/6-311++G(d,p) calculations.

	X	Y	Z
C	-1.185626	-0.528283	0.257598
H	-1.050122	-0.859842	1.285777
O	-1.149991	1.862468	0.084117
O	0.763527	0.835118	-0.413726
C	1.664236	-0.013090	0.194554
C	-0.546149	0.850855	0.002323
O	1.410975	-0.566623	1.220099
C	2.931270	-0.082760	-0.592360
F	-0.633581	-1.438723	-0.581455
F	-2.495779	-0.437481	-0.022947
H	3.664962	-0.665321	-0.042577
H	2.718939	-0.551140	-1.555261
H	3.299740	0.924975	-0.785377

Table C.48 Coordinates of CF_2H *trans*^{90} ADFAA M06-2X V_3 Transition State

Cartesian coordinates [in Å] of the V_3 transition state structure of the CF_2H *trans*^{90} conformer of acetic difluoroacetic anhydride from M06-2X/6-311++G(d,p) calculations.

	X	Y	Z
C	-1.194186	-0.524160	0.257229
H	-1.055315	-0.856506	1.284703
O	-1.132210	1.867160	0.094523
O	0.763544	0.820634	-0.433967
C	1.664125	-0.017821	0.180747
C	-0.542508	0.848648	-0.000019
O	1.404293	-0.580396	1.200706
C	2.961779	-0.075493	-0.562729
F	-0.658238	-1.439858	-0.585176
F	-2.505461	-0.418470	-0.014321
H	3.194894	-1.122494	-0.757498
H	2.917566	0.485217	-1.491915
H	3.743944	0.326444	0.082545

Table C.49 Coordinates of CH_3 *trans*^{120} ADFAA MP2 Minimum

Cartesian coordinates [in Å] of the minimum energy structure of the CH_3 *trans*^{120} conformer of acetic difluoroacetic anhydride from MP2/6-311++G(d,p) calculations.

	X	Y	Z
C	-2.371432	1.208652	0.518622
H	-3.456635	1.226162	0.428151
O	-2.476603	-1.174428	0.037239
O	-0.437802	-0.266657	0.483995
C	0.296545	0.102254	-0.573833
C	-1.870955	-0.180414	0.283198
O	-0.131269	0.465880	-1.645313
H	-2.063665	1.534792	1.515281
H	-1.920962	1.879368	-0.217077
C	1.791020	0.037514	-0.256200
F	2.079536	0.994108	0.668302
F	2.114089	-1.168542	0.265549
H	2.381836	0.217890	-1.154409

Table C.50 Coordinates of CH_3 *trans* ADFAA MP2 V_3 Transition State

Cartesian coordinates [in Å] of the V_3 transition state structure of the CH_3 *trans* conformer of acetic difluoroacetic anhydride from MP2/6-311++G(d,p) calculations.

	X	Y	Z
C	-2.284335	1.059405	0.519202
H	-2.953838	1.383082	-0.279356
O	-2.450858	-1.280383	-0.068584
O	-0.369571	-0.492148	0.341941
C	0.376310	0.195583	-0.534277
C	-1.794038	-0.322697	0.194846
O	-0.041253	0.834686	-1.472478
H	-2.859408	0.995150	1.447051
H	-1.474775	1.776125	0.639383
C	1.863086	0.101236	-0.190225
F	2.080760	0.808396	0.953112
F	2.224209	-1.183358	0.029146
H	2.470612	0.521895	-0.991709

Table C.51 Coordinates of CF_2H *trans*^{90} ADFAA MP2 Minimum

Cartesian coordinates [in Å] of the minimum energy structure of the CF_2H *trans*^{90} conformer of acetic difluoroacetic anhydride from MP2/6-311++G(d,p) calculations.

	X	Y	Z
C	-1.190319	-0.522570	0.271816
H	-1.084283	-0.803355	1.318315
O	-1.137053	1.877908	0.068254
O	0.759406	0.802968	-0.500901
C	1.662452	0.009277	0.191253
C	-0.543476	0.845573	-0.025939
O	1.417904	-0.428289	1.286616
C	2.914026	-0.163183	-0.610772
F	-0.622550	-1.484016	-0.506252
F	-2.501812	-0.443915	-0.043059
H	3.668907	-0.659486	-0.003202
H	2.684204	-0.767497	-1.492447
H	3.271212	0.809958	-0.953247

Table C.52 Coordinates of CF_2H *trans*^{90} ADFAA MP2 V_3 Transition State

Cartesian coordinates [in Å] of the V_3 transition state structure of the CF_2H *trans*^{90} conformer of acetic difluoroacetic anhydride from MP2/6-311++G(d,p) calculations.

	X	Y	Z
C	-1.289657	-0.536966	0.233274
H	-1.204126	-0.836065	1.276616
O	-1.209115	1.867709	0.094636
O	0.679761	0.787126	-0.496886
C	1.574015	0.007133	0.214711
C	-0.627847	0.831533	-0.025365
O	1.300240	-0.457146	1.292911
C	2.881076	-0.118664	-0.509709
F	-0.717011	-1.488563	-0.551309
F	-2.595297	-0.440769	-0.102613
H	3.130850	-1.179203	-0.582294
H	2.836648	0.330381	-1.499934
H	3.654784	0.369138	0.088153

Table C.53 Coordinates of Non-Planar *cis* AA M06-2X Minimum

Cartesian coordinates [in Å] of the minimum energy structure of the non-planar *cis* conformer of acetic anhydride from M06-2X/6-311++G(d,p) calculations.

	X	Y	Z
C	-2.328365	-0.804555	-0.390750
H	-2.210539	-0.927413	-1.468966
H	-2.295374	-1.796000	0.061995
H	-3.271362	-0.312036	-0.169602
O	-1.267965	1.103367	0.628698
O	0.000006	-0.660334	0.000037
C	1.196582	0.028871	-0.129182
C	-1.196585	0.028863	0.129191
O	1.267933	1.103369	-0.628707
C	2.328393	-0.804533	0.390716
H	2.210624	-0.927369	1.468940
H	2.295386	-1.795986	-0.062007
H	3.271375	-0.312010	0.169510

Table C.54 Coordinates of Non-Planar *cis* AA M06-2X V_3 Transition State

Cartesian coordinates [in Å] of the V_3 transition state structure of the non-planar *cis* conformer of acetic anhydride from M06-2X/6-311++G(d,p) calculations.

	X	Y	Z
C	-2.310250	-0.833919	-0.402674
H	-2.153514	-0.989786	-1.471685
H	-2.284607	-1.810286	0.082287
H	-3.264572	-0.343751	-0.230192
O	-1.299928	1.112088	0.595942
O	0.004169	-0.658360	0.063514
C	1.190894	0.029150	-0.112143
C	-1.204334	0.025341	0.129962
O	1.246975	1.101783	-0.619697
C	2.364189	-0.786661	0.352987
H	2.949119	-0.177711	1.042698
H	2.051313	-1.709078	0.834379
H	2.994289	-1.009317	-0.509047

Table C.55 Coordinates of Non-Planar *cis* AA MP2 Minimum

Cartesian coordinates [in Å] of the minimum energy structure of the non-planar *cis* conformer of acetic anhydride from MP2/6-311++G(d,p) calculations.

	X	Y	Z
C	-2.329761	-0.794025	-0.407523
H	-2.219248	-0.871562	-1.492534
H	-2.287062	-1.804005	0.005335
H	-3.278282	-0.318647	-0.161668
O	-1.261336	1.105494	0.658605
O	0.000000	-0.683388	0.000001
C	1.197239	0.027419	-0.136836
C	-1.197239	0.027419	0.136836
O	1.261336	1.105494	-0.658605
C	2.329761	-0.794024	0.407522
H	2.219249	-0.871563	1.492533
H	2.287063	-1.804004	-0.005336
H	3.278282	-0.318645	0.161668

Table C.56 Coordinates of Non-Planar *cis* AA MP2 V_3 Transition State

Cartesian coordinates [in Å] of the V_3 transition state structure of the non-planar *cis* conformer of acetic anhydride from MP2/6-311++G(d,p) calculations.

	X	Y	Z
C	2.295226	0.837181	-0.435449
H	2.117717	0.960585	-1.507296
H	2.265992	1.827717	0.023411
H	3.262251	0.364921	-0.268139
O	1.311548	-1.113861	0.620042
O	-0.010251	0.678501	0.098454
C	-1.189891	-0.031869	-0.113771
C	1.206862	-0.020897	0.140014
O	-1.226427	-1.103817	-0.652988
C	-2.378280	0.765262	0.353963
H	-2.078958	1.666070	0.886552
H	-2.983900	1.030497	-0.516123
H	-2.984481	0.126323	0.999712

Table C.57 Coordinates of CH_3 *trans*^{90} AA M06-2X Minimum

Cartesian coordinates [in Å] of the minimum energy structure of the CH_3 *trans*^{90} conformer of acetic anhydride from M06-2X/6-311++G(d,p) calculations.

	X	Y	Z
C	-1.468890	1.221447	0.510492
H	-0.825602	1.472045	1.353037
H	-1.236540	1.912900	-0.299253
H	-2.518404	1.308643	0.782242
O	-2.073048	-0.925252	-0.360549
O	0.063288	-0.690461	0.150681
C	1.172219	0.071580	-0.082545
C	-1.236124	-0.184066	0.036622
O	1.131176	1.172970	-0.544499
C	2.408563	-0.690115	0.290189
H	2.369560	-0.951892	1.348490
H	2.443328	-1.620272	-0.278319
H	3.283807	-0.081910	0.079368

Table C.58 Coordinates of CH_3 *trans* AA M06-2X R1 V_3 Transition State

Cartesian coordinates [in Å] of the R1 V_3 transition state structure of the CH_3 *trans* conformer of acetic anhydride from M06-2X/6-311++G(d,p) calculations.

	X	Y	Z
C	-1.646788	1.044805	0.572223
H	-0.809534	1.674885	0.856079
H	-2.250088	1.547597	-0.181915
H	-2.278694	0.851310	1.442030
O	-1.923946	-1.069284	-0.517048
O	0.102140	-0.669690	0.311183
C	1.118775	0.117848	-0.137396
C	-1.219586	-0.288250	0.027811
O	0.935325	1.071700	-0.835979
C	2.441811	-0.397537	0.342278
H	2.454545	-0.411325	1.432958
H	2.574632	-1.423362	-0.003602
H	3.235720	0.237885	-0.040293

Table C.59 Coordinates of CH_3 *trans*^{90} AA M06-2X R2 V_3 Transition State

Cartesian coordinates [in Å] of the R2 V_3 transition state structure of the CH_3 *trans*^{90} conformer of acetic anhydride from M06-2X/6-311++G(d,p) calculations.

	X	Y	Z
C	-1.474360	1.217011	0.522929
H	-0.835663	1.461818	1.370617
H	-1.238014	1.912994	-0.281822
H	-2.525396	1.302624	0.789480
O	-2.066567	-0.921411	-0.378985
O	0.061255	-0.693574	0.178433
C	1.165156	0.062238	-0.081404
C	-1.237437	-0.184482	0.040541
O	1.117310	1.153011	-0.569261
C	2.425142	-0.665177	0.292252
H	2.215188	-1.644418	0.713121
H	3.041714	-0.762848	-0.601723
H	2.975246	-0.053367	1.008154

Table C.60 Coordinates of CH_3 *trans*^{90} AA MP2 Minimum

Cartesian coordinates [in Å] of the minimum energy structure of the CH_3 *trans*^{90} conformer of acetic anhydride from MP2/6-311++G(d,p) calculations.

	X	Y	Z
C	-1.458657	1.185349	0.631537
H	-0.795999	1.380744	1.475382
H	-1.258749	1.932499	-0.138338
H	-2.502429	1.250081	0.939556
O	-2.056911	-0.885640	-0.450952
O	0.075388	-0.712477	0.213321
C	1.162073	0.064839	-0.105466
C	-1.227547	-0.183548	0.051854
O	1.078764	1.121021	-0.684343
C	2.424098	-0.615457	0.344000
H	2.420020	-0.704432	1.433283
H	2.463320	-1.624310	-0.072228
H	3.285519	-0.034881	0.017539

Table C.61 Coordinates of CH_3 *trans*^{120} AA MP2 Minimum

Cartesian coordinates [in Å] of the minimum energy structure of the CH_3 *trans*^{120} conformer of acetic anhydride from MP2/6-311++G(d,p) calculations.

	X	Y	Z
C	1.672163	1.072462	-0.712727
H	1.002852	1.886903	-0.427819
H	2.688576	1.288720	-0.386274
H	1.638442	0.960613	-1.799780
O	1.803920	-0.931821	0.646156
O	-0.110445	-0.573387	-0.512717
C	-1.137485	0.084708	0.106817
C	1.198854	-0.199434	-0.077739
O	-0.958860	0.918544	0.964327
C	-2.460883	-0.392772	-0.420790
H	-2.500425	-0.250113	-1.502992
H	-2.563641	-1.461668	-0.219542
H	-3.264244	0.159410	0.064410

Table C.62 Coordinates of CH_3 *trans* AA MP2 R1 V_3 Transition State

Cartesian coordinates [in Å] of the R1 V_3 transition state structure of the CH_3 *trans* conformer of acetic anhydride from MP2/6-311++G(d,p) calculations.

	X	Y	Z
C	-1.643113	1.043445	0.604289
H	-0.809092	1.638399	0.969592
H	-2.178452	1.591836	-0.171945
H	-2.338023	0.841042	1.424714
O	-1.906009	-1.056243	-0.549257
O	0.113685	-0.674409	0.377611
C	1.109255	0.102365	-0.151965
C	-1.211472	-0.283238	0.041734
O	0.891208	0.997938	-0.934596
C	2.449773	-0.338138	0.363110
H	2.483050	-0.212069	1.448086
H	2.592954	-1.398757	0.145240
H	3.231838	0.254656	-0.108760

Table C.63 Coordinates of CH_3 *trans*^{90} AA MP2 R2 V_3 Transition State

Cartesian coordinates [in Å] of the R2 V_3 transition state structure of the CH_3 *trans*^{90} conformer of acetic anhydride from MP2/6-311++G(d,p) calculations.

	X	Y	Z
C	-1.485964	1.176676	0.635065
H	-0.854618	1.367188	1.503716
H	-1.258312	1.927295	-0.123835
H	-2.540490	1.238830	0.904605
O	-2.029527	-0.893751	-0.481132
O	0.077454	-0.704481	0.268996
C	1.153953	0.060682	-0.096785
C	-1.227594	-0.187051	0.056879
O	1.057584	1.096889	-0.710284
C	2.444633	-0.581649	0.334876
H	2.998802	0.133555	0.947009
H	2.272022	-1.501341	0.890815
H	3.040918	-0.789080	-0.556607

Table C.64 Coordinates of CH_3 *trans*^{120} AA MP2 R2 V_3 Transition State

Cartesian coordinates [in Å] of the R2 V_3 transition state structure of the CH_3 *trans*^{120} conformer of acetic anhydride from MP2/6-311++G(d,p) calculations.

	X	Y	Z
C	1.666703	1.090290	-0.694087
H	0.993743	1.895098	-0.391112
H	2.683039	1.306188	-0.367136
H	1.629483	0.998559	-1.782867
O	1.812155	-0.936408	0.630863
O	-0.104742	-0.572237	-0.523421
C	-1.133995	0.071813	0.103178
C	1.203279	-0.195530	-0.080688
O	-0.961244	0.892548	0.974845
C	-2.469595	-0.378920	-0.423004
H	-2.996543	0.490686	-0.822474
H	-2.363037	-1.140891	-1.193112
H	-3.053979	-0.768784	0.413250

Appendix D: Supplementary Material for Chapter 4

Table D.1 Observed Transitions of TFAA-H_2O

J'	K_a'	K_c'	J''	K_a''	K_c''	Obs. Frequency (MHz)	Obs. - Calc. (MHz)
5	0	5	4	1	4	3175.007	0.001
4	1	4	3	0	3	3675.645	0.005
5	1	5	4	1	4	3739.558	0.001
5	0	5	4	0	4	3802.849	0.000
5	1	4	4	1	3	3895.140	-0.001
6	0	6	5	1	5	3989.080	-0.001
5	1	5	4	0	4	4367.401	0.001
6	1	6	5	1	5	4485.132	-0.001
6	0	6	5	0	5	4553.632	0.001
6	1	5	5	1	4	4671.286	0.000
7	0	7	6	1	6	4803.739	0.001
6	1	6	5	0	5	5049.685	0.001
7	1	7	6	1	6	5229.586	0.001
7	0	7	6	0	6	5299.792	0.002
7	1	6	6	1	5	5445.693	0.001
8	0	8	7	1	7	5615.524	-0.001
7	1	7	6	0	6	5725.637	-0.001
8	1	8	7	1	7	5972.844	0.000
8	0	8	7	0	7	6041.372	0.000
8	1	7	7	1	6	6217.931	0.000
8	1	8	7	0	7	6398.692	0.001
9	0	9	8	1	8	6421.531	0.001
9	1	9	8	1	8	6714.879	0.000
9	0	9	8	0	8	6778.854	0.005
12	5	8	12	4	8	6921.653	0.002
12	5	7	12	4	8	6921.730	0.001
12	5	8	12	4	9	6925.212	0.001
12	5	7	12	4	9	6925.286	-0.002
11	5	7	11	4	7	6929.514	0.001
11	5	6	11	4	7	6929.546	0.001
11	5	7	11	4	8	6931.298	-0.003
11	5	6	11	4	8	6931.333	0.000
10	5	6	10	4	6	6935.329	-0.003
10	5	5	10	4	6	6935.346	0.002
10	5	6	10	4	7	6936.167	-0.002
10	5	5	10	4	7	6936.184	0.003

Table D.1 Observed Transitions of TFAA-H_2O (cont'd)

J'	K_a'	K_c'	J''	K_a''	K_c''	Obs. Frequency (MHz)	Obs. - Calc. (MHz)
9	5	5	9	4	5	6939.570	-0.002
9	5	4	9	4	5	6939.570	-0.006
9	5	5	9	4	6	6939.936	0.004
9	5	4	9	4	6	6939.936	0.000
8	5	4	8	4	4	6942.599	0.003
8	5	3	8	4	4	6942.599	0.002
8	5	4	8	4	5	6942.738	0.004
8	5	3	8	4	5	6942.738	0.002
7	5	3	7	4	3	6944.692	0.003
7	5	2	7	4	3	6944.692	0.003
7	5	3	7	4	4	6944.734	-0.001
7	5	2	7	4	4	6944.734	-0.001
6	5	2	6	4	2	6946.088	0.008
6	5	1	6	4	2	6946.088	0.008
6	5	2	6	4	3	6946.088	-0.004
6	5	1	6	4	3	6946.088	-0.004
5	5	1	5	4	1	6946.957	0.003
5	5	0	5	4	1	6946.957	0.003
5	5	1	5	4	2	6946.957	0.000
5	5	0	5	4	2	6946.957	0.000
9	1	8	8	1	7	6987.518	-0.002
9	1	9	8	0	8	7072.200	0.002
10	0	10	9	1	9	7219.687	-0.001
10	1	10	9	1	9	7455.708	0.002
10	0	10	9	0	9	7513.039	0.002
10	1	10	9	0	9	7749.047	-0.008
10	1	9	9	1	8	7753.931	0.004
11	0	11	10	1	10	8008.898	-0.002
11	1	11	10	1	10	8195.374	0.002
11	0	11	10	0	10	8244.917	0.000
11	1	11	10	0	10	8431.390	0.000
4	4	1	3	3	0	8462.042	-0.002
4	4	1	3	3	1	8462.067	0.005
4	4	0	3	3	1	8462.067	0.005
4	4	0	3	3	0	8462.042	-0.002
11	1	10	10	1	9	8516.585	-0.002
12	0	12	11	1	11	8788.964	0.000

Table D.1 Observed Transitions of TFAA-H_2O (cont'd)

J'	K_a'	K_c'	J''	K_a''	K_c''	Obs. Frequency (MHz)	Obs. - Calc. (MHz)
12	0	12	11	0	11	8975.438	0.002
12	1	12	11	0	11	9120.432	0.001
5	4	1	4	3	1	9226.482	0.000
5	4	2	4	3	1	9226.482	0.003
5	4	1	4	3	2	9226.604	-0.003
5	4	2	4	3	2	9226.604	-0.001
13	0	13	12	1	12	9560.367	0.000
13	1	13	12	0	12	9816.559	0.000
6	4	3	5	3	2	9990.523	-0.003
6	4	2	5	3	2	9990.541	0.002
6	4	3	5	3	3	9991.024	-0.002
6	4	2	5	3	3	9991.042	0.003
14	0	14	13	1	13	10324.029	0.000
14	1	14	13	0	13	10519.502	0.001
7	4	4	6	3	3	10753.778	-0.004
7	4	3	6	3	3	10753.829	0.000
7	4	4	6	3	4	10755.280	0.000
7	4	3	6	3	4	10755.328	0.001
5	5	1	4	4	0	10770.517	0.001
5	5	0	4	4	0	10770.517	0.001
5	5	1	4	4	1	10770.517	0.000
5	5	0	4	4	1	10770.517	0.000
15	0	15	14	1	14	11081.066	0.000
15	1	15	14	0	14	11228.568	-0.001
8	4	5	7	3	4	11515.646	0.001
8	4	4	7	3	4	11515.784	0.000
8	4	5	7	3	5	11519.379	-0.001
8	4	4	7	3	5	11519.522	0.003
6	5	2	5	4	1	11535.049	0.001
6	5	1	5	4	1	11535.049	0.001
6	5	2	5	4	2	11535.049	-0.001
6	5	1	5	4	2	11535.049	-0.001
16	0	16	15	1	15	11832.620	-0.003
16	1	16	15	0	15	11942.879	0.000
9	4	6	8	3	5	12275.254	0.002
9	4	5	8	3	5	12275.613	0.001
9	4	6	8	3	6	12283.435	-0.001

Table D.1 Observed Transitions of TFAA-H_2O (cont'd)

J'	K_a'	K_c'	J''	K_a''	K_c''	Obs. Frequency (MHz)	Obs. - Calc. (MHz)
9	4	5	8	3	6	12283.797	0.002
7	5	3	6	4	2	12299.445	-0.002
7	5	2	6	4	2	12299.445	-0.002
7	5	3	6	4	3	12299.461	0.001
7	5	2	6	4	3	12299.461	0.001
8	5	4	7	4	3	13063.602	-0.001
8	5	3	7	4	3	13063.602	-0.002
8	5	4	7	4	4	13063.651	0.002
8	5	3	7	4	4	13063.651	0.000
6	6	0	5	5	0	13078.943	0.000
6	6	0	5	5	1	13078.943	0.000
6	6	1	5	5	0	13078.943	0.000
6	6	1	5	5	1	13078.943	0.000
18	0	18	17	1	17	13323.424	0.000
9	5	5	8	4	4	13827.373	0.003
9	5	4	8	4	4	13827.373	-0.001
9	5	5	8	4	5	13827.510	0.001
9	5	4	8	4	5	13827.510	-0.003
7	6	1	6	5	1	13843.482	-0.001
7	6	1	6	5	2	13843.482	-0.001
7	6	2	6	5	1	13843.482	-0.001
7	6	2	6	5	2	13843.482	-0.001
10	5	6	9	4	5	14590.554	-0.004
10	5	5	9	4	5	14590.570	0.000
10	5	6	9	4	6	14590.914	-0.004
10	5	5	9	4	6	14590.933	0.004
8	6	2	7	5	2	14607.942	-0.001
8	6	2	7	5	3	14607.942	-0.002
8	6	3	7	5	2	14607.942	-0.001
8	6	3	7	5	3	14607.942	-0.002
11	5	7	10	4	6	15352.919	0.001
11	5	6	10	4	6	15352.949	-0.001
13	4	9	12	3	10	15353.145	0.002
11	5	7	10	4	7	15353.754	-0.002
11	5	6	10	4	7	15353.787	-0.001
9	6	3	8	5	3	15372.262	-0.002
9	6	3	8	5	4	15372.262	-0.003

Table D.1 Observed Transitions of TFAA-H_2O (cont'd)

J'	K_a'	K_c'	J''	K_a''	K_c''	Obs. Frequency (MHz)	Obs. - Calc. (MHz)
9	6	4	8	5	3	15372.262	-0.002
9	6	4	8	5	4	15372.262	-0.003
7	7	0	6	6	0	15387.326	-0.001
7	7	0	6	6	1	15387.326	-0.001
7	7	1	6	6	0	15387.326	-0.001
7	7	1	6	6	1	15387.326	-0.001
10	6	4	9	5	4	16136.372	0.001
10	6	4	9	5	5	16136.372	-0.003
10	6	5	9	5	4	16136.372	0.001
10	6	5	9	5	5	16136.372	-0.003
8	7	1	7	6	1	16151.859	-0.003
8	7	1	7	6	2	16151.859	-0.003
8	7	2	7	6	1	16151.859	-0.003
8	7	2	7	6	2	16151.859	-0.003
11	6	6	10	5	5	16900.174	-0.004
9	7	2	8	6	2	16916.329*	-0.012
9	7	2	8	6	3	16916.329*	-0.012
9	7	3	8	6	2	16916.329*	-0.012
9	7	3	8	6	3	16916.329*	-0.012
10	7	3	9	6	3	17680.711*	-0.014
10	7	3	9	6	4	17680.711*	-0.014
10	7	4	9	6	3	17680.711*	-0.014
10	7	4	9	6	4	17680.711*	-0.014
8	8	0	7	7	0	17695.660	-0.003
8	8	0	7	7	1	17695.660	-0.003
8	8	1	7	7	0	17695.660	-0.003
8	8	1	7	7	1	17695.660	-0.003

* Denotes transitions measured with the chirped-pulse method

Table D.2 Observed Transitions of TFAA-D_2O

J'	K_a'	K_c'	J''	K_a''	K_c''	Obs. Frequency (MHz)	Obs. - Calc. (MHz)
9	1	9	8	1	8	6639.996	-0.002
9	0	9	8	0	8	6700.713	-0.001
9	1	8	8	1	7	6933.301	-0.002
9	1	9	8	0	8	6940.737	0.000
10	0	10	9	1	9	7184.086	-0.003
10	1	10	9	1	9	7371.552	0.001
10	0	10	9	0	9	7424.110	-0.001
10	1	10	9	0	9	7611.573	0.000
10	1	9	9	1	8	7690.832	0.002
11	0	11	10	1	10	7958.157	0.000
11	1	11	10	1	10	8101.815	-0.001
11	0	11	10	0	10	8145.620	0.001
11	1	11	10	0	10	8289.278	0.001
11	1	10	10	1	9	8443.541	0.001
12	0	12	11	1	11	8722.603	0.001
12	1	12	11	0	11	8974.571	0.000
14	7	7	14	6	8	9475.941	-0.001
14	7	8	14	6	8	9475.941	-0.001
14	7	7	14	6	9	9475.958	0.001
14	7	8	14	6	9	9475.958	0.001
13	0	13	12	1	12	9478.443	0.000
13	7	6	13	6	7	9480.204	0.002
13	7	7	13	6	7	9480.204	0.002
13	7	6	13	6	8	9480.204	-0.003
13	7	7	13	6	8	9480.204	-0.003
12	7	5	12	6	6	9483.612	-0.001
12	7	6	12	6	6	9483.612	-0.001
12	7	5	12	6	7	9483.612	-0.003
12	7	6	12	6	7	9483.612	-0.003
11	7	4	11	6	5	9486.301	0.001
11	7	5	11	6	5	9486.301	0.001
11	7	4	11	6	6	9486.301	0.001
11	7	5	11	6	6	9486.301	0.001
10	7	3	10	6	4	9488.375	0.000
10	7	4	10	6	4	9488.375	0.000
10	7	3	10	6	5	9488.375	0.000
10	7	4	10	6	5	9488.375	0.000

Table D.2 Observed Transitions of TFAA-D_2O (cont'd)

J'	K_a'	K_c'	J''	K_a''	K_c''	Obs. Frequency (MHz)	Obs. - Calc. (MHz)
9	7	3	9	6	3	9489.941	0.000
9	7	2	9	6	3	9489.941	0.000
9	7	3	9	6	4	9489.941	0.000
9	7	2	9	6	4	9489.941	0.000
8	7	2	8	6	2	9491.086	-0.003
8	7	1	8	6	2	9491.086	-0.003
8	7	2	8	6	3	9491.086	-0.003
8	7	1	8	6	3	9491.086	-0.003
5	5	1	4	4	0	10363.126	0.001
5	5	0	4	4	0	10363.126	0.001
5	5	1	4	4	1	10363.126	0.001
5	5	0	4	4	1	10363.126	0.001
7	4	4	6	3	3	10416.548	-0.001
7	4	3	6	3	3	10416.626	0.001
7	4	4	6	3	4	10418.687	-0.002
7	4	3	6	3	4	10418.764	-0.001
6	5	2	5	4	1	11121.304	0.001
6	5	1	5	4	1	11121.304	0.001
6	5	2	5	4	2	11121.304	-0.003
6	5	1	5	4	2	11121.304	-0.003
8	4	5	7	3	4	11171.175	-0.001
8	4	4	7	3	4	11171.405	0.002
8	4	5	7	3	5	11176.509	0.002
8	4	4	7	3	5	11176.737	0.002
7	5	3	6	4	2	11879.315	-0.001
7	5	2	6	4	2	11879.315	-0.002
7	5	3	6	4	3	11879.337	0.000
7	5	2	6	4	3	11879.337	-0.001
6	6	1	5	5	0	12581.722	0.001
6	6	0	5	5	0	12581.722	0.001
6	6	1	5	5	1	12581.722	0.001
6	6	0	5	5	1	12581.722	0.001
8	5	3	7	4	3	12637.023	-0.002
8	5	4	7	4	3	12637.023	0.000
8	5	4	7	4	4	12637.101	0.002
8	5	3	7	4	4	12637.101	0.000
7	6	2	6	5	1	13339.915	0.001

Table D.2 Observed Transitions of TFAA-D_2O (cont'd)

J'	K_a'	K_c'	J''	K_a''	K_c''	Obs. Frequency (MHz)	Obs. - Calc. (MHz)
7	6	1	6	5	1	13339.915	0.001
7	6	2	6	5	2	13339.915	0.001
7	6	1	6	5	2	13339.915	0.001
9	5	5	8	4	4	13394.238	0.006
9	5	4	8	4	4	13394.238	-0.002
9	5	5	8	4	5	13394.461	0.001
9	5	4	8	4	5	13394.461	-0.006
8	6	3	7	5	2	14098.009	0.000
8	6	2	7	5	2	14098.009	0.000
8	6	3	7	5	3	14098.009	-0.001
8	6	2	7	5	3	14098.009	-0.001
10	5	6	9	4	5	14150.697	0.005
10	5	5	9	4	5	14150.719	0.005
10	5	6	9	4	6	14151.279	-0.002
10	5	5	9	4	6	14151.297	-0.007
7	7	1	6	6	0	14800.274	0.001
7	7	0	6	6	0	14800.274	0.001
7	7	1	6	6	1	14800.274	0.001
7	7	0	6	6	1	14800.274	0.001
9	6	4	8	5	3	14855.933	0.002
9	6	3	8	5	3	14855.933	0.002
9	6	4	8	5	4	14855.933	0.000
9	6	3	8	5	4	14855.933	0.000
8	7	2	7	6	1	15558.463	0.000
8	7	1	7	6	1	15558.463	0.000
8	7	2	7	6	2	15558.463	0.000
8	7	1	7	6	2	15558.463	0.000
10	6	5	9	5	4	15613.593	0.006
10	6	4	9	5	4	15613.593	0.006
10	6	5	9	5	5	15613.593	-0.001
10	6	4	9	5	5	15613.593	-0.001
9	7	3	8	6	2	16316.586	0.001
9	7	2	8	6	2	16316.586	0.001
9	7	3	8	6	3	16316.586	0.001
9	7	2	8	6	3	16316.586	0.001
11	6	6	10	5	5	16370.860	-0.007
11	6	5	10	5	5	16370.860	-0.008

Table D.2 Observed Transitions of TFAA-D_2O (cont'd)

J'	K_a'	K_c'	J''	K_a''	K_c''	Obs. Frequency (MHz)	Obs. - Calc. (MHz)
11	6	6	10	5	6	16370.891	0.002
11	6	5	10	5	6	16370.891	0.001
8	8	1	7	7	0	17018.775	0.001
8	8	0	7	7	0	17018.775	0.001
8	8	1	7	7	1	17018.775	0.001
8	8	0	7	7	1	17018.775	0.001
10	7	4	9	6	3	17074.591	0.001
10	7	3	9	6	3	17074.591	0.001
10	7	4	9	6	4	17074.591	0.001
10	7	3	9	6	4	17074.591	0.001
9	8	1	8	7	1	17776.953	0.000
9	8	1	8	7	1	17776.953	0.000
9	8	1	8	7	1	17776.953	0.000
9	8	1	8	7	1	17776.953	0.000
11	7	5	10	6	4	17832.421	0.002
11	7	4	10	6	4	17832.421	0.002
11	7	5	10	6	5	17832.421	0.002
11	7	4	10	6	5	17832.421	0.002

Table D.3 Observed Transitions of TFAA-DOH

J'	K_a'	K_c'	J''	K_a''	K_c''	Obs. Frequency (MHz)	Obs. - Calc. (MHz)
8	0	8	7	1	7	5617.656	0.002
7	1	7	6	0	6	5661.855	-0.004
8	1	8	7	1	7	5938.996	0.000
8	0	8	7	0	7	6007.509	0.002
8	1	8	7	0	7	6328.845	-0.003
9	0	9	8	1	8	6417.373	-0.001
9	5	5	9	4	5	6756.463	0.010
9	5	4	9	4	5	6756.463	0.004
9	5	5	9	4	6	6756.974	0.007
9	5	4	9	4	6	6756.974	0.001
8	5	4	8	4	4	6760.046	0.001
8	5	3	8	4	4	6760.046	-0.001
8	5	4	8	4	5	6760.242	-0.002
8	5	3	8	4	5	6760.242	-0.003
7	5	3	7	4	3	6762.513	-0.009
7	5	2	7	4	3	6762.513	-0.009
7	5	3	7	4	4	6762.584	-0.004
7	5	2	7	4	4	6762.584	-0.005
6	5	2	6	4	2	6764.180	0.017
6	5	1	6	4	2	6764.180	0.017
6	5	2	6	4	3	6764.180	-0.001
6	5	1	6	4	3	6764.180	-0.001
5	5	1	5	4	1	6765.187	-0.005
5	5	0	5	4	1	6765.187	-0.005
5	5	1	5	4	2	6765.187	-0.009
5	5	0	5	4	2	6765.187	-0.009
9	1	9	8	0	8	6997.473	-0.003
10	0	10	9	1	9	7207.941	-0.003
10	1	10	9	0	9	7670.700	0.008
11	0	11	10	1	10	7988.646	0.001
5	5	1	4	4	0	10575.329	0.008
5	5	0	4	4	0	10575.329	0.008
5	5	1	4	4	1	10575.329	0.007
5	5	0	4	4	1	10575.329	0.007
6	5	2	5	4	1	11337.143	0.005
6	5	1	5	4	1	11337.143	0.005
6	5	2	5	4	2	11337.143	0.001

Table D.3 Observed Transitions of TFAA-DOH (cont'd)

J'	K_a'	K_c'	J''	K_a''	K_c''	Obs. Frequency (MHz)	Obs. - Calc. (MHz)
6	5	1	5	4	2	11337.143	0.001
7	5	3	6	4	2	12098.810	0.011
7	5	2	6	4	2	12098.810	0.010
7	5	3	6	4	3	12098.810	-0.007
7	5	2	6	4	3	12098.810	-0.008
6	6	1	5	5	0	12840.678	0.005
6	6	0	5	5	0	12840.678	0.005
6	6	1	5	5	1	12840.678	0.005
6	6	0	5	5	1	12840.678	0.005
8	5	4	7	4	3	12860.173	0.001
8	5	3	7	4	3	12860.173	-0.001
8	5	4	7	4	4	12860.237	-0.001
8	5	3	7	4	4	12860.237	-0.003
7	6	2	6	5	1	13602.508	0.004
7	6	1	6	5	1	13602.508	0.004
7	6	2	6	5	2	13602.508	0.004
7	6	1	6	5	2	13602.508	0.004
8	6	3	7	5	2	14364.220	-0.022
8	6	2	7	5	2	14364.220	-0.022
8	6	3	7	5	3	14364.220	-0.022
8	6	2	7	5	3	14364.220	-0.022
7	7	1	6	6	0	15105.985	0.002
7	7	0	6	6	0	15105.985	0.002
7	7	1	6	6	1	15105.985	0.002
7	7	0	6	6	1	15105.985	0.002
9	6	4	8	5	3	15125.821	0.004
9	6	3	8	5	3	15125.821	0.004
9	6	4	8	5	4	15125.821	0.003
9	6	3	8	5	4	15125.821	0.003
8	7	2	7	6	1	15867.812	0.000
8	7	1	7	6	1	15867.812	0.000
8	7	2	7	6	2	15867.812	0.000
8	7	1	7	6	2	15867.812	0.000
10	6	5	9	5	4	15887.143	0.003
10	6	4	9	5	4	15887.143	0.003
10	6	5	9	5	5	15887.143	-0.003
10	6	4	9	5	5	15887.143	-0.004

Table D.3 Observed Transitions of TFAA-DOH (cont'd)

J'	K_a'	K_c'	J''	K_a''	K_c''	Obs. Frequency (MHz)	Obs. - Calc. (MHz)
9	7	3	8	6	2	16629.577	0.001
9	7	2	8	6	2	16629.577	0.001
9	7	3	8	6	3	16629.577	0.001
9	7	2	8	6	3	16629.577	0.001
11	6	6	10	5	5	16648.109	0.000
11	6	5	10	5	5	16648.109	-0.001
11	6	6	10	5	6	16648.132	0.004
11	6	5	10	5	6	16648.132	0.003
8	8	1	7	7	0	17371.245	-0.001
8	8	0	7	7	0	17371.245	-0.001
8	8	1	7	7	1	17371.245	-0.001
8	8	0	7	7	1	17371.245	-0.001
10	7	4	9	6	3	17391.230	0.001
10	7	3	9	6	3	17391.230	0.001
10	7	4	9	6	4	17391.230	0.001
10	7	3	9	6	4	17391.230	0.001
12	6	7	11	5	6	17408.602	0.001
12	6	6	11	5	6	17408.602	-0.001
12	6	7	11	5	7	17408.650	-0.001
12	6	6	11	5	7	17408.650	-0.003

Table D.4 Observed Transitions of PiA-H_2O State A

J'	K_a'	K_c'	J''	K_a''	K_c''	Obs. Frequency (MHz)	Obs. - Calc. (MHz)
7	1	7	6	0	6	5510.848	0.001
8	0	8	7	1	7	6043.059	-0.001
8	1	8	7	0	7	6207.099	0.000
8	1	7	7	1	6	6566.857	-0.001
8	2	6	7	2	5	6690.671	0.001
9	0	9	8	1	8	6814.591	0.000
9	1	9	8	1	8	6853.178	-0.001
9	0	9	8	0	8	6877.882	0.000
9	1	9	8	0	8	6916.470	0.000
9	2	8	8	2	7	7160.898	0.000
9	1	8	8	1	7	7331.203	0.001
10	0	10	9	1	9	7574.818	0.001
10	1	10	9	1	9	7597.806	-0.001
10	0	10	9	0	9	7613.405	0.000
10	1	10	9	0	9	7636.395	0.000
5	4	2	4	3	1	8029.250	0.000
5	4	1	4	3	2	8031.579	0.002
12	0	12	11	1	11	9075.124	0.000
12	1	12	11	1	11	9082.879	-0.001
11	2	10	10	1	9	9084.364	0.000
12	0	12	11	0	11	9088.575	0.000
12	1	12	11	0	11	9096.331	0.001
5	5	1	4	4	0	9170.433	0.001
5	5	0	4	4	1	9170.447	0.000
7	4	3	6	3	4	9654.384	0.000
7	4	4	6	3	3	9626.288	-0.001
13	0	13	12	1	12	9819.784	0.000
13	1	13	12	0	12	9831.959	0.000

Table D.5 Observed Transitions of PiA-H_2O State B

J'	K_a'	K_c'	J''	K_a''	K_c''	Obs. Frequency (MHz)	Obs. - Calc. (MHz)
7	1	7	6	0	6	5510.872	0.000
8	0	8	7	1	7	6043.072	-0.001
8	1	8	7	0	7	6207.125	0.001
8	1	7	7	1	6	6566.874	0.000
9	0	9	8	1	8	6814.608	0.000
9	0	9	8	0	8	6877.903	-0.001
9	1	9	8	0	8	6916.494	-0.001
9	2	8	8	2	7	7160.915	0.000
10	1	10	9	1	9	7597.830	0.001
10	0	10	9	0	9	7613.429	0.001
5	4	2	4	3	1	8029.316	0.001
12	0	12	11	1	11	9075.148	0.000
12	1	12	11	1	11	9082.902	-0.003
11	2	10	10	1	9	9084.408	0.000
12	1	12	11	0	11	9096.357	0.000
7	4	3	6	3	4	9654.451	-0.001
7	4	4	6	3	3	9626.359	0.001
13	0	13	12	1	12	9819.811	0.001
13	1	13	12	0	12	9831.988	0.002

Table D.6 Observed Transitions of PiA-D_2O

J'	K_a'	K_c'	J''	K_a''	K_c''	Obs. Frequency (MHz)	Obs. - Calc. (MHz)
7	1	7	6	1	6	5284.981	0.000
7	0	7	6	0	6	5332.315	-0.001
7	2	6	6	2	5	5546.627	0.000
7	3	5	6	3	4	5632.970	0.000
7	1	6	6	1	5	5730.620	-0.001
7	2	5	6	2	4	5810.784	-0.001
8	1	8	7	1	7	6022.895	0.000
8	0	8	7	0	7	6054.467	0.000
8	2	7	7	2	6	6317.737	0.000
8	3	6	7	3	5	6437.625	0.003
8	1	7	7	1	6	6497.153	0.000
8	3	5	7	3	4	6527.459	0.000
8	2	6	7	2	5	6655.400	0.000
9	0	9	8	1	8	6729.856	0.000
9	1	9	8	1	8	6757.887	0.000
9	0	9	8	0	8	6777.757	0.000
9	1	9	8	0	8	6805.788	0.000
9	2	8	8	2	7	7081.613	-0.001
9	1	8	8	1	7	7243.191	0.001
10	0	10	9	1	9	7474.741	0.000
9	2	7	8	2	6	7486.957	0.001
10	1	10	9	1	9	7490.777	-0.001
10	0	10	9	0	9	7502.772	0.000
10	1	10	9	0	9	7518.809	0.000
10	1	9	9	2	8	7535.117	0.000
11	0	11	10	1	10	8213.233	0.001
11	1	11	10	1	10	8222.245	0.000
11	0	11	10	0	10	8229.269	0.000
11	1	11	10	0	10	8238.281	0.000

Table D.7 Observed Transitions of PiA-DOH

J'	K_a'	K_c'	J''	K_a''	K_c''	Obs. Frequency (MHz)	Obs. - Calc. (MHz)
8	0	8	7	1	7	6025.758	-0.001
8	1	8	7	1	7	6082.572	0.001
8	0	8	7	0	7	6117.650	0.001
8	1	8	7	0	7	6174.462	0.000
9	0	9	8	1	8	6791.802	0.001
9	1	9	8	1	8	6825.896	0.000
9	0	9	8	0	8	6848.613	-0.001
9	1	9	8	0	8	6882.708	0.000
9	2	8	8	2	7	7139.537	-0.001
9	1	8	8	1	7	7306.606	0.000
9	2	7	8	2	6	7524.209	0.001
10	0	10	9	1	9	7547.058	0.000
10	1	10	9	1	9	7567.056	0.001
10	0	10	9	0	9	7581.153	0.001
10	1	10	9	0	9	7601.149	-0.001
10	2	9	9	2	8	7905.154	0.001
10	1	9	9	1	8	8047.807	0.000
11	0	11	10	1	10	8295.185	-0.001

Table D.8 Observed Transitions of PiTFAA-H_2O State A

J'	K_a'	K_c'	J''	K_a''	K_c''	Obs. Frequency (MHz)	Obs. - Calc. (MHz)
7	1	7	6	1	6	5173.891	0.001
7	0	7	6	0	6	5239.859	0.000
7	2	6	6	2	5	5383.461	0.001
7	1	7	6	0	6	5404.266	0.000
7	1	6	6	1	5	5550.832	-0.002
7	2	5	6	2	4	5555.793	0.000
8	1	8	7	1	7	5901.254	0.002
8	0	8	7	0	7	5952.630	0.000
8	2	7	7	2	6	6140.249	0.002
8	1	7	7	1	6	6316.548	0.000
8	2	6	7	2	5	6371.917	-0.001
9	1	9	8	1	8	6625.919	-0.001
9	0	9	8	0	8	6663.551	0.000
9	1	9	8	0	8	6738.948	0.000
9	2	8	8	2	7	6892.498	0.000

Table D.8 Observed Transitions of PiTFAA-H_2O State A (cont'd)

J'	K_a'	K_c'	J''	K_a''	K_c''	Obs. Frequency (MHz)	Obs. - Calc. (MHz)
5	3	3	4	2	2	6987.072	0.000
9	1	8	8	1	7	7069.513	0.001
9	2	7	8	2	6	7184.018	0.000
10	0	10	9	1	9	7299.255	0.002
10	1	10	9	1	9	7348.356	-0.002
10	0	10	9	0	9	7374.650	0.000
10	1	10	9	0	9	7423.754	-0.002
10	2	9	9	2	8	7639.991	0.000
10	5	6	9	5	5	7765.319	0.001
10	3	8	9	3	7	7766.985	-0.006
10	3	8	9	3	7	7766.990	-0.001
10	1	9	9	1	8	7808.617	0.001
11	0	11	10	1	10	8037.668	0.001
11	1	11	10	1	10	8069.048	0.002
11	0	11	10	0	10	8086.775	0.003
11	1	11	10	0	10	8118.150	-0.002
11	2	10	10	2	9	8382.676	-0.001
11	1	10	10	1	9	8534.441	0.000
11	3	9	10	3	8	8539.544	-0.005
12	0	12	11	1	11	8768.673	0.001
11	2	9	10	2	8	8783.930	0.002
12	1	12	11	1	11	8788.421	0.001
6	6	1	5	5	0	11576.310	0.001
6	6	0	5	5	1	11576.310	0.001
7	6	2	6	5	1	12350.667	0.001
7	6	1	6	5	2	12350.667	-0.001

Table D.9 Observed Transitions of PiTFAA-H_2O State B

J'	K_a'	K_c'	J''	K_a''	K_c''	Obs. Frequency (MHz)	Obs. - Calc. (MHz)
7	1	7	6	1	6	5173.791	-0.001
7	0	7	6	0	6	5239.755	-0.001
7	2	6	6	2	5	5383.443	-0.006
7	1	6	6	1	5	5550.875	0.001
7	2	5	6	2	4	5555.893	-0.001
8	1	8	7	1	7	5901.134	0.001
8	0	8	7	0	7	5952.501	0.001
8	1	7	7	1	6	6316.571	0.001
8	2	6	7	2	5	6372.032	-0.002
9	1	9	8	1	8	6625.779	0.000
9	0	9	8	0	8	6663.397	0.001
9	2	7	8	2	6	7184.142	0.002
10	1	10	9	1	9	7348.195	-0.001
10	0	10	9	0	9	7374.472	-0.002
10	1	10	9	0	9	7423.533	-0.002
10	2	9	9	2	8	7639.938	0.000
10	3	8	9	3	7	7767.018	0.000
10	1	9	9	1	8	7808.571	-0.002
11	0	11	10	1	10	8037.513	-0.001
11	1	11	10	1	10	8068.863	0.002
11	1	11	10	0	10	8117.922	-0.001
11	2	10	10	2	9	8382.605	0.000
11	1	10	10	1	9	8534.355	0.000
12	0	12	11	1	11	8768.488	0.001
11	2	9	10	2	8	8784.035	0.000
6	6	1	5	5	0	11576.414	-0.004
6	6	0	5	5	1	11576.414	-0.004
7	6	2	6	5	1	12350.777	0.002
7	6	1	6	5	2	12350.777	0.000

Table D.10 Observed Transitions of PiTFAA-D_2O State A

J'	K_a'	K_c'	J''	K_a''	K_c''	Obs. Frequency (MHz)	Obs. - Calc. (MHz)
8	1	8	7	1	7	5814.912	0.001
8	0	8	7	0	7	5858.898	-0.001
8	1	8	7	0	7	5943.389	-0.001
8	2	7	7	2	6	6071.621	0.000
8	3	5	7	3	4	6210.781	0.001
8	1	7	7	1	6	6250.617	0.000
8	2	6	7	2	5	6337.488	0.001
9	0	9	8	1	8	6473.249	0.000
9	1	9	8	1	8	6527.160	0.000
9	0	9	8	0	8	6557.738	-0.002
9	1	9	8	0	8	6611.651	0.000
9	2	8	8	2	7	6812.142	-0.001
9	3	7	8	3	6	6928.808	0.000
9	1	8	8	1	7	6986.336	0.001
9	4	6	8	4	5	6935.612	0.001
9	3	6	8	3	5	7017.663	0.000
9	2	7	8	2	6	7141.193	0.001
10	0	10	9	1	9	7203.583	0.000
10	1	10	9	1	9	7237.181	0.001
10	0	10	9	0	9	7257.493	-0.001
10	1	10	9	0	9	7291.091	0.000
10	2	9	9	2	8	7547.128	-0.001
10	1	9	9	1	8	7706.280	-0.001
10	2	8	9	2	7	7934.778	-0.001
11	1	11	10	1	10	7945.534	0.000
11	0	11	10	0	10	7958.577	-0.001
11	2	10	10	2	9	8276.669	0.000
11	1	10	10	1	9	8412.735	0.002
11	3	9	10	3	8	8457.950	-0.002
11	4	8	10	4	7	8491.677	0.000

Table D.11 Observed Transitions of PiTFAA-D_2O State B

J'	K_a'	K_c'	J''	K_a''	K_c''	Obs. Frequency (MHz)	Obs. - Calc. (MHz)
8	2	7	7	2	6	6071.605	-0.001
8	3	5	7	3	4	6210.758	0.001
8	1	7	7	1	6	6250.597	-0.001
8	2	6	7	2	5	6337.463	0.001
9	0	9	8	1	8	6473.240	0.001
9	2	8	8	2	7	6812.125	-0.001
9	3	7	8	3	6	6928.785	-0.002
9	4	6	8	4	5	6935.590	0.002
9	1	8	8	1	7	6986.315	0.000
9	3	6	8	3	5	7017.635	-0.001
9	2	7	8	2	6	7141.165	0.001
10	2	9	9	2	8	7547.110	-0.002
10	1	9	9	1	8	7706.263	0.001
10	2	8	9	2	7	7934.747	0.000
11	2	10	10	2	9	8276.651	-0.001
11	1	10	10	1	9	8412.718	0.002
11	3	9	10	3	8	8457.926	-0.001
11	4	8	10	4	7	8491.647	-0.001

Table D.12 Observed Transitions of PiTFAA-DOH

J'	K_a'	K_c'	J''	K_a''	K_c''	Obs. Frequency (MHz)	Obs. - Calc. (MHz)
8	1	8	7	1	7	5871.682	0.000
8	0	8	7	0	7	5920.182	-0.002
8	2	7	7	2	6	6118.297	0.000
8	1	7	7	1	6	6296.356	0.000
8	2	6	7	2	5	6364.080	0.000
9	1	9	8	1	8	6591.971	0.000
9	0	9	8	0	8	6626.763	0.000
9	2	8	8	2	7	6866.552	0.000
9	1	8	8	1	7	7043.241	0.000
9	2	7	8	2	6	7173.769	0.000
10	0	10	9	1	9	7267.683	0.000
10	1	10	9	1	9	7310.020	0.000
10	0	10	9	0	9	7333.841	0.000
10	1	10	9	0	9	7376.178	0.000
10	2	9	9	2	8	7609.729	0.000
10	1	9	9	1	8	7775.397	0.000
10	2	8	9	2	7	7975.040	-0.001
11	0	11	10	1	10	7999.754	0.000
11	1	11	10	1	10	8026.343	0.001
11	0	11	10	0	10	8042.091	-0.001
11	1	11	10	0	10	8068.680	0.000

Table D.13 Coordinates of TFAA-H_2O Minimum

Cartesian coordinates [in Å] of the minimum energy structure of the trifluoroacetic anhydride – water complex from M06-2X/6-311++G(d,p) calculations.

	X	Y	Z
C	-2.439968	-0.327787	0.073954
O	-1.268254	1.694148	-0.529491
O	-0.112513	-0.248606	-0.248295
C	1.092750	0.237585	-0.694184
C	-1.216267	0.540460	-0.289125
O	1.251835	0.978454	-1.594106
C	2.239773	-0.468765	0.056930
O	0.980760	1.857680	1.259582
H	0.769864	2.723793	0.898643
H	1.501789	2.008739	2.051884
F	3.331629	0.277370	0.009698
F	1.943505	-0.725164	1.323432
F	2.491418	-1.630822	-0.554370
F	-2.569142	-1.323275	-0.801237
F	-3.537092	0.408078	0.052311
F	-2.293520	-0.850329	1.288531

Table D.14 Coordinates of PiA-H_2O Minimum

Cartesian coordinates [in Å] of the minimum energy structure of the pivalic anhydride – water complex from M06-2X/6-311++G(d,p) calculations.

	X	Y	Z
O	-1.195873	1.683251	0.071364
O	-0.131332	-0.284746	0.287120
C	0.994799	-0.044258	-0.482279
C	-1.260599	0.491581	0.115306
O	0.922203	0.528845	-1.525663
O	1.545855	2.659706	0.453379
H	0.585020	2.563817	0.414216
H	1.802364	2.701920	-0.471927
C	-2.519033	-0.346086	0.035568
C	-3.730372	0.581407	-0.030598
H	-4.642049	-0.016232	-0.097914
H	-3.790997	1.210845	0.859038
H	-3.675412	1.236080	-0.901621
C	-2.416437	-1.196884	-1.242209
H	-2.310014	-0.566409	-2.128028
H	-1.564492	-1.877995	-1.195361
H	-3.327518	-1.790083	-1.349169
C	-2.599892	-1.259011	1.268534
H	-2.645815	-0.673641	2.189949
H	-3.507919	-1.862932	1.203550
H	-1.740548	-1.928453	1.322680
C	2.218308	-0.703820	0.121861
C	2.312431	-0.392491	1.620672
H	1.461591	-0.805081	2.164582
H	3.226052	-0.842683	2.016730
H	2.348891	0.685987	1.783770
C	2.056184	-2.219623	-0.098028
H	1.987931	-2.458207	-1.162379
H	2.927615	-2.734295	0.313322
H	1.164291	-2.596722	0.406812
C	3.457012	-0.189889	-0.610507
H	4.341187	-0.706715	-0.230850
H	3.382435	-0.362923	-1.684931
H	3.583833	0.880849	-0.438741

Table D.15 Coordinates of PiTFAA-H_2O Conf 1 Minimum

Cartesian coordinates [in Å] of the minimum energy structure of conformer 1 of the pivalic trifluoroacetic anhydride – water complex from M06-2X/6-311++G(d,p) calculations.

	X	Y	Z
C	-1.056084	0.513759	-0.175301
O	-1.067526	1.673403	-0.434693
O	-0.001621	-0.287543	-0.013971
C	1.259680	0.030630	-0.602562
O	1.306325	0.657237	-1.603176
C	2.377351	-0.663520	0.139849
C	-2.346797	-0.296920	0.075958
F	-2.456454	-1.270217	-0.829424
F	-2.319058	-0.855002	1.286231
F	-3.409629	0.484313	-0.008220
C	3.689217	0.020685	-0.246164
H	3.685153	1.059448	0.088572
H	4.520848	-0.501260	0.231717
H	3.839108	0.006047	-1.326423
C	2.161426	-0.614279	1.656427
H	2.057025	0.415976	1.997886
H	1.273244	-1.174771	1.950496
H	3.028221	-1.065622	2.144775
C	2.370163	-2.126099	-0.348482
H	2.536066	-2.181586	-1.426582
H	3.175464	-2.666942	0.153582
H	1.425104	-2.617882	-0.109404
O	1.369864	2.440571	0.844612
H	1.928844	3.220013	0.823764
H	0.651516	2.616841	0.224806

Table D.16 Coordinates of PiTFAA-H_2O Conf 2 Minimum

Cartesian coordinates [in Å] of the minimum energy structure of conformer 2 of the pivalic trifluoroacetic anhydride – water complex from M06-2X/6-311++G(d,p) calculations.

	X	Y	Z
C	-0.879009	0.089495	0.657609
O	-0.958450	0.641327	1.700416
O	0.258799	-0.289387	0.027556
C	1.420165	0.474009	0.145552
O	1.376047	1.640264	0.377629
C	2.647912	-0.372265	-0.108156
C	-2.106869	-0.471005	-0.089308
F	-1.907818	-0.609039	-1.390042
F	-2.387062	-1.681799	0.416464
F	-3.160546	0.310017	0.109715
C	3.879619	0.528819	-0.037000
H	3.965267	1.001384	0.942800
H	4.774611	-0.070545	-0.215956
H	3.832449	1.317898	-0.789305
C	2.710024	-1.462045	0.974786
H	2.757222	-1.023725	1.974511
H	1.844394	-2.123718	0.921636
H	3.611146	-2.060052	0.822225
C	2.527190	-1.016751	-1.498869
H	2.449262	-0.256530	-2.279395
H	3.423358	-1.611504	-1.689127
H	1.655935	-1.669285	-1.560548
O	-1.112169	2.115087	-0.918699
H	-0.406041	2.531841	-0.410724
H	-1.888259	2.667924	-0.799749

Appendix E: Supplementary Material for Chapter 5

Table E.1 Observed Transitions of Parent Pivalic Acid

J'	K_p'	K_o'	J''	K_p''	K_o''	Obs. Frequency (MHz)	Obs. - Calc. (MHz)
1	0	1	0	0	0	4359.732*	0.001
6	2	4	6	1	5	4370.923*	0.000
5	3	2	5	2	3	4468.413*	0.000
3	2	2	3	1	3	4590.204*	0.000
4	3	1	4	2	2	4910.347*	0.000
1	1	1	0	0	0	5306.075*	-0.001
3	3	0	3	2	1	5312.158*	0.000
5	1	4	5	0	5	5378.791*	0.000
4	2	3	4	1	4	5421.368*	0.001
3	3	1	3	2	2	5727.795*	0.000
4	3	2	4	2	3	5949.674*	0.000
5	3	3	5	2	4	6348.985*	0.000
2	0	2	1	1	1	7680.779	-0.003
2	1	2	1	1	1	8341.865	-0.002
2	0	2	1	0	1	8627.125	-0.001
2	1	2	1	0	1	9288.213	0.001
2	2	1	1	1	0	11936.069	0.008
3	0	3	2	1	2	12080.139	-0.008
2	2	0	1	1	1	12405.967	-0.005
3	1	3	2	1	2	12460.680	-0.006
3	0	3	2	0	2	12741.232	0.000
3	2	2	2	2	1	13079.117	0.002
3	1	3	2	0	2	13121.768	-0.003
3	2	1	2	2	0	13417.047	-0.008
3	1	2	2	1	1	13578.787	-0.003
4	1	3	3	2	2	15621.560	0.001
3	2	2	2	1	1	15918.150	0.001
4	0	4	3	1	3	16348.666	0.006
4	1	4	3	1	3	16534.678	0.000
4	0	4	3	0	3	16729.205	0.006
4	1	4	3	0	3	16915.220	0.003
3	2	1	2	1	2	17481.152	-0.008
4	3	2	3	3	1	17587.724	0.004
4	2	3	3	2	2	17365.840	-0.008
3	2	1	2	1	2	17481.166	-0.001

* Denotes transitions measured with the cavity method

Table E.1 Observed Transitions of Parent Pivalic Acid (cont'd)

J'	K_p'	K_o'	J''	K_p''	K_o''	Obs. Frequency (MHz)	Obs. - Calc. (MHz)
4	3	2	3	3	1	17587.718	0.006
4	3	1	3	3	0	17671.785	-0.002
4	1	3	3	1	2	17960.915	-0.003
3	3	1	2	2	0	18714.584†	-0.003
3	3	0	2	2	1	18821.550†	0.004

* Denotes transitions measured with the cavity method

† Denotes transition with frequencies calculated from measured sideband peaks

Table E.2 Observed Transitions of OD Pivalic Acid

J'	K_a'	K_c'	F'	J''	K_a''	K_c''	F''	Obs. Frequency (MHz)	Obs. - Calc. MHz
1	0	1	2	0	0	0	1	4243.821*	-0.001
1	0	1	1	0	0	0	1	4243.897*	-0.001
3	2	2	3	3	1	3	3	4673.787*	0.000
3	2	2	4	3	1	3	4	4673.855*	-0.001
3	2	2	2	3	1	3	2	4673.880*	-0.001
5	3	2	5	5	2	3	5	4733.827*	0.000
5	3	2	6	5	2	3	6	4733.868*	-0.001
5	3	2	4	5	2	3	4	4733.879*	0.002
4	3	1	4	4	2	2	4	5182.469*	0.001
4	3	1	5	4	2	2	5	5182.532*	-0.002
4	3	1	3	4	2	2	3	5182.550*	0.000
1	1	1	1	0	0	0	1	5240.691*	0.001
1	1	1	2	0	0	0	1	5240.722*	-0.001
1	1	1	0	0	0	0	1	5240.769*	-0.002
4	2	3	4	4	1	4	4	5471.121*	0.001
4	2	3	5	4	1	4	5	5471.163*	-0.003
4	2	3	3	4	1	4	3	5471.180*	0.003
3	3	0	3	3	2	1	3	5563.799*	0.000
3	3	0	4	3	2	1	4	5563.907*	0.001
3	3	0	2	3	2	1	2	5563.945*	0.001
3	3	1	3	3	2	2	3	5940.344*	0.001
3	3	1	4	3	2	2	4	5940.448*	0.000
3	3	1	2	3	2	2	2	5940.481*	-0.004
4	3	2	4	4	2	3	4	6140.842*	0.000
4	3	2	5	4	2	3	5	6140.904*	-0.003

* Denotes transitions measured with the cavity method

Table E.2 Observed Transitions of OD Pivalic Acid (cont'd)

J'	K_a'	K_c'	F'	J''	K_a''	K_c''	F''	Obs. Frequency (MHz)	Obs. - Calc. MHz
4	3	2	3	4	2	3	3	6140.925*	0.002
5	3	3	5	5	2	4	5	6504.780*	0.001
5	3	3	6	5	2	4	6	6504.819*	-0.003
5	3	3	4	5	2	4	4	6504.830*	0.000
2	0	2	1	1	1	1	0	7407.973*	0.001
2	0	2	3	1	1	1	2	7408.068*	0.003
2	0	2	2	1	1	1	2	7408.145*	-0.001
2	0	2	2	1	1	1	1	7408.178*	-0.001
2	1	2	1	1	1	1	0	8123.947*	0.002
2	1	2	3	1	1	1	2	8124.018*	-0.001
2	1	2	2	1	1	1	1	8124.099*	0.000
2	0	2	3	1	0	1	2	8404.967*	0.001
2	0	2	2	1	0	1	1	8404.967*	-0.004
2	0	2	1	1	0	1	0	8405.036*	0.000
2	1	1	1	1	1	0	0	8851.178*	0.004
2	1	1	3	1	1	0	2	8851.259*	0.000
2	1	1	2	1	1	0	1	8851.333*	-0.004
2	1	2	2	1	0	1	1	9120.886*	-0.005
2	1	2	3	1	0	1	2	9120.923*	0.002
3	0	3	4	2	1	2	3	11709.540*	-0.004
3	0	3	4	2	1	2	3	11709.540*	-0.004
3	0	3	3	2	1	2	2	11709.588*	0.008
3	1	3	2	2	1	2	1	12139.090*	-0.001
3	1	3	4	2	1	2	3	12139.090*	0.000
3	1	3	3	2	1	2	2	12139.115*	0.003
2	2	0	3	1	1	1	2	12288.248*	0.002
3	2	2	2	2	2	1	1	12731.358*	-0.008
3	2	2	4	2	2	1	3	12731.414*	0.003
3	2	2	3	2	2	1	2	12731.493*	0.000
3	1	3	4	2	0	2	3	12855.039*	-0.005
3	1	3	2	2	0	2	1	12855.069*	0.005
3	2	1	2	2	2	0	1	13037.343*	-0.001
3	2	1	4	2	2	0	3	13037.392*	0.002
3	2	1	3	2	2	0	2	13037.470*	-0.003
3	1	2	2	2	1	1	1	13217.816*	0.001
3	1	2	4	2	1	1	3	13217.816*	0.001

* Denotes transitions measured with the cavity method

Table E.2 Observed Transitions of OD Pivalic Acid (cont'd)

J'	K_a'	K_c'	F'	J''	K_a''	K_c''	F''	Obs. Frequency (MHz)	Obs. - Calc. MHz
3	1	2	3	2	1	1	2	13217.840*	0.002
3	2	2	3	2	1	1	2	15722.049*	-0.001
3	2	2	4	2	1	1	3	15722.087*	0.002

* Denotes transitions measured with the cavity method

Table E.3 Observed Transitions of Parent PivSA

J'	K_p'	K_o'	J''	K_p''	K_o''	Obs. Frequency (MHz)	Obs. - Calc. (MHz)
5	0	5	4	0	4	6044.210*	-0.001
6	1	6	5	1	5	7164.513*	0.000
5	1	5	4	0	4	7186.558*	-0.001
6	0	6	5	0	5	7246.766*	0.000
6	2	5	5	2	4	7264.358*	0.001
6	2	4	5	2	3	7284.574*	-0.001
6	1	5	5	1	4	7360.116*	0.001
7	0	7	6	1	6	7385.964*	-0.001
7	1	7	6	1	6	8356.572*	0.000
7	0	7	6	0	6	8446.061*	0.000
7	2	6	6	2	5	8473.602*	-0.001
7	2	5	6	2	4	8505.678*	0.000
7	1	6	6	1	5	8584.381*	0.000
6	1	5	5	0	5	8992.201*	0.000
8	1	8	7	1	7	9547.784	0.001
8	0	8	7	0	7	9641.776	0.002
8	2	7	7	2	6	9682.169	0.001
8	2	6	7	2	5	9729.670	-0.002
8	1	7	7	1	6	9807.437	0.002
7	1	6	6	0	6	10329.817*	0.001
9	1	9	8	1	8	10738.083	0.003
9	0	9	8	0	8	10833.747	0.004
9	2	8	8	2	7	10889.961	0.003
9	3	7	8	3	6	10908.717	0.001
9	3	6	8	3	5	10911.703	-0.001
9	2	7	8	2	6	10956.621	0.006
9	1	8	8	1	7	11029.039	0.001

* Denotes transitions measured with the cavity method

Table E.3 Observed Transitions of Parent PivSA (cont'd)

J'	K_p'	K_o'	J''	K_p''	K_o''	Obs. Frequency (MHz)	Obs. - Calc. (MHz)
9	1	9	8	0	8	11614.696	0.000
8	1	7	7	0	7	11691.189	-0.001
10	1	10	9	1	9	11927.433	0.010
10	0	10	9	0	9	12022.001	-0.003
10	2	9	9	2	8	12096.875	-0.005
10	3	8	9	3	7	12122.236	0.002
10	3	7	9	3	6	12127.325	-0.011
10	2	8	9	2	7	12186.362	-0.005
10	1	9	9	1	8	12248.924	-0.002
11	1	11	10	1	10	13115.786	-0.001
11	0	11	10	0	10	13206.801	-0.001
11	2	10	10	2	9	13302.839	-0.006
11	3	9	10	3	8	13335.995	0.003
11	3	8	10	3	7	13344.229	-0.007
11	2	9	10	2	8	13418.572	-0.001
11	1	10	10	1	9	13466.802	-0.002
12	1	12	11	1	11	14303.175	0.005
12	0	12	11	0	11	14388.559	-0.004
12	2	11	11	2	10	14507.760	-0.007
12	3	10	11	3	9	14549.920	0.001
12	3	9	11	3	8	14562.646	-0.002
12	1	11	11	1	10	14682.356	-0.001
13	1	13	12	1	12	15489.590	0.001
13	0	13	12	0	12	15567.845	-0.001
13	2	12	12	2	11	15711.561	-0.005
13	6	8	12	6	7	15752.300	-0.007
13	6	7	12	6	6	15752.300	-0.007
13	5	9	12	5	8	15755.130	0.003
13	5	8	12	5	7	15755.130	-0.010
13	4	10	12	4	9	15760.190	-0.003
13	4	9	12	4	8	15760.868	-0.009
13	3	11	12	3	10	15763.915	-0.008
13	3	10	12	3	9	15782.835	0.001
13	2	11	12	2	10	15888.045	0.006
13	1	12	12	1	11	15895.244	-0.001
14	1	14	13	1	13	16675.075	0.000
14	0	14	13	0	13	16745.268	-0.001

Table E.3 Observed Transitions of Parent PivSA (cont'd)

J'	K_p'	K_o'	J''	K_p''	K_o''	Obs. Frequency (MHz)	Obs. - Calc. (MHz)
14	2	13	13	2	12	16914.161	-0.006
14	4	11	13	4	10	16974.764	0.004
14	4	10	13	4	9	16975.915	-0.003
14	3	12	13	3	11	16977.902	0.002
14	3	11	13	3	10	17005.074	0.006
14	1	13	13	1	12	17105.116	-0.003
14	2	12	13	2	11	17123.874	0.005
15	1	15	14	1	14	17859.677	0.001
15	0	15	14	0	14	17921.437	0.010

Table E.4 Observed Transitions of OD PivSA

J'	K_p'	K_o'	J''	K_p''	K_o''	Obs. Frequency (MHz)	Obs. - Calc. (MHz)
5	0	5	4	0	4	6018.689	-0.004
5	2	4	4	2	3	6030.292	-0.005
5	2	3	4	2	2	6043.359	-0.005
5	1	4	4	1	3	6114.696	-0.002
6	1	6	5	1	5	7129.992	0.000
6	0	6	5	0	5	7215.379	0.004
6	2	5	5	2	4	7235.149	0.001
6	2	4	5	2	3	7257.874	-0.004
6	1	5	5	1	4	7335.701	-0.002
7	1	7	6	1	6	8316.060	0.001
7	0	7	6	0	6	8408.429	0.003
7	2	6	6	2	5	8439.342	0.001
7	2	5	6	2	4	8475.360	0.002
7	1	6	6	1	5	8555.585	0.005
8	1	8	7	1	7	9501.183	0.000
8	0	8	7	0	7	9597.517	-0.002
8	2	7	7	2	6	9642.765	-0.003
8	3	6	7	3	5	9657.700	-0.001
8	3	5	7	3	4	9659.673	0.004
8	2	6	7	2	5	9696.017	0.000
8	1	7	7	1	6	9774.078	-0.001
9	1	9	8	1	8	10685.300	0.001
9	0	9	8	0	8	10782.530	0.002
9	2	8	8	2	7	10845.325	0.001

Table E.4 Observed Transitions of OD PivSA (cont'd)

J'	K_p'	K_o'	J''	K_p''	K_o''	Obs. Frequency (MHz)	Obs. - Calc. (MHz)
9	3	7	8	3	6	10866.340	0.012
9	3	6	8	3	5	10869.921	-0.004
9	2	7	8	2	6	10919.869	0.003
9	1	8	8	1	7	10990.924	0.001
10	1	10	9	1	9	11868.368	0.003
10	0	10	9	0	9	11963.562	0.001
10	2	9	9	2	8	12046.906	0.001
10	3	8	9	3	7	12075.257	-0.001
10	2	8	9	2	7	12146.676	0.000
10	1	9	9	1	8	12205.801	-0.003
11	1	11	10	1	10	13050.359	-0.005
11	0	11	10	0	10	13140.962	-0.004
11	2	10	10	2	9	13247.410	-0.002
11	3	9	10	3	8	13284.428	0.003
11	3	8	10	3	7	13294.332	-0.001
11	2	9	10	2	8	13375.972	-0.003
11	1	10	10	1	9	13418.382	-0.003
12	1	12	11	1	11	14231.304	0.004
12	0	12	11	0	11	14315.283	-0.002
12	2	11	11	2	10	14446.755	0.004
12	3	10	11	3	9	14493.738	-0.003
12	3	9	11	3	8	14509.019	-0.004
12	2	10	11	2	9	14607.089	0.002
12	1	11	11	1	10	14628.303	0.005

Table E.5 Observed Transitions of ^{34}S PivSA

J'	K_p'	K_o'	J''	K_p''	K_o''	Obs. Frequency (MHz)	Obs. - Calc. (MHz)
5	1	5	4	1	4	5928.717*	0.000
5	0	5	4	0	4	6000.395*	0.000
5	2	4	4	2	3	6010.406*	0.004
5	2	3	4	2	2	6021.669*	0.000
5	1	4	4	1	3	6089.654*	0.001
6	1	6	5	1	5	7112.993*	-0.001
6	0	6	5	0	5	7194.371*	0.000
6	2	5	5	2	4	7211.441*	0.000
6	2	4	5	2	3	7231.060*	0.002
6	1	5	5	1	4	7305.927*	0.001
7	1	7	6	1	6	8296.525*	0.000
7	0	7	6	0	6	8385.179*	0.000
7	2	6	6	2	5	8411.912*	0.000
7	2	5	6	2	4	8443.042*	-0.001
7	1	6	6	1	5	8521.234*	-0.002
8	1	8	7	1	7	9479.230*	0.000
8	0	8	7	0	7	9572.496*	-0.001
8	2	7	7	2	6	9611.723*	0.000
8	2	6	7	2	5	9657.845*	-0.002
8	1	7	7	1	6	9735.375*	0.001
9	1	9	8	1	8	10661.044*	-0.002
10	1	10	9	1	9	11841.932*	0.002

* Denotes transitions measured with the cavity method

Table E.6 Coordinates of Pivalic Acid Minimum

Cartesian coordinates [in Å] of the minimum energy structure of pivalic acid from M06-2X/6-311++G(3df,3pd) calculations.

	X	Y	Z
C	0.935643	-0.189803	0.000001
C	-0.569689	0.011840	0.000000
C	-1.249267	-1.352770	0.000014
H	-0.966892	-1.928411	0.879553
H	-2.330680	-1.218583	0.000014
H	-0.966894	-1.928428	-0.879513
C	-0.958471	0.803808	-1.254844
H	-2.040183	0.936510	-1.271874
H	-0.487516	1.784496	-1.262139
H	-0.667335	0.269852	-2.159468
C	-0.958472	0.803835	1.254827
H	-0.487520	1.784525	1.262100
H	-2.040185	0.936534	1.271855
H	-0.667333	0.269901	2.159463
O	1.609274	0.978561	0.000001
H	2.550008	0.761619	-0.000003
O	1.503984	-1.244745	0.000001

Table E.7 Coordinates of the Precursor Complex Minimum

Cartesian coordinates [in Å] of the minimum energy structure of the pivalic acid – SO_3 precursor complex from M06-2X/6-311++G(3df,3pd) calculations.

	X	Y	Z
S	-2.096780	-0.089061	0.015931
O	-2.609575	-0.962581	-0.966489
O	-2.003249	1.311358	-0.333951
O	-2.245827	-0.388693	1.390891
C	0.676089	0.295093	-0.083094
O	-0.255429	-0.537944	-0.152773
O	0.480676	1.564700	-0.029884
H	-0.506969	1.745112	-0.103829
C	2.104683	-0.178983	-0.012525
C	2.542173	0.036576	1.448551
H	3.570435	-0.306582	1.553201
H	2.495798	1.089155	1.720893
H	1.917393	-0.535839	2.133454
C	2.967443	0.671108	-0.950815
H	4.000722	0.337140	-0.870357
H	2.651759	0.555093	-1.987180
H	2.920712	1.724831	-0.687129
C	2.191993	-1.657596	-0.379423
H	1.842390	-1.832837	-1.395570
H	3.231722	-1.973591	-0.311967
H	1.597461	-2.269389	0.295077

Table E.8 Coordinates of PivSA Minimum

Cartesian coordinates [in Å] of the minimum energy structure of pivalic sulfuric anhydride from M06-2X/6-311++G(3df,3pd) calculations.

	X	Y	Z
S	-1.867867	-0.167596	0.077316
O	-2.590772	-1.261204	-0.428984
O	-2.105574	1.039325	-0.874716
O	-1.942468	0.244866	1.426623
C	0.650990	0.453592	-0.064193
O	-0.313808	-0.516568	-0.223323
O	0.368111	1.612706	0.012114
H	-1.522729	1.768613	-0.588865
C	2.035628	-0.148824	-0.009872
C	3.053835	0.984665	0.060859
H	2.892858	1.601387	0.942836
H	4.055740	0.560623	0.108278
H	2.988311	1.625588	-0.816695
C	2.263905	-1.006177	-1.261442
H	3.269720	-1.422222	-1.219014
H	1.551692	-1.826104	-1.316895
H	2.181465	-0.407788	-2.168472
C	2.113569	-1.024521	1.249954
H	3.118577	-1.438059	1.324583
H	1.916241	-0.439423	2.147744
H	1.402517	-1.846484	1.203898

Table E.9 Coordinates of the Seq. T.S. 1 Minimum

Cartesian coordinates [in Å] of the minimum energy structure of the first sequential reaction pathway transition state from M06-2X/6-311++G(3df,3pd) calculations.

	X	Y	Z
S	-1.957679	-0.080736	0.012001
O	-2.411914	-0.912842	-1.033891
O	-1.852169	1.334313	-0.278542
O	-2.196253	-0.431561	1.361261
C	0.812779	0.319489	-0.014554
O	-0.121734	-0.517394	-0.064245
O	0.617752	1.585723	0.001618
H	-0.376670	1.757486	-0.078002
C	2.230954	-0.192410	0.005828
C	3.219272	0.957336	0.179713
H	4.228959	0.549945	0.189302
H	3.143844	1.674199	-0.635339
H	3.052224	1.485624	1.116705
C	2.461941	-0.905094	-1.337225
H	3.476007	-1.301775	-1.347940
H	1.761598	-1.727120	-1.467824
H	2.356015	-0.214194	-2.173230
C	2.355070	-1.197483	1.158853
H	1.654750	-2.020402	1.038102
H	3.368451	-1.595815	1.164510
H	2.170093	-0.718648	2.119921

Table E.10 Coordinates of the Seq. T.S. 2 Minimum

Cartesian coordinates [in Å] of the minimum energy structure of the second sequential reaction pathway transition state from M06-2X/6-311++G(3df,3pd) calculations.

	X	Y	Z
O	-0.169567	-0.531228	0.195262
C	0.777065	0.353402	0.088480
O	0.538522	1.573069	0.028470
C	2.177531	-0.192771	0.008597
S	-1.850487	-0.111944	-0.026078
O	-2.023772	-0.326963	-1.413122
O	-2.491158	-0.933156	0.922718
O	-1.782201	1.322554	0.359848
H	-0.634664	1.671136	0.163239
C	3.185333	0.940992	0.173481
H	3.082005	1.421513	1.145132
H	4.190876	0.530611	0.096616
H	3.059052	1.698422	-0.596941
C	2.371073	-1.261896	1.089704
H	3.382527	-1.656832	1.008260
H	2.248534	-0.840000	2.086714
H	1.666140	-2.080510	0.968393
C	2.302573	-0.827731	-1.388727
H	3.306964	-1.235734	-1.492302
H	1.582002	-1.632580	-1.519210
H	2.150171	-0.086425	-2.172450

Table E.11 Coordinates of the Conc. T.S. Minimum

Cartesian coordinates [in Å] of the minimum energy structure of the concerted reaction pathway transition state from M06-2X/6-311++G(3df,3pd) calculations.

	X	Y	Z
S	-1.991347	0.124477	0.023454
C	0.642079	-0.330346	-0.031658
O	-0.304589	0.554427	-0.120898
O	0.406303	-1.551327	0.008074
H	-0.777177	-1.650355	-0.161408
C	2.060779	0.180361	-0.000062
O	-1.902972	-1.304488	-0.386119
O	-2.224691	0.312049	1.404844
O	-2.596234	0.957552	-0.938185
C	2.760386	-0.373242	-1.251470
H	2.294205	0.003530	-2.161478
H	3.799630	-0.048120	-1.240496
H	2.733301	-1.460670	-1.264537
C	2.719979	-0.392316	1.263469
H	3.758478	-0.065874	1.291053
H	2.223578	-0.031057	2.163578
H	2.693556	-1.479569	1.259531
C	2.105209	1.705206	0.011564
H	3.146330	2.022923	0.039037
H	1.639281	2.123896	-0.878165
H	1.597246	2.109991	0.884834

Figure E.1 Photograph of the Apparatus used to Synthesize SO_3

Appendix F: Supplementary Material for Chapter 6

Table F.1 Observed Transitions of Trimethylammonium Triflate

J'	K_a'	K_c'	F'	J''	K_a''	K_c''	F''	Obs. Frequency (MHz)	Obs. - Calc. MHz
4	1	4	4	3	1	3	3	3833.170*	0.001
4	1	4	3	3	1	3	2	3833.208*	-0.002
4	1	4	5	3	1	3	4	3833.229*	0.001
4	0	4	3	3	0	3	2	3909.880*	0.002
4	0	4	4	3	0	3	3	3909.912*	-0.001
4	0	4	5	3	0	3	4	3909.923*	0.001
4	2	3	4	3	2	2	3	3926.090*	0.000
4	2	3	5	3	2	2	4	3926.298*	0.001
4	2	3	3	3	2	2	2	3926.349*	-0.001
4	3	1	4	3	3	0	3	3931.007*	0.001
4	3	2	5	3	3	1	4	3931.197*	0.003
4	3	2	3	3	3	1	2	3931.367*	-0.002
4	3	1	5	3	3	0	4	3931.459*	0.001
4	3	1	3	3	3	0	2	3931.636*	0.003
4	2	2	4	3	2	1	3	3943.806*	0.000
4	2	2	5	3	2	1	4	3944.015*	0.000
4	2	2	3	3	2	1	2	3944.070*	0.001
4	1	3	4	3	1	2	3	4014.857*	-0.001
4	1	3	3	3	1	2	2	4014.895*	-0.001
4	1	3	5	3	1	2	4	4014.918*	0.001
5	1	5	5	4	1	4	5	4787.994*	0.000
5	1	5	5	4	1	4	4	4788.417*	0.000
5	1	5	4	4	1	4	3	4788.432*	-0.001
5	1	5	6	4	1	4	5	4788.449*	0.000
5	1	5	4	4	1	4	4	4788.965*	0.001
5	0	5	5	4	0	4	5	4874.059*	-0.001
5	0	5	4	4	0	4	3	4874.549*	-0.001
5	0	5	5	4	0	4	4	4874.576*	0.005
5	0	5	6	4	0	4	5	4874.576*	0.000
5	0	5	4	4	0	4	4	4875.192*	0.000
5	2	4	5	4	2	3	4	4905.483*	0.001

* Denotes transitions measured with the cavity method

Table F.1 Observed Trans. of Trimethylammonium Triflate (cont'd)

J'	K_a'	K_c'	F'	J''	K_a''	K_c''	F''	Obs. Frequency (MHz)	Obs. - Calc. MHz
5	2	4	6	4	2	3	5	4905.586*	-0.004
5	2	4	4	4	2	3	3	4905.598*	-0.003
5	4	2	5	4	4	1	4	4913.215*	0.005
5	4	1	5	4	4	0	4	4913.215*	-0.002
5	4	2	6	4	4	1	5	4913.624*	0.004
5	4	1	6	4	4	0	5	4913.624*	-0.003
5	4	2	4	4	4	1	3	4913.743*	0.001
5	4	1	4	4	4	0	3	4913.743*	-0.006
5	3	3	5	4	3	2	4	4915.062*	0.001
5	3	3	6	4	3	2	5	4915.297*	0.002
5	3	3	4	4	3	2	3	4915.355*	0.002
5	3	2	5	4	3	1	4	4915.982*	0.000
5	3	2	6	4	3	1	5	4916.215*	-0.001
5	3	2	4	4	3	1	3	4916.274*	0.001
5	2	3	5	4	2	2	4	4940.429*	-0.001
5	2	3	6	4	2	2	5	4940.540*	-0.001
5	2	3	4	4	2	2	3	4940.557*	0.004
5	1	4	5	4	1	3	5	5014.480*	0.002
5	1	4	5	4	1	3	4	5014.931*	-0.001
5	1	4	4	4	1	3	3	5014.950*	0.003
5	1	4	6	4	1	3	5	5014.966*	0.002
5	1	4	4	4	1	3	4	5015.518*	0.000
6	0	6	6	5	1	5	5	5255.774*	0.001
6	0	6	5	5	1	5	4	5255.835*	0.004
6	0	6	7	5	1	5	6	5255.835*	-0.001
5	1	5	4	4	0	4	3	5450.377*	0.001
5	1	5	6	4	0	4	5	5450.418*	0.003
5	1	5	5	4	0	4	4	5450.471*	-0.001
3	2	2	2	2	1	1	1	5479.293*	0.002
3	2	2	4	2	1	1	3	5479.434*	-0.001
3	2	2	3	2	1	1	2	5479.693*	-0.001
3	2	1	2	2	1	2	1	5624.708*	0.001

* Denotes transitions measured with the cavity method

Table F.1 Observed Trans. of trimethylammonium triflate (cont'd)

J'	K_a'	K_c'	F'	J''	K_a''	K_c''	F''	Obs. Frequency (MHz)	Obs. - Calc. MHz
3	2	1	4	2	1	2	3	5624.834*	0.001
3	2	1	3	2	1	2	2	5625.062*	0.003
6	1	6	6	5	1	5	6	5741.378*	0.002
6	1	6	6	5	1	5	5	5741.830*	-0.001
6	1	6	5	5	1	5	4	5741.837*	-0.001
6	1	6	7	5	1	5	6	5741.853*	0.002
6	1	6	5	5	1	5	5	5742.385*	-0.001
6	0	6	6	5	0	5	6	5831.158*	0.001
6	0	6	5	5	0	5	4	5831.655*	-0.002
6	0	6	6	5	0	5	5	5831.675*	0.002
6	0	6	7	5	0	5	6	5831.675*	0.000
6	0	6	5	5	0	5	5	5832.278*	0.000
6	2	5	6	5	2	4	6	5883.028*	0.001
6	2	5	6	5	2	4	5	5883.341*	0.000
6	2	5	5	5	2	4	4	5883.405*	0.001
6	2	5	7	5	2	4	6	5883.405*	0.000
6	2	5	5	5	2	4	5	5883.783*	0.000
6	5	2	6	5	5	1	5	5895.645*	0.000
6	5	1	6	5	5	0	5	5895.645*	0.000
6	5	2	7	5	5	1	6	5896.018*	0.002
6	5	1	7	5	5	0	6	5896.018*	0.002
6	5	2	5	5	5	1	4	5896.107*	0.001
6	5	1	5	5	5	0	4	5896.107*	0.001
6	4	3	6	5	4	2	5	5897.331*	0.001
6	4	2	6	5	4	1	5	5897.361*	-0.001
6	4	3	7	5	4	2	6	5897.570*	0.001
6	4	2	7	5	4	1	6	5897.599*	-0.003
6	4	2	5	5	4	1	4	5897.652*	-0.001
6	3	4	6	5	3	3	5	5899.975*	0.001
6	3	4	7	5	3	3	6	5900.111*	0.000
6	3	4	5	5	3	3	4	5900.135*	0.003
6	3	3	6	5	3	2	5	5902.420*	0.001

* Denotes transitions measured with the cavity method

Table F.1 Observed Trans. of Trimethylammonium Triflate (cont'd)

J'	K_a'	K_c'	F'	J''	K_a''	K_c''	F''	Obs. Frequency (MHz)	Obs. - Calc. MHz
6	3	3	7	5	3	2	6	5902.555*	-0.002
6	3	3	5	5	3	2	4	5902.582*	0.004
6	2	4	6	5	2	3	6	5942.730*	0.001
6	2	4	6	5	2	3	5	5943.053*	0.000
6	2	4	5	5	2	3	4	5943.121*	0.001
6	2	4	7	5	2	3	6	5943.121*	0.001
6	2	4	5	5	2	3	5	5943.511*	0.001
6	1	5	6	5	1	4	6	6011.824*	0.007
6	1	5	6	5	1	4	5	6012.300*	-0.003
6	1	5	5	5	1	4	4	6012.306*	-0.003
6	1	5	7	5	1	4	6	6012.328*	0.005
6	1	5	5	5	1	4	5	6012.891*	-0.003
10	4	7	9	10	3	8	9	6050.604*	-0.003
10	4	7	11	10	3	8	11	6050.619*	0.001
10	4	7	10	10	3	8	10	6050.721*	-0.001
11	4	8	10	11	3	9	10	6050.829*	0.000
11	4	8	12	11	3	9	12	6050.839*	0.003
11	4	8	11	11	3	9	11	6050.923*	0.000
7	4	3	6	7	3	4	6	6051.409*	0.000
7	4	3	8	7	3	4	8	6051.439*	0.001
7	4	3	7	7	3	4	7	6051.641*	0.001
9	4	6	8	9	3	7	8	6053.005*	-0.002
9	4	6	10	9	3	7	10	6053.022*	0.001
9	4	6	9	9	3	7	9	6053.148*	0.000
8	4	5	7	8	3	6	7	6056.613*	-0.001
8	4	5	9	8	3	6	9	6056.635*	0.001
8	4	5	8	8	3	6	8	6056.792*	0.001
6	4	2	5	6	3	3	5	6060.087*	0.000
6	4	2	7	6	3	3	7	6060.132*	0.000
6	4	2	6	6	3	3	6	6060.400*	0.001
7	4	4	6	7	3	5	6	6060.400*	-0.003
7	4	4	8	7	3	5	8	6060.433*	0.001

* Denotes transitions measured with the cavity method

Table F.1 Observed Trans. of Trimethylammonium Triflate (cont'd)

J'	K_a'	K_c'	F'	J''	K_a''	K_c''	F''	Obs. Frequency (MHz)	Obs. - Calc. MHz
7	4	4	7	7	3	5	7	6060.632*	-0.001
6	4	3	5	6	3	4	5	6063.720*	-0.001
6	4	3	7	6	3	4	7	6063.766*	0.000
6	4	3	6	6	3	4	6	6064.032*	0.000
7	0	7	7	6	1	6	6	6295.062*	0.003
7	0	7	6	6	1	6	5	6295.104*	0.006
7	0	7	8	6	1	6	7	6295.104*	0.000
6	1	6	5	5	0	5	4	6317.662*	-0.003
6	1	6	7	5	0	5	6	6317.691*	0.001
6	1	6	6	5	0	5	5	6317.731*	0.000
4	2	3	3	3	1	2	2	6392.787*	0.001
4	2	3	5	3	1	2	4	6392.870*	0.000
4	2	3	4	3	1	2	3	6393.058*	0.000
4	2	2	3	3	1	3	2	6692.334*	-0.004
4	2	2	5	3	1	3	4	6692.410*	0.000
4	2	2	4	3	1	3	3	6692.558*	-0.003
7	1	7	7	6	1	6	6	6693.274*	0.008
7	1	7	6	6	1	6	5	6693.274*	0.005
7	1	7	8	6	1	6	7	6693.274*	-0.004
7	3	5	7	6	3	4	6	6885.470*	0.002
7	3	5	8	6	3	4	7	6885.556*	0.000
7	3	5	6	6	3	4	5	6885.567*	0.003
7	3	4	7	6	3	3	6	6890.936*	0.001
7	3	4	8	6	3	3	7	6891.025*	0.001
7	3	4	6	6	3	3	5	6891.035*	0.003
7	1	6	6	6	1	5	5	7006.199	0.004
7	1	6	8	6	1	5	7	7006.199	-0.007
7	1	6	7	6	1	5	6	7006.199	0.005
7	1	7	6	6	0	6	5	7179.270*	-0.006
7	1	7	8	6	0	6	7	7179.298*	0.005
7	1	7	7	6	0	6	6	7179.328*	0.004
8	0	8	8	7	1	7	7	7325.511*	-0.004
8	0	8	7	7	1	7	6	7325.546*	0.005

* Denotes transitions measured with the cavity method

Table F.1 Observed Trans. of Trimethylammonium Triflate (cont'd)

J'	K_a'	K_c'	F'	J''	K_a''	K_c''	F''	Obs. Frequency (MHz)	Obs. - Calc. MHz
8	0	8	9	7	1	7	8	7325.546*	0.000
8	1	8	7	7	1	7	6	7642.664	0.002
8	1	8	8	7	1	7	7	7642.664	0.002
8	1	8	9	7	1	7	8	7642.664	-0.006
8	0	8	7	7	0	7	6	7723.712	0.001
8	0	8	8	7	0	7	7	7723.712	-0.009
8	0	8	9	7	0	7	8	7723.712	-0.009
8	2	7	8	7	2	6	7	7833.414*	-0.005
8	2	7	8	7	2	6	7	7833.414*	-0.005
8	2	7	7	7	2	6	6	7833.445*	0.003
8	2	7	9	7	2	6	8	7833.445*	-0.001
8	6	2	8	7	6	1	7	7861.805*	0.000
8	6	3	8	7	6	2	7	7861.805*	0.000
8	6	3	8	7	6	2	7	7861.805*	0.000
8	6	2	8	7	6	1	7	7861.805*	0.000
8	6	2	9	7	6	1	8	7862.033*	0.000
8	6	3	9	7	6	2	8	7862.033*	0.000
8	6	3	9	7	6	2	8	7862.033*	0.000
8	6	2	9	7	6	1	8	7862.033*	0.000
8	6	2	7	7	6	1	6	7862.065*	-0.006
8	6	3	7	7	6	2	6	7862.065*	-0.006
8	6	3	7	7	6	2	6	7862.065*	-0.006
8	6	2	7	7	6	1	6	7862.065*	-0.006
8	5	4	8	7	5	3	7	7863.846*	0.005
8	5	3	8	7	5	2	7	7863.846*	0.002
8	5	4	8	7	5	3	7	7863.846*	0.005
8	5	3	8	7	5	2	7	7863.846*	0.002
8	5	4	9	7	5	3	8	7864.004*	0.004
8	5	3	9	7	5	2	8	7864.004*	0.000
8	5	4	7	7	5	3	6	7864.029*	0.005
8	5	3	7	7	5	2	6	7864.029*	0.002
8	5	4	7	7	5	3	6	7864.029*	0.005
8	5	3	7	7	5	2	6	7864.029*	0.002

* Denotes transitions measured with the cavity method

Table F.1 Observed Trans. of Trimethylammonium Triflate (cont'd)

J'	K_a'	K_c'	F'	J''	K_a''	K_c''	F''	Obs. Frequency (MHz)	Obs. - Calc. MHz
8	4	5	8	7	4	4	7	7867.561*	0.003
8	4	5	8	7	4	4	7	7867.561*	0.003
8	4	5	9	7	4	4	8	7867.662*	0.000
8	4	5	9	7	4	4	8	7867.662*	0.000
8	4	5	7	7	4	4	6	7867.679*	0.005
8	4	5	7	7	4	4	6	7867.679*	0.005
8	4	4	8	7	4	3	7	7867.855*	0.003
8	4	4	8	7	4	3	7	7867.855*	0.003
8	4	4	9	7	4	3	8	7867.956*	0.000
8	4	4	9	7	4	3	8	7867.956*	0.000
8	4	4	7	7	4	3	6	7867.972*	0.004
8	4	4	7	7	4	3	6	7867.972*	0.004
8	3	6	8	7	3	5	7	7871.401*	0.001
8	3	6	8	7	3	5	7	7871.401*	0.001
8	3	6	9	7	3	5	8	7871.461*	0.001
8	3	6	7	7	3	5	6	7871.461*	-0.002
8	3	6	9	7	3	5	8	7871.461*	0.001
8	3	6	7	7	3	5	6	7871.461*	-0.002
8	3	5	8	7	3	4	7	7882.228*	0.002
8	3	5	8	7	3	4	7	7882.228*	0.002
8	3	5	9	7	3	4	8	7882.289*	0.002
8	3	5	7	7	3	4	6	7882.289*	0.000
8	3	5	9	7	3	4	8	7882.289*	0.002
8	3	5	7	7	3	4	6	7882.289*	0.000
8	2	6	8	7	2	5	7	7964.572*	-0.002
8	2	6	8	7	2	5	7	7964.572*	-0.002
8	2	6	7	7	2	5	6	7964.605*	0.004
8	2	6	9	7	2	5	8	7964.605*	0.000
8	2	6	9	7	2	5	8	7964.605*	0.000
8	2	6	7	7	2	5	6	7964.605*	0.004
8	1	7	7	7	1	6	6	7995.705	0.003
8	1	7	9	7	1	6	8	7995.705	-0.006
8	1	7	8	7	1	6	7	7995.705	0.002

* Denotes transitions measured with the cavity method

Table F.1 Observed Trans. of Trimethylammonium Triflate (cont'd)

J'	K_a'	K_c'	F'	J''	K_a''	K_c''	F''	Obs. Frequency (MHz)	Obs. - Calc. MHz
9	1	9	8	8	1	8	7	8590.053	0.006
9	1	9	9	8	1	8	8	8590.053	0.006
9	1	9	10	8	1	8	9	8590.053	-0.001
9	0	9	8	8	0	8	7	8661.035	0.010
9	0	9	9	8	0	8	8	8661.035	0.002
9	0	9	10	8	0	8	9	8661.035	0.002
9	2	8	9	8	2	7	8	8805.117*	-0.006
9	2	8	9	8	2	7	8	8805.117*	-0.006
9	2	8	10	8	2	7	9	8805.149*	0.006
9	2	8	10	8	2	7	9	8805.149*	0.006
9	7	2	9	8	7	1	8	8844.163*	-0.001
9	7	3	9	8	7	2	8	8844.163*	-0.001
9	7	3	9	8	7	2	8	8844.163*	-0.001
9	7	2	9	8	7	1	8	8844.163*	-0.001
9	7	2	10	8	7	1	9	8844.382*	0.000
9	7	3	10	8	7	2	9	8844.382*	0.000
9	7	3	10	8	7	2	9	8844.382*	0.000
9	7	2	10	8	7	1	9	8844.382*	0.000
9	7	2	8	8	7	1	7	8844.417*	0.002
9	7	3	8	8	7	2	7	8844.417*	0.002
9	7	3	8	8	7	2	7	8844.417*	0.002
9	7	2	8	8	7	1	7	8844.417*	0.002
9	6	3	9	8	6	2	8	8845.870*	0.001
9	6	4	9	8	6	3	8	8845.870*	0.001
9	6	3	10	8	6	2	9	8846.029*	-0.002
9	6	4	10	8	6	3	9	8846.029*	-0.002
9	6	4	10	8	6	3	9	8846.029*	-0.002
9	6	3	10	8	6	2	9	8846.029*	-0.002
9	6	3	8	8	6	2	7	8846.055*	0.003
9	6	4	8	8	6	3	7	8846.055*	0.003
9	6	4	8	8	6	3	7	8846.055*	0.003
9	6	3	8	8	6	2	7	8846.055*	0.003
9	5	4	9	8	5	3	8	8848.743*	-0.004

* Denotes transitions measured with the cavity method

Table F.1 Observed Trans. of Trimethylammonium Triflate (cont'd)

J'	K_a'	K_c'	F'	J''	K_a''	K_c''	F''	Obs. Frequency (MHz)	Obs. - Calc. MHz
9	5	4	10	8	5	3	9	8848.854*	-0.006
9	4	6	9	8	4	5	8	8853.881*	0.000
9	4	6	9	8	4	5	8	8853.881*	0.000
9	4	6	10	8	4	5	9	8853.957*	0.002
9	4	6	8	8	4	5	7	8853.957*	-0.003
9	4	5	9	8	4	4	8	8854.584*	0.000
9	4	5	9	8	4	4	8	8854.584*	0.000
9	4	5	10	8	4	4	9	8854.660*	0.003
9	4	5	8	8	4	4	7	8854.660*	-0.003
9	3	7	8	8	3	6	7	8857.569	0.002
9	3	7	10	8	3	6	9	8857.569	0.002
9	3	6	9	8	3	5	8	8877.079*	-0.001
9	3	6	9	8	3	5	8	8877.079*	-0.001
9	3	6	10	8	3	5	9	8877.125*	0.002
9	3	6	8	8	3	5	7	8877.125*	0.001
9	3	6	10	8	3	5	9	8877.125*	0.002
9	3	6	8	8	3	5	7	8877.125*	0.001
9	1	8	8	8	1	7	7	8979.821	0.001
9	1	8	10	8	1	7	9	8979.821	-0.006
9	1	8	9	8	1	7	8	8979.821	-0.001
9	2	7	9	8	2	6	8	8980.414*	-0.004
9	2	7	8	8	2	6	7	8980.441*	0.005
9	2	7	10	8	2	6	9	8980.441*	0.001
10	1	10	9	9	1	9	8	9535.530	0.002
10	1	10	10	9	1	9	9	9535.530	0.001
10	1	10	11	9	1	9	10	9535.530	-0.003
10	0	10	9	9	0	9	8	9594.906	0.000
10	0	10	10	9	0	9	9	9594.906	-0.006
10	0	10	11	9	0	9	10	9594.906	-0.005
10	1	9	9	9	1	8	8	9957.480	-0.001
10	1	9	11	9	1	8	10	9957.480	-0.007
10	1	9	10	9	1	8	9	9957.480	-0.004
11	1	11	10	10	1	10	9	10479.269	-0.001
11	1	11	11	10	1	10	10	10479.269	-0.002

* Denotes transitions measured with the cavity method

Table F.1 Observed Trans. of Trimethylammonium Triflate (cont'd)

J'	K_a'	K_c'	F'	J''	K_a''	K_c''	F''	Obs. Frequency (MHz)	Obs. - Calc. MHz
11	1	11	12	10	1	10	11	10479.269	-0.005
11	0	11	10	10	0	10	9	10527.048	-0.002
11	0	11	11	10	0	10	10	10527.048	-0.007
11	0	11	12	10	0	10	11	10527.048	-0.007
11	2	10	11	10	2	9	10	10740.764	0.003
11	2	10	10	10	2	9	9	10740.764	-0.004
11	2	10	12	10	2	9	11	10740.764	-0.007
11	7	4	12	10	7	3	11	10812.392	-0.001
11	3	8	10	10	3	7	9	10880.790	0.004
11	3	8	12	10	3	7	11	10880.790	0.003
12	1	12	11	11	1	11	10	11421.474	-0.002
12	1	12	12	11	1	11	11	11421.474	-0.003
12	1	12	13	11	1	11	12	11421.474	-0.006
12	0	12	11	11	0	11	10	11458.714	0.004
12	0	12	12	11	0	11	11	11458.714	0.000
12	0	12	13	11	0	11	12	11458.714	0.000
12	2	11	12	11	2	10	11	11704.377	0.007
12	2	11	11	11	2	10	10	11704.377	0.002
12	2	11	13	11	2	10	12	11704.377	-0.001
12	10	3	12	11	10	2	11	11791.383*	0.000
12	10	2	12	11	10	1	11	11791.383*	0.000
12	10	3	13	11	10	2	12	11791.572*	0.000
12	10	2	13	11	10	1	12	11791.572*	0.000
12	10	3	11	11	10	2	10	11791.596*	0.002
12	10	2	11	11	10	1	10	11791.596*	0.002
12	9	4	12	11	9	3	11	11792.607*	0.000
12	9	3	12	11	9	2	11	11792.607*	0.000
12	9	4	13	11	9	3	12	11792.761*	0.000
12	9	3	13	11	9	2	12	11792.761*	0.000
12	9	4	11	11	9	3	10	11792.779*	0.002
12	9	3	11	11	9	2	10	11792.779*	0.002
12	8	5	12	11	8	4	11	11794.337*	0.001
12	8	4	12	11	8	3	11	11794.337*	0.001
12	8	5	13	11	8	4	12	11794.457*	-0.001

* Denotes transitions measured with the cavity method

Table F.1 Observed Trans. of Trimethylammonium Triflate (cont'd)

J'	K_a'	K_c'	F'	J''	K_a''	K_c''	F''	Obs. Frequency (MHz)	Obs. - Calc. MHz
12	8	4	13	11	8	3	12	11794.457*	-0.001
12	8	5	11	11	8	4	10	11794.473*	0.003
12	8	4	11	11	8	3	10	11794.473*	0.003
12	7	6	12	11	7	5	11	11796.886*	0.000
12	7	5	12	11	7	4	11	11796.886*	0.000
12	7	6	13	11	7	5	12	11796.980*	0.001
12	7	5	13	11	7	4	12	11796.980*	0.000
12	7	6	11	11	7	5	10	11796.990*	0.002
12	7	5	11	11	7	4	10	11796.990*	0.002
12	6	7	12	11	6	6	11	11800.879*	0.003
12	6	6	12	11	6	5	11	11800.879*	-0.001
12	5	8	12	11	5	7	11	11807.585*	0.001
12	5	8	13	11	5	7	12	11807.636*	0.003
12	5	8	11	11	5	7	10	11807.636*	0.001
12	5	7	12	11	5	6	11	11807.771*	0.001
12	5	7	13	11	5	6	12	11807.822*	0.003
12	5	7	11	11	5	6	10	11807.822*	0.000
12	3	10	12	11	3	9	11	11813.508*	0.000
12	3	10	11	11	3	9	10	11813.527*	0.002
12	3	10	13	11	3	9	12	11813.527*	0.000
12	4	9	12	11	4	8	11	11818.128*	0.001
12	4	9	13	11	4	8	12	11818.161*	0.001
12	4	9	11	11	4	8	10	11818.161*	0.001
12	4	8	12	11	4	7	11	11823.691*	0.000
12	4	8	13	11	4	7	12	11823.725*	0.001
12	4	8	11	11	4	7	10	11823.725*	0.001
12	1	11	11	11	1	10	10	11889.615	-0.002
12	1	11	13	11	1	10	12	11889.615	-0.006
12	1	11	12	11	1	10	11	11889.615	-0.006
12	2	10	11	11	2	9	10	12022.623	-0.002
12	2	10	13	11	2	9	12	12022.623	-0.005
13	1	13	12	12	1	12	11	12362.373	0.004
13	1	13	13	12	1	12	12	12362.373	0.003

* Denotes transitions measured with the cavity method

Table F.1 Observed Trans. of Trimethylammonium Triflate (cont'd)

J'	K_a'	K_c'	F'	J''	K_a''	K_c''	F''	Obs. Frequency (MHz)	Obs. - Calc. MHz
13	1	13	14	12	1	12	13	12362.373	0.001
13	0	13	12	12	0	12	11	12390.644	0.004
13	0	13	13	12	0	12	12	12390.644	0.001
13	0	13	14	12	0	12	13	12390.644	0.001
13	2	12	13	12	2	11	12	12665.045	-0.003
13	2	12	12	12	2	11	11	12665.045	-0.007
13	2	12	14	12	2	11	13	12665.045	-0.009
13	1	12	12	12	1	11	11	12842.987	0.001
13	1	12	14	12	1	11	13	12842.987	-0.002
13	1	12	13	12	1	11	12	12842.987	-0.003
14	1	14	13	13	1	13	12	13302.170	0.001
14	1	14	14	13	1	13	13	13302.170	-0.001
14	1	14	15	13	1	13	14	13302.170	-0.002
14	2	13	14	13	2	12	13	13622.772	-0.007
14	2	13	13	13	2	12	12	13622.772	-0.010
14	2	13	14	13	2	12	13	13622.772	-0.007
14	2	13	13	13	2	12	12	13622.772	-0.010
14	1	13	13	13	1	12	12	13788.124	0.004
14	1	13	15	13	1	12	14	13788.124	0.001
14	1	13	14	13	1	12	13	13788.124	-0.001
15	1	15	14	14	1	14	13	14241.091	0.005
15	1	15	15	14	1	14	14	14241.091	0.004
15	1	15	16	14	1	14	15	14241.091	0.003
15	0	15	14	14	0	14	13	14256.447	-0.006
15	0	15	15	14	0	14	14	14256.447	-0.008
15	0	15	16	14	0	14	15	14256.447	-0.009
15	2	14	15	14	2	13	14	14577.610	-0.005
15	2	14	14	14	2	13	13	14577.610	-0.007
15	2	14	16	14	2	13	15	14577.610	-0.009
15	1	14	14	14	1	13	13	14726.097	0.000
15	1	14	16	14	1	13	15	14726.097	-0.003
15	1	14	15	14	1	13	14	14726.097	-0.004
16	1	16	15	15	1	15	14	15179.300	-0.003
16	1	16	16	15	1	15	15	15179.300	-0.004
16	1	16	17	15	1	15	16	15179.300	-0.005
16	0	16	15	15	0	15	14	15190.384	0.001
16	0	16	16	15	0	15	15	15190.384	-0.001

Table F.1 Observed Trans. of Trimethylammonium Triflate (cont'd)

J'	K_a'	K_c'	F'	J''	K_a''	K_c''	F''	Obs. Frequency (MHz)	Obs. - Calc. MHz
16	0	16	17	15	0	15	16	15190.384	-0.002
16	2	15	16	15	2	14	15	15529.673	-0.001
16	2	15	15	15	2	14	14	15529.673	-0.002
16	2	15	17	15	2	14	16	15529.673	-0.004
16	1	15	15	15	1	14	14	15658.582	-0.006
16	1	15	17	15	1	14	16	15658.582	-0.008
16	1	15	16	15	1	14	15	15658.582	-0.010
16	3	14	17	15	3	13	16	15733.750	-0.002
17	0	17	16	16	0	16	15	16124.873	-0.003
17	0	17	17	16	0	16	16	16124.873	-0.005
17	0	17	18	16	0	16	17	16124.873	-0.005
17	2	16	17	16	2	15	16	16479.136	0.004
17	2	16	16	16	2	15	15	16479.136	0.003
17	2	16	18	16	2	15	17	16479.136	0.002
17	1	16	16	16	1	15	15	16587.524	-0.008
17	1	16	18	16	1	15	17	16587.524	-0.010
18	2	17	19	17	2	16	18	17426.220	0.003
19	1	19	18	18	1	18	17	17991.187	0.001
19	1	19	19	18	1	18	18	17991.187	0.000
19	0	19	18	18	0	18	17	17995.094	0.001
19	0	19	19	18	0	18	18	17995.094	0.000

Table F.2 Coordinates of Trimethylammonium Triflate Minimum

Cartesian coordinates [in Å] of the minimum energy structure of trimethylammonium triflate from MP2/6-311++G(df,dp) calculations.

	X	Y	Z
S	0.616436	0.883956	0.035476
O	-0.034594	0.861669	-1.272647
O	1.482314	1.989110	0.354978
O	-0.348749	0.510746	1.114988
H	-1.595624	0.097409	0.479491
C	1.711841	-0.603863	0.003683
F	2.326929	-0.768269	1.162577
F	0.982682	-1.698237	-0.237666
F	2.620790	-0.496653	-0.950509
N	-2.553884	-0.215163	0.057550
C	-2.292665	-1.322537	-0.885752
H	-1.635109	-0.950585	-1.668366
H	-1.796848	-2.127749	-0.346171
H	-3.240616	-1.671241	-1.299649
C	-3.381627	-0.651047	1.197433
H	-2.877776	-1.476776	1.697376
H	-3.488196	0.181789	1.890709
H	-4.361216	-0.969986	0.837727
C	-3.135184	0.954135	-0.633500
H	-3.261576	1.757548	0.090963
H	-2.437966	1.267077	-1.408157
H	-4.100727	0.676436	-1.060026

Appendix G: Microwave Spectrum of Triflimidic Acid

Preface

The work described in Appendix G outlines the microwave and computational analysis of triflimidic acid. The introduction provides context for why this molecule is of fundamental interest, and the remainder of Appendix G catalogs the experimental and computational methods as well as the results.

Purpose

The analysis of gas phase complexes involving one or more strong acid molecules has long been the focus of many microwave studies. Microsolvation in amine and water complexation studies have shown that simple proton transfer is somewhat rare in the gas phase even for strong acids which readily transfer protons in solution. The recent study analyzing the mono-, di-, and trihydrates of triflic acid showed that three water molecules were necessary to facilitate proton transfer with the superacid.[1] Foundational studies by Legon and coworkers showed that proton transfer is uncommon for many acid-amine complexes with the exceptions of trimethylamine (TMA) with HI and HBr.[2] The recent study of trimethylammonium triflate described in Chapter 6 of this work added the superacid triflic acid to the list of acid-TMA complexes exhibiting proton transfer.[3]

Several of the previously mentioned studies in acid-amine studies have utilized the nuclear quadrupole coupling of the ^{14}N nucleus of the amine to experimentally measure the degree of proton transfer within the complex.[2,3] The quadrupole coupling is acutely sensitive to the electric field gradient about the ^{14}N nucleus and is therefore sensitive to the proximity of the positively charge proton to the nitrogen. In the microwave study of nitric acid – TMA, the ^{14}N nuclei of the acid and TMA were used to gauge the degree of proton transfer.[4] When referring to the extent of proton transfer, it is important to note that the degree of proton transfer is only defined by the metric that is used to define it.

Bis(trifluoromethanesulfonyl)amine, otherwise known as trifluoromethanesulfonimide (triflimidic acid) shown in Figure G.1, brings an interesting vantage point to gas phase proton transfer studies because the acidic proton in triflimidic acid is directly bonded to

the nitrogen atom. Therefore, the quadrupole moment of the acid's ^{14}N nucleus can be used to gauge the degree of proton transfer directly from the perspective of the transferring atom. Additionally, triflimidic acid is a stronger superacid than triflic acid[5] which has already been observed to exhibit proton transfer in the gas phase.[3] In this appendix, the microwave spectrum of triflimidic acid and its nuclear quadrupole coupling constants are presented as a necessary precursor to future complexation studies.

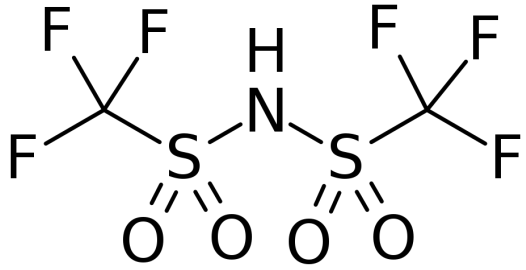

Figure G.1 Structure of Triflimidic Acid
A skeleton structural representation of triflimidic acid. Note that the geometry is shown later in Figure G.2.

Experimental and Computational Methods

The microwave spectrum of triflimidic acid was measured using our pulsed-nozzle Fourier transform tandem cavity[6] and chirped-pulse[7] microwave spectrometer.[8,9] The 95% pure sample of triflimidic acid obtained from Oakwood Chemical had a melting point of 46-47 °C and a boiling point of 90-91 °C. Data were initially measured with the broadband chirped-pulse method and the higher-resolution cavity method was subsequently used to resolve closely spaced hyperfine components and observe weaker transitions. Only *c*-type transitions were observed. Frequencies measured with the chirped-pulse method had accuracies of 12 kHz, while those measured with the cavity system had accuracies of 3 kHz. Triflimidic acid was introduced to the system by flowing 0.6 atm argon over a 3 g sample of solid superacid stored in a stainless steel reservoir. The resulting Ar-triflimidic acid mixture was then flowed through a 0.016 inch ID stainless steel hypodermic needle orthogonally oriented to the direction of microwave propagation of both the chirped-pulse and cavity spectrometers. Argon was additionally pulsed into the system with a stagnation pressure of 1.3 atm through a cone nozzle to facilitate the supersonic expansion. Although triflimidic acid is a solid at room temperature, no heating was necessary.

M06-2X/6-311++G(3df,3pd) geometry optimization and frequency calculations were performed for triflimidic acid using the Gaussian 16 suite.[10] A comparison of the computational results and the experimentally determined constants is shown in Table G.1.The calculated molecular structure of triflimidic acid is shown in Figure G.2 and the corresponding cartesian coordinates are included in Table G.2. Note that there is a C_2 axis of symmetry and dipole moments along the *a* and *b* principal axes are zero resulting in a *c*-type only spectrum. All observed transition frequencies, assignments, and residuals from the least squares fit are included in Table G.3.

Table G.1 Spectroscopic Constants of Triflimidic Acid

	Experimental	*M06-2X/6-311++G(3df,3pd)*	
A (MHz)	1017.89409(12)	1022	-0.4%
B (MHz)	333.566645(76)	337	-1.0%
C (MHz)	308.809009(94)	312	-1.0%
Δ_J (kHz)	0.00827(18)		
Δ_{JK} (kHz)	-0.00728(79)		
Δ_K (kHz)	0.0371(17)		
δ_J (kHz)	0.000788(72)		
$1.5\chi_{aa}$ (MHz)	1.0924(36)	1.00	8.5%
$0.25(\chi_{bb}-\chi_{cc})$ (MHz)	-1.0188(16)	-1.10	-8.0%
N^a	205 (175)		
RMS (kHz)	2.1		

(a) Number in parenthesis represents the number of distinct frequencies.

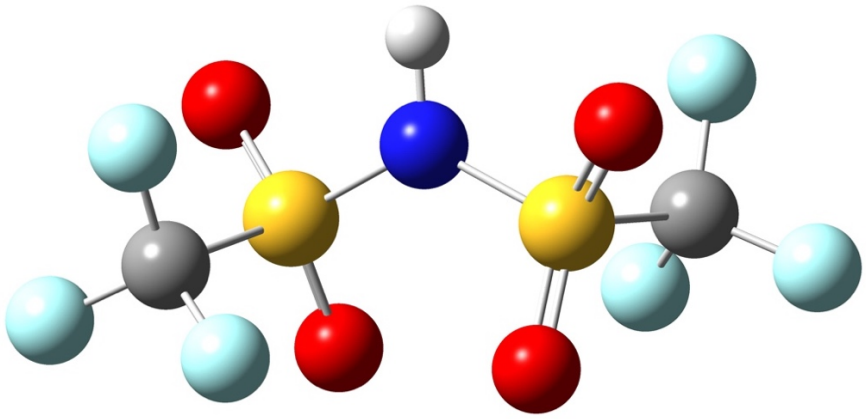

Figure G.2 Computational Structure of Triflimidic Acid
Optimized structure of triflimidic acid obtained with M06-2X/6-311++G(3df,3pd) calculations. Note the C_2 axis of symmetry through the N-H bond.

Table G.2 Coordinates of Triflimidic Acid Minimum

Cartesian coordinates [in Å] of the minimum energy structure of the triflimidic acid from M06-2X/6-311++G(3df,3pd) calculations.

	X	Y	Z
S	1.198387	-0.893321	0.094014
O	1.647911	-1.799021	1.085810
O	0.789712	-1.261380	-1.205815
C	2.526132	0.376163	-0.082678
F	2.123315	1.348926	-0.867264
F	2.818472	0.861361	1.110322
F	3.585575	-0.210824	-0.596527
N	0.000000	0.000000	0.814031
H	-0.000001	-0.000001	1.829040
S	-1.198387	0.893321	0.094014
O	-1.647911	1.799021	1.085810
O	-0.789712	1.261380	-1.205815
C	-2.526132	-0.376163	-0.082678
F	-2.818472	-0.861361	1.110322
F	-2.123315	-1.348926	-0.867264
F	-3.585575	0.210824	-0.596527

Table G.3 Observed Transitions of Triflimidic Acid

J'	K_a'	K_c'	F'	J''	K_a''	K_c''	F''	Obs. Frequency (MHz)	Obs. - Calc. MHz
7	3	4	7	6	2	4	6	7953.730	-0.002
7	3	4	8	6	2	4	7	7953.940	0.001
7	3	4	6	6	2	4	5	7953.973	-0.006
7	3	5	6	6	2	5	5	7997.074	0.001
7	3	5	8	6	2	5	7	7997.074	-0.001
7	3	5	7	6	2	5	6	7997.099	-0.003
5	4	1	5	4	3	1	4	8088.973	-0.001
5	4	1	6	4	3	1	5	8089.041	-0.002
5	4	1	4	4	3	1	3	8089.055	0.001
5	4	2	6	4	3	2	5	8089.118	-0.001

Table G.3 Observed Transitions of Triflimidic Acid (cont'd)

J'	K_a'	K_c'	F'	J''	K_a''	K_c''	F''	Obs. Frequency (MHz)	Obs. - Calc. MHz
5	4	2	4	4	3	2	3	8089.132	0.003
8	3	5	8	7	2	5	7	8575.050	0.002
8	3	5	9	7	2	5	8	8575.294	0.000
8	3	5	7	7	2	5	6	8575.334	0.000
6	4	2	6	5	3	2	5	8731.211	0.003
6	4	2	7	5	3	2	6	8731.279	0.001
6	4	2	5	5	3	2	4	8731.296	0.004
6	4	3	6	5	3	3	5	8731.514	0.003
6	4	3	7	5	3	3	6	8731.579	0.001
6	4	3	5	5	3	3	4	8731.596	0.005
9	3	6	9	8	2	6	8	9187.206	0.001
9	3	6	10	8	2	6	9	9187.492	0.000
9	3	6	8	8	2	6	7	9187.533	0.000
9	3	7	8	8	2	7	7	9310.135	-0.002
9	3	7	10	8	2	7	9	9310.147	0.002
9	3	7	9	8	2	7	8	9310.237	0.001
7	4	3	7	6	3	3	6	9372.934	-0.002
7	4	3	8	6	3	3	7	9373.002	-0.003
7	4	3	6	6	3	3	5	9373.021	0.003
7	4	4	7	6	3	4	6	9373.835	-0.002
7	4	4	8	6	3	4	7	9373.896	-0.002
7	4	4	6	6	3	4	5	9373.912	0.002
5	5	0	5	4	4	0	5	9481.964	-0.001
5	5	0	5	4	4	0	4	9482.305	-0.001
5	5	0	4	4	4	0	3	9482.326	0.000
5	5	0	6	4	4	0	5	9482.340	0.002
5	5	0	4	4	4	0	4	9482.754	-0.002
10	3	7	10	9	2	7	9	9789.244	0.000
10	3	7	11	9	2	7	10	9789.566	0.000
10	3	7	9	9	2	7	8	9789.606	0.000
11	2	10	10	10	1	10	9	9836.125	-0.002
11	2	10	12	10	1	10	11	9836.200	-0.001
10	3	8	9	9	2	8	8	9975.093	-0.001
10	3	8	11	9	2	8	10	9975.106	0.001
10	3	8	10	9	2	8	9	9975.227	-0.001
8	4	4	8	7	4	5	7	10013.782	0.000
8	4	4	9	7	4	5	8	10013.849	-0.002

Table G.3 Observed Transitions of Triflimidic Acid (cont'd)

J'	K_a'	K_c'	F'	J''	K_a''	K_c''	F''	Obs. Frequency (MHz)	Obs. - Calc. MHz
8	4	4	7	7	4	5	6	10013.864	0.001
8	4	5	8	7	3	5	7	10016.012	0.001
8	4	5	9	7	3	5	8	10016.065	-0.002
8	4	5	7	7	3	5	6	10016.081	0.002
13	2	11	12	12	1	11	11	10255.712	-0.001
13	2	11	14	12	1	11	13	10255.724	0.001
13	2	11	13	12	1	11	12	10255.910	0.000
11	3	8	11	10	2	8	10	10381.081	0.001
11	3	8	12	10	2	8	11	10381.429	-0.002
11	3	8	10	10	2	8	9	10381.469	0.000
11	8	4	11	11	7	4	11	10446.865	0.000
11	8	3	11	11	7	5	11	10446.865	0.000
11	8	4	12	11	7	4	12	10446.959	-0.002
11	8	3	12	11	7	5	12	10446.959	-0.002
11	8	4	10	11	7	4	10	10446.970	0.000
11	8	3	10	11	7	5	10	10446.970	0.000
10	8	3	10	10	7	3	10	10447.575	-0.002
10	8	2	10	10	7	4	10	10447.575	-0.002
10	8	3	11	10	7	3	11	10447.688	-0.002
10	8	2	11	10	7	4	11	10447.688	-0.002
10	8	3	9	10	7	3	9	10447.701	0.000
10	8	2	9	10	7	4	9	10447.701	0.000
9	8	2	9	9	7	2	9	10448.104	0.000
9	8	1	9	9	7	3	9	10448.104	0.000
9	8	2	10	9	7	2	10	10448.239	-0.001
9	8	1	10	9	7	3	10	10448.239	-0.001
9	8	2	8	9	7	2	8	10448.256	0.001
9	8	1	8	9	7	3	8	10448.256	0.001
13	1	12	12	12	0	12	11	10473.666	-0.004
13	1	12	14	12	0	12	13	10473.762	0.003
12	2	11	11	11	1	11	10	10614.260	-0.002
12	2	11	13	11	1	11	12	10614.330	0.001
12	2	11	12	11	1	11	11	10615.063	0.001
11	3	9	10	10	2	9	9	10647.029	-0.001
11	3	9	12	10	2	9	11	10647.044	0.001
11	3	9	11	10	2	9	10	10647.198	0.000
9	4	5	9	8	3	5	8	10653.224	-0.002

Table G.3 Observed Transitions of Triflimidic Acid (cont'd)

J'	K_a'	K_c'	F'	J''	K_a''	K_c''	F''	Obs. Frequency (MHz)	Obs. - Calc. MHz
9	4	5	10	8	3	5	9	10653.298	-0.001
9	4	5	8	8	3	5	7	10653.308	-0.003
9	4	6	9	8	3	6	8	10658.084	-0.002
9	4	6	10	8	3	6	9	10658.135	0.000
7	5	2	7	6	4	2	6	10767.309	-0.002
7	5	3	7	6	4	3	6	10767.317	0.000
7	5	2	8	6	4	2	7	10767.364	-0.002
7	5	3	8	6	4	3	7	10767.372	0.000
7	5	2	6	6	4	2	5	10767.372	-0.001
7	5	3	6	6	4	3	5	10767.381	0.001
14	2	12	13	13	1	12	12	10961.402	-0.001
14	2	12	15	13	1	12	14	10961.421	0.002
14	2	12	14	13	1	12	13	10961.694	-0.001
12	3	9	12	11	2	9	11	10963.721	0.000
12	3	9	13	11	2	9	12	10964.085	-0.002
12	3	9	11	11	2	9	10	10964.124	0.001
10	4	6	10	9	3	6	9	11290.581	0.001
10	4	6	11	9	3	6	10	11290.658	-0.002
10	4	6	9	9	3	6	8	11290.673	0.003
10	4	7	10	9	3	7	9	11300.182	0.001
10	4	7	11	9	3	7	10	11300.222	-0.001
10	4	7	9	9	3	7	8	11300.234	0.004
12	3	10	11	11	2	10	10	11326.931	-0.001
12	3	10	13	11	2	10	12	11326.947	0.001
12	3	10	12	11	2	10	11	11327.133	0.000
14	1	13	13	13	0	13	12	11364.382	0.001
14	1	13	15	13	0	13	14	11364.465	0.001
6	6	0	6	5	5	0	5	11518.089	-0.001
6	6	1	6	5	5	1	5	11518.089	-0.001
6	6	0	5	5	5	0	4	11518.104	0.000
6	6	1	5	5	5	1	4	11518.104	0.000
6	6	0	7	5	5	0	6	11518.115	0.002
6	6	1	7	5	5	1	6	11518.115	0.002
13	3	10	13	12	2	10	12	11539.305	0.000
13	3	10	14	12	2	10	13	11539.670	-0.001
13	3	10	12	12	2	10	11	11539.706	0.001
15	2	13	14	14	1	13	13	11691.083	-0.001

Table G.3 Observed Transitions of Triflimidic Acid (cont'd)

J'	K_a'	K_c'	F'	J''	K_a''	K_c''	F''	Obs. Frequency (MHz)	Obs. - Calc. MHz
15	2	13	16	14	1	13	15	11691.107	0.001
15	2	13	15	14	1	13	14	11691.466	0.001
11	4	7	11	10	3	7	10	11924.947	-0.001
11	4	7	12	10	3	7	11	11925.038	-0.001
11	4	7	10	10	3	7	9	11925.052	0.001
11	4	8	11	10	3	8	10	11942.523	-0.001
11	4	8	12	10	3	8	11	11942.560	0.000
11	4	8	10	10	3	8	9	11942.565	-0.001
13	3	11	12	12	2	11	11	12015.721	-0.001
13	3	11	14	12	2	11	13	12015.739	0.001
13	3	11	13	12	2	11	12	12015.955	-0.001
9	5	4	9	8	4	4	8	12051.654	-0.003
9	5	4	10	8	4	4	9	12051.703	-0.005
9	5	4	8	8	4	4	7	12051.715	0.000
9	5	5	9	8	4	5	8	12051.729	-0.001
9	5	5	10	8	4	5	9	12051.777	-0.004
9	5	5	8	8	4	5	7	12051.789	0.001
14	3	11	14	13	2	11	13	12111.000	0.001
14	3	11	15	13	2	11	14	12111.351	0.000
14	3	11	13	13	2	11	12	12111.381	0.000
7	6	1	7	6	5	1	6	12160.646	-0.001
7	6	2	7	6	5	2	6	12160.646	-0.001
7	6	1	8	6	5	1	7	12160.688	0.001
7	6	2	8	6	5	2	7	12160.688	0.001
16	2	14	15	15	1	14	14	12446.208	-0.001
16	2	14	17	15	1	14	16	12446.236	0.001
16	2	14	16	15	1	14	15	12446.672	-0.001
12	4	8	12	11	3	8	11	12555.229	-0.001
12	4	8	13	11	3	8	12	12555.336	-0.002
12	4	8	11	11	3	8	10	12555.350	0.001
12	4	9	12	11	3	9	11	12585.458	-0.002
12	4	9	13	11	3	9	12	12585.490	0.001
15	3	12	15	14	2	12	14	12682.768	0.001
15	3	12	16	14	2	12	15	12683.089	-0.001
15	3	12	14	14	2	12	13	12683.116	0.001
10	5	5	10	9	4	5	9	12693.310	-0.001
10	5	5	11	9	4	5	10	12693.358	-0.002

Table G.3 Observed Transitions of Triflimidic Acid (cont'd)

J'	K_a'	K_c'	F'	J''	K_a''	K_c''	F''	Obs. Frequency (MHz)	Obs. - Calc. MHz
10	5	5	9	9	4	5	8	12693.367	0.001
10	5	6	10	9	4	6	9	12693.499	-0.002
10	5	6	11	9	4	6	10	12693.547	-0.001
10	5	6	9	9	4	6	8	12693.556	0.001
14	3	12	13	13	2	12	12	12714.239	-0.002
14	3	12	15	13	2	12	14	12714.258	0.000
14	3	12	14	13	2	12	13	12714.505	-0.001
8	6	2	8	7	5	2	7	12803.161	-0.001
8	6	3	8	7	5	3	7	12803.161	-0.001
8	6	2	9	7	5	2	8	12803.209	0.002
8	6	3	9	7	5	3	8	12803.209	0.002
11	5	6	11	10	4	6	10	13334.414	-0.005
11	5	6	12	10	4	6	11	13334.467	0.000
11	5	7	11	10	4	7	10	13334.854	-0.004
11	5	7	12	10	4	7	11	13334.904	0.000
9	6	3	9	8	5	3	8	13445.584	-0.002
9	6	4	9	8	5	4	8	13445.584	-0.002
9	6	3	10	8	5	3	9	13445.630	-0.001
9	6	4	10	8	5	4	9	13445.630	-0.001
7	7	0	7	6	6	0	6	13553.864	-0.002
7	7	1	7	6	6	1	6	13553.864	-0.002
7	7	0	8	6	6	0	7	13553.884	0.001
7	7	1	8	6	6	1	7	13553.884	0.001
12	5	7	12	11	4	7	11	13974.786	0.005
12	5	7	13	11	4	7	12	13974.827	-0.002
12	5	7	11	11	4	7	10	13974.843	0.008
12	5	8	12	11	4	8	11	13975.719	0.004
12	5	8	13	11	4	8	12	13975.758	-0.002
12	5	8	11	11	4	8	10	13975.773	0.007
10	6	4	10	9	5	4	9	14087.869	0.003
10	6	5	10	9	5	5	9	14087.869	0.001
10	6	4	11	9	5	4	10	14087.913	0.004
10	6	5	11	9	5	5	10	14087.913	0.002
8	7	1	8	7	6	1	7	14196.443	0.011
8	7	2	8	7	6	2	7	14196.443	0.011
8	7	1	9	7	6	1	8	14196.463	-0.001
8	7	2	9	7	6	2	8	14196.463	-0.001

Table G.3 Observed Transitions of Triflimidic Acid (cont'd)

J'	K_a'	K_c'	F'	J''	K_a''	K_c''	F''	Obs. Frequency (MHz)	Obs. - Calc. MHz
13	5	8	13	12	4	8	12	14614.142	-0.002
13	5	8	14	12	4	8	13	14614.194	0.001
13	5	9	13	12	4	9	12	14615.994	-0.002
13	5	9	14	12	4	9	13	14616.041	0.001
9	7	2	9	8	6	2	8	14838.968	-0.002
9	7	3	9	8	6	3	8	14838.968	-0.002
9	7	2	10	8	6	2	9	14839.007	0.000
9	7	3	10	8	6	3	9	14839.007	0.000